الجمهورية الجزائرية الديمقراطية الشعبية

République Algérienne Démocratique et Populaire

Ministère de L'Enseignement Supérieur et de la Recherche Scientifique

Université Ferhat ABBAS Sétif 1

UNIVERSITÉ SETIF1-FERHAT ABBAS

FACULTÉ DE TECHNOLOGIE

THÈSE

Présentée au Département d'automatique et systèmes intelligents

Pour l'obtention du diplôme de

DOCTORAT

Domaine : Sciences et Technologie

Filière: Automatique **Option: Automatique et systèmes**

Par

BOUGUERRA Assala

THÈME

Contrôle et gestion d'un système hybride PV-Pile à combustible par les techniques intelligentes

Soutenue le 13/04/2026 devant le Jury :

Lazhar RAHMANI	Professeur	Univ. Ferhat Abbas Sétif 1	Président
BADOUD Abd Essalam	Professeur	Univ. Ferhat Abbas Sétif 1	Directeur de thèse
MEKHILEF Saad	Professeur	Université de technologie de Swinburne - Australie	Co-Directeur
Belkacem OULD BOUAMAMA	Professeur	Ecole polytechnique de Lille - France	Examinateur
Diab MOKEDDEM	Professeur	Univ. Ferhat Abbas Sétif 1	Examinateur
BAHI Tahar	Professeur	Univ. Badji Mokhtar, Annaba	Examinateur

الجمهورية الجزائرية الديمقراطية الشعبية

People's Democratic Republic of Algeria

Ministry of Higher Education and Scientific Research

Université Ferhat ABBAS Sétif 1

UNIVERSITY OF SETIF1- FERHAT ABBAS
FACULTY OF TECHNOLOGY

THESIS

Presented to the Automatic and Intelligent Systems Department

To obtain the degree of

Ph.D

Domain : Sciences and Technology

Field: Automatic **Option: Automatic and systems**

By

BOUGUERRA Assala

TITLE

Control and management of a hybrid PV-Fuel Cell system using intelligent techniques

Defended on 13/04/2026 before the Jury:

Lazhar RAHMANI	Professor	Ferhat abbas setif 1 university	President
Abd Essalam BADOUD	Professor	Ferhat abbas setif 1 university	Supervisor
Saad MEKHILEF	Professor	University of Swinburne of Technology - Australia	Co-Supervisor
Belkacem OULD BOUAMAMA	Professor	Polytechnic School of Lille - France	Examiner
Diab MOKEDDEM	Professor	Ferhat abbas setif 1 university	Examiner
BAHI Tahar	Professor	University of Badji Mokhtar, Annaba	Examiner

Acknowledgements

In the name of Allah, the Most Kind and the Most Merciful. I am deeply grateful to Allah, the infinite source of knowledge and wisdom, for providing me with the strength, willpower, and clear purpose necessary to complete my PhD journey. Without His divine guidance and boundless mercy, this achievement would not have been possible.

I am truly grateful to my supervisors, ***Professor Abd Essalem BADOUD*** *and* ***Professor Saad MEKHILEF****. Their excellent guidance, constant support, and valuable encouragement have been crucial to improving this research. I would like to extend my sincere appreciation to* ***Pr. Saad MEKHILEF*** *for his kindness in granting full access to the experimental facilities and equipment of* ***Power Electronics and Renewable Energy Research Laboratory (PEARL) at the University of Malaya (UM) in Malaysia****, which was very crucial in obtaining and verifying the results presented in this thesis. His insightful guidance and innovative ideas significantly enhanced the scientific merit and quality of this research work. I am truly grateful to them for allowing me to pursue my doctoral research under their guidance.*

I would like to sincerely thank the eminent members of my thesis committee, ***Professor Lazhar RAHMANI****,* ***Professor*** **Belkacem OULD BOUAMAMA,** ***Professor*** **Diab MOKEDDEM,** *and* ***Professor BAHI Tahar*** *for their meticulous examinations, constructive criticism, and valuable suggestions, which significantly improved the quality and scientific value of this dissertation.*

I would like to sincerely thank ***Dr. Karam Khairullah Mohamed*** *for his much-appreciated help in the experimental verification of this research. His technical expertise and practical experience greatly assisted in the successful completion of experimental work. I would also like to express my sincere gratitude to* ***Dr.Djamel Ziane*** *from the IRENA research team at the University of Nantes for his valuable contribution to the experimental verification of other parts of this work, and to* ***Dr****.* **Jihed Hmad** *for his continuous support and assistance throughout the completion of this research.*

I am deeply grateful to ***Professor Chouder Aissa*** *for his invaluable advice during the initial stages of my work, which played a crucial role in laying a solid foundation in this field. Their feedback greatly improved the quality and content of this thesis.*

I would like to thank the ***Automatic Laboratory of Setif (LAS)*** *for giving me the tools and space I needed to do my research. I highly appreciate the collaboration and the successful interactions with my colleagues that greatly contributed to the academic and personal dimensions of this work.*

I am most thankful to ***my family****, whose unending love, deep faith, and unshakeable prayers have been my greatest. This milestone is as much theirs as it is mine.*

BOUGUERRA Assala

DEDICATION

To the moon of my sky, who taught me patience and the true meaning of challenge:

***My dear father**,*

To the sun that dawned from a flicker in the void,

whose steadfast light guided my academic journey's darkest hours:

My beloved mother,

To the steadfast branches of my family tree, whose presence has given me strength, stability, and a deep sense of belonging:

My cherished brothers Abd el Latif and Mohamed Youcef and sisters Donia, Hadil, Meryam, and Manal

To the companions who shared in my journey with loyalty and encouragement:

Dear friends—Rania, Khaldiya, Hala and Khaoula

To the land of one and a half million martyrs, whose history and hope still motivate us:

My beloved homeland, Algeria

To those who illuminated my academic path, nurtured my curiosity, and shaped my scientific vision:

Professor Abd Essalem BADOUD and Professor Saad MEKHILEF

With profound respect and heartfelt gratitude

I dedicate this work.

BOUGUERRA Assala

Abstract

This thesis emphasizes designing, improving, and validating new enhanced control and power management approaches for a hybrid standalone photovoltaic-fuel cell (PV-FC) system, especially under challenging circumstances involving multiple energy sources. The primary aim is to develop effective control strategies to mitigate the challenges presented by varying weather conditions, nonlinear output characteristics, and fluctuating load demands that impact system efficiency, stability, and dependability.

The most significant contribution of this thesis is the enhanced pufferfish optimization algorithm (EPFOA), which improves MPPT in solar energy systems. This strategy was evaluated against four established metaheuristic methods: PSO, GWA, AOA, and SOA, in the context of rapidly fluctuating irradiance and intricate shading circumstances. The EPFOA exhibited the ability to consistently identify the global maximum power point using just two tuning parameters, successfully overcoming local maxima and ensuring enhanced output power without oscillations around the MPP. Experiments conducted under intricate real-world conditions demonstrated significantly enhanced tracking speed, accuracy, and robustness.

The proposed approaches demonstrated substantial enhancements in resilience, efficiency, and dynamic response relative to current techniques, validated by comprehensive simulations and real-time hardware-in-the-loop experiments. The EPFOA was recognized for its stability under real operating situations, confirming its practical application.

On the other hand, an improved FSSO was proposed for the control of polymer electrolyte membrane fuel cells (PEMFC) under fluctuating pressure and temperature circumstances. The FSSO was evaluated against the traditional control method (CSO) and proved effective in achieving reduced settling times and improved stability while accurately tracking the MPP despite changes in the environment.

Ultimately, an efficient EHOA energy control approach has been developed to regulate the operation of several energy sources and ensure the continuous availability of power to fulfill load demand. This approach efficiently allocates energy, emphasizes renewable sources, and prevents the system from surpassing the operational thresholds of any component, so guaranteeing a consistent power supply to meet demand. The findings demonstrate that the hybrid system can rapidly adapt to environmental changes and the requirements of the load. This outcome demonstrates that the proposed EHOA control, compared to other conventional and contemporary management techniques, may be effectively implemented in practical applications. This research has established a scalable and methodical framework for integrating hybrid renewable energy systems, supporting various topologies, sizes, and operating requirements, beyond basic technological efficiency.

By providing a scalable framework for dependable, sustainable, and intelligent hybrid energy systems, the established solutions tackle fundamental issues in the integration of renewable energy.

Keywords: Hybrid energy system, PV-fuel cell, intelligent control, energy management strategy, MPPT, renewable energy, EPFOA, FSSO, EHOA, Load demand, GMPP.

Résumé

Cette thèse met l'accent sur la conception, l'amélioration et la validation de nouvelles approches renforcées de contrôle et de gestion de l'énergie pour un système hybride autonome photovoltaïque-pile à combustible (PV-PAC), en particulier dans des circonstances difficiles impliquant de multiples sources d'énergie. L'objectif principal est de développer des stratégies de contrôle efficaces pour atténuer les défis posés par les conditions météorologiques variables, les caractéristiques de sortie non linéaires et les demandes de charge fluctuantes qui affectent l'efficacité, la stabilité et la fiabilité du système.

La contribution la plus significative de cette thèse est l'algorithme d'optimisation amélioré du poisson-globe (Enhanced Pufferfish Optimization Algorithm - EPFOA), qui améliore la MPPT (Recherche du Point de Puissance Maximale) dans les systèmes d'énergie solaire. Cette stratégie a été évaluée par rapport à quatre méthodes métaheuristiques établies : l'optimisation par essaims de particules (PSO), l'algorithme du loup gris (GWO), l'arithmétique algorithme d'optimisation (AOA) et l'algorithme d'optimisation du serpent (SOA), dans le contexte d'une irradiation à fluctuations rapides et de conditions d'ombrage complexes. L'EPFOA a démontré sa capacité à identifier systématiquement le point de puissance maximale global (GMPP) en utilisant seulement deux paramètres de réglage, surmontant avec succès les maxima locaux et assurant une puissance de sortie accrue sans oscillations autour du MPP. Les expériences menées dans des conditions complexes de terrain ont montré une vitesse de poursuite, une précision et une robustesse significativement améliorées.

Les approches proposées ont démontré des améliorations substantielles en termes de résilience, d'efficacité et de réponse dynamique par rapport aux techniques actuelles, validées par des simulations complètes et des expériences en temps réel de type "Hardware-in-the-Loop". L'EPFOA a été reconnu pour sa stabilité dans des situations opérationnelles réelles, confirmant son applicabilité pratique.

D'autre part, un algorithme d'optimisation de la recherche de l'écureuil volant (FSSO) a été proposé pour le contrôle des piles à combustible à membrane échangeuse de protons (PEMFC) dans des conditions de pression et de température fluctuantes. Le FSSO a été évalué par rapport à l'algorithme d'optimisation de la recherche du coucou (CSO) et s'est avéré efficace pour obtenir des temps d'établissement réduits et une stabilité améliorée tout en assurant un suivi précis du MPP malgré les changements environnementaux.

Enfin, une approche de contrôle de l'énergie par an algorithme d'optimisation des troupeaux de wapitis (EHOA) a été développée pour réguler le fonctionnement de plusieurs sources d'énergie et garantir la disponibilité continue de l'électricité afin de satisfaire la demande de charge. Cette approche alloue efficacement l'énergie, privilégie les sources renouvelables et empêche le système de dépasser les seuils opérationnels de tout composant, garantissant ainsi un approvisionnement en énergie stable pour répondre à la demande. Les résultats démontrent que le système hybride peut s'adapter rapidement aux changements environnementaux et aux exigences de la charge. Ce résultat montre que le contrôle EHOA proposé, comparé à d'autres techniques de gestion conventionnelles et contemporaines, peut être mis en œuvre efficacement dans des applications pratiques. Cette recherche a établi un cadre évolutif et méthodique pour l'intégration de systèmes hybrides d'énergie renouvelable, prenant en charge diverses topologies, tailles et exigences opérationnelles, au-delà de la simple efficacité technologique.

En fournissant un cadre évolutif pour des systèmes d'énergie hybrides fiables, durables et intelligents, les solutions établies abordent les problèmes fondamentaux de l'intégration des énergies renouvelables.

Mots-clés : Système d'énergie hybride, PV-pile à combustible, contrôle intelligent, stratégie de gestion de l'énergie, MPPT, énergie renouvelable, EPFOA, FSSO, EHOA, Demande de charge, GMPP.

الملخص

تُركز هذه الأطروحة على تصميم وتحسين والتحقق من صحة أساليب جديدة مُحسّنة للتحكم وإدارة الطاقة لنظام هجين مستقل يعمل بخلايا الوقود الكهروضوئية (PV-FC)، لا سيما في ظل ظروف صعبة تتضمن مصادر طاقة متعددة. والهدف الرئيسي هو تطوير استراتيجيات تحكم فعّالة للتخفيف من التحديات التي تفرضها الظروف الجوية المتغيرة، وخصائص الخرج غير الخطية، وتقلبات الطلب على الطاقة، والتي تؤثر على كفاءة النظام واستقراره وموثوقيته.

وتتمثل أهم مساهمة لهذه الأطروحة في خوارزمية تحسين سمكة البخاخ المُحسّنة (EPFOA)، التي تُحسّن من تتبع نقطة القدرة القصوى (MPPT) في أنظمة الطاقة الشمسية. وقد تم تقييم هذه الاستراتيجية مقارنةً بأربع طرق استكشافية مُثبتة: PSO وGWA وAOA وSOA، في سياق إشعاع شمسي سريع التذبذب وظروف تظليل معقدة. وقد أظهرت خوارزمية EPFOA قدرةً على تحديد نقطة القدرة القصوى العالمية باستمرار باستخدام مُعاملَي ضبط فقط، متجاوزةً بنجاح القيم القصوى المحلية، ومُضمنةً قدرة خرج مُحسّنة دون تذبذبات حول نقطة القدرة القصوى. أظهرت التجارب التي أُجريت في ظروف واقعية معقدة تحسنًا ملحوظًا في سرعة التتبع ودقته ومتانته.

وأظهرت المناهج المقترحة تحسينات كبيرة في المرونة والكفاءة والاستجابة الديناميكية مقارنةً بالتقنيات الحالية، وهو ما تم التحقق منه من خلال عمليات محاكاة شاملة وتجارب محاكاة الأجهزة في الوقت الفعلي. وقد حظي نظام EPFOA بالتقدير لاستقراره في ظروف التشغيل الحقيقية، مما يؤكد جدواه العملية.

من جهة أخرى، تم اقتراح نظام FSSO مُحسَّن للتحكم في خلايا وقود غشاء البوليمر الإلكتروليتي (PEMFC) في ظل ظروف الضغط ودرجة الحرارة المتقلبة. وقد تم تقييم نظام FSSO مقارنةً بطريقة التحكم التقليدية (CSO)، وأثبت فعاليته في تقليل أوقات الاستقرار وتحسين الاستقرار مع تتبع دقيق لنقطة الطاقة القصوى (MPP) على الرغم من تغيرات البيئة.

وفي النهاية، تم تطوير منهج فعال للتحكم في الطاقة EHOA لتنظيم تشغيل مصادر الطاقة المتعددة وضمان استمرارية توافر الطاقة لتلبية الطلب على الطاقة. يوزع هذا المنهج الطاقة بكفاءة، ويركز على مصادر الطاقة المتجددة، ويمنع النظام من تجاوز عتبات التشغيل لأي مكون، مما يضمن إمدادًا ثابتًا بالطاقة لتلبية الطلب. تُظهر النتائج قدرة النظام الهجين على التكيف السريع مع التغيرات البيئية ومتطلبات الأحمال. وتُبين هذه النتيجة إمكانية تطبيق نظام التحكم EHOA المقترح، مقارنةً بتقنيات الإدارة التقليدية والمعاصرة الأخرى، بفعالية في التطبيقات العملية. وقد أرست هذه الدراسة إطارًا منهجيًا قابلًا للتطوير لدمج أنظمة الطاقة المتجددة الهجينة، يدعم مختلف التكوينات والأحجام ومتطلبات التشغيل، متجاوزًا الكفاءة التقنية الأساسية.

ومن خلال توفير إطار عمل قابل للتطوير لأنظمة طاقة هجينة موثوقة ومستدامة وذكية، تعالج الحلول المُطورة قضايا جوهرية في دمج الطاقة المتجددة.

الكلمات المفتاحية: نظام طاقة هجين، خلية وقود كهروضوئية، تحكم ذكي، استراتيجية إدارة الطاقة، تتبع نقطة القدرة القصوى (MPPT)، طاقة متجددة، EPFOA، FSSO، EHOA، طلب الحمل، GMPP.

Table of Contents

List of Figures XII

List of Tables XV

List of Acronyms XVI

List of Symbols XX

CHAPTER 1 : INTRODUCTION 1

1.1 Background 1

1.1.1 Overview of renewable energy sources 1

1.1.2 Importance of hybrid renewable power systems 4

1.1.3 Motivation for integrating SPV and FC systems 7

1.2 Problem Statement 7

1.3 Research Questions 8

1.4 Objectives and contributions of the thesis 8

1.5 Structure of thesis 10

CHAPTER 2 : MODELING OF POWER SOURCES 12

2.1 Introduction 12

2.2 A PV solar cell's mathematical model 14

2.2.1 Model of Ideal Solar cell 15

2.2.2 Model of Practical PV cell 16

2.2.3 The effect of temperature and irradiance on SPV systems 17

2.2.4 The effect of Partial shading conditions 19

2.3 Fuel Cell 21

2.3.1 Principles of fuel cells 21

2.3.2 Different types of FCs 21

2.3.3 Polymer electrolyte membrane fuel cell (PEMFC) 23

2.3.3.1 Static model of PEMFC 24

2.3.3.2 Dynamic model of PEMFC 27

2.3.4 The influence of pressure and temperature on PEMFC efficiency 28

2.4 Power Electronic Converters (PECs) 30

2.4.1 DC-DC power converters 30

2.4.1.1 Boost converter 32

2.4.1.1.1 The mode state ''ON'' 33

2.4.1.1.2 The mode state ''OFF'' 33

2.4.1.2 SEPIC converter 34
2.4.1.3 Buck-Boost converter 35
2.4.1.3.1 The mode state ''ON'' 35
2.4.1.3.2 The mode state ''OFF'' 35

2.5 Energy Storage systems 36
2.5.1 Model of lithium-ion battery 36

2.6 Conclusion 37

CHAPTER 3 : LITERATURE REVIEW ON CONTROL AND POWER MANAGEMENT OF HYBRID STANDALONE POWER SYSTEMS 39

3.1 Introduction 39

3.2 Maximum Power Point Tracking (MPPT) Techniques: 40
3.2.1 MPPT-based PV system descriptions for DC-to-DC applications 41
3.2.1.1 MPPT approach based on current or voltage control 41
3.2.1.2 MPPT approach based on duty cycle control 41
3.2.2 Overview of the several MPPT approaches and their categorization 42
3.2.2.1 Conventional MPPT Control Approaches 43
3.2.2.1.1 Perturb And Observe (P&O) approach 44
3.2.2.1.2 Incremental conductance (IC) approach 45
3.2.2.1.3 Hill Climbing (HC) 47
3.2.2.1.4 Constant voltage approach 48
3.2.2.1.5 Open Circuit Voltage (OCV) approach 49
3.2.2.1.6 Short Circuit Current (SCC) approach 49
3.2.2.1.7 An approach based on Lookup Table (LT) 50
3.2.2.2 Advanced MPPT approaches 51
3.2.2.2.1 Smart MPPT strategies 51
3.2.2.2.1.1 Fuzzy Logic Controller (FLC) approach 51
3.2.2.2.1.2 Artificial neural network approach 52
3.2.2.2.1.3 Adaptive Neuro Fuzzy Inference System (ANFIS) 54
3.2.2.2.1.4 The Bayesian Network (BN) 55
3.2.2.2.1.5 Fibonacci series approach (FS) 56
3.2.2.2.1.6 Gauss Newton approach (GNA) 56
3.2.2.3 Metaheuristic MPPT approaches 57
3.2.2.3.1 Social spider strategy for optimization 57
3.2.2.3.2 Zebra optimization algorithm 57
3.2.2.3.3 Snake optimization algorithm (SOA) 57
3.2.2.3.4 Coot optimization approach 58
3.2.2.3.5 Rat optimization approach (ROA) 58
3.2.2.3.6 Falcon optimization approach 58
3.2.2.3.7 Dung beetle approach 59
3.2.2.3.8 Atomic orbital search approach 59
3.2.2.4 Hybrids MPPT approaches 60
3.2.2.4.1 Grey Wolf Equilibrium Optimization (GWEO) approach 61

3.2.2.4.2 FLC-P&O approach 61
3.2.2.4.3 Artificial Bee Colony-Perturb and Observe (ABC-P&O) approach 61
3.2.3 An overview of MPPT control of PEMFC 63
3.2.3.1 Jaya MPPT approach 63
3.2.3.2 Modified PSO MPPT approach 65
3.2.3.3 Adaptive Genetic Algorithm-Based ANFIS MPPT approach 66

3.3 An overview of energy management approaches 68
3.3.1 Categorization of energy management approaches 68
3.3.1.1 Rule based approaches 69
3.3.1.2 Optimization based approaches 70
3.3.1.3 AI-based approaches 71

Conclusion 72

CHAPTER 4 : INTELLIGENT CONTROL APPROACHES FOR A STANDALONE HYBRID PV-PEMFC SYSTEM 73

4.1 Introduction 73

4.2 The Development of an MPPT Controller for Photovoltaic Systems 73
4.2.1 The Conventional Pufferfish Optimization Approach (CPFOA) 73
4.2.1.1 Inspiration of Pufferfish 73
4.2.1.2 Initialization 74
4.2.1.3 Mathematical Model of conventional PFOA 75
4.2.1.4 Exploration phase: Predatory attack on the pufferfish 75
4.2.1.5 Exploitation phase: Defensive Strategy of Pufferfish against Predators 75
4.2.1.6 Iterative Process 76
4.2.2 Proposed Enhanced Pufferfish Optimization Approach (EPFOA)-Based MPPT 76
4.2.2.1 Enhancements in Initialization 76
4.2.2.2 Enhancements in Exploration 77
4.2.2.3 Levy Flights in Optimization: A General Overview 77
4.2.2.4 Enhancements in Exploitation 79
4.2.2.5 Adjustment of the condition of termination 81
4.2.3 Metaheuristic approaches used in comparative study 81
4.2.3.1 Particle Swarm Optimization (PSO) 81
4.2.3.2 Grey Wolf Approach (GWA) 83
4.2.3.3 Arithmetic optimization approach (AOA) 84
4.2.3.3.1 Initialization of AOA 84
4.2.3.3.2 Exploration stage 85
4.2.3.3.3 Exploitation stage 85
4.2.3.4 Snake optimization algorithm (SOA) 85
4.2.4 Validation of EPFOA Under different conditions 86
4.2.4.1 Test of Performance of the proposed EPFOA under changing irradiance conditions 86
4.2.4.2 Test of Performance of the proposed EPFOA under Partial shading conditions 92

4.3 The Development of an MPPT Controller for PEMFCs 102

4.3.1 Flying Squirrel Search Optimization Method 103
4.3.1.1 Application of the FSSO Method to the Tracking of GMPPs 104
4.3.1.1.1 Getting started 104
4.3.1.1.2 Fitness Evaluation 104
4.3.1.1.3 Declaration and Arrangement 105
4.3.1.1.4 Location recency 105
4.3.1.1.5 Current Seasonal Monitoring Status 105
4.3.1.1.6 Change Routine 106
4.3.1.1.7 Evaluation of Convergence 106
4.3.1.1.8 Returning to the initial state 106
4.3.1.2 Cuckoo search optimization (CSO) 108
4.3.2 Results and discussion 111
4.3.2.1 Standard Test conditions 111
4.3.2.2 Fast change in temperature levels 112
4.3.2.3 Fast change in Pressures levels 114
4.3.2.4 Sudden change in pressure and temperature levels 116

4.4 Conclusion 120

CHAPTER 5 : DESIGN OF ENERGY MANAGEMENT AND POWER FLOW STRATEGIES 121

5.1 Introduction 121

5.2 A brief overview of the different power management approaches used 121
5.2.1 Proportional-integral (PI) control approach 121
5.2.2 The Equivalent Consumption Minimization Approach (ECMA) 122
5.2.3 The External Energy Maximization Approach (EEMA) 122
5.2.4 PARTICLE SWARM OPTIMIZER 123
5.2.5 The proposed Elk Herd Optimization Approach 123
5.2.5.1 Inspiration of EHOA 123
5.2.5.2 The EHOA's mathematical model 124
5.2.5.2.1 Initialization of EHOA population 124
5.2.5.2.2 Rutting Season 124
5.2.5.2.3 Calving Season 125
5.2.5.2.4 Selection Season 125

5.3 Simulation setup and discussion 129

5.4 Conclusion 138

CHAPTER 6 : CONCLUSIONS 139

6.1 General conclusion 139

6.2 Perspectives & Future Directions 140

References.. 141

List of Figures

Figure 1.1: Annual CO_2 emissions [2]..1
Figure 1.2: CO_2 emissions from fossil fuels and land use change,World ,2023 [2]. 2
Figure 1.3: Electricity production by source in 2024 [4]..3
Figure 1.4: (a) Annual change in electricity generation(TWh),(b) Electricity generation for solar power (TWh) ,(c) Global solar capacity ,and (d) Global electricity generation per source [4]..4
Figure 2.1: The structure of the proposed hybrid PV-PEMFC standalone system..13
Figure 2.2: The single-diode model equivalent electrical circuit of a PV cell [43]. 15
Figure 2.3 : (I) P-V and (II) I-V characteristics of the SPR-200-BLK PV module at varied levels of illumination. 17
Figure 2.4 : (I) P-V and (II) I-V characteristics of the SPR-200-BLK PV module at different temperature ranges. 18
Figure 2.5: Solar irradiance patterns for PV module under (I) uniform and (II) non-uniform shading scenarios. 19
Figure 2.6: I-V (I) and P-V (II) curves under uniform and non-uniform shading conditions...........................20
Figure 2.7 : Different types of FCs. 22
Figure 2.8 : Schematic of the PEMFC functioning [59]. 24
Figure 2.9 : The dynamic electrical circuit equivalent of PEMFC [63]. 28
Figure 2.10 : (I) the P-I and (II) V-I properties of PEMFC at various pressures and steady temperatures......29
Figure 2.11: ((I) the P-I and (II) V-I properties of PEMFC at different temperatures and steady pressures. ..29
Figure 2.12 : several common DC–DC converter topologies [75]. 31
Figure 2.13 : (a) ON and (b) OFF modes boost converter circuits [73],[80]. 33
Figure 2.14: (a) ON and (b) OFF modes Buck-Boost converter circuits [80]. 36
Figure 2.15: The model of the battery [81]...37
Figure 3.1: Structure of MPPT approach based on (a) current or voltage (b) duty cycle controls [86]. 41
Figure 3.2: Categorization of MPPT approaches...43
Figure 3.3: Classification of conventional approaches...43
Figure 3.4: Flowchart of P&O strategy [92]...44
Figure 3.5 : Flowchart of IC approach [92]. 47
Figure 3.6: Flowchart of HC approach [97]...47
Figure 3.7: Flowchart of constant voltage approach [99]. 48
Figure 3.8: Flowchart of LT approach [99]. 50
Figure 3.9: Flowchart of FLC approach [99]..52
Figure 3.10: The architecture of ANN [99]. 53
Figure 3.11: The ANFIS approach flowchart [104]. 54
Figure 3.12: The architecture of ANFIS [95]. 55
Figure 3.13: The architecture of BN [95]. 55
Figure 3.14: The flowchart of Jaya MPPT approach [60]. 64
Figure 3.15: The modified PSO flowchart [117]. 66
Figure 3.16 : Flowchart of adaptive genetic algorithm-Based ANFIS MPPT approach [118]...........................67
Figure 3.17: Power management strategies [128]. 69
Figure 4.1: PFOA flowchart [144]..80
Figure 4.2: PSO approach flowchart [157]. 82
Figure 4.3: The GW strategy flowchart [157]. 83
Figure 4.4: Simulation Setup...86
Figure 4.5: Photovoltaic system Simulink model controlled by proposed MPPT techniques. 86
Figure 4.6: The profile of irradiance...87

Figure 4.7: Power dynamics under changing irradiance. 87
Figure 4.8: Power output zoom in. 89
Figure 4.9: The output voltage of PV. 90
Figure 4.10: The output current of PV. 90
Figure 4.11: Duty cycle response of PV. 90
Figure 4.12: The P-V curve of the proposed EPFOA. 91
Figure 4.13: A visual representation of each approach's tracking time and mean tracking time under change irradiance conditions. 92
Figure 4.14: A visual representation of each approach's efficiency and average efficiency under change irradiance conditions. 92
Figure 4.15 : Block diagram of the Proposed EPFOA under PSCs. 93
Figure 4.16: A MATLAB simulation of the suggested MPPT approaches Under Partial Shading Circumstances. 93
Figure 4.17: The P–V properties of PS scenarios used. 94
Figure 4.18: Simulation results of comparison between the proposed EPFOA with SOA, AOA, GWA, and PSO under three PSC. 98
Figure 4.19: A visual representation of each approach's efficiency and average efficiency under three PS scenarios. 99
Figure 4.20: A visual representation of each approach's tracking time and mean tracking time under three PS scenarios. 99
Figure 4.21 : System architecture utilizing two of the MPPT approaches: (a) FSSOS and (b) CSO. 102
Figure 4.22: The foraging habit of the flying squirrel [175]. 104
Figure 4.23: The flowchart of FSSO MPPT [59]. 108
Figure 4.24: CSO flowchart [59]. 110
Figure 4.25: The FSSO and CSO MPPT approaches are evaluated in typical operational circumstances concerning (a) power, (b) current, and (c) voltage. 112
Figure 4.26: The profile of varying levels of temperature. 112
Figure 4.27 : The FSSO and CSO MPPT approaches are evaluated under change temperature conditions concerning (a) power, (b) current, and (c) voltage. 113
Figure 4.28 : The profile of varying levels of pressure. 115
Figure 4.29: The FSSO and CSO MPPT approaches are evaluated under change pressure conditions concerning (a) power, (b) current, and (c) voltage. 115
Figure 4.30: The FSSO and CSO MPPT approaches are evaluated under different pressure and temperature conditions concerning (a) power, (b) current, and (c) voltage. 117
Figure 4.31: power settling time graphical representation. 118
Figure 5.1: Families of elk herds [182]. 126
Figure 5.2 : A flowchart delineating the basic EHOA [184]. 127
Figure 5.3: the proposed methodology that includes EHOA. 127
Figure 5.4: Configurations for power management approaches: (a) PI approach [81], (b) Equivalent consumption minimization approach [81], (c) External energy maximization approach [81], (d) PSO, and (e) EHOA. 129
Figure 5.5: Power flow for the suggested hybrid renewable energy system. 130
Figure 5.6 : Irradiance profile. 130
Figure 5.7: Load profile. 131
Figure 5.8: Power production versus the amount of power needed. 131
Figure 5.9: PV, PEMFC, and battery power response using (a) PI, (b) ECMS, (c) EEMS, (d) PSO, and (e) EHOA. 133
Figure 5.10: DC Link Voltage. 134

Figure 5.11: The SOC response of the battery for the proposed power management approaches. 134
Figure 5.12: Hydrogen consumption in (Ipm) for the proposed power management approaches. 135
Figure 5.13: Hydrogen consumption in (gm) for the proposed power management approaches. 135
Figure 5.14: Efficiency of the proposed power management approaches. 136
Figure 5.15: Graphical representation of the proposed power management approaches: (a) Hydrogen consumption, and (b) Efficiency...137

List of Tables

Table 1.1 : Comparison of the performance of various topologies against the proposed configuration.............6
Table 2.1 : Key PV Module Parameters under Standard Test Conditions. 18
Table 2.2 : Comparison of several categories of FCs [48],[49],[53]. 22
Table 2.3: The PEMFC specifications [59]...26
Table 2.4 : Comparative analysis of the characteristics of the most used non-isolated converters [74]............31
Table 2.5: The components of each converter equation [71]. 36
Table 3.1: The potential differences in the direction of the HC approach [92]. 48
Table 3.2: Comparison of Conventional approaches [99]. 50
Table 3.3 : Comparison between smart MPPT strategies [99],[92],[95]. 56
Table 3.4 : Comparison between Metaheuristic MPPT approaches. 60
Table 3.5: Comparison between hybrid MPPT strategies. 62
Table 3.6: Comprehensive comparison between the performances of different MPPT categories...................62
Table 3.7 : Analysis of prevalent and recent MPPT approaches utilized in fuel cells regarding performance, tracking duration, oscillation, advantages, limitations, and complexity. 67
Table 3.8: The most common and recent power management strategies used in the literature........................71
Table 4.1 : Summary of comparative study evaluation under change irradiance conditions. 91
Table 4.2 : Tuning parameters and random numbers for methods used. 99
Table 4.3: Summary of comparative study analysis between five metaheuristic approaches under PSCs.....100
Table 4.4 : A comprehensive comparison between the proposed EPFOA and the common and currently used MPPT approaches for PV. 101
Table 4.5: Parameter for the boost converter. 103
Table 4.6: Parameters Used in FSSO and CSO MPPT strategies. 107
Table 4.7: The results of comparative evaluation [59]. 118
Table 4.8: A comprehensive comparison between the proposed FSSO and the common and currently used MPPT approaches for PEMFC [59]. 119
Table 5.1: The hybrid power system part's electrical details. 130
Table 5.2 : Comparison between different performance metrics for the proposed power management approaches...136
Table 5.3 : A comprehensive comparison between the proposed EHOA and the common and currently used EMSs. 137

List of Acronyms

A-ECMS	Adaptive Equivalent Consumption Minimization Strategy
AGA	Adaptive Genetic Algorithm
ANFIS	Adaptive Neuro Fuzzy Inference System
AFCs	Alkaline Fuel Cells
AOA	Arithmetic Optimization Algorithm
ABC	Artificial Bee Colony
ABC-P&O	Artificial Bee Colony-Perturb and Observe
AI	Artificial Intelligence
ANN	Artificial Neural Networks
AOA	Arithmetic Optimization Approach
AOS	Atomic Orbital Search
BA	Back Propagation Algorithm
BS	Battery Storage
BSB	Battery Storage Bank
BN	Bayesian Network
BFV	Best Fixed Voltage
BWO	Beluga Whale Optimization
CO2	Carbon dioxide
COS	Coot Optimization Strategy
CV	Constant Voltage
CCM	Continuous Conduction Mode
CPFOA	Conventional Pufferfish Optimization Approach
CSE	Conventional Sources of Energy
CS	Convergence Speed
COA	Coyote Optimization Algorithm
CS	Cuckoo Search
DRB	Deterministic Rules-Based
DEO	Differential Evolution Optimization
DCFCs	Direct Carbon Fuel Cells
DMFCs	Direct Methanol Fuel Cells
DCM	Discontinuous Conduction Mode
DDM	Double-Diode Model
DBA	Dung Beetle Approach
DP	Dynamic Programming

EO	Equilibrium Optimization
ECMA	Equivalent Consumption Minimization Approach
ECMS	Equivalent Consumption Minimization Strategy
EEMA	External Energy Maximization Approach
EEMS	External Energy Maximization Strategy
EHOA	Elk herd Optimization Algorithm
EM	Energy Management
EMCS	Energy Management Control Strategy
EMS	Energy Management Strategy
ESS	Energy Storage System
ESSs	Energy Storage Systems
EPFOA	Enhanced Pufferfish Optimization Approach
FOA	Falcon Optimization Approach
FS	Fibonacci Series Approach
FSM	Finite State Machine
FSs	Flying Southern Squirrels
FSSOA	Flying Squirrel Search Optimization Algorithm
FDSMS	Frequency decoupling and state machine strategy
FC	Fuel Cell
FCs	Fuel Cells
FL	Fuzzy Logic
FLC	Fuzzy Logic Controller
FRBC	Fuzzy Rule-Based Control
GTO	Gaussian-Type Orbitals
GNA	Gauss Newton Approach
GA	Genetic Algorithms
GW	Gigawatts
GMPP	Global Maximum Power Point
GESs	Green Energy Sources
GHGEs	Greenhouse Gas Emissions
GHSs	Green Hydrogen Systems
GWA	Grey Wolf Algorithm
GWO	Grey Wolf Optimization
GWEO	Grey Wolf Equilibrium Optimization
HHO	Harris hawks optimizer
HCM	Hill Climbing Method
HESSs	Hybrid Energy Storage Systems
H2	Hydrogen
HPSs	Hybrid Power Systems
HRESs	Hybrid Renewable Energy Systems
HSs	Hybrid Systems

ISDM	Ideal Single-Diode Model
IPFOA	Improved Pufferfish Optimization Algorithm
IC	Incremental Conductance Method
I-V	Current-Voltage
LCAO	Linear Combination of Atomic Orbitals
LMPPs	Local Maximum Power Points
LPPs	Local Power Peaks
LT	Lookup Table
ML	Machine Learning
MPP	Maximum Power Point
MPPs	Maximum Power Points
MPPT	Maximum Power Point Tracking
MFCs	Microbial Fuel Cells
MBO	Mine-Blast Optimization
MPC	Model Predictive Control
MCFCs	Molten Carbonate Fuel Cells
MAS	Multi-Agent Systems
NASA	National Aeronautics and Space Administration
NLD	Nonlinear Programming
OCV	Open Circuit Voltage
OS	Optimum Solution
PSCs	Partial Shading Conditions
PSO	Particle Swarm Optimization
P&O	Perturb and Observe Technique
PAFCs	Phosphoric Acid Fuel Cells
PV	Photovoltaic
PEMFC	Polymer Electrolyte Membrane Fuel Cell
PEM	Polymer Electrolyte Membranes
PECs	Power Electronic Converters
PSUs	Power Storage Units
P-V	Power-Voltage
PSO	Particle Swarm Optimization
PI controller	Proportional-integral controller
PEMFCs	Proton Exchange Membrane Fuel Cells
PWM	Pulse Width Modulation
ROA	Rat Optimization Approach
RNN	Recursive Neural Networks
RL	Reinforcement Learning
REs	Renewable Energies
RE	Renewable Energy
RES	Renewable Energy Source

RESs	Renewable Energy Sources
RS	Random Solution
SSA	Salp Swarm Algorithm
SCI	Short Circuit Current
SDM	Single-Diode Model
SEPIC	Single-Ended Primary-Inductance
SCOA	Sculptor Optimization Algorithm
STO	Slater-Type Orbitals
SDMC	Sliding Mode
SOA	Snake Optimization Algorithm
SOFCs	Solid Oxide Fuel Cells
SOA	Snake Optimization Algorithm
SSOS	Social Spider Optimization Strategy
SPV	Solar Photovoltaics
STC	Standard Test Conditions
SMM	State Machine Method
SOC	State Of Charge
SDP	Stochastic Dynamic Control Strategy
SCP	Supercapacitor
SDGs	Sustainable Development Goals
TDM	Triple-Diode Model
U.S	United States
WOA	Whale Optimization Approach
WT	Wind Turbines
ZOA	Zebra Optimization Technique

List of Symbols

(I_{PV})	The output current of an ideal solar cell
(I_{ph})	The photocurrent
I_d	The diode current
I_s	The saturating current
q	An electron charge is equal to
V_{oc}	Voltage of the open circuit in Volts
N_s	Number of associated series cells
K	Boltzmann's factor
A	The diode ideality factor
T_o	The real time temperature in Kelvin (K)
(R_p)	Parallel resistance
(R_s)	Series resistance
V_{PV}	The output voltage
I_{sc}	The Current of short circuit at standard conditions (STC)
Ki	Coefficient of temperature for I_{sc} cell
T_r	The reference temperature in Kelvin (K)
G	The Solar radiation (W/m²)
G_{ref}	The Solar radiation at STC (W/m²)
(I_{rs})	Reversal saturating current
(Eg)	The band energy gap
(I_{sc})	Short Circuit Current
(P_{MPP})	Maximum Power Output
(V_{MPP})	Voltage at Maximum Power Point
(I_{MPP})	Current at Maximum Power Point
MWC	The water content of the membrane
(T)	The temperature of fuel cell
(P_{H_2})	The partial pressures of hydrogen
(P_{O2})	The partial pressures of oxygen
V_{cell}	The generated voltage of the fuel cell
V_{con}	The concentration loss caused by excess water flooded in the catalyst fuel cell
V_{Nernst}	The reverse open-circuit output voltage (thermoelectric abilities) of the single cell
ΔG	Liberated energy Gibbs (J/mol)
ΔS	The change entropy
F	Unchanged Faraday
R	The factor of global gas

T	The temperature cell during the process
V_{act}	The drop in activation voltage
I_{FC}	Current of the fuel cell
$CO_2\,(atm)$	The concentration of oxygen
$\xi_i\,(i=1-4)\,(\xi_1, \xi_2, \xi_3, \text{ and } \xi_4)$	The FC characteristic coefficients
V_{ohmic}	Ohmic over-voltage drop
R_C	The primary resistance to contact
R_M	The resistance of the PEMFC
t_m	The electrolyte membrane's size (cm)
r_m	The resistance of electrolyte membrane's $(\Omega \cdot cm)$
λ_m	Content of water membrane
A	The fuel cell active surface space $(70\ \text{cm}^2)$
B	An empirical constant that changes based on the cell and how it operates
$j_{\max}$	The maximum density of current
j	The maximum current
(V_{FC})	The output voltage of FC
(P_{FC})	The output power of FC
CH_2	The concentration of hydrogen
C	Capacitor
V_C	The dynamic voltage across the corresponding electrical capacitor (C)
τ	The RC circuit's constant time
(D)	Diode
(L)	Inductor
(S)	An adjustment switch
(R)	Resistive load
T	The switching period
D	the constant duty cycle
$V_{battery}$	Battery voltage
E_0	Constant voltage battery
Q	Capacity of battery
K	Polarization constant
R_b	The internal resistance of a battery

A_b	Amplitude of the exponential zone
it	The charge of the battery right now
i^*	Current battery filtered
B	The constant of time in the exponential zone
Pol_{res}	Polarization resistance
I_{ref}	The reference current
V_{ref}	The reference voltage
dP_{PV}	The change in power
(dI)	Photovoltaic cell current
(dV)	Photovoltaic cell voltage
K_v	Constant value
(E)	Error
(ΔE)	Change in error
P	Module output power
V	Module output voltage
(D)	Duty cycle
SoC	State of charge
P_{Load}	The power of load
P_{PV}	The PV output power
P_{FC}	The FC output power
$P_{Battery}$	The battery output power

Chapter 1 : Introduction

1.1 Background

1.1.1 Overview of renewable energy sources

For hundreds of years, the globe has relied heavily on fossil fuels such as coal, oil, and natural gas. This reliance has resulted in significant environmental consequences, including increased carbon dioxide (CO2) emissions, which contribute to global warming and climate change [1]. The Global Carbon Budget 2024 and Our World in Data report that CO2 emissions were low prior to the Industrial Revolution. Growth continued incrementally until the mid-twentieth century, with worldwide emissions reaching 6 billion tons by 1950. The total nearly doubled to 20 billion tons by 1990. Since then, industrialized nations like China and the United States have been the primary contributors to emissions, which increased sharply to 37.79 billion tons annually in 2023 as shown in Figure 1.2. China remains the largest emitter with an estimated peak of 11.90 billion tons in 2023. Emissions have significantly increased as a result of rapid production. Recent data indicates that emissions in the United States (U.S) are stabilizing and continuing to decline as outlined in Figure 1.1.

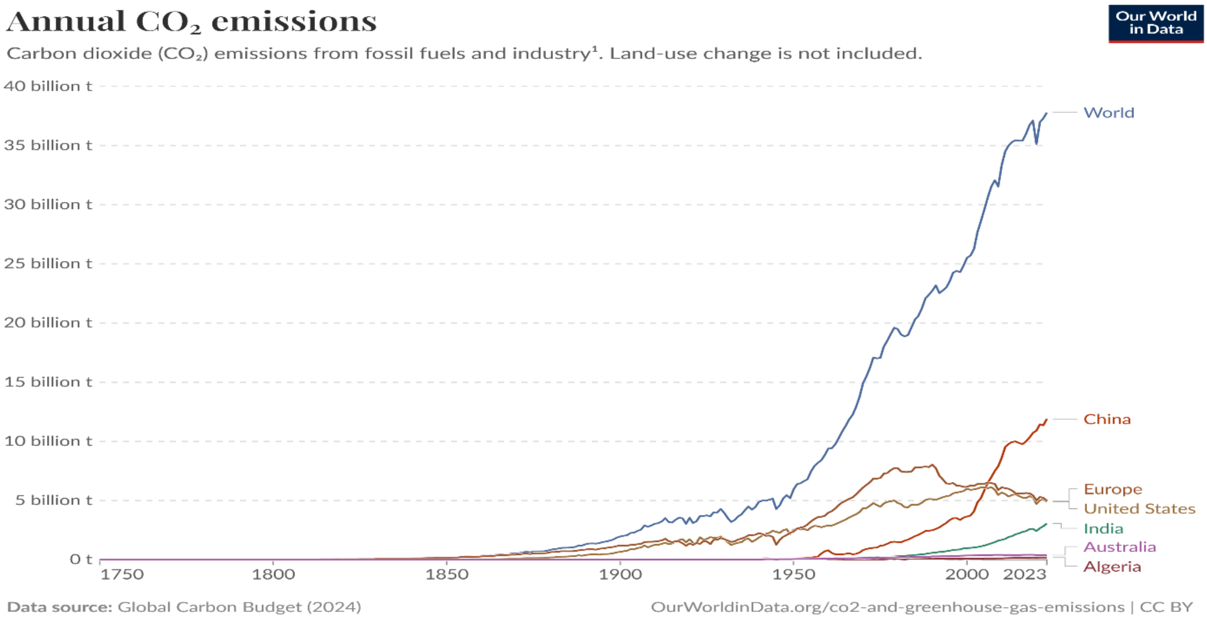

Figure 1.1: Annual CO2 emissions [2].

The recent reports of the Global Carbon Budget (2024) and Paris agreement [3] indicate that the use of fossil fuels must be stopped and the CO2 emissions need to be reduced by 45% by 2030 and completely by 2050 to prevent global warming. Consequently, this change is necessary to mitigate the effects of climate change on ecosystems and industries around the world. For these reasons, fossil fuel reliant on infrastructure must be replaced by cleaner, renewable energy sources [2].

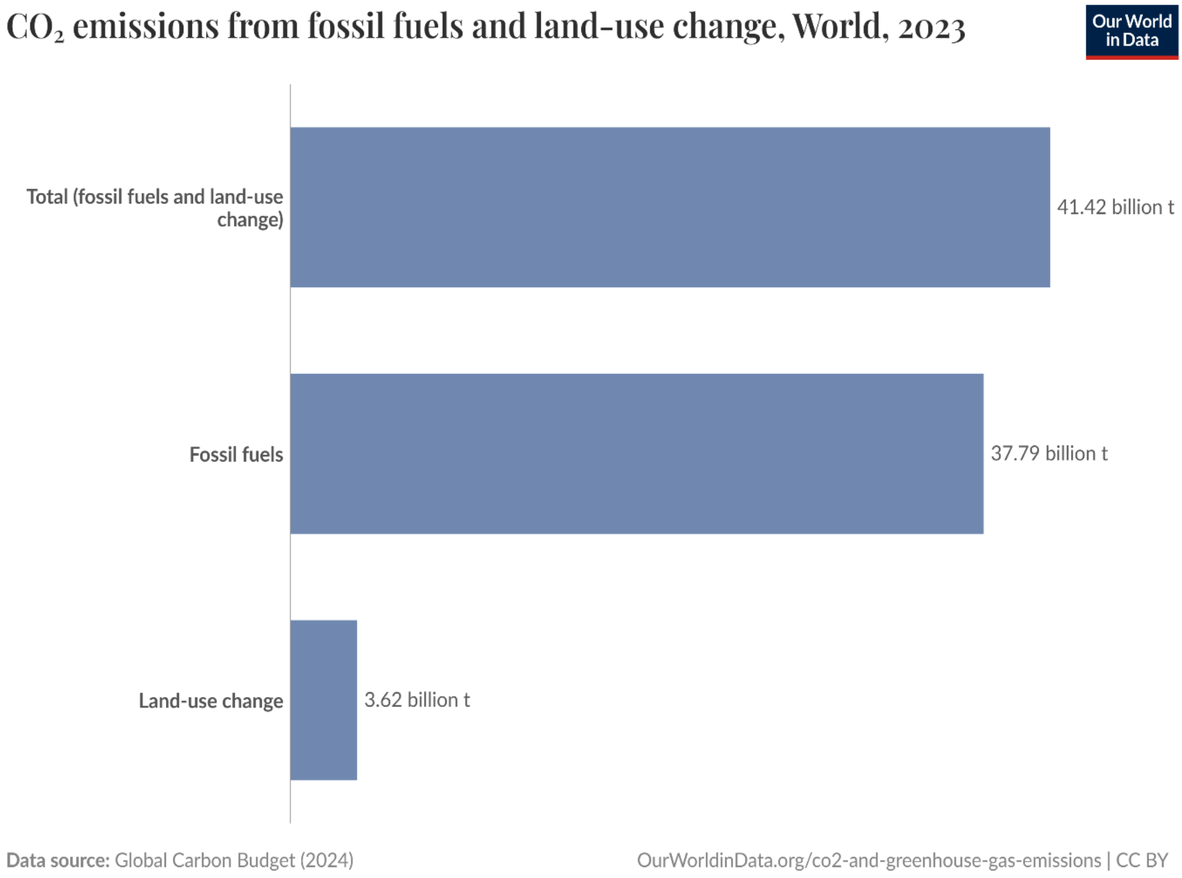

Figure 1.2: CO2 emissions from fossil fuels and land use change,World ,2023 [2].

As depicted in Figure 1.3, renewable energy, projected to contribute to 41% of global electricity generation by 2024, is pivotal to this transition. Nevertheless, solar photovoltaic (PV) technology, although exhibiting rapid expansion, constitutes merely 7% of global electricity generation, primarily due to the substantial initial costs linked to the installation of solar photovoltaic systems, despite notable technological advancements and cost reductions over time.

The Ember Global Electricity Review 2025 reports that renewable energy sources contributed a record 858 TWh of generation in 2024, representing a 49% increase from the prior record established in 2022. Solar power experienced an unprecedented surge of 474 TWh, marking the highest annual growth in absolute terms and the most rapid increase in six years, with a 29% rise. Solar energy has been a key driver for the growth of electricity generation, doubling its capacity every three years. In 2024, solar generation attained 2,131 TWh, sufficient to power the equivalent of all of India. This swift expansion has not only addressed the increasing global demand for electricity but also substantially reduced dependence on costly fossil fuels, thereby avoiding a 12% increase in fossil generation that would have been necessary in the absence of solar energy [4].

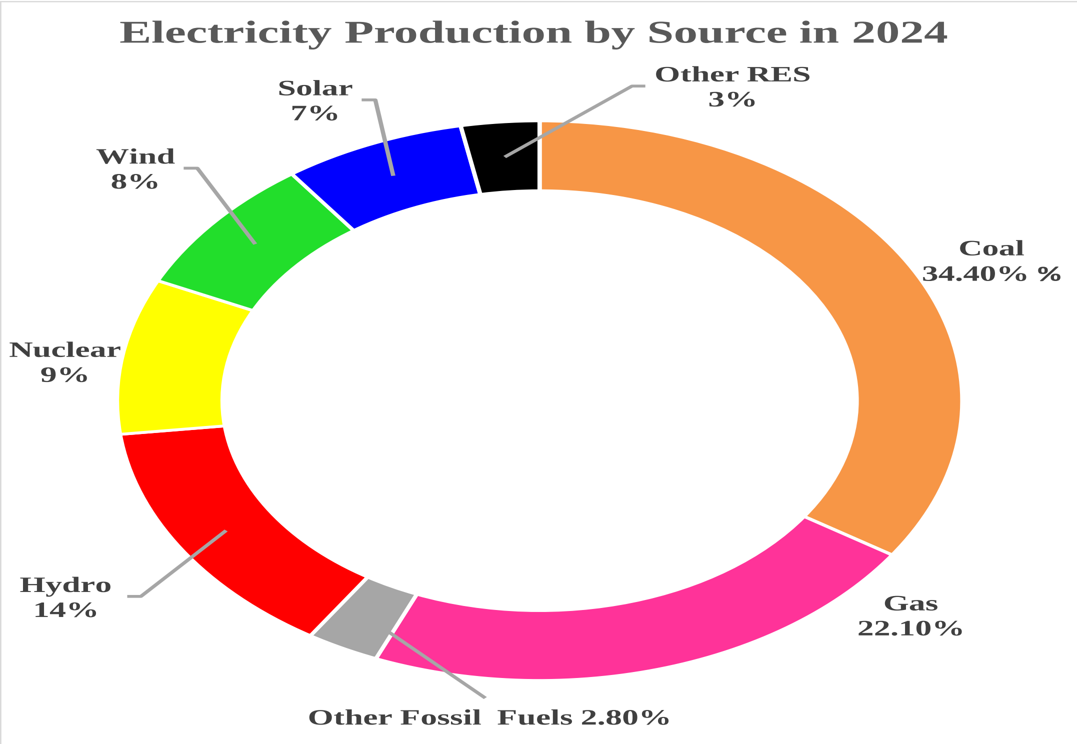

Figure 1.3: Electricity production by source in 2024 [4].

Outstanding capacity installations further accelerate the remarkable rate of growth in solar energy. In 2024, the world added 585 gigawatts (GW) of solar power, which was more than twice as much as in 2022 and 30% more than in 2023. In 2022, the installed solar power exceeded 1 terawatt, and the subsequent 1 terawatt was installed within only two years. Solar power has been the primary generator of new electricity generation worldwide for the last three years and continues to be the fastest-growing power source for the twenty years in a row, as presented in Figure 1.4.

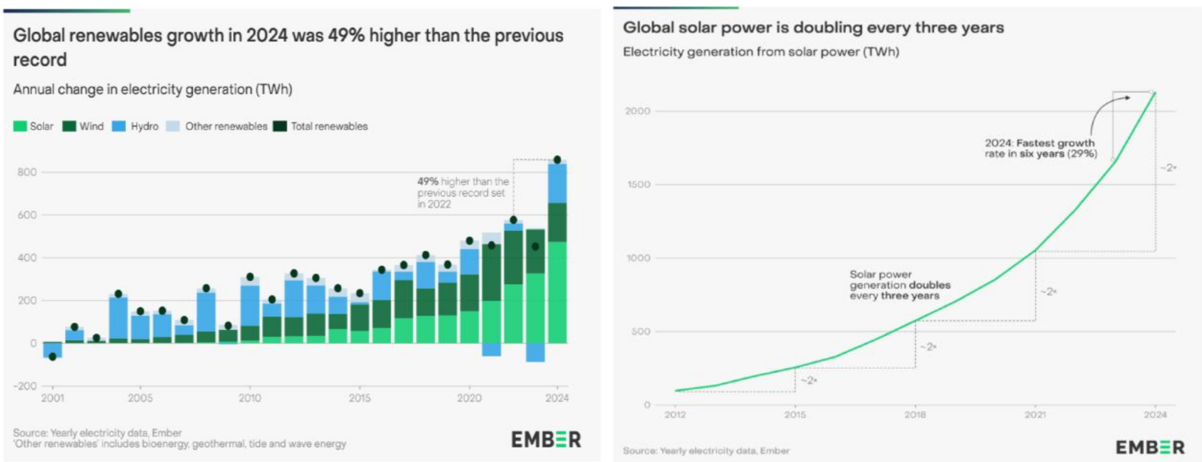

(a) **(b)**

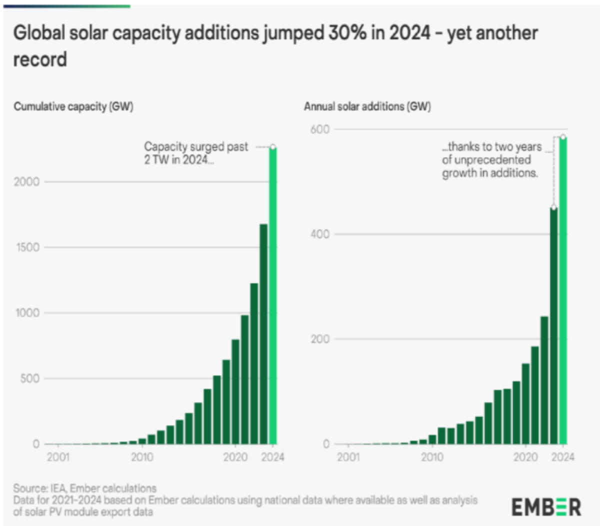

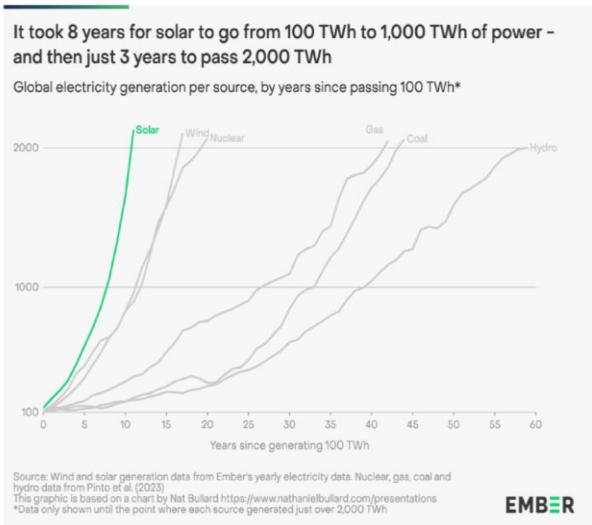

(c) **(d)**

Figure 1.4: (a) Annual change in electricity generation(TWh),(b) Electricity generation for solar power (TWh) ,(c) Global solar capacity ,and (d) Global electricity generation per source [4].

Solar photovoltaic (SPV), whose price has decreased by nearly 380 times since 1977, is a key driver in the global shift to renewable energy (RE) and mitigating the climate change crisis because of its abundant input energy, clean energy source, scalability, low ongoing maintenance costs, silent operation, and easy installation[5],[6]. This decrease has made SPV more affordable and viable with traditional energy sources. If the use of solar photovoltaic continues to grow, it will surpass wind power in 2027 and become the leading renewable energy source (RES) by 2029. In the future years, RES like PV, wind turbines (WT), and fuel Cells (FCs) will make a considerable effect on the supply of energy available around the world [4].

Hybridization of SPV and FCs is an encouraging remedy for the intermittency of solar energy. Solar PV produces enough energy during the day to sustain a steady power supply, but FCs can store excess energy and deliver it when there is not enough sunlight. The hybrid technology enhances the scalability and reliability of renewable systems of power [7]. The transition from traditional fossil fuel systems, particularly gas turbines, to RESs like SPV is causing a paradigm shift in the world's power infrastructure [8]. Solar PV, a low-carbon, cost-effective alternative, is rapidly replacing gas turbines in the power generation sector. This transition in energy production encourages the development of sustainable, independent systems powered by RE [9]. Along with SPV systems, wind , and fuel cells are now acknowledged as the main technology in the field of renewable energies (REs) [10]. FCs generate a clean, net-zero emission that only consists of vaporized water by converting the chemical energy of hydrogen or other fuels into electrical power. The role of FCs in energy systems will become more significant as the efficiency of hydrogen production increases [11]. This advantage is particularly applicable when RESs, such as SPVs, are used to power hybrid systems (HSs). Additionally, HSs can support energy independence in transportation, industry, and backup power systems for residential and commercial structures [12]. This advantage is especially beneficial in off-grid or rural areas where conventional electricity utilities are either nonexistent or insufficient [13].

1.1.2 Importance of hybrid renewable power systems

Increasing apprehensions regarding climate change and the depletion of conventional energy sources (CSE), and the resulting increase in the price of petroleum have made hybrid renewable energy systems (HRESs) even more crucial. They are essential to the quest for environmental causes. By mitigating fossil fuel reliance, augmenting the use of RE, and using more accurate energy storage and management systems, hybrid clean energy sources support us in achieving our carbon-neutral targets. Photovoltaic and wind energy are renewable, location-dependent, safe for the environment, and practical sources of alternative power because of advances in renewable energy systems. But one common problem concerning solar energy, which has a crucial place among alternative sources of power, is its intermittent nature at night or in shadowing conditions. During most of the year, standalone PV power systems cannot supply valuable electricity. Since fluctuations in solar power do not correspond to the periodic distribution of demand, such a problem is largely caused by reliance on unpredictable sunny hours. In contrast to weather-dependent solar and wind power, fuel cells generate steady output not affected by environmental, temporal, or spatial variables, making them an extremely potent green power source. Consequently, a power source that supports the SPV energy is introduced into the system to achieve reliability and system continuity [12] [13].

Hydrogen energy systems are increasing in significance because of their ability to safely store renewable energy while also promoting zero-carbon power generation through green hydrogen systems (GHSs), which include electrolysis powered by clean sources such as wind and PV power. Advances in hydrogen storage technology, including advanced components and reduction techniques, have substantially raised the viability of employing hydrogen in hybrid systems. Hybrid power systems use more than one sustainable energy source. Hybrid power systems (HPSs) are an interesting subject of research all around the world. The hybrid renewable energy system is increasingly acknowledged for its capacity to provide consumers with high-efficiency, reliable power more efficiently than a single sustainable source. RESs have become more reliable and consistent over the past few years with the support of hydrogen (H2)-based fuel cell hybrid power systems. Hydrogen is considered the key renewable energy source, with the potential to address concerns such as oil and natural resource depletion, global warming, and environmental degradation [7].

As the benefits of solar, wind, and fuel cell technologies became widely recognized, system developers began looking into their integration. A "hybrid renewable energy system" is any energy system that combines one or more renewable energy sources with a CSE, or that uses two or more RESs, such as wind, fuel cells, or SPV systems. HRES are often the most reliable and cost-effective method to generate electricity in rural areas. However, in a hybrid renewable energy system, FC and SPV can reduce power production oscillations, which significantly reduces the need for energy storage [13].

Over the last ten years, HRES have gained recognition as practical substitutes for electricity generation, allowing designers to take advantage of the benefits of both conventional and renewable energy sources. In order to meet demand during times of high load or when the source of clean energy is inadequate battery storage is continuously integrated into the HRES. Battery storage (BS) reduces the gap between the timing of peak loads and the maximum power generation. The HRES design is primarily determined by the performance of a single system. Individual components have to be initially modeled to accurately predict performance, and then their combination must be assessed to consistently meet demand. Researchers use this methodology because, if the power output predictions from these individual components are sufficiently accurate, the resulting combination will provide electricity at the lowest possible cost [13].

By combining RESs with high-efficiency energy storage technologies, hybrid energy systems generate stable electricity while reducing their dependence on nonrenewable energy sources. Energy storage through improved energy management results in increased stability and flexibility in energy generation. While conventional systems use a single power source and basic control systems, they are inefficient with low performance and flexibility. The inefficiency of coal and natural gas power generation leads to energy losses during both production and distribution. Hybrid energy storage systems (HESSs) can be used to continuously sustain necessary loads during electricity outages [12].

According to the existing literature, researchers have proposed many different power source combinations that include renewable energy systems, traditional generators, and energy storage systems. Previous research works effort was primarily focused on single-source designs (i.e., independent wind or photovoltaic systems); although they are relatively simple to implement, they also exhibit significant intermittency and lower levels of reliability due to limited interaction between multiple energy sources. To address these constraints, researchers have progressively embraced hybrid energy supplier configurations, integrating two or more sources such as photovoltaic-battery, wind-diesel, or wind-photovoltaic systems, wherein complementing generation profiles enhance energy accessibility and system resilience. The suggested configuration for a hybrid green power system is PV–FC–Battery, which allows for the integration of renewable generation with both short- and long-term storage solutions. It guarantees that the energy system continues to have reliability, resiliency, and self-sufficiency. The proposed topology will be compared with a table that illustrates the various trade-offs (cost, efficiency, reliability, scalability, environmental impact, and control complexity) of the various HES topologies. The analysis shows that while the PV–Battery and PV–Diesel–Battery topologies will be more affordable and easier to use over the short term, the PV–FC–Battery offers the highest overall efficiency considering the combined durability, green extended storage, and emissions; therefore, it is the most suitable topology for off-grid, high-priority, and next-generation energy systems.

Table 1.1 : Comparison of the performance of various topologies against the proposed configuration.

Topology	**Efficiency**	**Reliability**	**Capital cost**	**Operating cost**	**Emissions**	**Scalability**	**Control complexity**	**Application**
Proposed (PV-FC-Battery)	**High**	**Very High**	**High**	**Low**	**Zero**	**High**	**Very High**	Vital utilities, off-grid microgrids, isolated communities.
PV-Battery[14], [15]	High	Medium	Low-Medium	Low	Zero	Medium	Low	Small-scale commercial and residential
Wind-Battery [16]	Medium	Medium-high	Medium	Low	Zero	Medium	Medium	Coastal microgrids and isolated regions.
PV-Wind[17],[18]	Medium	Low-Medium	Low-Medium	Low	Zero	High	Low	Grid-linked hybrids and renewable energy sources.
PV-Wind-Battery[19],[20]	Medium	High	Medium	Low	Zero	Medium	Medium	Rural microgrids and islands.
PV-Diesel [21]	Medium	High	Low-Medium	High	Medium-High	High	Low-Medium	Hybrid backup systems and electricity for rural areas

PV-Diesel-Battery [21],[22]	Medium	Very high	Medium	High	High	Medium	Medium	Emergency power and telecom towers.
Wind-Diesel [23],[24]	Medium	High	Medium	High	High	Medium	Medium	Isolated power grids and supplementary generating.
PV-Battery-Supercapacitor [25],[26]	High	Medium	Medium	Low	Zero	Medium	Medium	Support for EV charging and improved power quality.
Fuel cell-Battery-Supercapacitor [27]	High	Very high	High	Medium	Low-Medium	Medium	High	Transportation systems, data centres, and military systems.
PV-Wind-FC-Battery [28]	High	Extremely high	Very high	Low	Zero	High	Very high	Maritime systems and smart microgrids.

1.1.3 Motivation for integrating SPV and FC systems

The combination of fuel cell and PV systems is to mitigate the intermittent and unreliable nature of RESs, particularly solar energy. SPV, as a contributor to energy from renewable sources, still has to grow. The availability of solar energy to achieve a continuous flow of electricity is difficult to sustain because of its dependency on the sun, which provides energy during daylight hours. It will still need a second power source to ensure reliability even when solar energy cannot be extracted at night or under shaded conditions. Fuel cells will provide a guaranteed and stable source of power that can be produced at any time of day in any condition, with fuel cells producing an energy supply that is not affected by weather and availability of solar energy sources. Both reliability and permanence of the RE systems will be enhanced substantially by integrating both technologies to develop a hybrid system, which will provide a consistent energy source. This integration provides more energy security, reduced operating expenses, and a more sustainable energy option for meeting varying energy demand, all while decreasing dependence on CSE, as well as improving energy management.

1.2 Problem Statement

Research has focused considerable attention on hybrid PV and FC systems because they have the potential to provide resilient and green power sources. Several research studies have illustrated the barriers to desired effectiveness and performance. One of the most significant issues with solar energy is its inconsistent and unpredictable nature, as photovoltaic systems can only generate electricity during sunny conditions, leading to higher power production throughout the day but no output at night or when shaded. Additionally, since there are many factors that can change depending on the conditions of the energy production (i.e., the load demand for the energy users, solar radiation, cell temperature, etc.), using solar energy can introduce issues such as oscillating power output and increased complexity for integrating these clean RESs. Difficulty intensifies with rapid, severe changes in irradiance intensity. Factors including cloud cover, dust accumulation, trees, and building shadows impact how much sunlight solar panels are exposed to. Partial shading has unique effects on the power-voltage curve such that series-connected modules will have different outputs. The P-V curve also It gets complicated when there is only one global maximum power point (GMPP) and many local peaks, so conventional methods for maximum power point tracking (MPPT) will be less effective in locating the GMPP. To address these challenges while providing tracking efficiency in solar energy systems using intelligent and adaptive algorithms, it is important to locate the GMPP reliably in several scenarios, explore previous P-V curves, and adapt the dynamic conditions in real-time.

Despite the potential of fuel cells as a green source of energy, there are fundamental challenges to their overall use and performance. One of the major issues is optimizing fuel consumption, because fuel cells use a consistent source of fuel, such as hydrogen or methanol; thus, minimizing fuel consumption is essential to improving fuel cell efficiency. Ultimately, suboptimal fuel consumption leads to increased operational expenses and poor efficiency. In addition, fuel cell performance and lifetime can also be affected by factors such as pressure, temperature, and humidity. Operating in a changing environment can also influence performance and can make it difficult to sustain an optimum performance level over time. These challenges require advanced approaches for improving fuel cell performance, cost minimization, and increasing accuracy in different environmental conditions.

The last issue to address is power management. When optimizing the use of renewable sources of energy, it is crucial to have an efficient strategy of power management approach. A power management approach must focus on three elements: (1) sustaining a continuous supply of power to satisfy variations in demand, (2) reducing costs, and (3) minimizing fuel consumption (H2). It is also essential to prolong the lifetime of components to be sustainable and economical. When implementing this method, we are primarily dealing with considerations regarding the type and properties of energy storage, the sizing of the system, environmental variations, and the power demand data over time. These are the issues that allow us to manage the periodic variations in load demand and energy sources, which frequently cause substantial fluctuations in the DC link voltage and, as a result, system performance.

1.3 Research Questions

In this section, we outline the specific research questions that this thesis will seek to address. The challenges of the hybrid PV-FC system sparked such questions. The studies focus on maximizing energy production, enhancing system resiliency, and improving overall performance.

Question 01: How could MPPT approaches be improved to accurately find the GMPP under partial shading and fast-varying irradiance conditions?

Question 02: How advanced control strategies can be developed with the aim to optimally maximize and stabilize PV output response to fast changes in environmental inputs?

Question 03: How to ensure efficiency for fuel cells and consumption of hydrogen, in a PV-FC hybrid system, while still achieving reliability and lifetime of each component?

Question 04: How do we develop more robust energy management approaches that consider abrupt changes in the load demand profiles and DC link voltage?

1.4 Objectives and contributions of the thesis

Developing an efficient control strategy and selecting the appropriate hybrid system is a challenging task, particularly when multiple energy sources are included. We need to select the right renewable energy sources and implement an efficient energy management strategy for a hybrid stand-alone system, which will include SPV, FC, and a battery storage bank (BSB). Efficient control systems are crucial, as the system's performance and efficiency can be significantly affected by variable operating conditions. This dissertation has concentrated on the improvement of control strategies for photovoltaic system and proton exchange membrane (PEMFC) FC, while developing a control strategy for energy management for a hybrid stand-alone system PV-FC-BSB-SCP by optimizing to achieve higher efficiencies at different operating conditions.

The unpredictable and inconsistent nature of solar energy leads to low conversion efficiency, which presents a significant barrier to the growth of sustainable energy. When partial shading occurs, the nonlinearity in the P-V characteristics of the solar array can result in multiple local power peaks (LPPs). Traditional MPPT methods, which are typically designed for uni-modal P-V curves, are unable to distinguish between global and local maxima. Consequently, these methods can experience reduced performance, particularly when the initial operating point is far from the actual GMPP. This thesis aims to enhance advances in MPPT strategies, in which the efficiency of tracking GMPP would be more accurate and efficient.

On the other hand, this research aims to develop an optimal algorithm to improve the output power and efficiency of the PEMFC specifically under varying pressure and temperature conditions.

The primary goal of the thesis is to implement effective power management that enhances the dynamic performance of the hybrid standalone system PV-FC-BSB to disturbances caused by changes in load demands and in SPV power output. This approach achieves its goal by providing reliable control of the DC bus voltage while the hybrid system meets the load demand. The main focus of the proposed EMCS is to increase the lifespan of the energy sources and mitigate the degradation in fuel cell performance. The EMCS also aims to minimize hydrogen consumption, which has a direct contribution to the total energy production cost and assists in maintaining an efficient and sustainable operation throughout its useful life cycle.

This dissertation presents several new control techniques for improving performance and the efficiency of RE systems as key contributions to achieving the goals and addressing the challenges, which can be summarized as follows:

- We designed, simulated, and validated an improved pufferfish optimization algorithm (IPFOA), a new MPPT controller specifically tailored for solar power systems operating under complex and changing scenarios, particularly in the presence of partial shading conditions (PSCs). This algorithm allows for fast and accurate tracking of the GMPP, resulting in lower steady-state oscillations and minimal tracking error, which indicates greater stability and improved convergence. The proposed technique is flexible, accurate, and robust when deployed in complex real-world solar panel issues affected by uneven and changing shading and fast-varying conditions; it performed better than both existing and more advanced MPPT algorithms.
- Proposing an advanced technique for fuel cells (FC) termed the Flying Squirrel Search Optimization Algorithm (FSSOA). This algorithm improves fuel cell (FC) performance, specifically for proton exchange membrane fuel cells (PEMFC), increasing efficiency and adaptability across diverse pressure and temperature conditions.
- Proposing and developing an optimized energy management strategy (EMS) for a hybrid green power system based on the elk herd optimization algorithm (EHOA). The

system proposed for this dissertation includes fuel cells (FC), a battery storage bank (BSB), and photovoltaics (PV), all of which have been considered. The main challenge for this type of system with power sources is to properly share the load demand across the various types and amounts of power sources without exceeding their operational limits, making the energy management control strategy (EMCS) crucial for managing this load-sharing process. The main focus of the energy management strategy is to reduce the hydrogen consumption, extend the lifetime of the power sources in the system, monitor the battery state of charge, stabilize the DC bus voltage, and improve overall system efficiency. To evaluate the implementation of the EHOA in the EMCS, the EHOA was compared against other strategies, such as the Proportional-Integral (PI) control approach, the Equivalent Consumption Minimization approach (ECMA), the external energy maximization strategy (EEMS), and particle swarm optimization (PSO), based on minimum hydrogen consumption and overall efficiency. The obtained results confirmed the EHOA outperformed in efficiency and reduced hydrogen fuel consumption, thereby increasing lifespan.

In summary, all of these contributions have provided a full collection of solutions for the improvement of performance, efficiencies, and stabilities in hybrid RE systems.

1.5 Structure of thesis

To provide a clear overview, each chapter of this research is outlined concisely as follows:

Chapter 2:

The second chapter aims to present a detailed model of the components for the suggested hybrid system, which will be used in the next chapters for control, including both simulation and implementation, as well as the energy management approach. We will start with a detailed investigation of photovoltaic technology, proceeding from the cell to the module, and discuss the impact of temperature, irradiance, and shading on SPV performance. Next, we will concentrate on fuel cell technology in detail, discussing the various fuel cell types, in particular PEMFC, along with their static and dynamic models. This chapter will describe the impact of temperature and pressure on fuel cell efficiency. We will also introduce the various power converters that are part of the system, notably the DC-DC converters, and will show the model of the battery included for energy storage and management of the system.

Chapter 3:

This chapter provided a detailed description of the control methods commonly utilized in hybrid power systems, including an introduction to MPPT methods for photovoltaic and fuel cell systems. The chapter concludes with an overview of energy management approaches for efficient power flow.

Chapter 4:

The present chapter discusses improved control methods for the HRES studied in this research. A new IPFOA MPPT controller is proposed, improved, and simulated specifically for PV systems in the MATLAB-Simulink environment for sudden changes in temperature and irradiance, then tested with real-time implementation for complicated shaded situations. This chapter presents also an evaluation of FSSO control method design and implementation for the PEMFC, as well as a comparison of performance with cuckoo search (CS) under variable pressures and temperatures.

Chapter 5:

The fifth chapter presents a novel power management approach to manage optimal load demand control of a stand-alone hybrid system comprising PV, FC, and Battery. The EHOA EMCS is compared with various current and conventional methods, including, PI, ECMS, EEMS, and PSO, to establish its efficiency and performance.

Chapter 6:

The last chapter highlights the key results of the dissertation. However, considering the advances in current research, there are new implications to still examine. Furthermore, several critical difficulties require consideration in future projects.

Chapter 2 : Modeling of power sources

2.1 Introduction

The topic of renewable energy has been a major focus for many researchers for a long time. Over the last fifty years, increases in global energy demand have heightened the importance of energy security in national energy planning and finally drawn attention to the environmental degradation from fossil fuel production. The latest energy studies conclude that energy demand will exceed 50% by 2040, creating a critical shortfall of fossil fuel resources and increased environmental disasters. Countries are implementing RE technology to enhance energy security and strengthen their initiatives against global warming. The government is essential for the extensive implementation of SPV energy technology, which provides a clean source of power production with no carbon footprint. The modular design, secure structure, and minimal maintenance needs led governments to favor photovoltaic systems over alternative green energy sources (GESs). In recent decades, countries have implemented several policy mechanisms for the implementation of SPV systems [29],[9]. Despite the solar resource being more predictable and exhibiting less significant fluctuations, solar production ceases during the night and is diminished at dawn and dusk, leading to an energy deficit due to the decreased incident radiation. Consequently, reliance on just one energy source is constrained and insufficient [30].

In efforts to address the above issues, researchers are undertaking valuable research into a possible alternative: GESs that are perpetual and independent of environmental impact. Hydrogen is becoming a viable green power source and is expected to contribute up to 24% of the global energy supply by 2050. Employing hydrogen for energy not only decreases CO2 emissions but also stores it as compressed or liquid gas, thus avoiding the problems with batteries and all other types of energy storage. The fuel cell is probably the most prominent example of several well-known H2-fueled technologies with a diverse range of possible topologies and profound implications for a greener energy supply. Many researchers have developed hybridization approaches to increase energy output efficiency while decreasing greenhouse gas emissions (GHGEs). One hybrid option is combining photovoltaic and fuel cell (PV-FC) technologies that are among the key components in the green revolution pathways to overcome the intermittency of photovoltaics while generating a more dependable and cost-effective operating system [10],[9]. These hybrid systems can bolster efficiency and dependability, being firmly suited for rural areas facing unique challenges to promote infrastructure for standalone power plants that govern energy access issues, an ongoing struggle indicated by the 2030 United Nations Sustainable Development Goals (SDGs) [31].

The use of hybrid systems that combine various energy sources effectively addresses the drawbacks of single components [32]; however, an alternate system is essential for a reliable electricity supply. Currently, the energy storage for small and medium sizes primarily uses batteries and, for some specific applications, supercapacitors. For large-scale storage, hydro pumping in wet areas stores potential energy. Energy storage devices are needed for solar energy related to storage assurance because solar is unpredictable, to meet the load profile, and to provide demand and supply system security. The first role of energy storage systems (ESSs) is in the short term; they manage excess energy or insufficient energy, thus ensuring reliability and the electrical supply response or responding during load changes. The second, or long-term, role of energy storage devices is providing demand when generation does not maintain the load. In the past, various batteries and, more recently, supercapacitors have been involved in short-term ESSs. SCPs show a better dynamic response than BSB, allowing them to handle demand changes and deliver energy almost immediately. Furthermore, they have operated safely without producing any toxic gasses. Supercapacitors protect batteries by minimizing degradation and prolonging their longevity through their extended lifespan. They are capable of charging and discharging at a high rate, making them useful for many applications. SCPs have a long cycle life, operate in severe temperatures, and have low maintainability. Their eco-friendly components render them a significant contribution to energy storage options. Conversely, batteries have poorer dynamic response and possess a limited lifespan determined by the number of charging and discharging cycles. The rising importance of BSB is mostly due to their considerable load capacity and the ability to sustain a greater discharge current percentage in both extent and duration. These properties enhance the security of the system response, as batteries can endure prolonged problems and shortfalls in production, as well as dynamic variations in demand. In the battery system, it was essential to efficiently regulate the charging process through an effectively regulated energy management system [30], [33].

Hybrid renewable electric energy generation systems are now necessary for most electric networks, with stand-alone systems including water pumping, telecommunication systems, educational institutions, government-funded organizations, and the private sector to provide the next generation with a future of clean energy [33],[34].

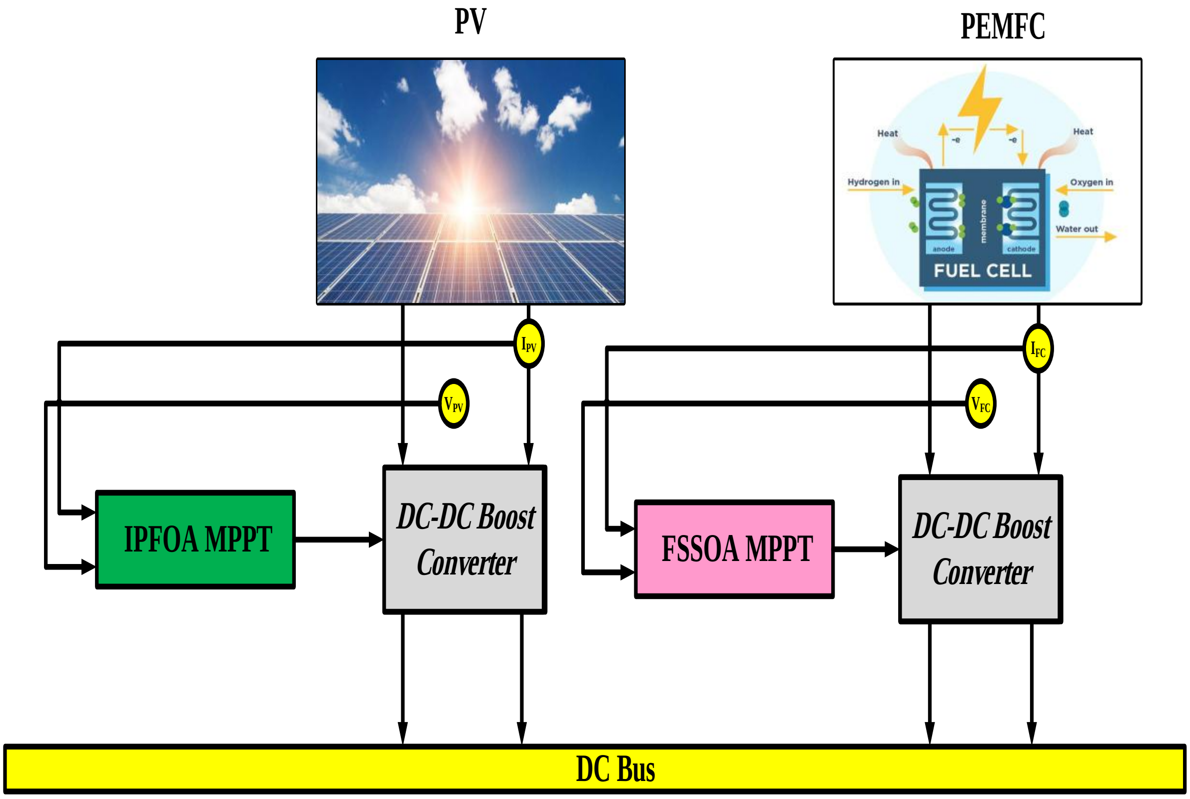

Figure 2.1: The structure of the proposed hybrid PV-PEMFC standalone system.

As shown in Figure 2.1, the hybrid standalone system (with the PV system as the main energy source and PEMFC as the alternate energy source) shows excellent reliability and efficiencies. The photovoltaic system and fuel cell are connected by a DC-link, allowing for efficient transfer of energy and control of voltage. The PV system consisted of series and parallel arrays connected with a capacitor at the input of the DC-DC boost converter to support power regulation and improve efficiencies. When the boost converter is configured with MPPT, the efficiencies of the SPV array in power extraction are improved. The PEMFC, when connected to a suitable DC-DC boost converter, elevates the voltage to the required level, while

MPPT control ensures optimal energy output from the FC as needed. Following this structure, the PV source will supply consistent power to the load, with the backup of the proton exchange membrane fuel cells used during periods of insufficient solar radiation.

This chapter aims to present a detailed model of the components for the proposed hybrid system, which will be utilized in the subsequent chapters for the control and energy management strategy. First, a detailed study of photovoltaic technology will be undertaken, covering everything from cell to module, while presenting the influence of temperature, irradiance, and shading on SPV system. Then, the focus will be on fuel cell technology in detail, describing the various types of FCs, particularly PEMFC, along with their static and dynamic models. This chapter presents the influence of temperature and pressure on the efficiency of a FC. Various specifications of the power converters that are part of the system will also be presented, specifically regarding DC-DC power converters. In addition, the battery model will be presented as part of the energy storage and management of the system.

2.2 A PV solar cell's mathematical model

A solar cell converts photons into clean, continuous electricity. Single cells, when connected in parallel or series, form PV modules that can subsequently be combined to form PV arrays. Most commercial photovoltaic cells use single-crystalline and polycrystalline silicon, followed by various semiconductors and various manufacturing processes. The two forms of silicon photovoltaic cells are leaders in the market because of their advantages in cost and efficiency, depending on the manufacturing process [35], [36]. While the first silicon-based solar cell was fabricated from a single-crystalline silicon wafer and announced in 1954 [37], today's focus has shifted to new solar technologies, including perovskite solar cells (the first production line started in November 2024). These new technologies are expected to revolutionize the solar power industry [38].

To predict solar cell performance under various climatic conditions, photovoltaic system simulations use various models, including the single-diode model (SDM), double-diode model (DDM), and triple-diode model (TDM). The SDM is the most popular type due to its ease of use and design [39]. The ideal single-diode model (ISDM) is the simplest and least accurate of all single-diode models. While the ISDM is simple to use, it is limited in its ability to accurately model the performance of a solar cell at the maximum power point (MPP). Some models may omit the shunt resistance to simplify the simulation. Despite simplification in the models, they exhibit inefficiencies when temperatures change. Even with this limitation, the SDM can still be useful as an electrical equivalent circuit model because it simplifies modeling solar cell behavior and offers useful insights on the design and optimization of solar energy systems [40],[41]. The SDM replicates the solar cell as an electrical circuit, as shown in Figure 2.2, using a p-n junction as a diode, a photocurrent generator, and two resistors to represent losses such as Joule heating and recombination. For accurate simulation, this model requires the ideality factor, photocurrent, diode saturation current, series resistance, and shunt resistance [42].

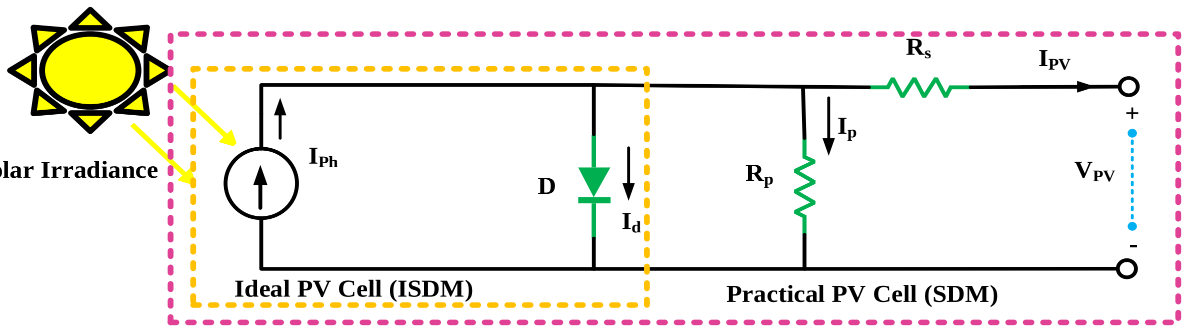

Figure 2.2: The single-diode model equivalent electrical circuit of a PV cell [43].

2.2.1 Model of Ideal Solar cell

The orange dotted line shows that the solar photovoltaic can be modeled as an ideal solar cell (I_{ph}) in parallel with a diode, as in Figure 2.2. The output current of an ideal solar cell (I_{PV}) is defined in Equation(2.1), which is derived from Kirchhoff's first law [42].

$$I_{PV} = I_{ph} - I_d \tag{2.1}$$

The diode current I_d equation, presented in Eq.(2.2), delineates the I-V characteristics of photovoltaic solar cells according to semiconductor principles.

$$I_d = I_s \left[\exp\left(\frac{qV_{oc}}{N_s KAT_o} \right) - 1 \right] \tag{2.2}$$

Where:

I_s : The saturating current.

q : An electron charge is equal to $1.602 \times 10^{-19} C$.

V_{oc} : Voltage of the open circuit in Volts.

N_s : Number of associated series cells.

K : Boltzmann's factor, which is equivalent to $1.380 \times 10^{-23} J / K$.

A : The diode ideality factor.

T_o : The real time temperature in Kelvin (K).

Replacing the value of I_d into Equation (2.1) gives the output current I_{PV} of an ideal solar cell, as illustrated in Equation(2.3).

$$I_{PV} = I_{ph} - I_s \left[\exp\left(\frac{qV_{oc}}{N_s KAT_o} \right) - 1 \right] \tag{2.3}$$

In the ideal case, a solar cell offers a highly accurate representation of the photon-generated current, which precisely corresponds to the intensity of the lighting and irradiation. Some factors are omitted from the ideal case model; however, they significantly influence the output of a photovoltaic device in real-world scenarios.

2.2.2 Model of Practical PV cell

The pink dotted line in Figure 2.2 depicts a more accurate circuit representation of a solar PV cell. This model type is recognized as the real or practical single diode model, comprising parallel resistance (R_p) and series resistance (R_s). In theory, R_p and R_s are neglected, but, in practice, it is infeasible to disregard these resistances, as the efficiency of the PV solar cell is influenced by these parameters.

R_s represents the series resistance in the current passage and is regarded as losses associated with the Joule influence, usually arising from metallic grids, semiconductor components, the collecting bus, and its links. R_p represents parallel resistances associated with current leakage due to cell thickness and surface impacts and is referred to as shunt resistance. The influence of R_s is significant due to the increase in cell resistance in the photovoltaic module relative to R_p. The impact of R_p is only visible when a significant number of PV modules are included in a SPV system. Thus, when R_s is accounted for and R_p is considered indeterminate with V_{PV} is the output voltage, the diode current equation (2.2) has been modified to equation (2.4).

$$I_d = I_s \left[\exp\left(\frac{q\left(V_{PV} + I_{PV} R_s\right)}{N_s K A T_o} \right) - 1 \right] \tag{2.4}$$

The revised Eq.(2.5) considered R_s based on the modifications made to Eq. (2.3).

$$I_{PV} = I_{ph} - I_s \left[\exp\left(\frac{q\left(V_{PV} + I_{PV} R_s\right)}{N_s K A T_o} \right) - 1 \right] \tag{2.5}$$

Assuming the PV cells are arranged in a series-parallel configuration, N_p represents the number of series cells arranged. The output current I_{PV} may be calculated, resulting in a modification of Equation(2.5), which is represented in Equation (2.6) by the following formula:

$$I_{PV} = N_p * I_{ph} - N_p * I_s \left[\exp\left(\frac{q\left(V_{PV} + I_{PV} R_s\right)}{N_s K A T_o} \right) - 1 \right] \tag{2.6}$$

Considering the formulas already mentioned for photovoltaic cell modeling, certain parameters must be defined for modeling, based on the chosen PV module model. This model requires the calculation of I_{ph}, I_{rs}, and I_s, which can be determined from the below formulas. The photocurrent (I_{ph}) is directly related to the reflected radiation and unaffected by voltage (V_{PV}) or series resistance (R_s); it exhibits a linear dependence on sunlight and is affected by temperature, as seen in Equation(2.7).

$$I_{ph} = \left[I_{sc} + Ki\left(T_o - T_r\right) \right] * \frac{G}{G_{ref}} \tag{2.7}$$

Whereas:

I_{sc}: The Current of short circuit at standard conditions (STC).

Ki : Coefficient of temperature for I_{sc} cell.

T_r : The reference temperature in Kelvin (K).

G : The Solar radiation (W/m²).

G_{ref} : The Solar radiation at STC (W/m²).

Using formulas (2.8) and(2.9), saturating current (I_s) and reversal saturating current (I_{rs}) are computed as follows:

$$I_{rs} = I_{sc} / \left[\exp\left(\frac{qV_{oc}}{N_s KAT_o} \right) - 1 \right] \tag{2.8}$$

$$I_s = I_{rs} \left[\frac{T_o}{T_r} \right]^3 \exp\left[\left(\frac{qEg}{AK} \right) \left(\frac{1}{T_r} - \frac{1}{T_o} \right) \right] \tag{2.9}$$

Whereas the band energy gap (Eg), which is equivalent to $1.1\,\text{eV}$ and the ideality factor (A) were derived from the chosen model provided by the designer of the specified module.

2.2.3 The effect of temperature and irradiance on SPV systems

The performance of photovoltaic cells and modules is influenced by environmental factors, including sunlight intensity and temperature; thus, it is necessary to effectively model the PV module based on the previously given formulas for accurately predicting the effects of weather variations on the output of PV. The chosen photovoltaic module for the present study is the Sun Power SPR-200-BLK PV module. The electrical characteristics under Standard Test Conditions (STC) $\left(G_{ref} = 1000\ W/m^2 and\ \mathrm{T}_r = 25\ ^\circ C\right)$ are outlined in **Table 2.1**.

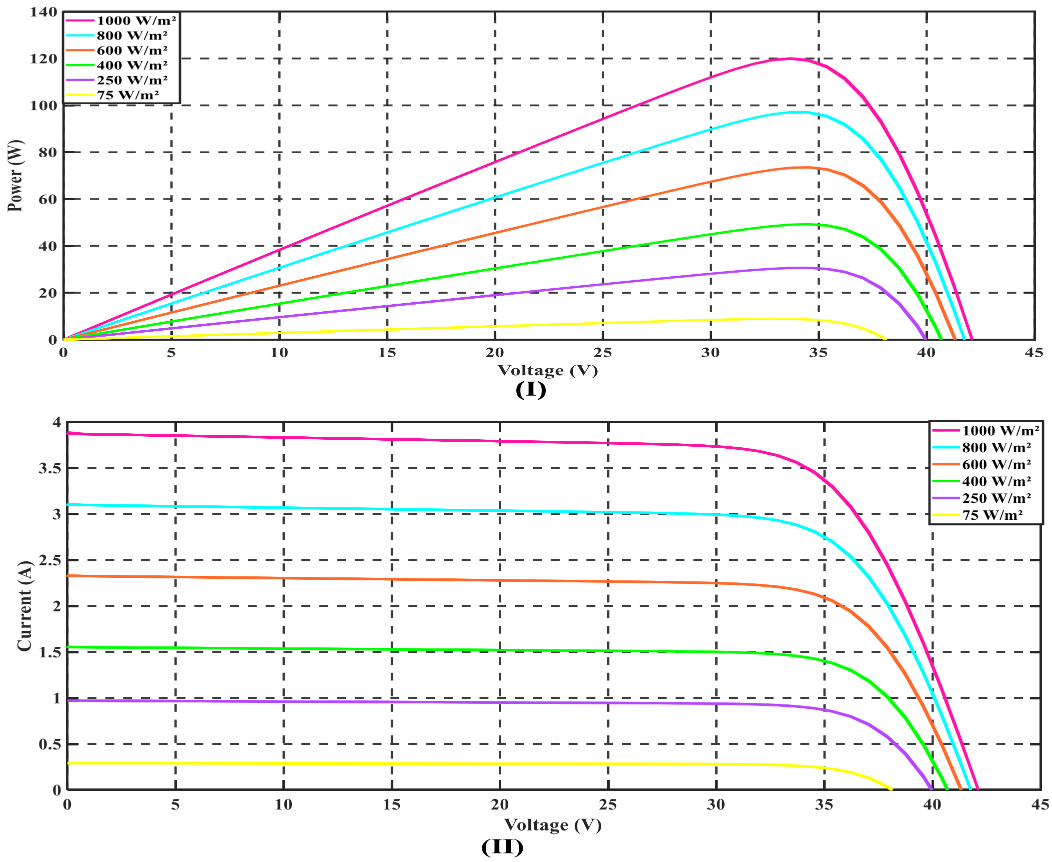

Figure 2.3 : (I) P-V and (II) I-V characteristics of the SPR-200-BLK PV module at varied levels of illumination.

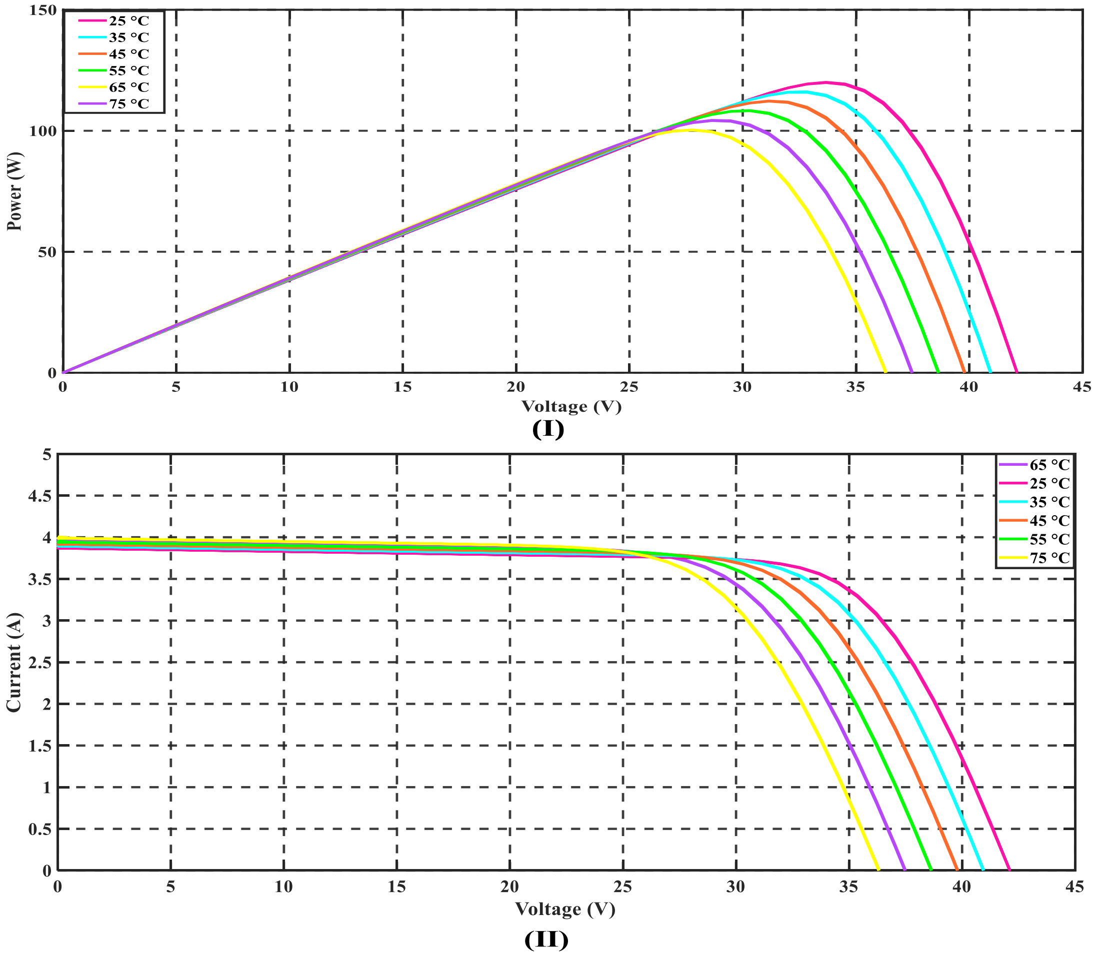

Figure 2.4 : (I) P-V and (II) I-V characteristics of the SPR-200-BLK PV module at different temperature ranges.

The output characteristic curves of the SPR-200-BLK photovoltaic module for various sun irradiation and temperature conditions are shown in Figure 2.3 and Figure 2.4. The photovoltaic module has a non-linear characteristic that varies depending on moving solar radiation, temperature, and load conditions. The operational point (maximum power point) of a solar panel may be determined using both the (P-V) and (I-V) curves, at which point the panel will be able to obtain its peak power production. This point will fluctuate based on the amount of illumination and temperature, and each curve will demonstrate a different operating point based on that shift. The maximum power point shows the highest power output possible under specified conditions. Therefore, to overcome this issue, an MPPT controller is necessary to identify a singular global peak point.

Table 2.1 : Key PV Module Parameters under Standard Test Conditions.

PV Module Type	**Sun Power SPR-200-BLK**
Open Circuit Voltage (V_{oc})	47.8 V
Short Circuit Current (I_{sc})	5.403 A
Maximum Power Output (P_{MPP})	200.12 W
Voltage at Maximum Power Point (V_{MPP})	40 V

Current at Maximum Power Point (I_{MPP})	5.003 A

The performance of PV modules depends on alternative levels of irradiation, because different levels of irradiation will change the performance of the module. As irradiation increases, so does the total number of photons impacting a module similarly. This impact demonstrably improves efficiency as well as power output. In Figure 2.3, when irradiation is low, radiation affects short-circuit current strongly but has no effect on open-circuit voltage. On the other hand, temperature has a strong impact on open-circuit voltage and minimal or no effect on short-circuit current. Therefore, the maximum power output of the panel is decreasing, as shown in Figure 2.4.

2.2.4 The effect of Partial shading conditions

A single solar panel generates some voltage; therefore, a series of interconnected panels is necessary to achieve a significantly higher voltage. Interconnect all of them in parallel to make a solar array capable of generating sufficient electricity. Partial shading on the solar panel may result from structures, trees, moving clouds, snow, dust, bird droppings, and other environmental obstacles. It disperses solar energy widely across the external layers of several photovoltaic panels within the array. Under the PSC, a shaded panel operates at a negative voltage if a photovoltaic string contains a panel receiving less sunlight than the other panels; hence, it dissipates rather than generating power. This technique produces the hotspot phenomenon—localized heating of the darkened panel. The hotspot effect is detrimental as it can compromise the module's cover and damage its cells. Typically equipped with opposing parallel bypass diodes, which provide an alternative passage for excess current generated by fully illuminated panels, solar panels mitigate the hotspot effect [44],[45],[46].

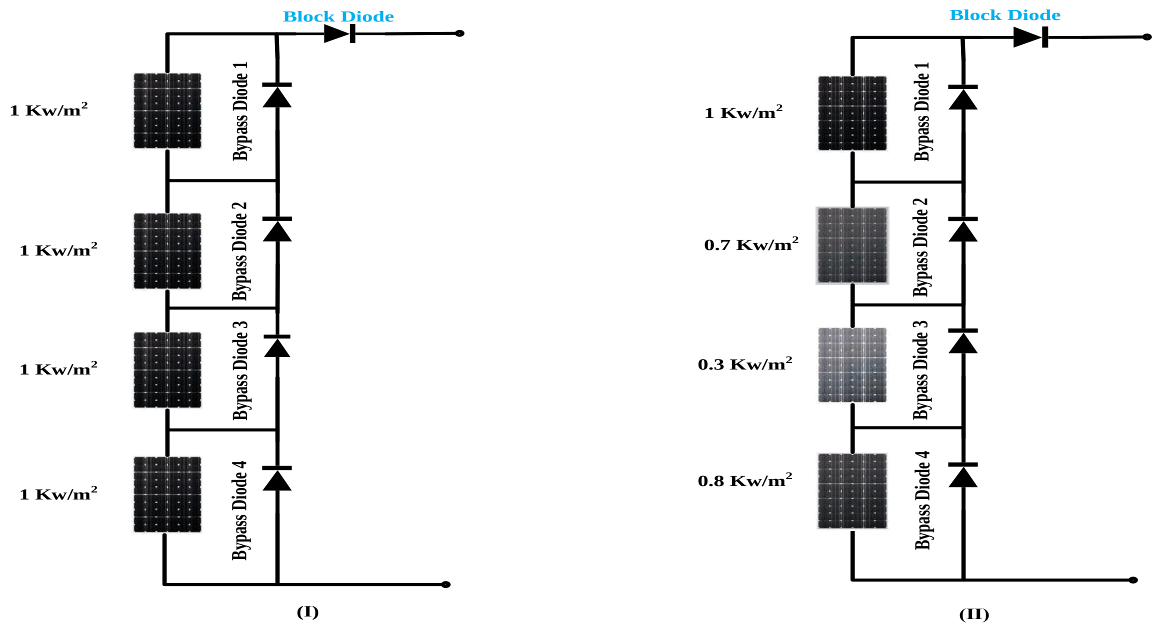

Figure 2.5: Solar irradiance patterns for PV module under (I) uniform and (II) non-uniform shading scenarios.

In shaded conditions, parallel-connected solar strings may generate reverse circulation currents. Reverse-flowing currents induce heat losses when shaded solar panels absorb the redirected electrical output. Each photovoltaic string is connected in series with a diode that eliminates reverse currents, thus assuring that the electrical current flows unidirectionally from the string to the load. Figure 2.5 depicts the interconnections of these diodes to the photovoltaic array. A decrease in array current under consistent shading conditions reduces the output power of the PV array; this reduction is directly related to the solar irradiation reflected on the array surface. The P-V characteristic curve exhibits a singular maximum power point and is consistent. Thus, a fundamental MPPT system may identify that distinct peak. Using bypass diodes modifies the photovoltaic characteristic curve, leading to several maximum power points (MPPs), comprising one global maximum power point and several local maximum power points (LMPPs), as depicted in Figure 2.6 . The construction of the PV array and the arrangement of shading establish the LMMP number. As the number of local maximum power points rises, it becomes increasingly difficult to extract optimal power from a solar array using PSCs. Although not applicable in this scenario, conventional MPPT algorithms are proficient at detecting the distinct MPP even in shaded conditions. Specific shadows in the traditional MPPT approach may lead to failures in the MPP tracker, resulting in inaccurate power loss and failure to identify the optimum power point.

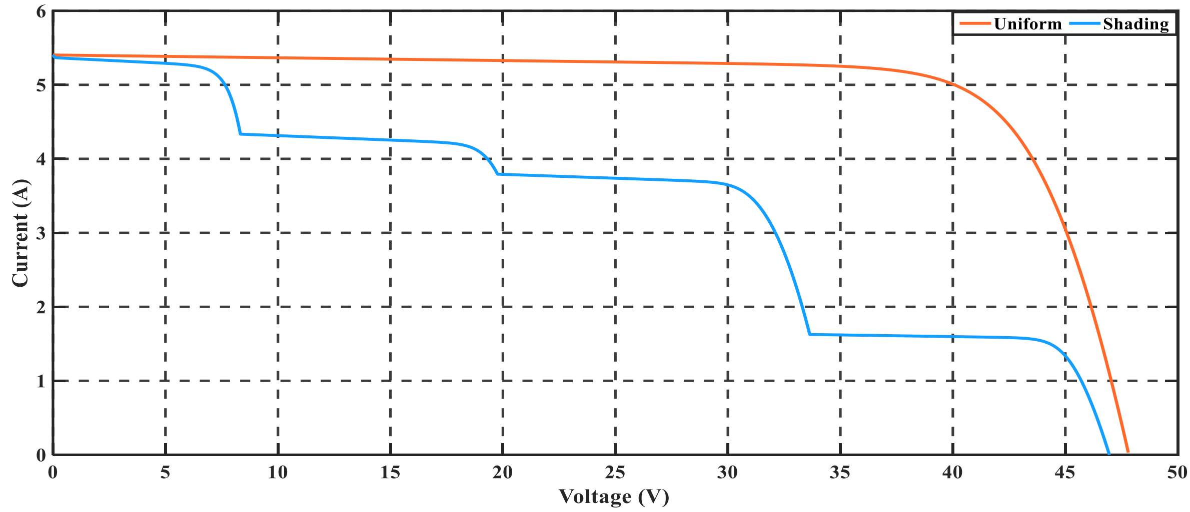

(I)

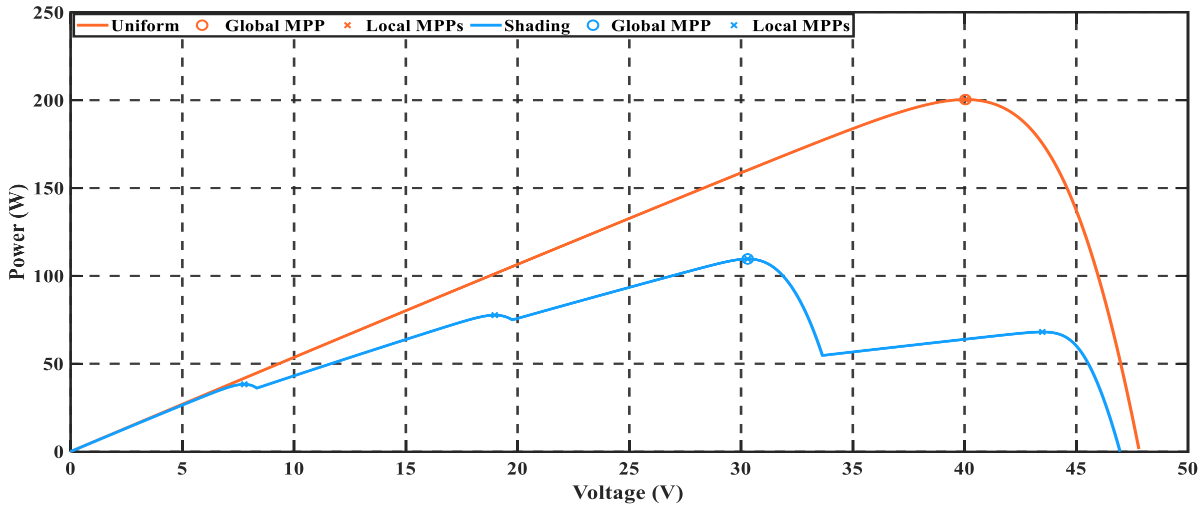

(II)

Figure 2.6: I-V (I) and P-V (II) curves under uniform and non-uniform shading conditions.

2.3 Fuel Cell

2.3.1 Principles of fuel cells

Fuel cells are one of the top 21st-century energy sources. Since then, researchers have focused on these technologies to provide sustainable energy generation solutions that reduce environmental impact, improve reliability and availability, and foster new energy domains. In the drive to greener fuels, petroleum and natural gas alternatives must be found quickly. As a greener alternative to fossil fuels, fuel cells are widely promoted. Pure hydrogen fuel cells emit no greenhouse emissions. Fuel cells may minimize pollution and greenhouse gas emissions because their only output is water. Fuel cells use hydrogen from natural sources for transport, energy transmission, and storage, reducing oil use and increasing green power. Fuel cells can use hydrogen, natural gas, biogas, and methanol, convert energy up to 60% efficiently, and reduce air pollution and other criteria pollutants. FCs provide reliable grid supply, silent operation, little maintenance, and more. Due to their wide range of applications, FCs can solve major power sector issues in commercial, residential, industrial, and transport. Fuel cells are electrochemical cells that convert chemical energy into electricity. The electrochemical reaction generates clean, efficient electricity from fuel via an intrinsic oxidation-reduction mechanism. Fuel reactions are continuously and instantly turned into electrical energy without burning to prolong power production until oxygen and fuel supplies run out. NASA (National Aeronautics and Space Administration) used fuel cells to power space shuttles and satellites a century after their invention in 1838. Several companies, commercial structures, and residential buildings use these devices as primary or secondary electrical sources [47].

2.3.2 Different types of FCs

Consideration of the various types of FCs is important, as it simplifies apprehending the benefits and drawbacks of each type and helps identify the most suitable applications for each type. For decades to come, this knowledge can help construct cleaner, more sustainable power systems. Fuels are classified based on the electrolytes used and the electrochemical reactions taking place inside the fuel cell stack. In most FCs, hydrogen is the main fuel. A variety of factors, including catalysts, operating temperature, efficacy, fuel type, thermal control, footprint, usage, costs, and functioning speed, influence the range of fuel cell forms, producing variants appropriate for various applications. Among the conventional fuel cells currently being considered are polymer-electrolyte membranes, alkaline, direct methanol, phosphoric acid, solid oxide, molten carbonate, and reversible fuel cells [48],[49],[50].

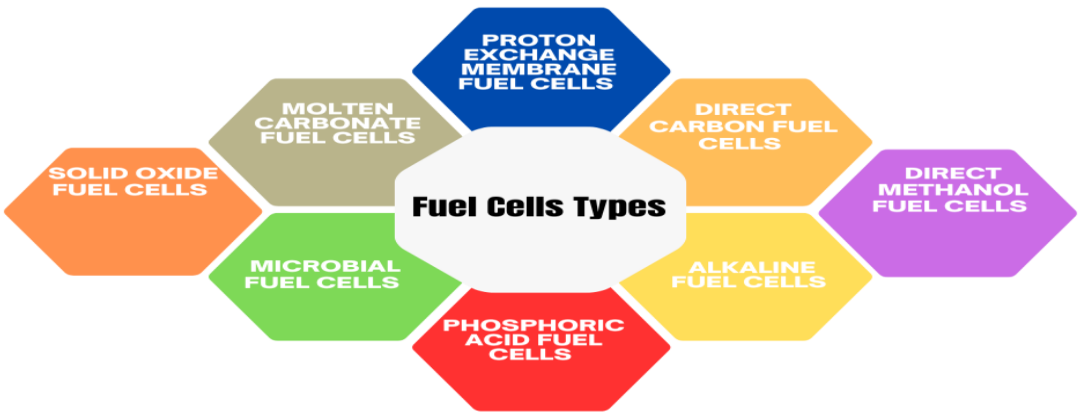

Figure 2.7 : Different types of FCs.

Based on the choice of fuel and electrolyte, FCs are divided into eight main groups, as shown in Figure 2.7. The eight principal types of fuel cells are molten carbonate fuel cells (MCFCs), direct carbon fuel cells (DCFCs), proton exchange membrane fuel cells (PEMFCs), solid oxide fuel cells (SOFCs), direct methanol fuel cells (DMFCs), alkaline fuel cells (AFCs), phosphoric acid fuel cells (PAFCs), and microbial fuel cells (MFCs), an emerging type of FC, have recently attracted the interest of experts in the field. With the exception of the electrolyte and fuel, the fundamental principles of fuel cells are nearly identical. Every FC comprises three primary components. The electrolyte, electrodes, and external circuit form a singular FC. Connection elements are frequently employed for the stacking of numerous FCs [51],[52]. Table 2.2 summarizes the wide range of characteristics of all the examined FC forms, including their benefits, applications, and limits.

Table 2.2 : Comparison of several categories of FCs [48],[49],[53].

FC Types	MCFCs	DCFCs	PEMFCs	SOFCs	DMFCs	AFCs	PAFCs	MFCs
Operating temperature (°C)	600 -700	600 - 800	30 -100	500 - 1000	20 - 90	50 -200	150 -220	20 -40
Electrical efficiency (%)	>60	>80	40 -50	50 -60	20 - 40	50 -60	40 - 50	Low reliant on microbial effectiveness and organic content
System power (Kw)	<1 -100	-	<1 -250	<1 -3000	0.001 -100	10 -100	50 -100	-
Applications	Utility electricity and large distributed generation	Carbon capture and storage (CCS), the use of carbon-rich waste, and grid-scale electricity generation	Transportation, small distributed generation, vehicles, backup power, and portable power	Utility electricity, large distributed generation , and auxiliary power	Vehicle and Mobile	Space, military, backup power, and transport	distributed generation	Biosensors, organic waste power, treatment of wastewater, and remote power
Cell fuel	Hydrogen	Coal, biochar, and other forms of solid carbon	Hydrogen	Hydrogen	Methanol	Hydrogen	Hydrogen	Organic materials (waste and wastewater)
Advantages	A solid electrolyte ,higher performance, fuel durability, resistant electrolyte, appropriate for combined heat and power, hybrid and gas turbine cycles, and Can utilize various kinds of catalysts	Higher efficiency, fuel availability, reduced emissions, and appropriateness for waste-to-energy operations	A solid electrolyte mitigates corrosion and electrolyte management issues, reduced temperature, and rapid starting and load adjustment	Higher performance, fuel durability, resistant electrolyte, appropriate for combined heat and power, hybrid and gas turbine cycles, and Can utilize various kinds of catalysts	Decreased expenses resulting from the lack of a fuel reformer, substantial power density, and low level of temperature	A broader spectrum of durable substances facilitates the use of more inexpensive materials, reduced temperature , The cathode reaction occurs more rapidly with alkaline electrolytes , resulting in enhanced	appropriate for combined heat and power (CHP) systems and enhanced resilience to fuel contaminants	Two-purpose (waste processing and power production), renewable power supply, and ecologically sustainable

						performance			
Challenges	Elevated temperature erosion and degradation of cell parts, prolonged initialization duration, and reduced power density	High-temperature breakdown of materials, carbon depositing, and fuel preparing (grinding of solid carbon)	Costly catalysts and susceptible to fuel pollutants	Elevated temperature erosion and degradation of cell parts, prolonged initialization duration, and restricted number of shutdowns	Poor efficiency methanol permeability	CO2 sensitivity in fuel and air, management of electrolytes made from water, and conductivity of polymer electrolyte	Costly catalysts, prolonged initialization duration, and sensitivity to sulfur	Reduced power density, microbial performance fluctuates with ambient circumstances, and material expenses

2.3.3 Polymer electrolyte membrane fuel cell (PEMFC)

Fuel cells are electrochemical devices that convert the chemical energy stored in fuels into electricity; they are suitable for electrifying electrical devices and vehicles. The intriguing functional characteristics of the polymer electrolyte membrane fuel cell, or PEMFC, entice researchers to look deeper into it. Various FCs forms work at distinct temperatures; nevertheless, the PEMFC is preferred and represents an attractive alternate power source due to its basic architecture, rapid starts, increased power density, excellent efficiency, low temperature of operation, silent production of energy, significant electrical output, efficient reactions that can be improved by a catalyst, and environmentally friendly operation. However, two obstacles impede widespread application: reliability and durability. The initial stage is to develop an exact PEMFC model to simulate the PEMFC system utilizing the MPPT approach. Considering the mathematical modeling and features of PEMFC systems is key [54],[51],[55],[52].

Figure 2.8 illustrates the schematic configuration of the PEM fuel cell functioning. The fuel cell requires fuel (Hydrogen) and air as its two inputs. The chemical process of conversion generates electricity, utilizing hydrogen as a fuel source. A PEMFC comprises a stack of fuel cells, each consisting of two electrodes and an electrolyte. The cathode and anode serve as the two electrodes, while the electrolyte consists of polymer electrolyte membranes (PEM). An electrolyte divides hydrogen ions into positive and negative charges. Hydrogen and oxygen are supplied to the fuel cells, resulting in energy generation through an electrochemical procedure. In a PEMFC, only two products are heat and water [56]. All resulting chemical reactions can be described in the formulas below [57],[58]:

Anode oxidation reaction:

$$H_2 = 2H^+ + 2e^- \tag{2.10}$$

Reduction process occurring at the cathode:

$$O_2 + 4H^+ + 4e^- = 2H_2O \tag{2.11}$$

Overall chemical reactions of the PEMFC:

$$\frac{1}{2}O_2 + 2H^+ + 2e^- = H_2O + Electricity + Heat \tag{2.12}$$

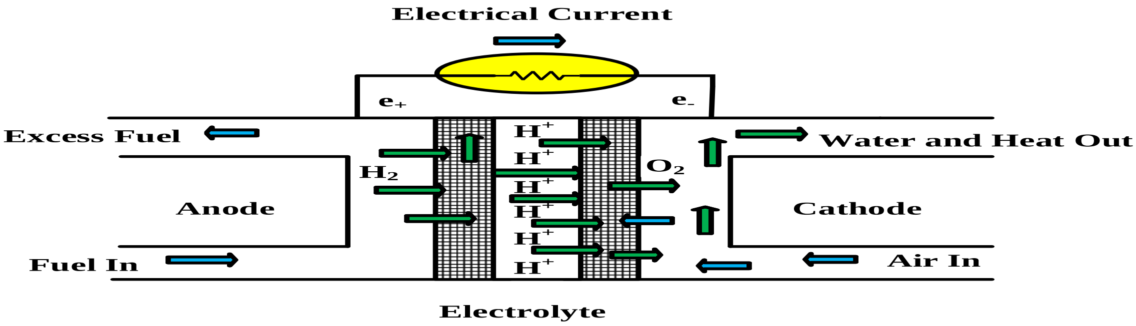

Figure 2.8 : Schematic of the PEMFC functioning [59].

2.3.3.1 Static model of PEMFC

The voltage of the PEMFC is impacted by the water content of the membrane $(MWC) = 27.7$, the temperature of fuel cell (T), and the partial pressures of hydrogen (P_{H_2}) and oxygen (P_{O2}), respectively. The voltage from FC also has nonlinear V-I properties due to the voltage drop from concentration, ohmic losses, and activation. Taking these drops into account, the output voltage of PEMFC can be described by the following equation [60]:

$$V_{cell} = E_{Nernst} - V_{act} - V_{ohmic} - V_{con} \tag{2.13}$$

V_{act} denotes the activation loss resulting from the chemical process, V_{cell} represents the generated voltage of the fuel cell, V_{con} indicates the concentration loss caused by excess water flooded in the catalyst fuel cell, and V_{ohmic} refers to the Ohmic loss caused by the inner resistance of the FC. V_{Nernst} represents the reverse open-circuit output voltage (thermoelectric abilities) of the single cell, expressed as:

$$E_{Nernst} = \frac{\Delta G}{2F} + \frac{\Delta S}{2F}(T - T_0) + \frac{RT}{2F}\left[\ln(P_{H_2}) + \frac{1}{2}\ln(P_{O_2})\right] \tag{2.14}$$

Whereas:

ΔG : Liberated energy Gibbs (J / mol).

ΔS : The change entropy.

F : Unchanged Faraday.

R : The factor of global gas.

T : The temperature cell during the process.

V_{Nernst} can be defined by equation (2.15) as follows:

$$E_{Nernst} = 1.229 - 8.5\times10^{-4}\left(T - 298.15\right) + 4.308\times10^{-5}\left(\ln\left(P_{H_2}\right) + 0.5\ln\left(P_{O_2}\right)\right) \quad (2.15)$$

The drop in activation voltage V_{act} is described as:

$$V_{act} = \left[\xi_1 + \xi_2 + \xi_3 T\ \ln\left(CO_2\right) + \xi_4 T\ \ln\left(I_{FC}\right)\right] \quad (2.16)$$

Where I_{FC} is the current of the fuel cell, $CO_2\,(atm)$ is the concentration of oxygen defined by equation (2.17) , and $\xi_i\ (i = 1-4)$ are the FC characteristic coefficients.

$$CO_2 = \frac{P_{O_2}}{\left(5.08\times10^{6}\right)\times\exp\left(-498/T\right)} \quad (2.17)$$

Ohmic over-voltage drop, or V_{ohmic} , is computed as follows:

$$V_{ohmic} = I_{FC}\left(R_M + R_C\right) \quad (2.18)$$

The V_{ohmic} resistance of the fuel cell can be reduced by employing materials that conduct and an electrolyte membrane. R_C in equation (2.18) denotes the primary resistance to contact, which is expected to remain constant as it is unaffected by the temperature of the FC's operation. R_M denotes the resistance of the PEM and is determined by the expressions below:

$$R_M = \frac{r_m t_m}{A} \quad (2.19)$$

$$r_m = \frac{181.6\left[1 + 0.03\left(I_{FC}/A\right) + 0.0062\left(T/303\right)\left(I_{FC}/A\right)^{2.5}\right]}{\left[\lambda_m - 0.634 - 3\left(I_{FC}/A\right)\right]\exp\left[\left(4.18\left(T - 303/T\right)\right)\right]} \quad (2.20)$$

With:

t_m : The electrolyte membrane's size (cm) .

r_m : The resistance of electrolyte membrane’s $(\Omega\cdot cm)$.

λ_m : Content of water membrane.

A : The fuel cell active surface space $(70\ \text{cm}^2)$.

The loss voltage (V_{con}) resulting from excessive water inundation in the FC catalysis is expressed as:

$$V_{con} = -B\ \ln\left(1 - \frac{j}{j_{\max}}\right) \quad (2.21)$$

Where:

B : An empirical constant that changes based on the cell and how it operates.

$j_{\max}$: The maximum density of current.

j : The maximum current.

$$V_{FC} = N_{FC} V_{cell} \tag{2.22}$$

$$P_{FC} = V_{FC} I_{FC} \tag{2.23}$$

The total number of FCs is represented by $[N_{FC} = 128]$, whereas (V_{FC}), (I_{FC}), and (P_{FC}) represent the output voltage, current, and power of the FC . **Table 2.3** provides a full description of the PEMFC's parameters.

Table 2.3: The PEMFC specifications [59].

Parameters	Values	Description
MWC	27.7	The water content of molecules
A	70 cm^2	The fuel cell active surface space
N_{FC}	128	The total number of FCs
P_{O_2}	1 atm	Oxygen pressure level
P_{H_2}	1.5 atm	Hydrogen pressure level
T	328 Kalven	The temperature cell during the process
CO_2	$P_{O_2} / \left(5.08\times10^{-5} * \exp\left((-498)/T\right)\right)$	The concentration of oxygen
$j_{\max}$	1.5 A/cm^2	The maximum density of current.
B	0.0016 V	An empirical constant that changes based on the cell and how it operates
j	$\frac{I_{FC}}{A}$	The maximum current
ξ_1	-0.514	All values of the cell model variables
ξ_2	$0.00286+\left(0.0002*\ln(A)\right)+\left(4.3*\ln(CH_2)*1\times10^{-5}\right)$	All values of the cell model variables
ξ_3	0.41×10^{-4}	All values of the cell model variables
ξ_4	-0.93×10^{-4}	All values of the cell model variables
CH_2	$P_{H_2} / \left(1.1\times10^{-6}\right) * \exp\left(-77/T\right)$	The concentration of hydrogen

2.3.3.2 Dynamic model of PEMFC

The term "double layer charging" describes the behavior of a PEMFC. Electrons that are transferred at the anode pass through the external load before reaching the cathode when hydrogen ions arrive at the same time. As a result, at the membrane-cathode interface, two charged layers with different polarities form. An electrical capacitor is what this layer does. An electrical potential that matches the previously mentioned concentration and activation voltages $(V_{act}$ and $V_{con})$ can be generated by collecting charges. Consequently, the activation and concentration voltages allow current to pass for a particular period. The ohmic decrease in voltage relates immediately to variations in current [61],[62]. This dynamic behavior can be modeled using an equivalent electrical circuit model, as illustrated in Figure 2.9. The resistors R_{ohm}, R_{act}, and R_{con} indicate ohmic, activation, and concentration over-voltages, respectively, while the capacitor C represents the delay of these over-voltages in reaction to fuel cell current changes.

The voltage formula of the cell can be written as follows, where V_C is defined as the dynamic voltage across the corresponding electrical capacitor (C):

$$\frac{dV_C}{dt} = \frac{1}{C} \cdot I_{FC} - \frac{1}{\tau} \cdot V_C \tag{2.24}$$

τ represents the RC circuit's constant time, which is shown by:

$$\tau = C \cdot (R_{act} + R_{con}) \tag{2.25}$$

As a result, the general cell voltage formula is now expressed as follows:

$$V_{cell} = E_{Nernst} - V_{ohm} - V_C \tag{2.26}$$

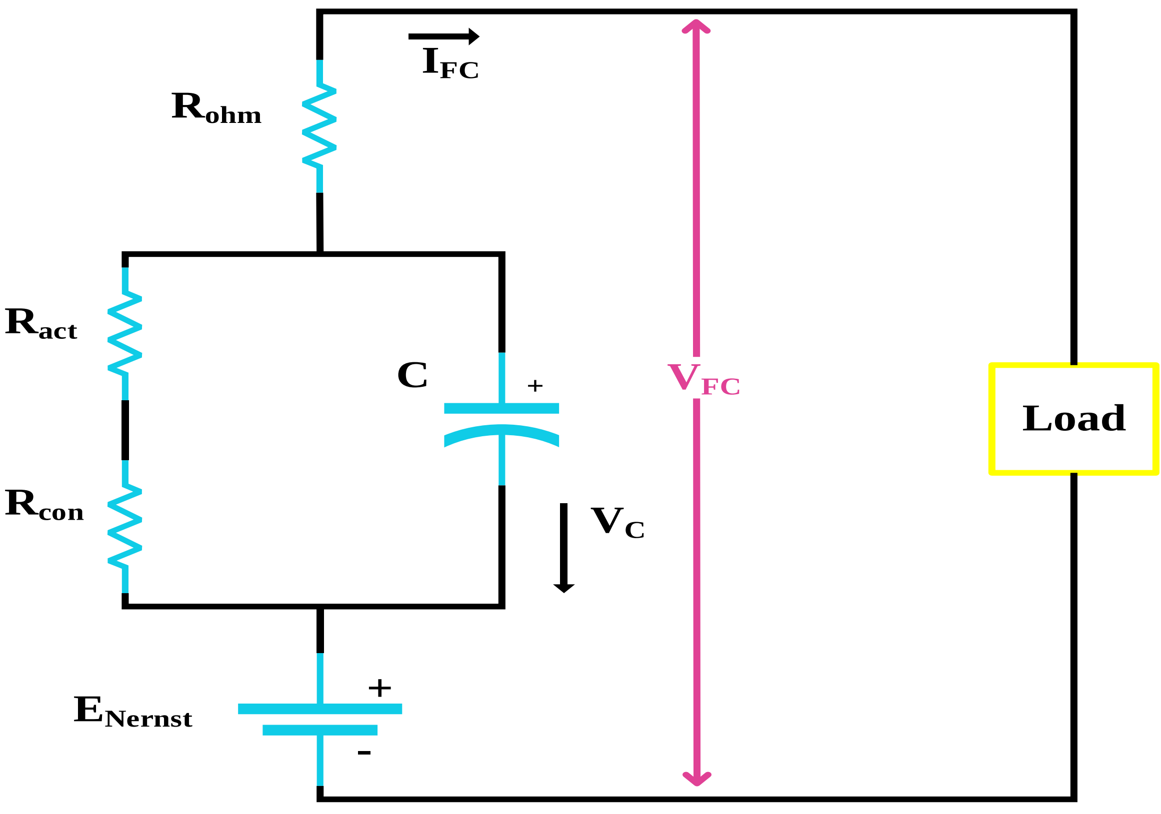

Figure 2.9 : The dynamic electrical circuit equivalent of PEMFC [63].

2.3.4 The influence of pressure and temperature on PEMFC efficiency

The properties of the PEMFC model have nonlinear behavior in its output. V-I and P-I curves are exclusively based on cell variables like temperature (T), membrane water content (MWC), hydrogen partial pressure (P_{H_2}), and oxygen pressure (P_{O_2}). These factors affect the PEMFC performance but specifically the power output. To understand this relationship, Figure 2.10 shows the power-current and voltage-current maintains at $T = 328$ K and different hydrogen and oxygen pressures. The PEMFCs are very sensitive to pressure because their movement of products and reactants has such a significant effect on cell performance. A decrease in pressure (such as 1 atm) reduces response rate and energy production, while its increase ($from$ 1.5 atm to 3 atm ; see Figure 2.10) improves response rate and reactant availability. E_{Nemest} Law states that reactant and product partial pressure increases also increase the operating voltage, which enhances power output [64]. Figure 2.11 illustrates the voltage-current and power-current corresponding to P_{H_2} of 1.5 atm and P_{O_2} of 1 atm the different operating temperatures. Increasing temperature ($from$ 328 Kalven to 373.15 Kalven ; see Figure 2.11) typically improves PEMFC performance by increasing hydrogen crossover and membrane conductivity. The equation of E_{Nemest} shows that the output voltage is dependent on temperature. The E_{Nemest} equation relates the effect of temperature on output voltage. With increased temperature, the stronger reaction dynamics associated with activity increase and the output voltage increases. Due to the negative thermodynamic relationship between open circuit voltage and temperature, the voltage increases are nearly sufficient for overcoming losses. Increases in temperature also produce increases in leakage current; however, leakage current density will remain constant at a specific temperature. Continued extreme temperature operation could impact the longevity of the PEMFC. Higher temperatures will also increase the elevated concentration potential correlation, as they allow higher current densities to be achieved with less mass crossover. Temperature has a direct effect on protons moved across the cell membrane; increasing temperatures will result in faster reaction speeds between the anode and cathode. However, at a higher temperature, even if the materials were chosen, higher temperatures and faster reaction speeds can change the physical structural properties of the materials over time. Thus, to achieve optimal performance, all parameters would require an exact value. Overall, low temperatures ($from$ 328 Kalven to 288.15 Kalven) would potentially damage the reaction conditions and further entrench the relationship between longevity and performance [65],[66],[67].

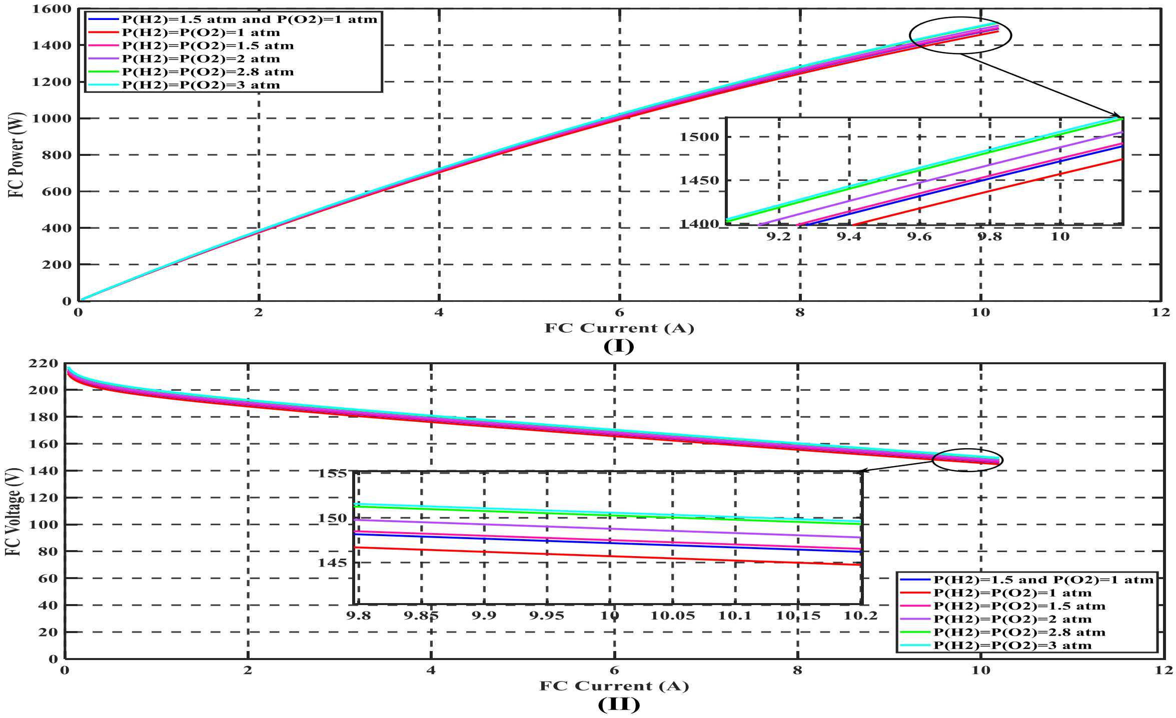

Figure 2.10 : (I) the P-I and (II) V-I properties of PEMFC at various pressures and steady temperatures.

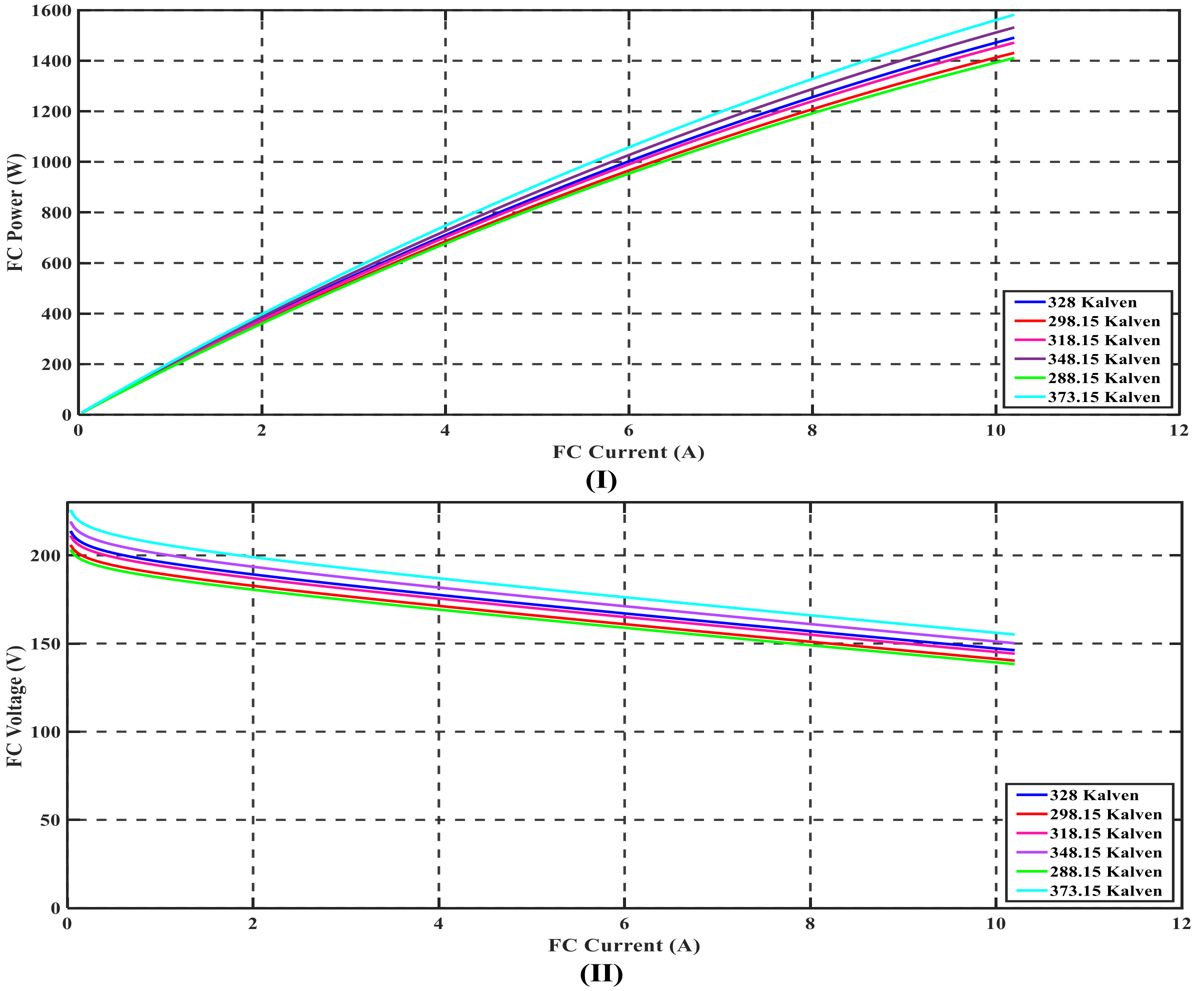

Figure 2.11: ((I) the P-I and (II) V-I properties of PEMFC at different temperatures and steady pressures.

2.4 Power Electronic Converters (PECs)

Power electronic converters (PECs) serve as essential components in the field of electricity, providing the properties required for effective energy conversion, management, and distribution across numerous systems, particularly in RE applications. Power converters are advanced power electronics that convert electrical power from one form to another, allowing for seamless integration of the source and load while controlling and increasing voltage to achieve the desired output voltage. The converter's duty cycle must be controlled to maintain a consistent voltage. As renewable energy sources (RESs) proliferate and are increasingly adopted in various combinations (such as photovoltaics and fuel cells), with or without power storage units (PSUs) including supercapacitors and batteries, hybrid systems (HSs) continue to gain prominence. Factors that can impact power output include the pressure and temperature affecting a PEMFC system, as well as external environmental conditions like irradiance and temperature for a PV system. PECs are required to regulate the output voltage of PV or PEMFC and optimize conversion efficiency by minimizing the power losses due to these fluctuations [68],[69],[70],[71]. Dynamic voltage regulation is employed by these converters to provide a stable power supply within the operational range of the power source and PSU. Converters enhance power flow between various components of a system and ease integration of RESs with storage technologies. In addition, bidirectional power flow is beneficial to PSUs, which may store excess power when it is high and discharge during low productivity or demand. PECs can be rectifiers (AC to DC converters), DC-to-DC converters, inverters (DC to AC converters), and others [71],[72]. This work is concerned with DC-DC converters that can offer improved power efficiency, consistent voltage regulation, and operationally reliable power management to standalone HSs.

2.4.1 DC-DC power converters

Several studies have examined many different kinds of DC-DC converters for green energy technologies and storage to enhance performace. DC-DC converters convert an uncontrolled DC voltage into a regulated DC output voltage by functioning as switching mode regulators. These converters take a crucial and critical role, particularly when integrated with substantial and costly systems such as photovoltaic and fuel cell technologies. Consequently, modeling those converters has emerged as a significant subject recently, following the introduction of the state-space averaging technique. The output of those converters must remain constant regardless of load disturbances [72],[73]. DC-DC converters are classified into three main technologies according to their operational modes. There are three modes: hard switching mode, linear mode, and soft switching mode. This thesis focuses on the hard switching mode, which can be further classified into non-isolated and isolated converters based on their galvanic isolation. Despite the benefits and drawbacks of both classes, non-isolated DC-DC configurations remain a more beneficial and viable choice for integration with green power systems. Boost, buck, buck-boost, zeta, SEPIC, and cuk are the predominant non-isolated converters utilized in power systems. The formulae listed in Table 2.5 were used for calculating each converter's components. The primary criteria for choosing DC-DC converters in photovoltaic or proton exchange membrane fuel cell applications are cost, efficiency, energy transfer, and the capacity to sustain output despite fluctuations in input. Table 2.4 illustrates a comparative analysis of the characteristics of the most prevalent non-isolated converters regarding efficiency, complexity, cost, and other factors [71],[72],[74].

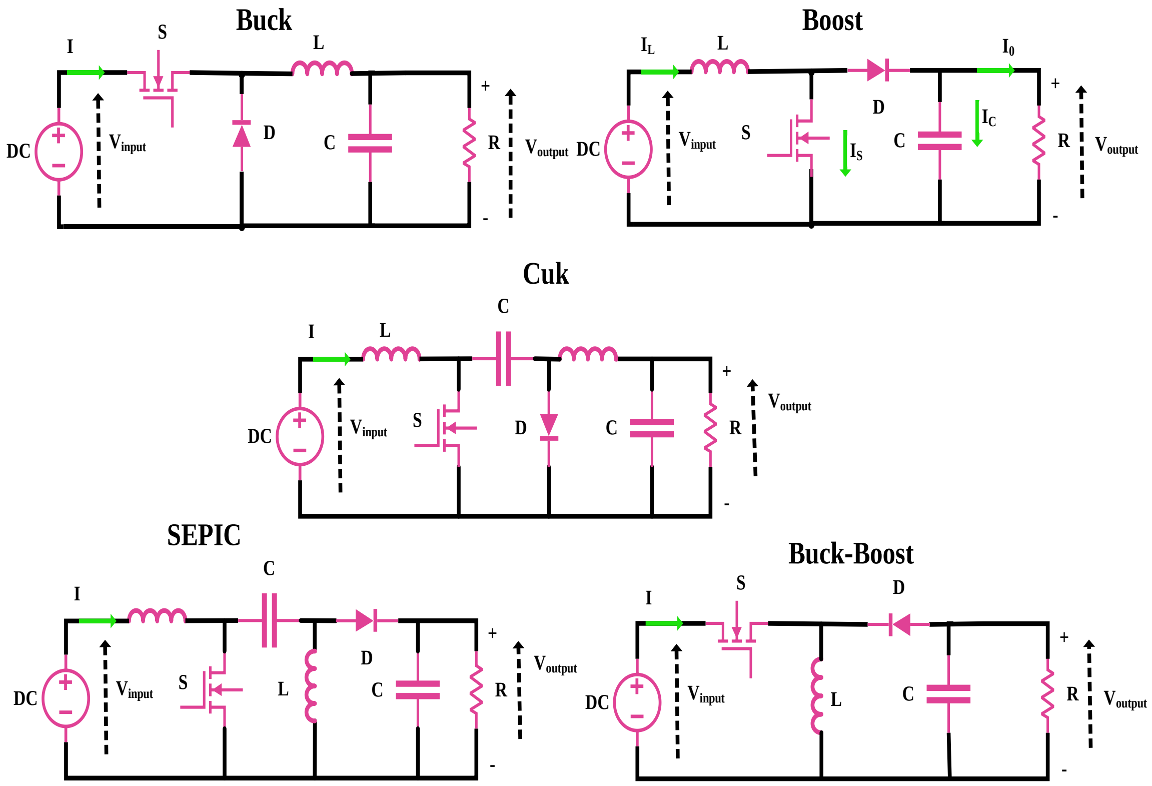

Figure 2.12 : several common DC–DC converter topologies [75].

This study enhances energy extraction from PV modules operating under shaded conditions with variations in both irradiance and temperature levels by using boost and SEPIC converters for maximum power point tracking in PV systems. In the case of the PEMFC, a boost converter is exclusively used for MPPT to maximize the FC output and ensure optimal performance during power conversion. In this energy management technique, boost converters are also employed to manage the flow of power from both the PV and PEMFC technologies to facilitate their seamless integration. Output power flow from and to the supercapacitor and battery is used with a buck-boost converter for flexibility in voltage regulation during charge and discharge cycles. This approach ensures a hybrid configuration is stable and operates efficiently while guaranteeing synergy between the PV system, PEMFC, and PSU for effective power management.

In

Figure 2.12, several common DC–DC converter topologies are illustrated. Each of the converters has a power MOSFET and a diode that represents the switch, but if desired, the switch can also be implemented using BJTs, IGBTs, or thyristors. There is also research suggesting that IGBTs can be used to function as a switch for implementation in multiple converters in power systems. At least, it does clarify that the electronic switches adapted in this work will be used [76],[74],[75].

Table 2.4 : Comparative analysis of the characteristics of the most used non-isolated converters [74].

Converter	**Cost**	**Efficiency**	**Average Efficiency of Tracking**	**Complexity of the hardware**	**Components that transfer power**
Cuk [71]	Medium	High	High	Medium	Capacitor and inductor

Boost [70],[71]	Low	High	Medium	Low	Inductor
Buck [71],[77]	Medium	High	Medium	Low	Inductor
Buck-Boost [77],[71],[75]	Low	Medium	High	Medium	Inductor
SEPIC [75],[71]	Medium	Medium	High	High	Capacitor and inductor

2.4.1.1 Boost converter

A boost converter is termed "boost" due to its voltage output being higher than its input voltage. A highly effective power electrical equipment elevates the input voltage without employing a transformer. During the boost operation, all the power input to the system is maintained the same as the output power by decreasing the current. Figure 1 illustrates that the boost converter comprises a DC input voltage source, a diode (D), an inductor (L), an adjustment switch (S), and a resistive load (R) linked to a filter capacitor (C) in a standalone system output. The predominant electronic switch utilized is a power MOSFET; however, research indicates that IGBT can also be utilized in switching applications. Typically, pulse width modulation (PWM) technologies are employed for switching in simple circuit designs. Consequently, the PWM modulated signal must fluctuate between states of ON and OFF to adjust the output voltage. The correlation between the input and output voltage of a step-up converter is determined by the duty cycle of the control switch. The voltage that is generated can be modified by changing the ON duration of the switch[69],[76],[78]. Consequently, the mean voltage of the output can be defined as a function of the duty cycle "D" [79].

The converter can thus function in two different modes based on its power capacity for storage and the duration of the switch time. The two operating modes are called continuous mode of conduction (CCM) and discontinuous mode of conduction (DCM), which indicate situations with and without a pause interval, respectively. As depicted in Figure 2, when the switch S is in the ON position, the current in the inductor rises linearly, and the diode remains OFF during this period. When the switch S is OFF, the energy stored in the inductor is released through the diode into the output of the RC circuit. The converter's designation implies that the output voltage will periodically exceed the input voltage. The switching period is T, and the switch is closed for DT and open for $(1-D)T$, where D is the constant duty cycle [79],[73],[78].

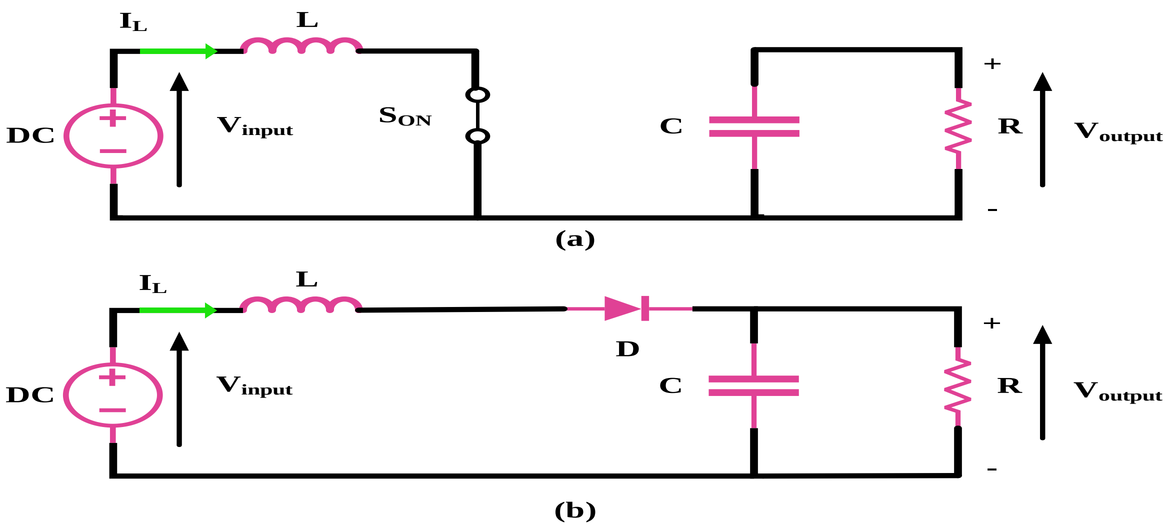

Figure 2.13 : (a) ON and (b) OFF modes boost converter circuits [73],[80].

The state-space model of the boost converter in both ON and OFF modes is primarily shown as follows [73]:

2.4.1.1.1 The mode state ''ON''

As the capacitor passes through the load, the inductor is charged by the supplied voltage source, as shown in Figure 2.13 (a). The voltage formulas can be expressed as:

$$V_{input} - L\frac{dI_L}{dt} = 0 \tag{2.27}$$

$$\frac{V_C}{R} + C\frac{dV_C}{dt} = 0 \tag{2.28}$$

The aforementioned two formulas can be expressed as follows by expressing the output voltage as $V_{output} = V_C$ and the state vector as $x = [I_L \quad V_C]^T$:

$$\begin{bmatrix} \frac{dI_L}{dt} \\ \frac{dV_C}{dt} \end{bmatrix} = \begin{bmatrix} 0 & 0 \\ 0 & -\frac{1}{RC} \end{bmatrix} \begin{bmatrix} I_L \\ V_C \end{bmatrix} + \begin{bmatrix} \frac{1}{L} \\ 0 \end{bmatrix} V_{input} \tag{2.29}$$

$$V_{output} = \begin{bmatrix} 0 & 1 \end{bmatrix} \begin{bmatrix} I_L \\ V_C \end{bmatrix} \tag{2.30}$$

2.4.1.1.2 The mode state ''OFF''

When in OFF mode, the diode discharges the power stored in the inductor to the output RC circuit; the voltage equations are as follows:

$$V_{input} - V_C - L\frac{dI_L}{dt} = 0 \tag{2.31}$$

$$I_L - \frac{V_C}{R} - C\frac{dV_C}{dt} = 0 \tag{2.32}$$

The aforementioned formulas for determining the subsequent state formulas for the OFF phase have been revised as:

$$\begin{bmatrix} \frac{dI_L}{dt} \\ \frac{dV_C}{dt} \end{bmatrix} = \begin{bmatrix} 0 & -\frac{1}{L} \\ \frac{1}{C} & -\frac{1}{RC} \end{bmatrix} \begin{bmatrix} I_L \\ V_C \end{bmatrix} + \begin{bmatrix} \frac{1}{L} \\ 0 \end{bmatrix} V_{input} \tag{2.33}$$

$$V_{output} = \begin{bmatrix} 0 & 1 \end{bmatrix} \begin{bmatrix} I_L \\ V_C \end{bmatrix} \tag{2.34}$$

A converter model is created during a single switching period using the state space average method. Consequently, a single space characterization that appropriately describes the behavior of the circuit over the full period T must be used in place of the state space representations of the two modes. The state space averaging method produced the averaged modified model, which is expressed as follows:

$$A = A_1 d + A_2 (1 - d) \tag{2.35}$$

$$B = B_1 d + B_2(1-d) \tag{2.36}$$

Whereas A_1, A_2, B_1, and B_2 are defined by:

$$A_1 = \begin{bmatrix} 0 & 0 \\ 0 & -\frac{1}{RC} \end{bmatrix}, A_2 = \begin{bmatrix} 0 & -\frac{1}{L} \\ \frac{1}{C} & -\frac{1}{RC} \end{bmatrix}, B_1 = \begin{bmatrix} \frac{1}{L} \\ 0 \end{bmatrix}, B_2 = \begin{bmatrix} \frac{1}{L} \\ 0 \end{bmatrix}$$

Use the aforementioned matrices in equations (2.35) and (2.36) to determine the duty cycle, denoted as d, at any given time.

$$\frac{d}{dt}\begin{bmatrix} I_L \\ V_C \end{bmatrix} = \begin{bmatrix} 0 & -\frac{(1-d)}{L} \\ \frac{1-d}{C} & -\frac{1}{RC} \end{bmatrix}\begin{bmatrix} I_L \\ V_C \end{bmatrix} + \begin{bmatrix} \frac{1}{L} \\ 0 \end{bmatrix} V_{input} \tag{2.37}$$

$$V_{output} = \begin{bmatrix} 0 & 1 \end{bmatrix}\begin{bmatrix} I_L \\ V_C \end{bmatrix} \tag{2.38}$$

Equation (2.37) can be used to calculate the steady-state model of the boost converter by:

$\frac{d}{dt}\begin{bmatrix} I_L \\ V_C \end{bmatrix} = 0$ With: $d = D$

Equation (2.37) changes to:

$$\begin{bmatrix} 0 \\ 0 \end{bmatrix} = \begin{bmatrix} 0 & -\frac{(1-D)}{L} \\ \frac{1-D}{C} & -\frac{1}{RC} \end{bmatrix}\begin{bmatrix} I_L \\ V_C \end{bmatrix} + \begin{bmatrix} \frac{1}{L} \\ 0 \end{bmatrix} V_{input} \tag{2.39}$$

$$V_{output} = \begin{bmatrix} 0 & 1 \end{bmatrix}\begin{bmatrix} I_L \\ V_C \end{bmatrix} \tag{2.40}$$

Employing equations (2.39) and(2.40), the steady-state relationship between V_{output} and V_{input} can be expressed as:

$$\frac{V_{output}}{V_{input}} = \frac{1}{1-D} \tag{2.41}$$

2.4.1.2 SEPIC converter

Like a buck-boost converter, a single-ended primary-inductance converter can increase or decrease voltage, but in some designs, like the Cuk converter, the SEPIC converter incorporates an inductor at the input. This conversion to a current pulse makes it continuous and allows precise MPPT efficiency to be achieved. While the capacitor C_1 provides isolation between the input and output (to protect from output overload and short circuit) as illustrated in Figure 2.12, a conventional SEPIC design also has the advantage of the same polarity of input and output voltages compared to Cuk and Buck-Boost structures. Buck-boost converter drawbacks, such as reversed load voltage and fluctuating load current, can be overcome by SEPIC. Buck–boost converters exhibit lower efficiency compared to SEPIC and Cuk converters. Moreover, the SEPIC converter, identical to the Cuk converter, possesses the beneficial characteristic of having the switch control terminal grounded. Conversely, the SEPIC converter exhibits a discontinuous output current, necessitating a substantial output capacitor filter to mitigate current fluctuations [74],[71].

2.4.1.3 Buck-Boost converter

Due to its simple and affordable design, the buck-boost converter is the most commonly used in switch regulation. This converter combines the previously mentioned boost and buck designs, where the boost converter raises the output voltage levels and the buck converter lowers them. The same components used in the previously discussed converters shown in Figure 2.12 are used to construct a buck-boost converter. The load capacitor and input voltage are connected in parallel with the inductor. The switch or transistor is between the input and the inductor, while the diode is between the inductor and the load capacitor. By switching the voltage polarity, this converter can increase or decrease the output voltage in relation to the input voltage. The converter structure is currently being studied to enhance the performance of power systems. The uses for the combined converter technology are diverse, encompassing power management, vehicle purposes, stand-alone structures, and electrically connected power production systems[77],[71],[75]. The state-space model of the Buck-Boost converter in both ON and OFF modes is primarily shown as follows[80]:

2.4.1.3.1 The mode state ‘’ON”

The equation(2.42), and Figure 2.14 shows the state when the switch is closed (ON).

$$\begin{bmatrix} \frac{dI_L}{dt} \\ \frac{dV_C}{dt} \end{bmatrix} = \begin{bmatrix} 0 & 0 \\ 0 & -\frac{1}{C} \end{bmatrix} \begin{bmatrix} I_L \\ V_C \end{bmatrix} + \begin{bmatrix} \frac{1}{L} \\ 0 \end{bmatrix} V_{input} \tag{2.42}$$

2.4.1.3.2 The mode state ‘’OFF”

However, the equation(2.43), and **Figure *2.14*** shows the state when the switch is opened (OFF).

$$\begin{bmatrix} \frac{dI_L}{dt} \\ \frac{dV_C}{dt} \end{bmatrix} = \begin{bmatrix} 0 & \frac{1}{L} \\ -\frac{1}{C} & -\frac{1}{C} \end{bmatrix} \begin{bmatrix} I_L \\ V_C \end{bmatrix} + \begin{bmatrix} 0 \\ 0 \end{bmatrix} V_{input} \tag{2.43}$$

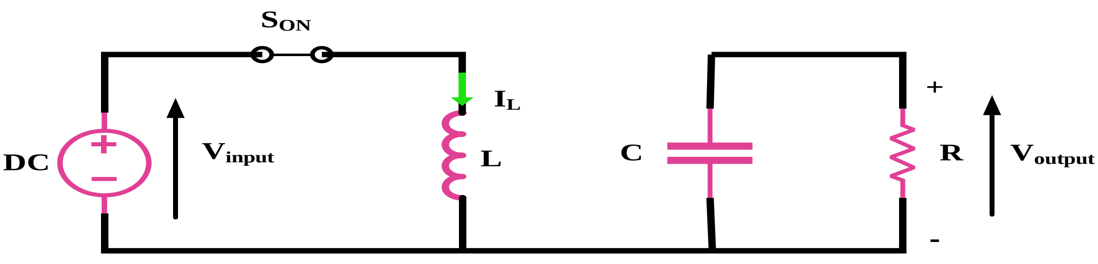

(a)

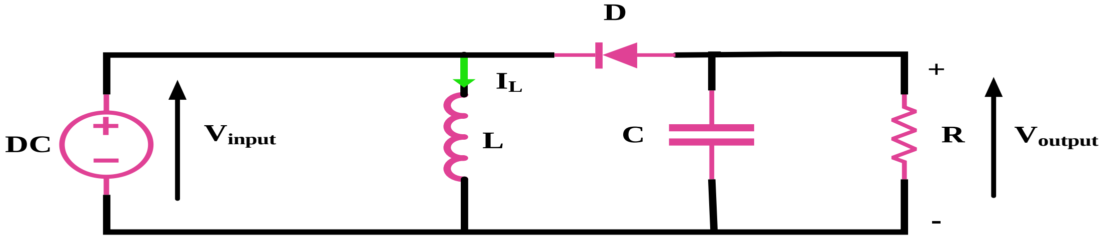

(b)

Figure 2.14: (a) ON and (b) OFF modes Buck-Boost converter circuits [80].

Table 2.5: The components of each converter equation [71].

Converter	$\frac{V_{output}}{V_{input}}$	C_1	C_2	L_1	L_2
Boost	$\frac{1}{1-D}$	$\frac{V_{output} \cdot D}{\Delta V_{C1} \cdot f_s \cdot R}$	-	$\frac{V_{input} \cdot D}{\Delta I_{L1} \cdot f_s}$	-
SEPIC	$\frac{D}{1-D}$	$\frac{V_{output} \cdot D}{\Delta V_{C1} \cdot f_s \cdot R}$	$\frac{V_{output} \cdot D}{\Delta V_{C2} \cdot f_s \cdot R}$	$\frac{V_{input} \cdot D}{\Delta I_{L1} \cdot f_s}$	$\frac{V_{input} \cdot D}{\Delta I_{L2} \cdot f_s}$
Buck-Boost	$-\frac{D}{1-D}$	$\frac{V_{output} \cdot D}{\Delta V_{C1} \cdot f_s \cdot R}$	-	$\frac{V_{input} \cdot D}{\Delta I_{L1} \cdot f_s}$	-

2.5 Energy Storage systems

Energy storage systems (ESS) are often used in stand-alone combined RE systems to overcome the problem of RES intermittency. Supercapacitors (SCPs), batteries, and flywheels are the most popular types of energy storage technologies. The primary objective of ESSs is to control extra or not enough power over a short period. This makes sure that they are reliable and can quickly adapt to changes in power supply during loads. The secondary, or long-term, objective of energy storage systems is to meet needs when output cannot keep up with demand. In temporary energy storage systems, SCPs usually have a more efficient dynamic reaction than BSBs. This makes it easier to quickly deliver energy and handle changes in demand. SCPs function well without releasing toxic gases, and they protect batteries by slowing down their degradation and extending their life. Their advantage is because they have a longer cycle life and can charge and discharge quickly. They operate effectively at extreme temperatures with minimal maintenance and are environmentally sustainable. BSBs are highly regarded for their high load capacity and high current release capacity, which make system response more reliable by making up for long periods of low production and changes in demand. Battery systems need a way to manage energy so that they can control the charging process effectively. There are many kinds of batteries, but the lithium-ion kind is the most common. The lithium-ion battery works better than conventional batteries (95%) [80],[30]. The PSU model used in this study is described in the following section.

2.5.1 Model of lithium-ion battery

RE systems are inconsistent, variable, and uncertain, so a BSB is needed to keep power generation and fix RES problems. This research uses lithium-ion batteries, which have a higher energy density than any other type (NiMH, lead-acid, or NiCd) and are efficient, long-lasting, and able to work under extreme temperatures. The state of charge (SOC) of the battery is considered to achieve optimal performance. There are multiple technological considerations when selecting a battery configuration—including longevity, capacity, discharge rate, size, sensitivity to temperature, maintenance, and cost. For the reasons stated previously, this work uses lithium-ion batteries. Correspondingly, the modified Shepherd fitting curve model contains voltage polarization when calculating battery discharge voltage. Additionally, a filtered battery voltage is taken with the battery current for the calculation of the polarization resistance to ensure the simulation is accurate. The model of a battery illustrated in Figure 2.15 and its voltage, $V_{battery}$, in a model of a lithium-ion battery is written as follows [81], [82], [83]:

$$V_{battery} = E_0 - K\frac{Q}{Q-it}it - R_b i + A_b e^{-(B.it)} - K\frac{Q}{Q-it}i^* \tag{2.44}$$

With:

E_0 : Constant voltage battery.

Q : Capacity of battery.

K : Polarization constant.

R_b : The internal resistance of a battery.

A_b : Amplitude of the exponential zone.

it : The charge of the battery right now.

i^* : Current battery filtered.

B : The constant of time in the exponential zone.

The battery voltage rises sharply when it reaches full charge, which is shown by the polarization resistance change that follows:

$$Pol_{res} = K\frac{Q}{it-0.1Q} \tag{2.45}$$

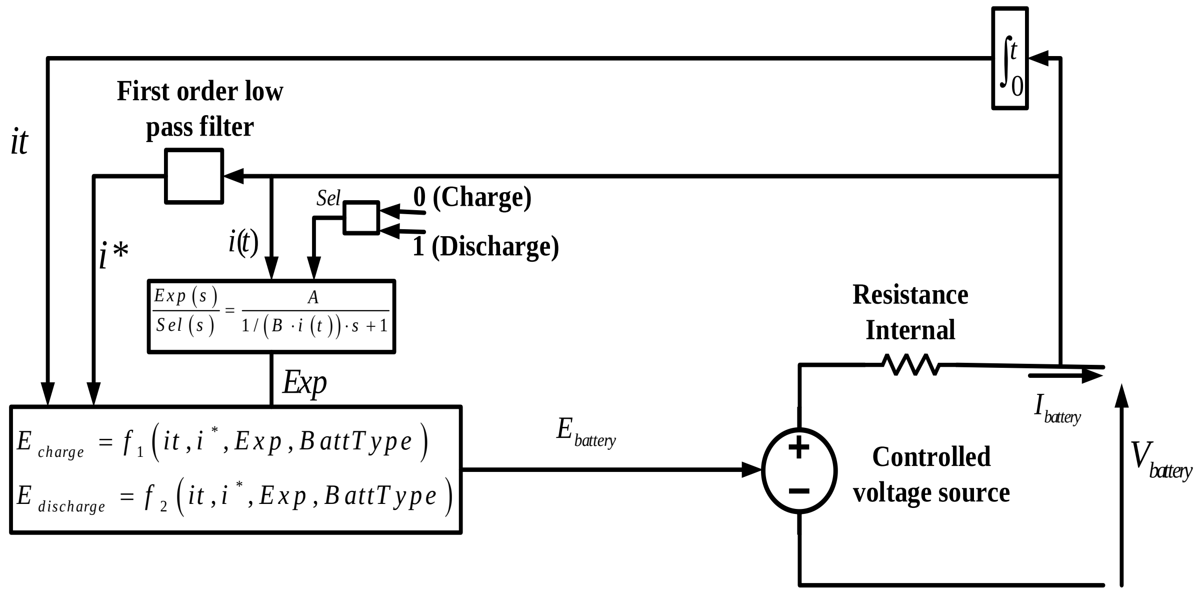

Figure 2.15: The model of the battery [81].

2.6 Conclusion

This chapter's objective is to present a comprehensive model of the components of the proposed hybrid system, which will be utilized in the upcoming chapters for the energy management and control approach. Initially, photovoltaic technology was explored in detail from cells to modules, with an emphasis on the effects of temperature, irradiance, and shading on SPV systems, ultimately leading to an overview of fuel cell technology. The discussion featured the static and dynamic models of different types of fuel cells, with an emphasis on proton exchange membrane FCs, and the chapter analyzed how pressure and temperature impact fuel cell efficiency. The features of the system's power converters, specifically the DC-DC power converters such as boost, SEPIC, and buck-boost, were illustrated and discussed to partially represent and accurately model the electrical circuitry. The model of battery is also presented as component of the energy storage and management system.

Chapter 3 : Literature review on control and power management of hybrid standalone power systems

3.1 Introduction

Renewable energy technologies continue to maintain public attention as practical and environmentally friendly options. Solar is one of the most recognized sources of clean energy, designed to have some distinct advantages over traditional fossil fuel-based production. Photovoltaic systems produce no emissions, are long-lasting, and are almost maintenance-free. However, many renewable energy sources have a very low output range [84]. Additionally, they also have a high upfront cost. Nonetheless, photovoltaic systems continue to have lower operating efficiency due to their reliance on weather conditions, stifling the growth of solar power systems in energy markets. Rapid shifts in solar radiation and partial shadowing conditions (PSCs) are the key variables that reduce PV efficiency. Furthermore, both scenarios have a negative impact on the output power and energy efficiency of solar systems. As a result, most solar systems include a maximum power point tracker. This tracker aims to optimize the extraction of power and increase the output of energy from solar systems. The MPP tracker, during the sudden change in irradiance level, may fail to detect weather differences, resulting in power outages due to insufficient monitoring of the new MPPs. Subsequently, in the context of PSCs, the emergence of multiple maximum power points (MPPs) due to changed electrical properties of the photovoltaic array may confuse the maximum power point tracker, causing it to operate at a local maximum power point (LMPP) rather than ensuring optimal power from the global maximum power point (GMPP), resulting in significant power losses [85]. Perovskite and tandem cells are two recent technologies in solar cell design and construction that have made considerable advancements. Even though the processes are necessary, the overall performance of the system should be improved continually. The MPPT is a recognized concept in solar power. The objective is to improve an MPPT that, by adapting the I-V operating point to the load characteristics, harvests and sustains the maximum power from PV panels under a range of environmental conditions. The converter can function at or near the MPP on the P-V feature curve if the PV panel's outputs, voltage, or current are adjusted to provide the optimum power. It should be noted that MPPT is utilized for other green energy sources, like FCs, in addition to producing electricity from SPV [86],[87].

Fuel cells are another clean energy option that is capable of ensuring even more efficient and stabilized performance when it comes to power generation from different sources. Fuel cells provide clean and stable sources of energy. Because of how they work and how easy it is to operate and get flexibility out of them, FCs can be a strong contender for a variety of applications for power generation. However, fuel cells do not work optimally, since their ability to generate electricity is heavily reliant on several factors related to systems, environments, and other variables, such as temperature and pressure. An enhanced MPPT approach is developed and implemented in a power electronics interface for fuel cell combinations to address this issue. The main goal of this accurate method is to extract the maximum output out of the power source by obtaining the highest power out of the power converter. Fuel cells have very nonlinear operating characteristics, which limit the maximum power output they can provide. Clean energy has both benefits and drawbacks. For example, green energy has a lesser effect on the environment, but it can also be expensive and dependent on weather conditions. Although an alternative energy source is necessary for optimal power supply, hybrid systems that utilize multiple generating sources provide viable, safe, and efficient technologies to reduce the drawbacks of single sources and the challenges associated with relying solely on one. Currently, the primary technologies of energy storage in small and medium-sized systems are batteries and, in certain cases, supercapacitors. Power storage is required to meet load profiles, as solar supply sources cannot supply total demand at all times. Power storage is necessary for supplying demand, stabilizing the system, and reliability. To support the operation of a standalone hybrid power system sustainably, suitable energy management systems need to be implemented [88],[89],[30],[32],[7].

This chapter provides an overview of the most common control strategies for standalone hybrid PV-PEMFC systems. The sections that discuss PV systems contain descriptions of the different categories of MPPT methods, along with their drawbacks and recent advances in the field. The chapter provides an overview of various techniques for MPPT for PEMFC, encompassing both conventional and intelligent methodologies. An overview of energy management approaches used in hybrid systems is presented.

3.2 Maximum Power Point Tracking (MPPT) Techniques:

The power output in photovoltaic systems attains its peak at a point known as the "Maximum Power Point" (MPP), the location of which fluctuates continually. The variable generation of electricity and voltage based on weather conditions poses a significant challenge in the solar energy field. These variables encompass factors such as shade, sunlight intensity, temperature, and load properties. This influences the specified photovoltaic output power for a particular system, as the systems are designed to generate an established amount of power prior to implementation. The extraction of maximum power is not assured for all electrical loads [90],[91],[92].

Monitoring the peak power of the PV generator necessitates that the operating point be at the MPP, which is a position on the photovoltaic curve indicating the maximum power a particular photovoltaic module can generate at a specific time. Consequently, the MPP must be consistently monitored using MPPT techniques. MPPT is a strategy used to optimize power extraction from PV modules by adjusting the operating voltage or current, typically necessitating a switching converter to regulate PV power output. Each MPPT controller aims to ensure that the power-voltage derivative on the P-V characteristics curve is equal to zero. To apply the MPPT algorithm, the duty cycle of the converter is varied until the source impedance is equal to the load impedance according to the measured output voltage and current of the PV module. When the impedance matching is aligned, the MPP will be tracked. Photovoltaic systems are more efficient and produce more electrical energy when using solar tracking methods. A significant issue in MPPT systems arises during voltage tracking and the precise adjustment of the duty ratio to optimize the peak output power from the PV system [87],[91].

To maximize the energy flow from the PV panel to the load, researchers and industry experts have developed various MPPT strategies with designs that have been published in the literature. Each strategy has unique needs, limitations, and uses. The performance of the particular technique depends on its ability to track in quickly changing climatic conditions. As a result, these methods are classified on the basis of the tracking characteristics of PSCs and sudden changes in light levels. However, when developing new MPPT designs for PV systems, factors such as cost, lost power, complexity, and means of implementation are considered [92],[93],[94]. This study examined MPPT in PV systems, detailing the differences in classification, the limitations of traditional methods, and the switch to more advanced MPPT techniques.

3.2.1 MPPT-based PV system descriptions for DC-to-DC applications

3.2.1.1 MPPT approach based on current or voltage control

The current- or voltage-based MPPT method works by estimating the reference current or voltage $(I_{ref}$ or $V_{ref})$ and then calculating the error between the reference and the observed photovoltaic current or voltage. The converter requires extracting the MPP from the PV panel because a regulator such as PI, PID, sliding mode (SDMC), backstepping, etc., uses this error to calculate the duty cycle. I_{ref} or V_{ref} equals I_{MPP} or V_{MPP} at the MPP. As illustrated in Figure 3.1 (a), The MPPT controller is connected to the DC/DC converter. It is evident the DC system is solely shown below. To make it suitable for a stand-alone or grid-connected photovoltaic system, it can be improved by adding more power electronic components, like inverters or grid components [86].

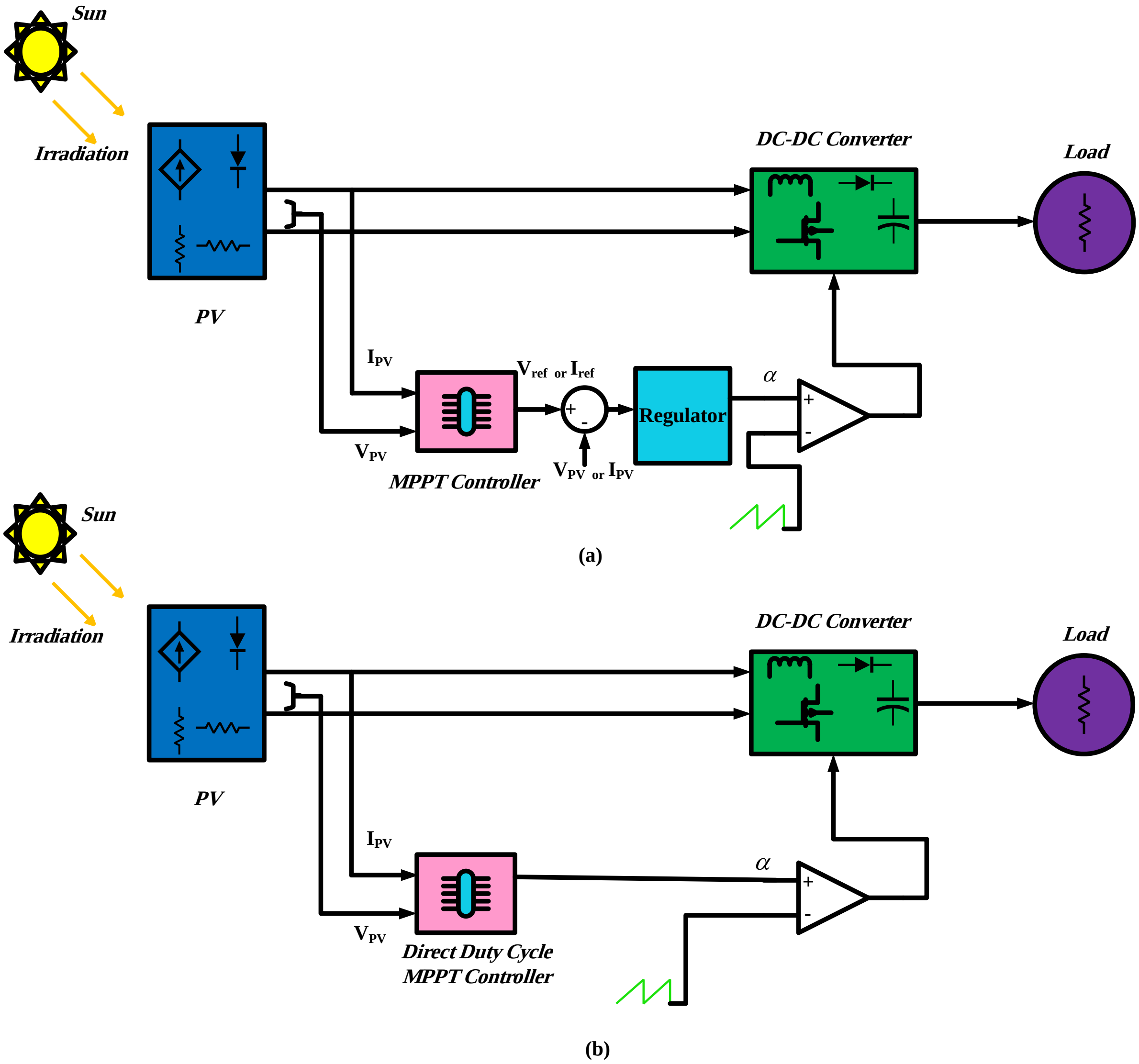

Figure 3.1: Structure of MPPT approach based on (a) current or voltage (b) duty cycle controls [86].

3.2.1.2 MPPT approach based on duty cycle control

As illustrated in Figure 3.1 (b), another popular type of MPPT technique, which differs from the first type, depends on the DC/DC converter's duty cycle regulation. This method is referred to as a "duty cycle control-based MPPT approach." The regulator is not required because the MPPT controller controls the duty cycle. The positive aspects of this technique over current- or voltage-based MPPT methods include a simpler MPPT design, less computation time, and no need for tuning because no regulator is used. As a result, this method offers an MPPT system that is adjusted to achieve the best possible performance results [86].

3.2.2 Overview of the several MPPT approaches and their categorization

A primary problem in solar photovoltaic systems is monitoring and extraction of the maximum power point under fluctuating external conditions, including temperature, irradiance, and partial shade. In 1968, the MPPT controller, a crucial component of photovoltaic systems utilizing MPPT, was initially implemented in space systems to tackle this issue. Since then, improvements in tracking speed, robustness, precision, effectiveness, and simplicity have been made to the MPPT controller. To accurately find the MPP when the output voltage, current, or product (power) changes suddenly, MPPT methods need to have high response rates. MPPT is a part of PV system technology because the main goal is to produce the maximum power possible to the load or grid [95],[96]. There are many different MPPT methods, and each one has benefits as well as drawbacks. Since there are restrictions in every system, each of them must determine the best approach. For example, climate, sunlight time, and overall budget are just a few of the factors to consider. Some MPPT approaches also adopt different designations. Various methodologies exist within these categories, including the attributes of the method and the tracking strategy. Typically, these are categorized into classes such as indirect, direct, soft computing, or standard intelligent approaches, based on the use case approach. MPPT techniques can be classified based on the methods of tracking into constant parameters, measurement and comparison, mathematical computation, trial and error, and intelligent approaches. While indirect strategies provide the MPP based on concepts, they do not provide the power features of the PV system. Direct techniques measure the power, current, and voltage of a PV system using sensors; therefore, the MPP is determined by analyzing these measurements. The predominant classification encompasses MPPT, including traditional methodologies, AI-based strategies, advanced soft computing approaches (bio-inspired), and hybrid methods [97]. This thesis analyzes the MPPT techniques based on this categorization due to their accuracy, as indicated in Figure 3.2.

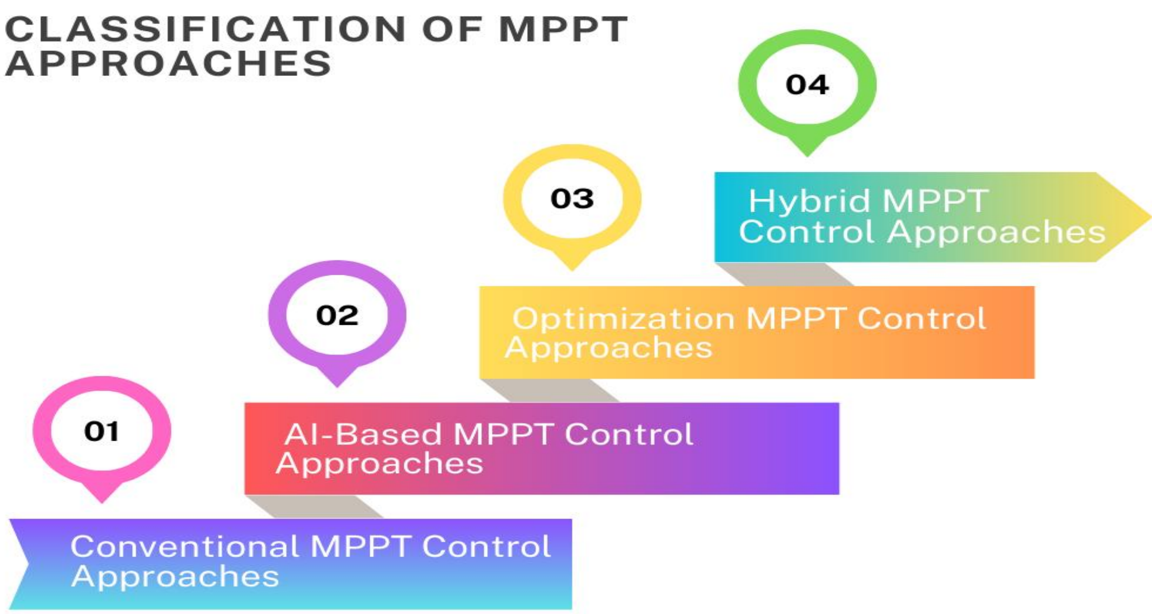

Figure 3.2: Categorization of MPPT approaches.

3.2.2.1 Conventional MPPT Control Approaches

Classic approaches are usually used to improve the output of power in PV systems due to their simplicity, performance in tracking the MPP, and relatively low computational requirements. Furthermore, these strategies serve as an overview and are regarded as conventional benchmarks for comparisons with current methods. The literature identifies the most recognized MPPT techniques as the classic perturb and observe and incremental conductance methods. This section provides an overview of the most prevalent classical approaches, including the perturb and observe technique (P&O), which is iterative in its behavior. These techniques rely on the identification of oscillations by keeping three successive slope values, subsequently leading to the method's divergence from the maximum power point (MPP) position. The incremental conductance method (IC) relies on the analysis of the P-V property curve. The approach was introduced in 1993 and aimed to address certain limitations of the P&O technique. The approaches under discussion comprise constant voltage (CV), open circuit voltage (OCV), short circuit current (SCI), and the hill climbing method (HCM) [95].

The classical approaches have been readily employed in practical applications because of their simplicity. When exposed to uniform radiation, they perform at their peak. However, these methods have drawbacks such as poor accuracy, long tracking times, and low adaptability to external changes. The relatively poor tracking efficiency is generally due to sudden changes in weather conditions, having slower responses, and more significant variations near the MPP. Furthermore, it is difficult to efficiently mitigate the effects of partial shading due to its effects and how they affect the performance of the classic methods. In general, the relatively low tracking efficiency obtained arises from abrupt weather changes, slower response times, and larger variations near the MPP. Furthermore, because partial shading has effects that lower the performance of conventional methods, it is challenging to address effectively. The system becomes confused and converges on local optimal solutions, which results in a large loss of solar panel output power. Similarly, the GMPP does not always match the solution to a multi-peak optimization problem. Recent implementations of intelligent techniques, optimization techniques, and hybrid techniques aim to overcome the limitations of classic methods and improve MPPT control performance while fulfilling specific needs [98],[99],[91].

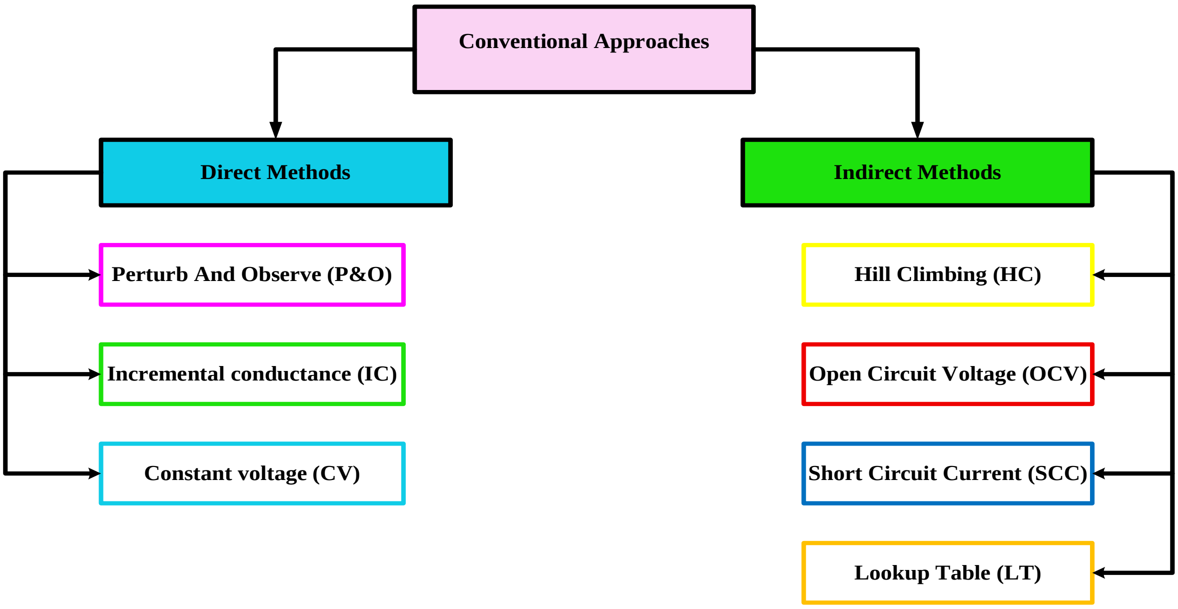

Figure 3.3: Classification of conventional approaches.

3.2.2.1.1 Perturb And Observe (P&O) approach

The P&O approach is a widely utilized control technique in commercial MPPT controllers due to the algorithm's low complexity and simplicity of implementation. The review of the literature indicates that this strategy depends on the trial-and-error approach to identify and pursue the MPP. The method works by making a small change to a control variable and then observing how the desired function responds until the slope reaches zero. The operational procedure of the perturbation and observation approach demonstrates the change of the system's constant functioning point, necessitating adjustments to the perturbation step size and observation time step size [95],[100].

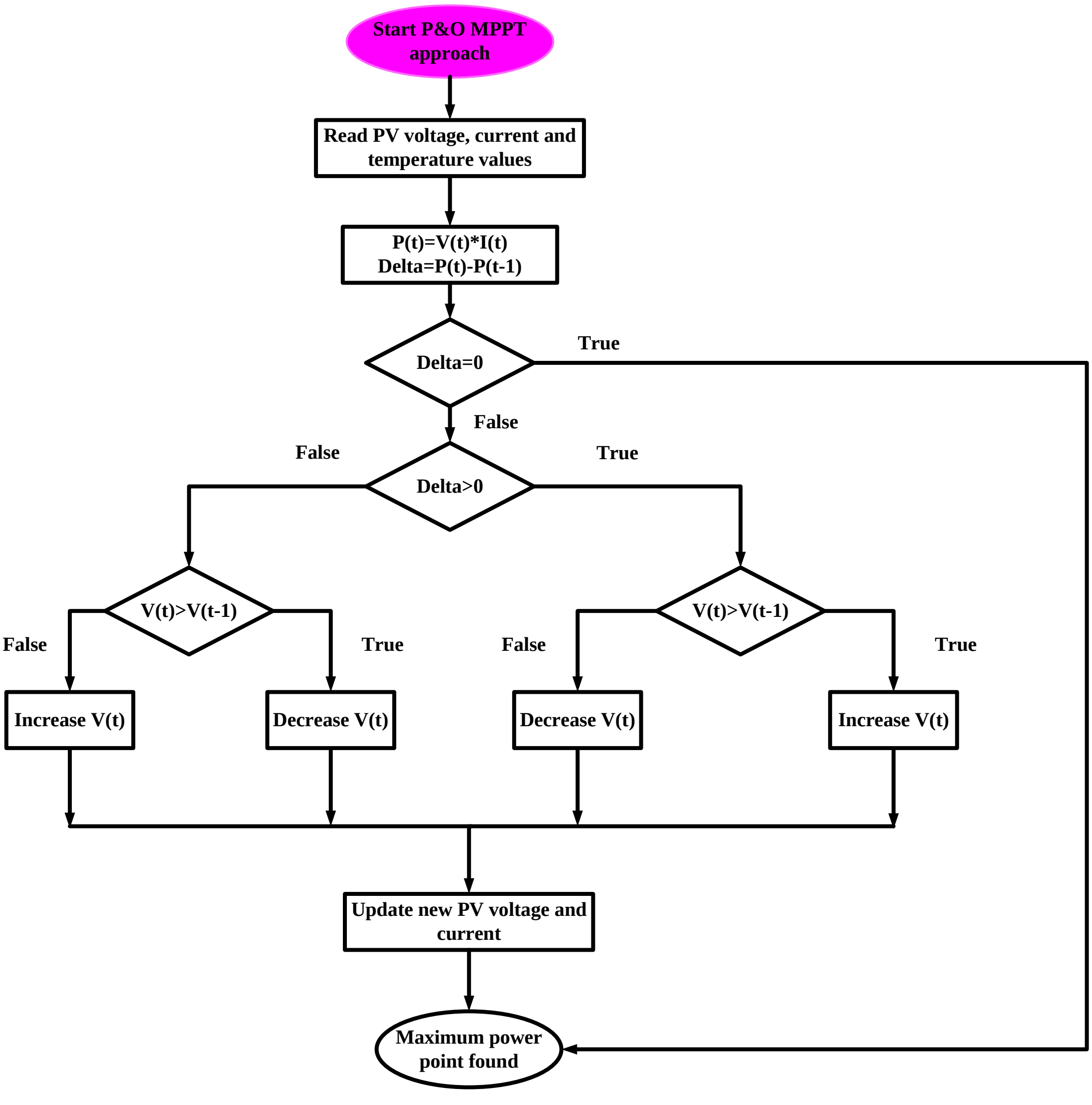

Figure 3.4: Flowchart of P&O strategy [92].

The current and voltage are measured at the PV module output to determine its power output value. Then, the difference in voltage and power is found by comparing the new values to the old ones. At the highest operating point, the change in power, dP_{PV} , is zero. However, if dP_{PV} is not zero, the approach will seek to identify the optimal solution by progressively adjusting the voltage with a fixed step size. If the operating point of the PV system is positioned on the left side, the method will pursue the maximum power point by adjusting the system towards the right side, and conversely if it is on the right side. The principal benefit of P&O is its straightforward design and ease of implementation, making it suitable for diverse applications. However, its drawbacks include a propensity to oscillate around the MPP and potential inefficiencies in partial shadows. Figure 3.4 illustrates a flowchart corresponding to this strategy [101],[102],[99].

The maximum power point at the end of each P-V curve is shown by equation(3.1). Equations (3.2) and (3.3) can be used to determine whether the MPP is pointing left or right [92].

$$\frac{dP_{PV}}{dV_{PV}} = 0 = MPP \tag{3.1}$$

$$\frac{dP_{PV}}{dV_{PV}} \succ 0 \quad \text{Left side of MPP} \tag{3.2}$$

$$\frac{dP_{PV}}{dV_{PV}} \prec 0 \quad \text{Right side of MPP} \tag{3.3}$$

3.2.2.1.2 Incremental conductance (IC) approach

This approach was first identified in 1983. The definitive version of the conventional incremental conductance computational design was introduced in 1995. This technology involves the controller measuring incremental variations in the voltage and current of the photovoltaic array to predict the impact of changes in voltage. This approach necessitates increased computational time in the controller; however, it can monitor more swiftly fluctuating situations compared to the P&O strategy. It resembles the algorithm used in P&O in its ability to induce stable fluctuations in the generated power[95].

This solution fundamentally utilizes the same approach as P&O to attain MPP; however, it exploits the distinctive relationship of the I-V (current-voltage) graph. This computation comprehends the estimations of voltage and current in photovoltaic cells and calculates the derivatives of photovoltaic cell current (dI) and photovoltaic cell voltage (dV). The photovoltaic current-voltage curve is used to determine the direction of movement at the operating point. The P&O methodology, characterized by moderate uncertainty and enhanced subsequent performance, possesses all the attributes that render it the best-recognized approach in the scientific literature for uniform circumstances. The IC method relies on the condition that the derivative of the output power P concerning the panel voltage V equals zero at the MPP. This approach utilizes the entire dataset to figure out the slope of the system's P-V curve and monitor the maximum power point. If the slope of the P-V curve, or the derivative of the PV array power $\left(\frac{dP}{dV}\right)$, is zero, then only the tracking operation is achieved. Rapidly shifting environmental circumstances complicate the monitoring of the MPP, resulting in an exponential decline in tracking efficiency due to the continual alteration of the P-V curve. Maintaining the operational point under those circumstances is very difficult. Numerous adaptive step size methodologies are being developed to extract the MPP without fluctuations [99],[92],[102]. Figure 3.5 illustrates a flowchart of IC approach and the mathematical formulas for determining the position of the maximum power point on the Power-Voltage (P-V) curve is delineated by equations as follows [92]:

$$P = V * I \tag{3.4}$$

$$\frac{dP}{dV} = \frac{d(VI)}{dV} \tag{3.5}$$

When power is at its highest (peak power point),

$$\frac{dP}{dV}=0,\ \frac{I}{V}+\frac{dI}{dV}=0 \tag{3.6}$$

If the right side of the curve is, where the operational point is located, then

$$\frac{dP}{dV}\prec 0,\quad \text{then if} \tag{3.7}$$

$$\frac{I}{V}+\frac{dI}{dV}\prec 0,\quad \text{V is decreased,} \tag{3.8}$$

$$\text{if } \frac{I}{V}+\frac{dI}{dV}\succ 0,\quad \text{V is increased,} \tag{3.9}$$

If the left side of the curve is, where the operational point is located, then

$$\frac{dP}{dV}\succ 0,\qquad \text{then if,} \tag{3.10}$$

$$\frac{I}{V}+\frac{dI}{dV}\succ 0,\quad \text{V is increased,} \tag{3.11}$$

$$\text{if } \frac{I}{V}+\frac{dI}{dV}\prec 0,\quad \text{V is decreased,} \tag{3.12}$$

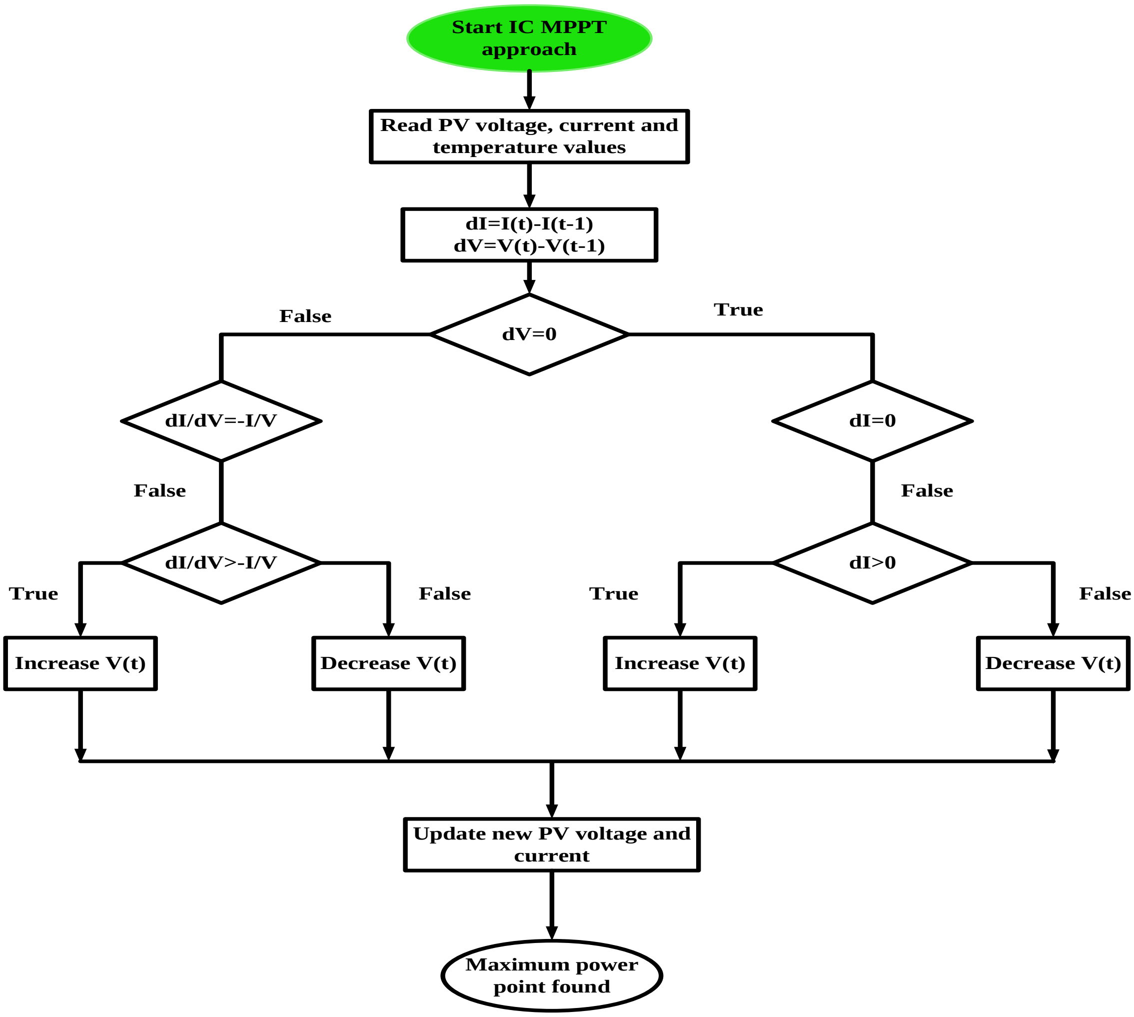

Figure 3.5 : Flowchart of IC approach [92].

3.2.2.1.3 Hill Climbing (HC)

A common approach used in PV systems to increase the output of power is called Hill Climbing (HC) MPPT. The flowchart of this method is illustrated in Figure 3.6 . It involves continuously changing the operating point to determine the maximum power that a photovoltaic module can produce. Changing the duty cycle of the converter is the HC method. It is not exactly the same as P&O, even though it keeps a similar basis. While the hill-climbing approach requires a change in the duty cycle, the perturb and observe approach requires a modification in the terminal voltage in order to use MPPT. As the photovoltaic output varies from its maximum value at any given time, the duty cycle used for the converter's regulation continuously adapts. The alteration of the duty ratio determines the change in the duty cycle direction, which in turn affects the tracking direction on the module's P-V characteristics. The duty cycle is calculated using the formula as follow [91],[86],[92],[99],[97]:

$$D(i) = D(i-1) \pm \text{Step} \tag{3.13}$$

Where Step is the step size, $D(i)$ is the duty ratio at the $i\text{th}$ iteration that controls the converter, and $D(i-1)$ is the duty at the $(i-1)\text{th}$ iteration. Depending on the approach used, the step size S may be preset. Depending on where the power point is on the curve, the step size can be either positive or negative. Step will be negative if power and voltage change, whether for a positive or negative. As shown in Table 3.1, a distinct sign for the power change signifies that Step will be positive.

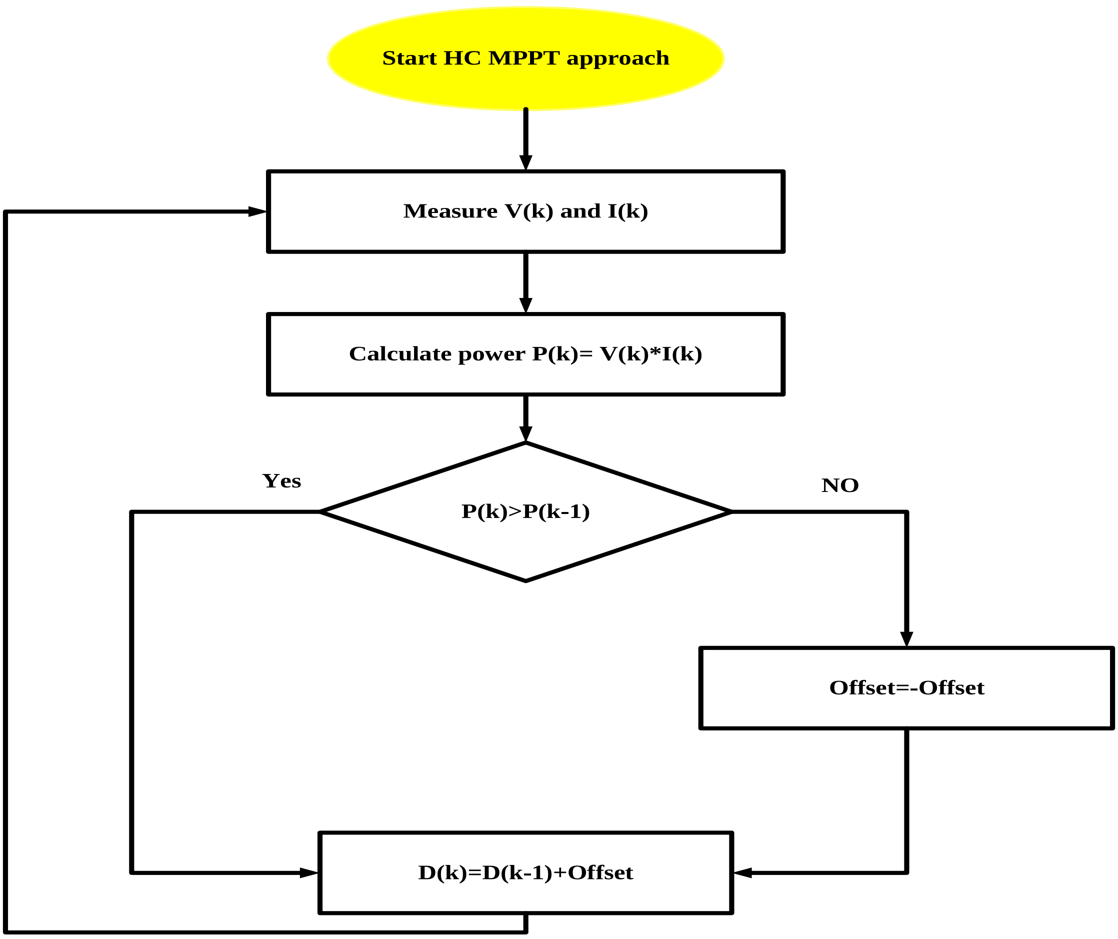

Figure 3.6: Flowchart of HC approach [97].

Table 3.1: The potential differences in the direction of the HC approach [92].

Δ*P*	+	+	-	-
ΔV	-	-	+	-
The perturbation variable's direction	+	-		+

3.2.2.1.4 Constant voltage approach

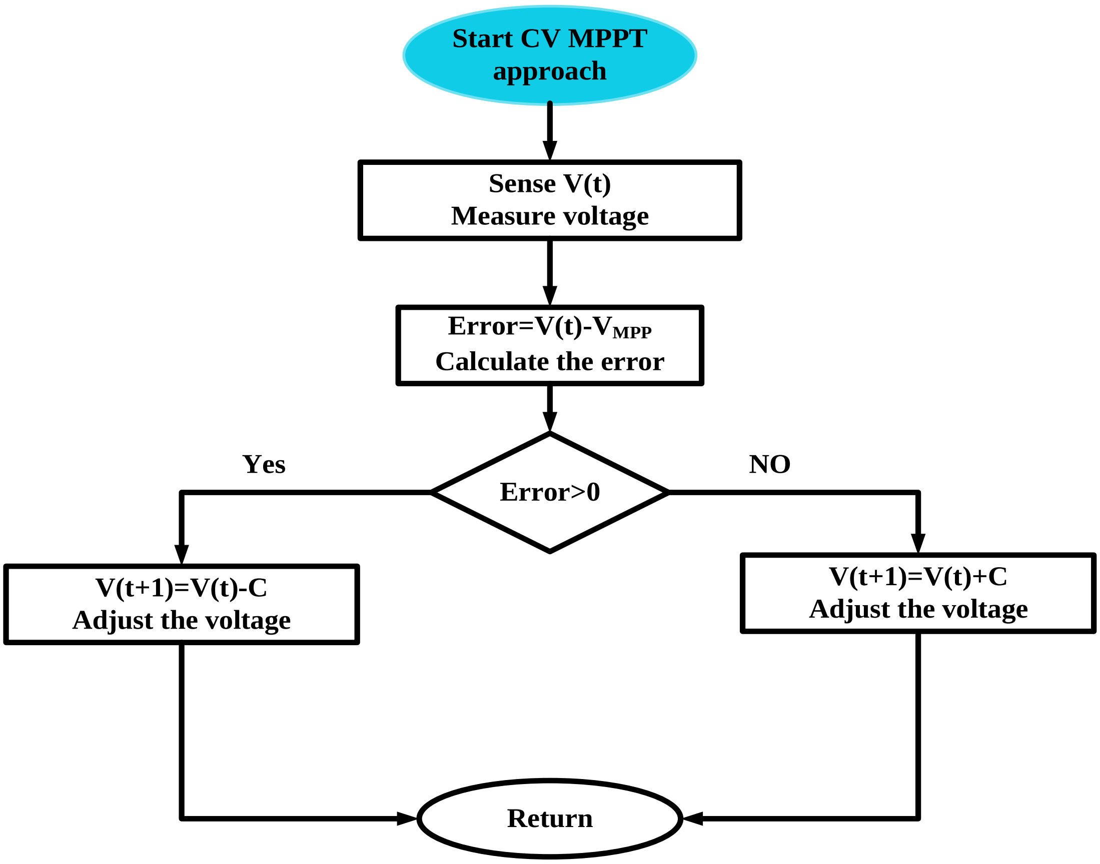

Figure 3.7: Flowchart of constant voltage approach [99].

The most basic MPPT control system is the Constant Voltage (CV) approach, also known as "The Best Fixed Voltage (BFV) Technique." By regulating the solar panel's voltage to maintain a steady reference voltage equal to the feature PV module's VMPP, the PV module's point of operation is kept near the MPP. The fixed voltage range typically ranges from 72% to 80% of the VOC. The CV approach neglects the effects of temperature and irradiance on the module and assumes that the constant reference voltage accurately represents the actual MPP. Consequently, the reference voltage needs to be adjusted for different locations, and the point of operation is not precisely aligned with the MPP. A feedback-controlled loop controls the DC-to-DC converter's duty cycle, and a single voltage sensor in the CV circuit tracks the PV array voltage (V_{PV}). All that is needed to implement constant voltage MPPT control is array voltage monitoring. It can be performed using both analog and digital technology. The given formula, where K is a constant with a range of 0.72 to 0.8, illustrates the relationship between the voltage at the maximum power point (V_{MPP}) and the open-circuit voltage (V_{OC}) and its flowchart is presented in Figure 3.7. The key benefit of the CV strategy is its simple operation, making it inexpensive and suitable for low-efficiency requirements. Its key disadvantage is that it cannot adapt to changing environmental conditions (for example, changing light and temperature), so it extracts less power than more adjustable MPPT techniques. Thus, although P&O and IC may have advantages for some low irradiance situations, the CV method is the most effective. Those methods are commonly pursued as an integrative technology to combine with other MPPT methods; however, the CV method may become less effective in situations where there is significant variation in the amount of light or heat [99],[87],[97],[92],[95],[91].

$$V_{MPP} = V_{OC} \times K \tag{3.14}$$

3.2.2.1.5 Open Circuit Voltage (OCV) approach

The Open Circuit Voltage (OCV) MPPT, an additional offline method, estimates the open circuit voltage is an offline metric that approximates the maximum power point voltage. The correlation between V_{MPP} and V_{OC} is delineated below [92]:

$$V_{MPP} = K_v * V_{OC} \tag{3.15}$$

The K_v constant value is typically established within the range of 0.7 to 0.8 and can be obtained from the manufacturer's data sheet. This technique is predicated on calculation, as indicated in the aforementioned condition. The OCV technique posits that the voltage at the MPP equals the product of the open-circuit voltage of the solar module and the coefficient K_v. The technique's simplicity makes it straightforward to use, but removing the load during each VOC measurement causes problems with the power supply, which lowers system performance. As a result, this approach is not recommended in areas where the load's supply continuity is crucial [91].

3.2.2.1.6 Short Circuit Current (SCC) approach

Similar to the OCV monitoring method, this tracking technique is based on the linear correlation found between the short-circuit current (I_{SC}) and the photovoltaic current at the maximum power point (I_{MPP}). The fill variable, weather, and PV cell design have significant effects on the corresponding constant K_1, as shown in the formula below. The calculated constant for polycrystalline solar panels is roughly 0.85. Usually, a PV test is performed at regular intervals of roughly two minutes to identify the constant. Once it has been received, the system uses the updated estimate until the subsequent calculation is performed. As a result, the control chart and the OCV technique are identical. As a result, this method has the same benefits and drawbacks as the OCV control method. Due to the previously mentioned constraint, this approach is ineffective at the accurate MPP and is instead merely an estimate. This technique performs well for high-voltage, low-current tasks. Furthermore, power loss results from inconsistent I_{SC} assessments required for continuous operation [92],[91].

$$I_{MPP} = K_1 * I_{SC} \tag{3.16}$$

K_v falls between 0.78 and 0.92.

3.2.2.1.7 An approach based on Lookup Table (LT)

The Lookup Table (LT) MPPT strategy uses data that has already been calculated and stored in a lookup table to extract maximum energy out of PV systems. The method generates a table that matches the optimal voltage or current values to obtain maximum power harvesting with different external conditions (e.g., light and temperature). By utilizing the real-time measures for determining the optimum point of operation, the lookup table gives the system the optimum point of operation when it is in operation. One of the benefits of the LT approach is that it has a rapid "response time," which is a result of using predetermined data values rather than intricate real-time calculations. The main problem with this method is that its effectiveness depends on how accurate and reliable the field data used to make it is. The procedure may not work as well if the weather is different from what was used to make the lookup table [99]. The flowchart of this approach is shown in Figure 3.8.

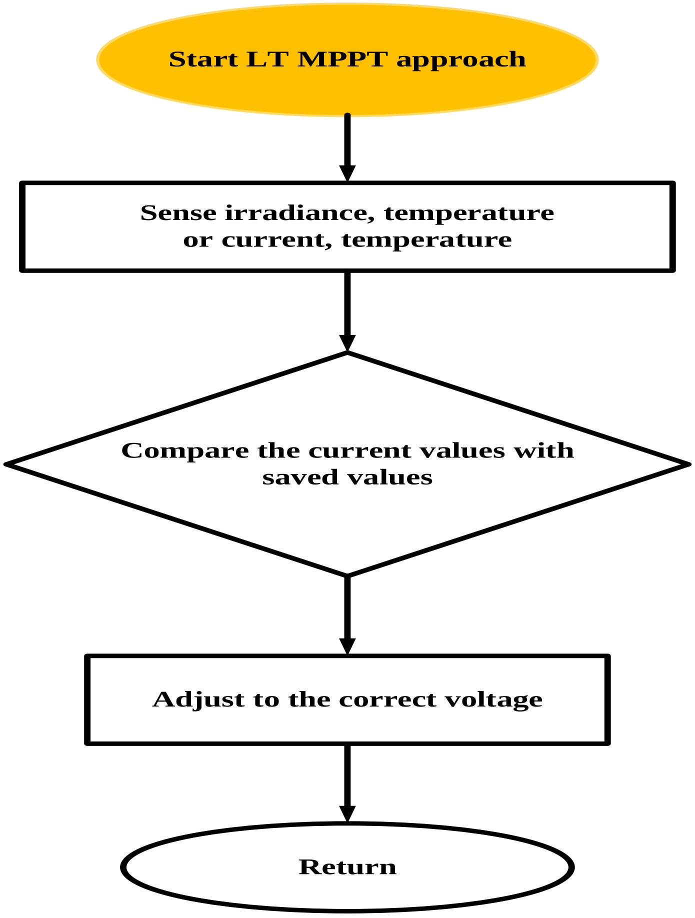

Figure 3.8: Flowchart of LT approach [99].

Table 3.2: Comparison of Conventional approaches [99].

MPPT approach	P&O	IC	HC	CV	OCV	SCC	LT
Cost	Low	Medium	Low	Low	Low	Low	Low
True MPPT	Yes	Yes	Yes	No	No	No	Varies
Speed of tracking	Slow	Medium	Medium	Slow	Slow	Slow	Fast

Circuitry	Digital and analog	Digital	Digital	Analog	Digital and analog	Digital and analog	Digital
Difficulty of implementation	Low	Medium	Low	Low	Low	Low	Low
Accuracy	Medium	Medium	Medium	Low	Low	Low	High
MPP monitoring ability under PSCs	No	No	No	No	No	No	No
sensed variables	Current and voltage	Current and voltage	Current and voltage	Voltage	Voltage	Current	Current, temperature or irradiance ,temperature

3.2.2.2 Advanced MPPT approaches

Advanced MPPT techniques are primarily distinguished by their capacity to learn and adjust to intricate and fluctuating external factors, hence enhancing precision as well as effectiveness in monitoring the MPP relative to conventional methods. They can be classified into three primary categories: intelligent strategies, metaheuristic strategies, and hybrid approaches. Each category has unique benefits and can be chosen according to specific circumstances [99].

3.2.2.2.1 Smart MPPT strategies

The integration of smart strategies in SPV systems has become more realistic and attractive with significant improvements in processing power and cost reductions. Soft computing, or AI MPPT technologies, is prevalent to address the drawbacks inherent in classic approaches, including low tracking speed, steady-state fluctuations, and GMPP tracking under partial shading situations. These approaches have numerous benefits, such as the ability to control function appropriately when handling system nonlinearities and flexibility and also adaptability [103]. The widely used soft computing or artificial intelligence-based strategies for MPPT used in solar systems include fuzzy logic (FL), the Fibonacci series approach, artificial neural networks (ANN), the adaptive neuro fuzzy inference system (ANFIS), and the Bayesian network (BN).

3.2.2.2.1.1 Fuzzy Logic Controller (FLC) approach

Fuzzy logic serves as a connector between human knowledge and linguistic expressions inside a control system. A solar system that enhances MPPT through fuzzy logic is referred to as an intelligent system. Despite the ambiguity of the inputs, the system is capable of tracking. The algorithm's simplicity in modeling mathematically constitutes a significant benefit. Fuzzy logic serves as a connector between human knowledge and linguistic expressions inside a control system. A solar system that enhances MPPT through fuzzy logic is referred to as an intelligent system. Despite the ambiguity of the inputs, the system is capable of tracking. The algorithm's simplicity in modeling mathematically constitutes a significant benefit. To enhance the power output of PV systems, the FLC MPPT method uses a rule-based system to handle data that is uncertain or hard to predict. Due to the use of fuzzy logic, a series of if-then rules determines the appropriate control actions based on the correlations between input variables such as voltage and current and the desired output. There are three steps in the FLC strategy. The first step, fuzzification, transforms numerical data into linguistic values using membership functions. To reach a decision in the second phase, the rule table evaluates these entries. Defuzzification, the last stage, turns linguistic information into exact numerical values. The FLC procedure uses fuzzy rules to assess the rate of power change and the power difference between the previous and the current powers. The feature of the FLC procedure is that it does not rely on an accurate mathematical model of the system to mitigate a wide range of uncertainties and circumstances, whether it be varying illumination or temperature variation. Due to its flexibility, it can adapt to difficult scenarios in addition to partial shading. The major drawback is the complexity of designing and tuning the fuzzy rules that may need extensive expertise. Often used as inputs to the FLC method are the functions for error (E) and change in error (ΔE), and the corresponding equations are given below. In the given formulas, P and V stand for module output power and voltage, respectively, with (n) and $(n-1)$ for the current value and the value from the previous sampling interval, respectively. The control signal is generated in accordance with these formulas in order to maximize power output [99],[101].

$$E(n) = \frac{\Delta P}{\Delta V} = \frac{P(n) - P(n-1)}{V(n) - V(n-1)} \tag{3.17}$$

$$\Delta E = E(n) - E(n-1) \tag{3.18}$$

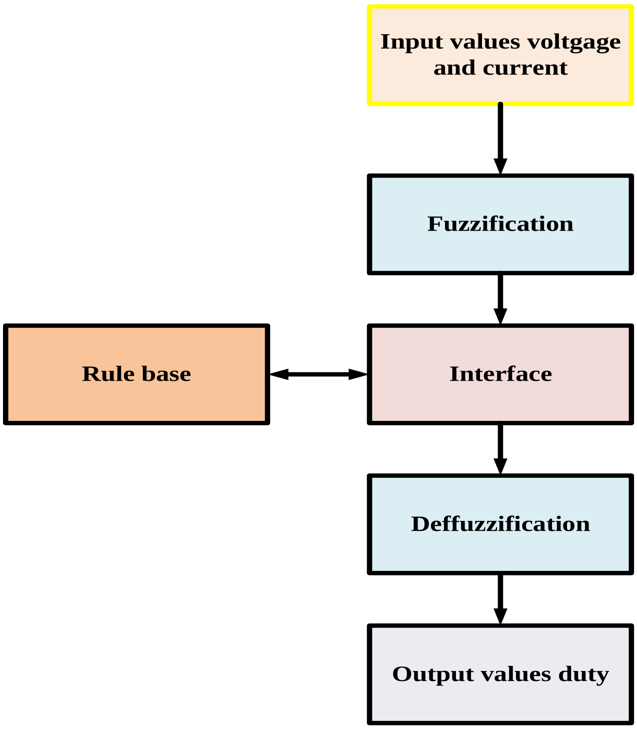

Figure 3.9: Flowchart of FLC approach [99].

3.2.2.2.1.2 Artificial neural network approach

This is the optimal solution for tackling the most intricate issues. The intelligence-driven ANN will effectively accomplish this duty. These applications for ANN will necessitate no comprehensive knowledge regarding the system and mathematical models. This approach enables them to tackle challenges that are far more intricate by precisely defining the input-output system. ANN is an intelligence-driven enhanced MPPT method, owing to the intrinsic characteristics of the method of learning and the biological characteristics of neurons. Artificial Neural Networks (ANN) are a soft-computing methodology modeled after the human central nervous system. To construct a network analogous to a biological neural network, these machine-learning models are depicted with interconnected neurons (artificial nodes). Connection weights are adjusted throughout the training process until the optimal fit, or the reference voltage related to the MPP, is achieved. The ANN methodology is characterized by its structure, which comprises several nodes that are interconnected. As represented in Figure 3.10, three layers are commonly found in these nodes. The input layer is the first layer that represents the area where data is gathered; the hidden layer is the second layer that indicates the area where data requires complicated processing; and the output layer is the third layer that represents the area where results are given out. The variables used as inputs for the ANN MPPT methodology may encompass attributes of the PV array, including PV current (I_{PV}) and voltage (V_{PV}), environmental variables such as solar irradiance (G) and ambient temperature (T), or a combination of both. The outputs generally comprise reference signals, including MPP current (I_{MPP}), MPP voltage (V_{MPP}), or the duty cycle (D) for regulating the DC-to-DC converter. To achieve high accuracy, numerous studies analyzed the use of artificial neural networks for maximum power point tracking. However, in addition to its advantages, ANN MPPT may have some limitations that can affect accuracy and performance. Training must be directly related to the solar energy system and its operational conditions. The ANN will require periodic retraining and validation over a long time (months to years) to achieve point accuracy under differing environmental conditions. More research is needed to determine if the approach developed for one PV system can be utilized successfully for tracking MPPT on another system [92],[103],[91],[97].

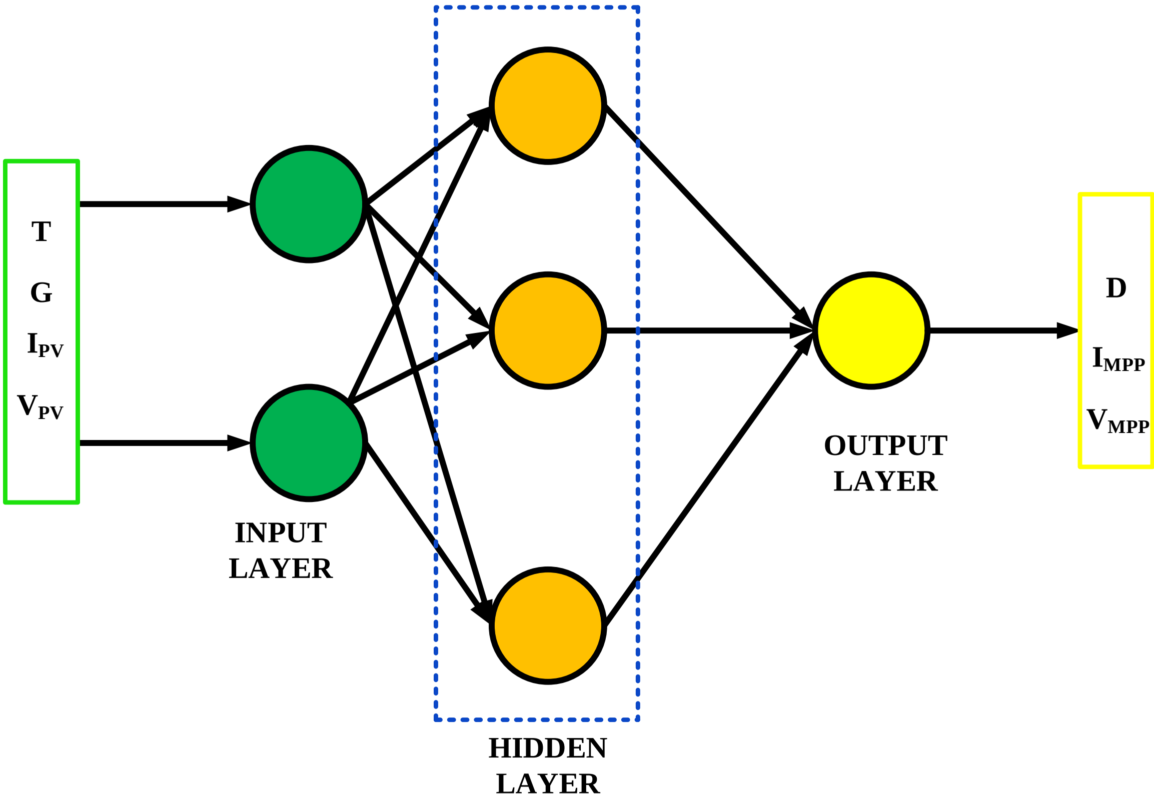

Figure 3.10: The architecture of ANN [99].

3.2.2.2.1.3 Adaptive Neuro Fuzzy Inference System (ANFIS)

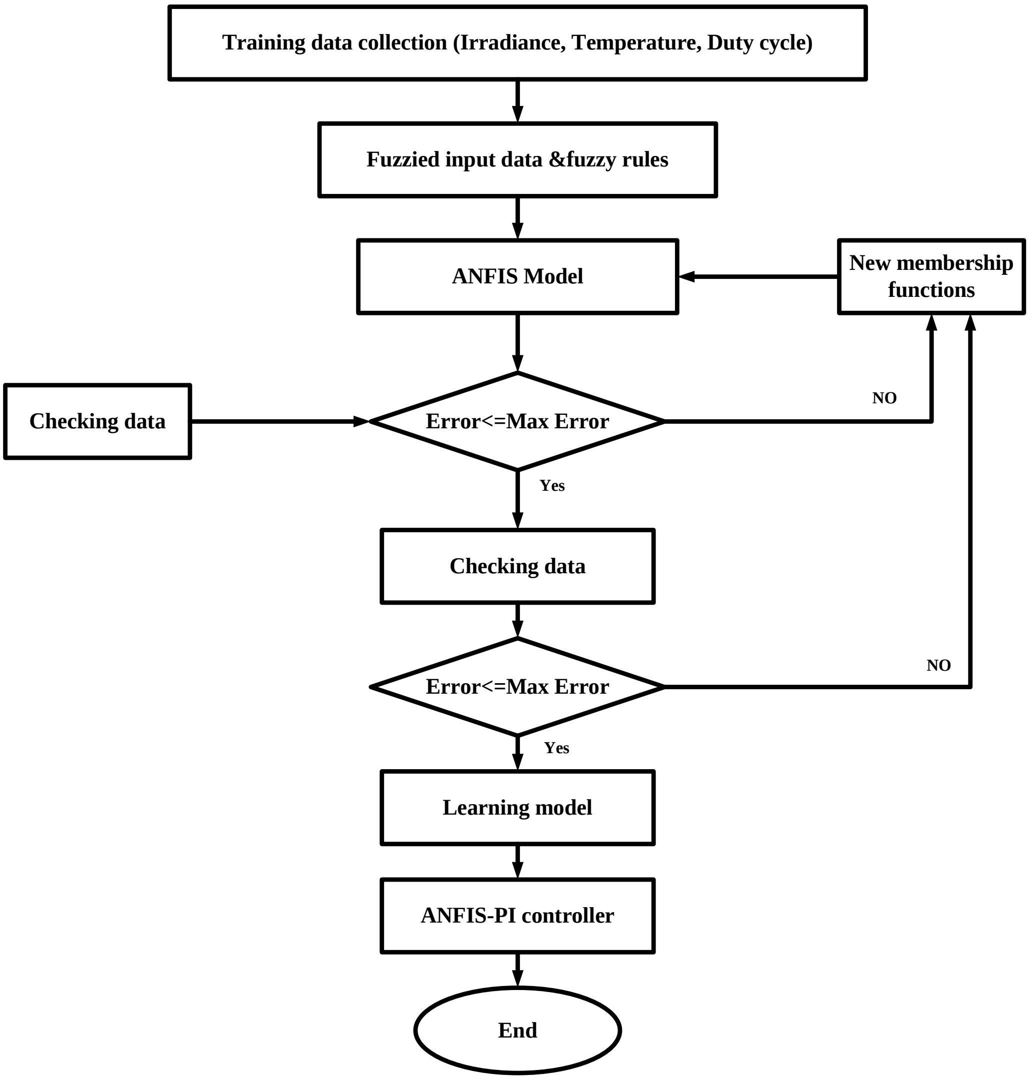

Figure 3.11: The ANFIS approach flowchart [104].

The ANFIS-based controller utilizes two MPPT methods: ANN and FLC, which provide a more efficient integrated MPPT method. It is also implemented in other fields, such as MPPT for PV systems, because of its ability to encompass uncertainty and non-linearity. This method directly generates function memberships yielding fuzzy results using precise input, such as temperature and irradiation, which will ultimately be fuzzified. Therefore, the fuzzy variables obtain a fuzzy output through a compositional method by using a predetermined set of rules that link these inputs to the desired MPPT outcome. Defuzzification converts the ambiguous result into a specific value, and it is usually performed using methods such as the centroid method. To further enhance the system, training strategies, such as backpropagation, are applied by modifying membership functions and rule functions to reduce the difference between the predicted and actual MPP. Iteratively modify the rule base, inference approaches, and membership functions to reduce this outcome, as illustrated in Figure 3.12 . The benefit of the ANFIS-based MPPT technique is its adaptability; the distortions are captured and corrected as it learns, resulting in a robust tracking system, essential when environmental conditions can change quickly. In addition, when comparing ANN and ANFIS approaches, the one that employs ANFIS will provide a lower mean percentage error in the prediction. ANFIS is more qualified because it has a higher accuracy and learning ability, and the predicted data is more accurate when using the maximum volume of inputs. ANFIS integrates data-driven and knowledge-based methodologies. Forecasting utilizing ANFIS, an approach based on data, provides a flow from multivariate data to the output. It is crucial to acknowledge that although the preceding information offers a general outline of the mathematical structure, the complexities of ANFIS, particularly regarding MPPT, are mathematical and can be fairly intricate. The optimization techniques, including genetic algorithms (GA), can be employed to learn the ANFIS membership functions and enhance efficiency. The integration of GA with ANFIS in MPPT applications synergizes the advantages of both methodologies, resulting in enhanced effectiveness and durability of solar power systems [104],[95].The flowchart of the ANFIS approach illustrated in Figure 3.11.

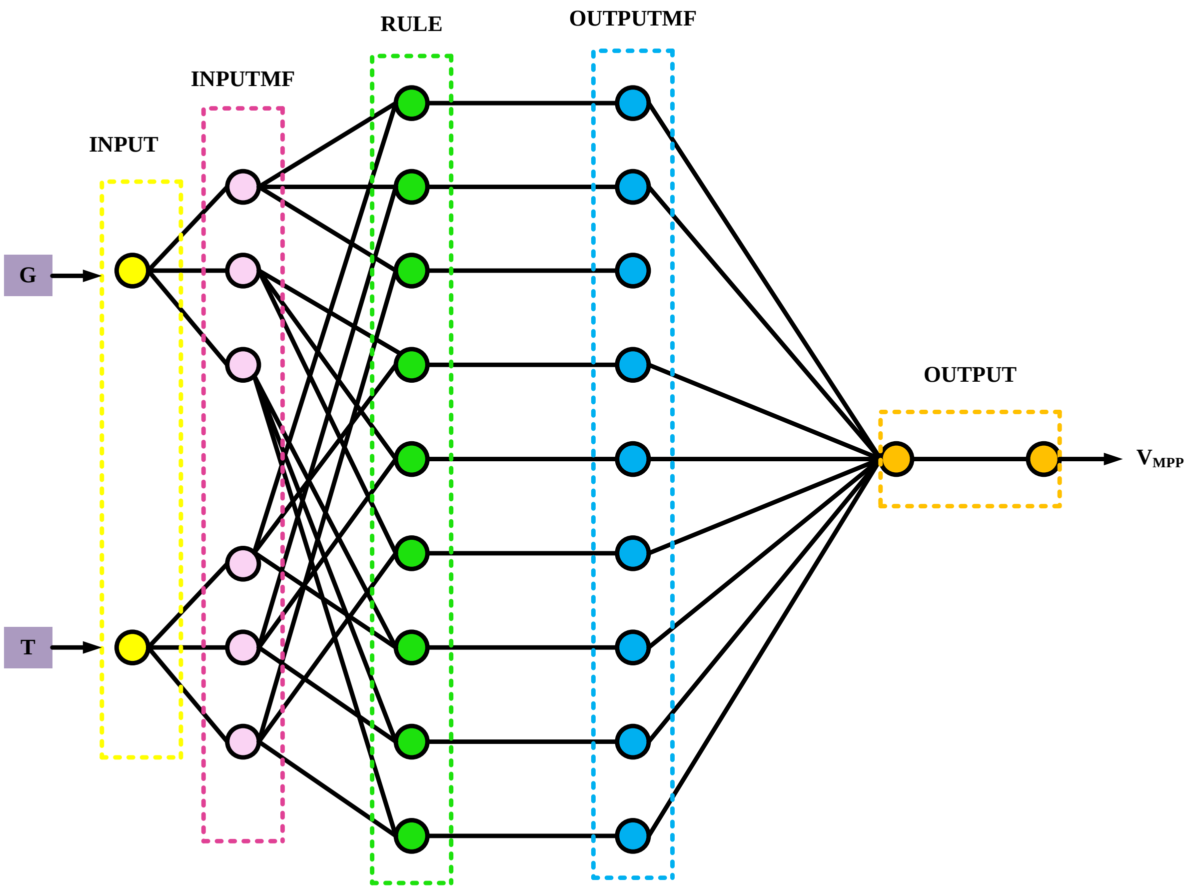

Figure 3.12: The architecture of ANFIS [95].

3.2.2.2.1.4 The Bayesian Network (BN)

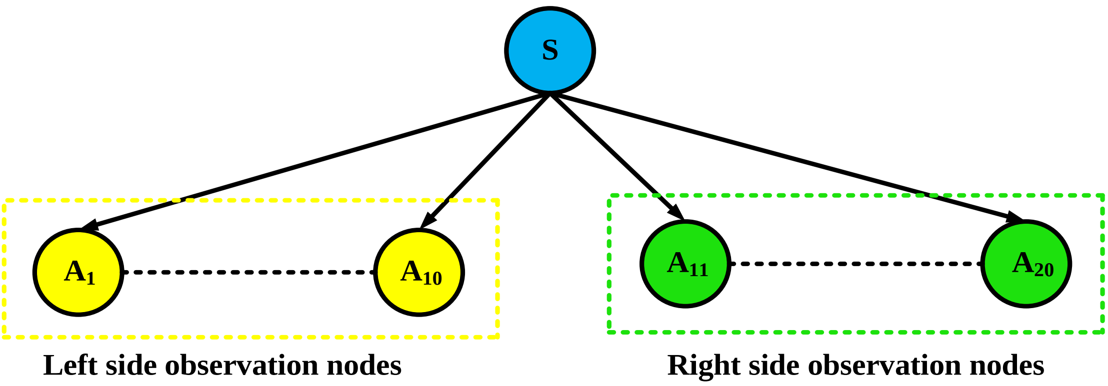

Figure 3.13: The architecture of BN [95].

The Bayesian network (BN), a technique for modeling the probability distribution of multiple random factors used in information fusion, is shown in Figure 3.13. In the literature, Bayesian networks are utilized to pinpoint the exact direction of motion of the output voltages from solar arrays to ascertain the reason for functioning at the MPP [95].

3.2.2.2.1.5 Fibonacci series approach (FS)

To improve the monitoring of the MPP in solar systems, the Fibonacci Series (FS) method of MPPT uses ideas from the Fibonacci sequence, a mathematical series in which each value is the sum of the two preceding values. Similar to interval reducing methods, this approach systematically reduces the area search process for the MPP by modifying the operation's starting point using the Fibonacci increment concept. By reducing the search area with each iteration, this approach has features like simplicity, ease of use, and efficiency in convergence to the MPP. Additionally, it usually avoids oscillations near the MPP, producing dependable results. However, limitations include the ability to converge slowly compared to more sophisticated methods and its vulnerability to changing conditions. To ensure optimal performance in a variety of atmospheric conditions, the FS MPPT procedure requires precise variable adjustment. The repeated sequence is shown in the formula below, where R stands for the PV curve locations that are used to track the MPP [99].

$$R(n+2) = R(n+1) + Rn, (n = 1, 2, 3, \ldots \text{ and } R1 = R2 = 1) \tag{3.19}$$

3.2.2.2.1.6 Gauss Newton approach (GNA)

Compared to similar mathematical calculation algorithms, the GNA has a faster tracking speed and employs a root-locating technique. The method determines the direction and number of iterations required to solve the controlling formula by using both the first and second derivatives of the power change. Its complex construction, which comes from the sophisticated computational modeling required, is its drawback. Further studies in this field can simplify all of this complexity [91].

Table 3.3 : Comparison between smart MPPT strategies [99],[92],[95].

Approaches	**Measured Metrics**	**Type of circuitry**	**Cost**	**Accuracy**	**Speed of monitoring MPP**	**True MPPT**	**Difficulty of Application**
ANN	Voltage and current	Digital	Medium	Medium	Medium	Yes	Medium
ANFIS	Voltage and current	Digital	Medium	High	Medium	Yes	Medium
FLC	Voltage and current	Digital and analog	Low	Medium	Slow	Yes	Low
BN	Voltage and current	Digital	High	High	Medium	Yes	High

FS	Voltage and current	Digital	Medium	Medium	Medium	Yes	Medium
GNA	Voltage and current	Digital	High	High	Medium	Yes	High

3.2.2.3 Metaheuristic MPPT approaches

Advanced solutions for solar system optimization are offered by metaheuristic MPPT techniques, particularly in circumstances where standard approaches might not work. They are a vital tool for maximizing the efficiency of PV systems because of their capacity to handle complexity, variable conditions, and multiple objectives [99].

3.2.2.3.1 Social spider strategy for optimization

A meta-heuristic swarm optimization technique that incorporates cooperative social-spider behavior was introduced in [105]. The social spider optimization strategy (SSOS) aims to imitate spider interactions while adhering to the bio-inspired principles of spider populations. Because of interpersonal interactions among swarm members, a colony of social spiders can work in a dispersed fashion while remaining coherent. SSOS proposes that the entire world operates as a network in which spiders communicate by vibrations influenced by their weight and proximity to one another. In contrast to other swarm-based optimization approaches, the algorithm searches with two independent agents, separated by the spider's sex. Each agent group exhibits diverse behaviors and is distributed 65% to 90% in favor of females within the colony.

3.2.2.3.2 Zebra optimization algorithm

Similar to locating a MPP on the PV curve, Metaheuristic Optimization Algorithms carry out a generalized search for an optimal solution inside a specified space. Under PSCs, a novel zebra optimization technique (ZOA) is presented in [106]; it is a well-known nature-inspired heuristic optimization approach with broad applicability, robust adaptability, high efficacy, and global optimization potential. In real-world applications, these techniques are acknowledged for their effectiveness and dependability. Zebras are considered both potential solutions to the problem and members of the population in ZOA. Their quest for food and protection from predators are examples of their innate social behavior. Each zebra mathematically represents a potential solution within the search region. The values of the selection criteria determine each zebra's location within the search space. As a result, each zebra in the ZOA can be represented by vectors. Within ZOA, each zebra can be represented as a vector, with the components of the vector representing the values of the variables that need to be optimized in order to arrive at the best possible solution.

3.2.2.3.3 Snake optimization algorithm (SOA)

Fatma introduced the SOA metaheuristic technique in 2022 [107], which mimics snake mating behavior to solve various optimization challenges. When food is abundant and temperatures are low, both male and female snakes compete for the best mates. This study presents a simple and effective optimization strategy that involves quantitatively simulating and modeling dietary and reproductive behaviors and patterns. Snake reproduction is influenced by mating seasons, cold temperatures, and food availability; when these conditions are met, rival males will compete for the female's attention. It is up to the female to decide whether or not to reproduce. Nonetheless, if any of these elements are missing, the snakes will seek or eat the available food. This strategy, known as the search process, comprises two stages: exploration and exploitation. In the interest of curiosity, the snakes will investigate environmental conditions, such as seeking a cooler habitat, and if there is no food, they will begin foraging. In terms of exploitation, if food is available, snakes will check the temperature to see if it is hot or cold; if the temperature is high, they will focus completely on digesting the current meal. Mating will occur when food is available and the temperature is low. As a result, each male will compete to find the most attractive female, while each female will try to find the most notable man. During the mating season, each pair will reproduce based on the availability of food resources. If copulation occurs within the allotted region, the female may lay eggs, which will eventually hatch into baby snakes [108].

3.2.2.3.4 Coot optimization approach

Iraj Naruei proposed the Coot Optimization strategy (COS) in 2021[109]. It is acknowledged as one of the metaheuristic optimization techniques that draws inspiration from the collective behavior of water birds belonging to the Rallidae family of rails and coot swarms. In order to mimic the foraging behavior of coot swarms, the algorithm simultaneously creates an imitation population of coots and adjusts their locations based on a set of rules. The two distinct movement patterns that bird's exhibit on water surfaces—erratic movements in the first phase and regular movements in the second phase—are replicated by the COS. As a result, four types of coot motions on the water surface are considered: random motion, chain motion, group leader positional changes, and leader movement to direct a group to the best positions [110].

3.2.2.3.5 Rat optimization approach (ROA)

A biologically inspired optimization technique, the rat swarm optimizer method was initially introduced in 2020. The main source of motivation for this algorithm is the aggressive and predatory behavior of rats in their natural habitat. Known for their aggressive nature, rats are naturally socially complex animals that engage in activities like jumping, chasing, and fighting. The main motivation for this effort is the violent behavior displayed during the hunt and battle with the prey. Rats attack their prey collectively because of their social nature. Mathematically, this behavior is described by the assumption that the best search agent knows where the prey is, and other search agents can modify their placements according to the best search agent found so far [111].

3.2.2.3.6 Falcon optimization approach

Metaheuristics are algorithms inspired by nature that are used to approximate difficult optimization problems. Patterns of animal swarming behavior, like those exhibited by ants, cuckoos, bees, pigeons, and bats, have been used by metaheuristic algorithms. Among the remarkable properties inherent in metaheuristics are identity, flexibility, illation-free instruments, and the ability to avoid local optima. The hunting behavior of a falcon served as the inspiration for the metaheuristic approach put forth by [112]. An efficient method for handling stochastic population-based problems is the falcon optimization approach (FOA), which is a three-phase process that necessitates adjustments to a large number of parameters. The hunting strategy employed by falcons in flight to locate prey served as the model for the suggested method. To meet their unique dietary requirements, reclusive falcons modify their hunting tactics. Consequently, novel strategies are developed, and outstanding models uphold flight-related presumptions. According to Tucker, among birds, falcons are the best flyers. Appropriate targets are examined at various phases of advanced hunting to determine if they surpass the requirements for aerial success. The falcon is one of the fastest animals on the planet; reports of its stoops reaching 200 mph (320 km/h) have been made. A system of tiny tubercles in their beaks facilitates easy breathing for falcons. They control the flow of air through ducts with high velocity. Hunting is mostly done during the day, including in the morning and evening. Small and medium-sized birds and invertebrates such as locusts, worms, grasshoppers, and crickets constitute the majority of their diet. The falcon uses various techniques to get to its target. Each trajectory's first segment is a logarithmic spiral where the falcon maintains a remarkable level of precision in keeping its head in line and its eyes on the prey; the second segment is a linear path where the falcon moves straight toward the prey and descends when it is in sight. Therefore, there are three phases to the mechanism that a falcon uses to move. In phase 1, the falcon hunts for prey; in phase 2, it extends its dive in a logarithmic spiral; and in phase 3, it completes the dive, which may or may not lead to a successful prey catch. A falcon's behavior rapidly adapts to its experiences under various circumstances [113].

3.2.2.3.7 Dung beetle approach

A novel MPPT technique for PV systems using the Dung beetle approach (DBA) method was presented, which was inspired by the movement, foraging, stealing, and reproduction behaviors of dung beetles. The rolling ball behavior, such as moving the manure ball to the best storage location, is indicated by the global search in the DBA technique. Local searches, such as breeding, foraging, and thieving, are then used to move around the storage balls and further explore the best placement. The dung beetle MPPT controller works by first establishing the dung beetle population, then evaluating the fitness values of different populations, and finally identifying the best individuals. Each subgroup was then subjected to cooperative optimization. The rolling dung beetle and the dancing dung beetle were hunted all over the world. Breeding and foraging dung beetles conducted the local search, minimizing the search range by dynamically modifying the mating and habitats in response to changes in R variables. To improve tracking effectiveness, thief dung beetles look for the best foraging sites[43].

3.2.2.3.8 Atomic orbital search approach

In quantum chemistry, atomic orbital search (AOS) approach is a computer technique used to ascertain the electrical makeup of atoms and molecules. The AOS method depends on the Schrödinger formula's resolution, which describes how electrons move through a system. For most relevant systems, the Schrödinger equation is a partial differential equation that cannot be solved exactly. As a result, the AOS approach is one of the estimated approaches used to solve the problem. The AOS method starts with the assumption that a linear combination of atomic orbitals (LCAO), which are the solutions to the Schrödinger model for solitary atoms, can be used to express the wave function of the system. Another name for these atoms' orbitals is fundamental functions. The secular formula, a matrix equation, is then solved to determine the values of the LCAO's coefficients. Using the variable concept and the LCAO ansatz, the secular formula is derived from the Schrödinger problem. The variational notion states that when the function of waves is chosen from a set of functions called experiment variables, the energy of the system falls. The initialization phase and the self-consistency phase are the two stages of the AOS method. In the startup stage, the secular equation is solved for the first time and the atomic orbitals are chosen. The secular formula is iteratively resolved during the self-consistency phase until the LCAO parameters converge to a predetermined threshold. In the AOS method, the choice of atomic orbitals is essential since it affects the calculation's accuracy and efficiency. Gaussian-type orbitals (GTO) are the most commonly employed types of atomic orbitals. GTOs are functions, which involve multiplying the Gaussian function times a polynomial. GTOs are used for their convenience, flexibility, and mathematical simplicity. GTOs can describe valence and core orbitals, and are very easy to integrate. Another popular choice are Slater-type orbitals (STO), which are defined by a polynomial multiplied by a radial function. Despite having less flexibility than GTOs, STOs are more physically motivated. An efficient tool for determining the electronic structure of atoms and molecules is the AOS algorithm. It has been used to study a wide range of systems, including solids, big biomolecules, and small molecules. The method is very compatible with parallel computing and is relatively easy to implement. However, the AOS algorithm has a number of shortcomings. Its dependence on the LCAO approximation, which might not be accurate for systems with strong electron correlation, is its main drawback. The AOS method's high computational overhead makes calculations time-consuming for large systems, which is another disadvantage. To sum up, the atomic orbital search process is a useful computer method used to ascertain the electrical makeup of atoms and molecules. The approach is based on solving the Schrödinger equation and using the LCAO approach, which comprises choosing atomic orbitals, resolving the secular equation, and performing a self-consistency step. An electron's transition between various orbitals when its energy levels fluctuate is analogous to the quantum staircase. An electron moves to a higher energy level in the outer orbital when it absorbs energy below its binding threshold. An electron moves to a lower level of energy within its orbital if it absorbs more energy than its binding threshold [45]. Table 3.4 presents a comparison of metaheuristic MPPT techniques.

Table 3.4 : Comparison between Metaheuristic MPPT approaches.

MPPT approaches	**Approach type**	**Measured Metrics**	**Type of circuitry**	**Cost**	**Accuracy**	**Tracking Speed**	**Tree GMPP in shading**	**Complexity of application**
SSOS	Swarm-intelligence	Voltage and current	Digital	Medium	Very high	Very Fast	Yes	High
ROA	Swarm-intelligence	Voltage and current	Digital	Medium	Very high	Fast	Yes	Medium-high
ZOA	Bio-Inspired	Voltage and current	Digital	Medium	High	Medium-Fast	Yes	Medium-high
SOA	Bio-Inspired	Voltage and current	Digital	Medium	Very high	Very Fast	Yes	High
FOA	Bio-Inspired	Voltage and current	Digital	Medium	High	Medium-Fast	Yes	High
DBA	Bio-Inspired	Voltage and current	Digital	Medium	High	Medium	Yes	Medium
COS	Swarm-intelligence	Voltage and current	Digital	Medium	Very high	Very fast	Yes	High
AOS	Physics-Based	Voltage and current	Digital	Medium	High	Medium	Yes	Medium

3.2.2.4 Hybrids MPPT approaches

Hybrid MPPT approaches combine various MPPT strategies to enhance PV systems' performance and adaptability in complex or rapidly fluctuating conditions. These approaches outperform standalone algorithms in tracking speed, accuracy, and maximum power point identification under partial shade. Hybrid approaches are commonly used for determining the MPP under partial shading, as both approaches benefit from their effective integration [101],[99].

3.2.2.4.1 Grey Wolf Equilibrium Optimization (GWEO) approach

Similar to determining the MPP on a PV curve, the goal of meta-heuristic optimization techniques is to identify the optimal solutions within a specified search space. Grey Wolf Equilibrium Optimization (GWEO) is a novel hybrid approach that skillfully combines the benefits of Equilibrium Optimization (EO) and Grey Wolf Optimization (GWO) methodologies. GWO is good at moving through the solution space, but it lacks a random perturbation process, which could lead to a halt at local optima. On the other hand, EO has a narrower search space and less exploration power, but compensates by employing a random perturbation approach that enhances its ability to avoid local optima. The hybrid GWEO technique creates a balanced methodology by combining the unpredictability of EO with the organized exploration capability of GWO. Throughout optimization, GWEO's improved population updating technique continuously adjusts the balance between exploration and exploitation. This flexibility guarantees that even in intricate, dynamic environments, the approach retains a high tracking efficiency. In terms of convergence speed, robustness, and electricity generation efficiency, the combined method performs better than either GWO or EO alone. Furthermore, by combining the benefits of its predecessor techniques while maintaining lower variable difficulty and attaining faster convergence, GWEO outperforms conventional techniques like GA, PSO, and EA. This makes GWEO a useful tool for solving the MPP problem in dynamic PV systems since it enables it to generate a variety of non-dominated solutions. The combination of GWO and EO represents a significant breakthrough in PV system optimization by demonstrating the causal relationship between their synergistic abilities and the increased effectiveness of the MPPT strategy [114].

3.2.2.4.2 FLC-P&O approach

The FLC-P&O hybrid approach to improve MPPT in PV systems by combining the P&O method with fuzzy logic control (FLC). The FLC increases the system's responsiveness to changing external conditions, such as fluctuating temperature and irradiance, by adaptively adjusting the perturbation step size in response to system inputs, such as changes in power and voltage. The P&O technique perturbs and monitors power fluctuations to modify the voltage to follow the MPP once the fuzzy controller has established the optimal step size. The combined approach shows better flexibility in response to changing conditions, reduces oscillations around the MPP, and increases tracking accuracy. However, it adds complexity, requires careful fuzzy rule adjustment, and uses more computer power, making it more resource-intensive than less complex methods [115].

3.2.2.4.3 Artificial Bee Colony-Perturb and Observe (ABC-P&O) approach

In order to optimize the tracking of the GMPP in a photovoltaic system, this work proposes a hybrid approach that combines the well-known perturb and observe method with the artificial bee colony (ABC) algorithm. By adjusting the reference voltage while keeping an eye on the photovoltaic system's output power, the P&O method aims to create fluctuations. The voltage reference adjustment continues in the same direction if the current measured power $P(n)$ is greater than the previous sampled value $P(n-1)$. On the other hand, it is reversed. To determine the MPP, the PV module's voltage is compared to the maximum voltage. A small change in the reference voltage causes the photovoltaic module's power to increase. The &O technique is used by the proposed MPPT algorithm both at system startup and when there is constant solar radiation. Additionally, dynamic step adjustments are made to the reference voltage to reduce low power oscillations in the steady state and enable quick tracking of the MPP during transients. On the other hand, the foraging habits of honeybee colonies serve as the model for the ABC. The ABC algorithm serves as a new method for determining the photovoltaic module's MPP in the presence of constant illumination. The ABC is only used in the ABC-P&O strategy when there are irradiance variations in order to determine the voltage reference that initiates the P&O approach for GMPP [116]. The Table 3.5 summarizes the performance metrics of recent and common hybrid MPPT strategies, while Table 3.6 presents a comprehensive comparison between the performances of different MPPT categories.

Table 3.5: Comparison between hybrid MPPT strategies.

MPPT approaches	**Measured Metrics**	**Type of circuitry**	**Cost**	**Tracking Speed**	**Tree GMPP in shading**	**Complexity of application**	**Accuracy**
FLC-P&O	Voltage and current	Digital	Low-Medium	Medium-Fast	Not exact (partial)	Medium	High
ABC-P&O	Voltage and current	Digital	Medium	Fast	Yes	Medium-High	Very high
GWOE	Voltage and current	Digital	Medium-High	Very Fast	Yes	High	Very high

Table 3.6: Comprehensive comparison between the performances of different MPPT categories.

Category	**MPPT strategy**	**Steady-state oscillation**	**Convergence speed**	**Effectiveness in uniform Shade**	**Effectiveness in partial Shade**	**Complexity**
Classical approaches	**P&O**	High	Medium	Medium-high	Low	Low
	IC	Low	Medium-Fast	High	Low	Low-medium
	HC	High	Medium	Medium	Low	Low
	CV	Very low	Very fast	Low-Medium	Low	Low
	OCV	Very low	Slow-medium	Medium	Low	Low
	SCC	Very low	Fast	Medium	Low	Low
	LT	Very low	Fast	Medium-high	Medium	Low-medium
Smart	**ANN**	No oscillation	Very fast	Very High	Very high	Medium
	ANFIS	No oscillation	Very fast	High	High	High
	FLC	Low	Fast	High	Medium	High
	BN	No oscillation	Fast	High	Very high	High
	FS	Very low	Medium-Fast	High	Medium	High

	GNA	Very low	Fast	High	Very high	High
Metaheuristic	**SSOS**	Very Low	Very fast	Very High	Very High	Low
	ROA	Very Low	Fast	High	High	Low
	ZOA	Low	Medium-Fast	High	High	Medium
	SOA	Very low	Very fast	Very High	Very High	Low
	FOA	Low	Medium-Fast	High	High	Medium
	DBA	Medium	Medium	High	Medium	High
	COS	Very low	Very fast	Very High	Very High	Low
	AOS	Medium	Medium	Medium	Medium	High
Hybrid	**FLC-P&O**	Very low	Medium-Fast	High	High	Medium
	ABC-P&O	Low	Fast	High	Medium	Medium
	GWOE	Very low	Very fast	Very high	Very high	High

3.2.3 An overview of MPPT control of PEMFC

Among the various fuel cell technologies, proton exchange membrane fuel cells (PEMFCs) have been the subject of current research. The most common type of fuel cell that uses hydrogen gas as fuel is the proton exchange membrane fuel cell (PEMFC) [55].

Despite its significant efficiency, the fuel cell's power output is not always ideal because of its variable internal components. To ensure optimal power harvesting, a maximum power point tracking technique via the power electronics interface is required. The use of PEMFCs in hybrid standalone systems is the primary focus of the current study. Therefore, the control mechanisms used in producing electricity are the focus of our studies. Depending on whether the fuel cell serves as a primary or secondary energy source, different control objectives apply. As the main source, the control system aims to give the grid or load a steady voltage and frequency. On the other hand, controlling power flow to satisfy system demand is the goal when acting as a backup source. The PEMFC is introduced in this thesis as an additional power source that guarantees steady output power in accordance with a specified reference. For this goal, this literature has proposed a number of control techniques, which will be looked at in the next section, as detailed in Table 3.7 .

3.2.3.1 Jaya MPPT approach

A recently developed meta-heuristic method for handling complex, non-linear, constrained optimization problems is the Jaya approach. The two main parameters used in this method are "number of iterations" and "population size," which sets it apart from other heuristic approaches. The application of the Jaya strategy is simple and straightforward because these parametric values are easily defined for any optimization issue [60].

In the MPPT monitoring of the fuel cell, the amount of electricity produced by the P_{FC} is considered the objective function.

First, a random population set of size (n) that corresponds to the duty cycle is created, $D = \{d_1, d_2, ..., d_n\}$. FC measurements for a particular set of duty cycles D are used to calculate the power output P_{FC}. Candidates with optimal and suboptimal function values are assigned using two range parameters, d_{best} and d_{worst}, respectively. The population set is updated using the best and worst options in every cycle. The following is the update rule for the i^{th} candidate in the k^{th} iteration of the Jaya method

$$d_i^{k+1} = d_i^k + r_1\left(d_{best} - d_i^k\right) - r_2\left(d_{worst} - d_i^k\right) \tag{3.20}$$

$$d_i^{k+1} = \begin{cases} d_i^{k+1}, iff \ \left(d_i^{k+1}\right) > f\left(d_i^k\right) \\ d_i^k, iff \ \left(d_i^{k+1}\right) \le f\left(d_i^k\right) \end{cases} \tag{3.21}$$

Actual and updated values are denoted by d_i^k and d_i^{k+1} in this context, while optimal and suboptimal solutions among all options are denoted by d_{best} and d_{worst} ; r_1 and r_2 are stochastic numbers between 0 and 1. $r_1\left(d_{best} - d_i^k\right)$ Indicates the solution that is closest to optimality, while $r_2\left(d_{worst} - d_i^k\right)$ indicates the least desirable solution that should be shunned. When either the maximum iteration limit is reached or the difference between the optimal and suboptimal values of $\left(d_{best} - d_{worst}\right) <\in$ is determined, the termination process begins [60]. The jaya approach is detailed in flowchart below.

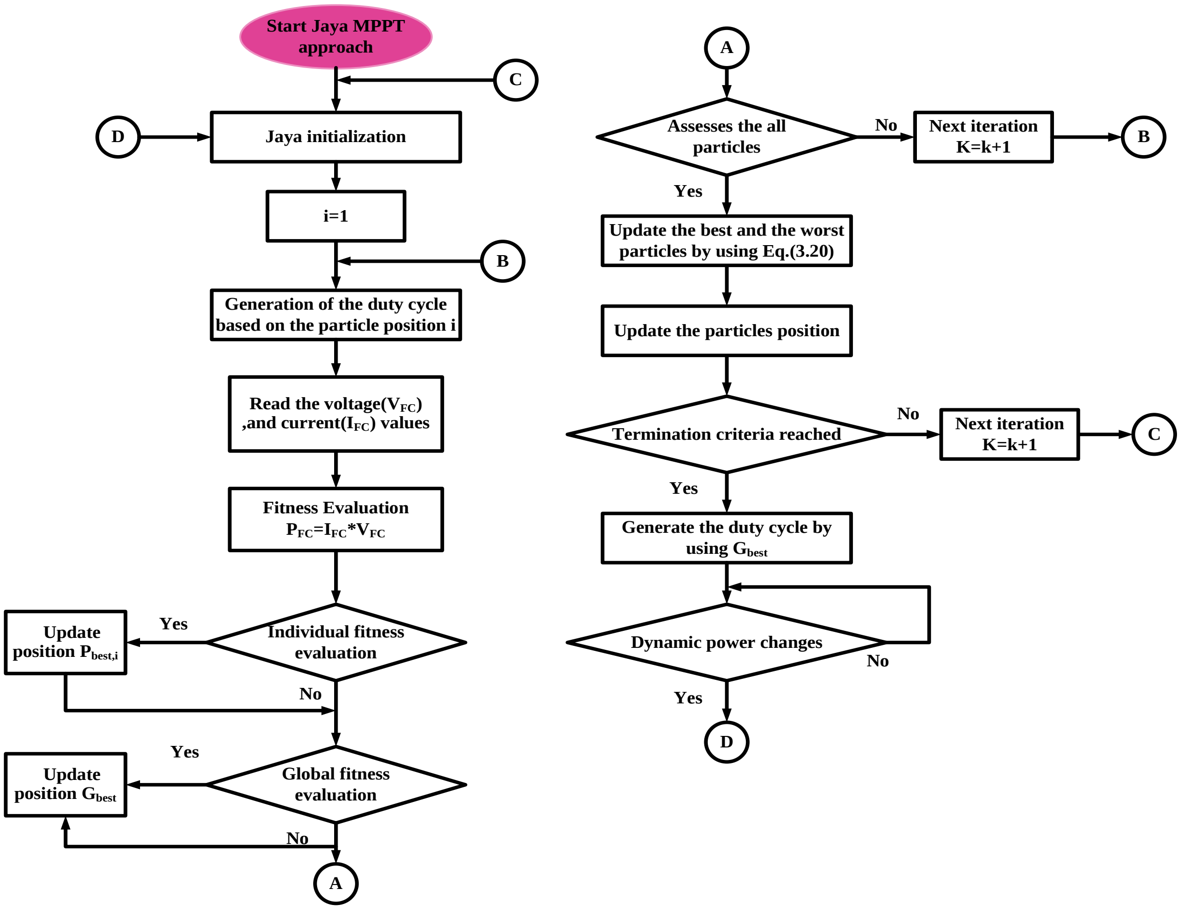

Figure 3.14: The flowchart of Jaya MPPT approach [60].

3.2.3.2 Modified PSO MPPT approach

In 1995, Kennedy and Eberhart presented a population-focused PSO approach. An intelligent optimization technique called particle swarm optimization (PSO) mimics the cooperative behavior of flocks of fish or birds. The PSO algorithm's design is based on how living things interact with one another, both singly and in a swarm. Because of its straightforward algorithmic structures and quick convergence rates, which can be readily controlled by a small number of variables, this population-based optimization technique is frequently used by researchers in both academic and industrial settings. Each swarm is referred to as a particle in the PSO algorithm, which moves with a particular velocity in order to determine the global optimum position in the optimization process. The ideal particle in the vicinity, known as P_{best} , dictates the particle's location. The ideal particle, known as G_{best} , was generated by every particle. The location of the particle X_i is updated as [117]:

$$X_i^{k+1} = X_i^k + \theta_i^{k+1} \tag{3.22}$$

Where the velocity element that determines the perturbation size is denoted by θ_i .

The following process is used to evaluate the speed:

$$\theta_i^{k+1} = w\,\theta_i^k + C_1 R_1 \left[P_{besti} - X_i^k \right] + C_1 R_2 \left[G_{best} - X_i^k \right] \tag{3.23}$$

Let $i = 1, 2, ...N$, where N the size of the swarm is, C_1 and C_2 are the velocity factors, w is the inertia weight, and R_1 and R_2 are random factors. The global optimal position is represented by G_{best} , while the specific optimal position is indicated by $\in U(0,1)$, P_{besti} . Formula (3.24) can be expressed as follows if a location replaces the duty cycle and the step size indicates velocity:

$$d_i^{k+1} = d_i^k + \theta_i^{k+1} \tag{3.24}$$

In formula(3.23), the inertia weight diminishes linearly from $w_{\max}$ to $w_{\min}$. Adjust the inertia weight using formula(3.25).

$$w^k = w_{\max} - \left((w_{\max} - w_{\min}) * k \right) / k_{\max} \tag{3.25}$$

The maximum number of iterations is denoted by $k_{\max}$, where k is the number of iterations. The Figure 3.15 is illustrated the flowchart of the modified PSO approach.

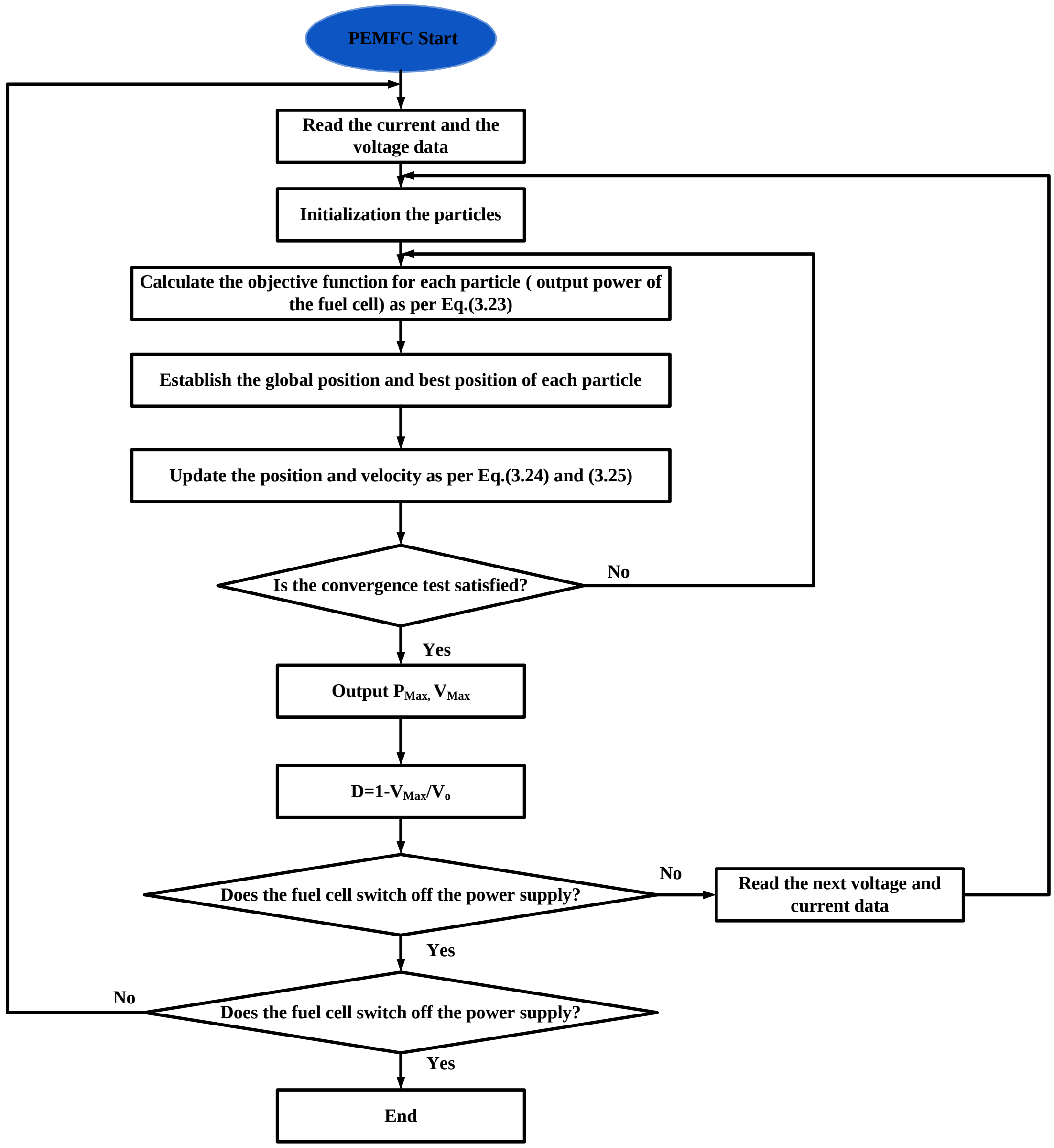

Figure 3.15: The modified PSO flowchart [117].

3.2.3.3 Adaptive Genetic Algorithm-Based ANFIS MPPT approach

One crucial component of converter-powered green power systems is the ability to track the maximum power point. The fuel cell stack's nonlinear properties have a direct impact on how the electric vehicle system that depends on it operates, and it produces variable output power that is dependent on operating temperature conditions. To improve the electric vehicle system's power supply rating, the adaptive genetic algorithm-based ANFIS technique is used. The recommended controller works in three stages: first, it determines the fuel stack's ideal voltage under various temperature conditions; second, it trains the ANFIS controller using a suitable dataset; and third, it generates switching signals for the DC-DC converter. The dataset for the ANFIS controller is obtained using the back propagation algorithm (BA). The ANFIS controller can monitor any local MPP of the fuel stack system under various operating temperature conditions thanks to the BP data training technique. The fuel stack system datasets are trained using the AGA concept in order to provide duty pulses for the boost converter using the ANFIS technique. The greatest power output of this proposed method offsets its drawbacks, which include increased design difficulty and higher implementation costs [118].

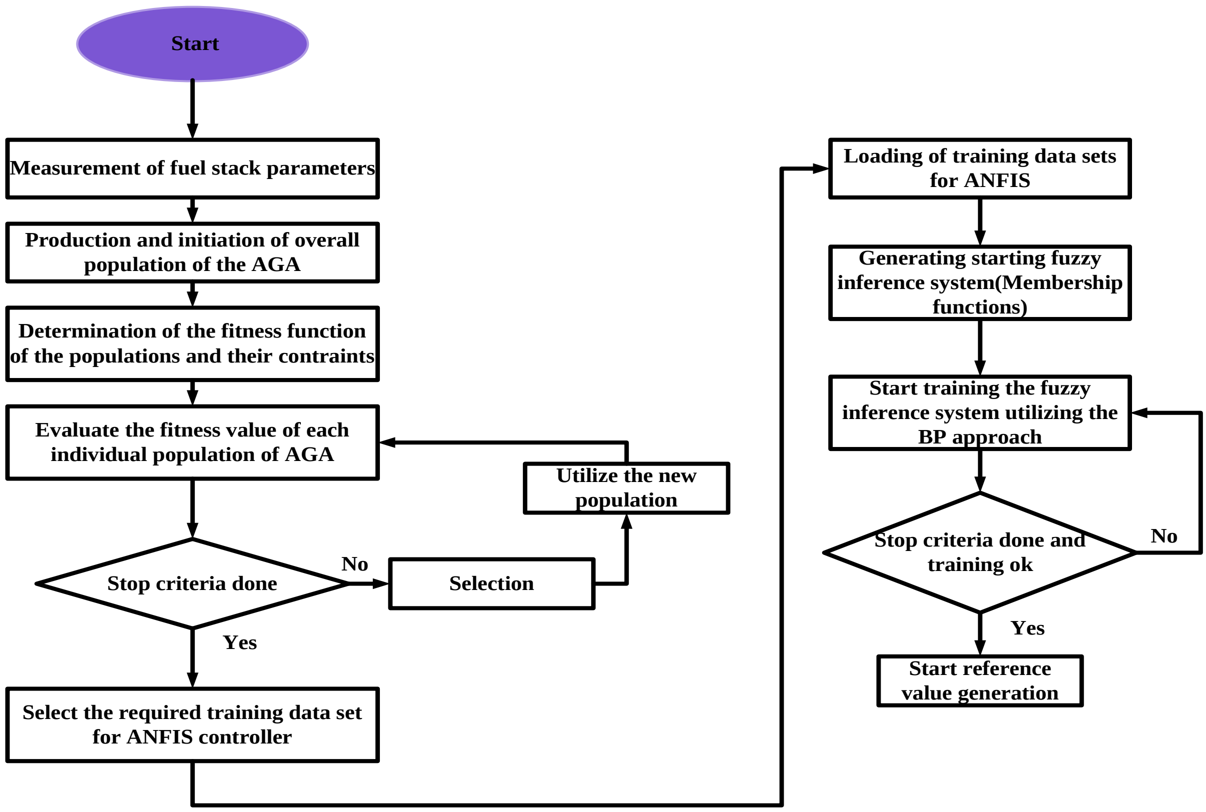

Figure 3.16 : Flowchart of adaptive genetic algorithm-Based ANFIS MPPT approach [118].

Table 3.7 : Analysis of prevalent and recent MPPT approaches utilized in fuel cells regarding performance, tracking duration, oscillation, advantages, limitations, and complexity.

MPPT approach	Performance	Tracking duration	Oscillation	Advantages	Limitations	Complexity
FLC [67], [119]	High	Medium	Low	Resilient to nonlinearity	Poor rule-based tuning	Medium
Incremental Conductance Sliding Mode [120]	Very High	Fast	Very Low	Quick convergence, robustness, and fewer oscillations	Complex tuning and chattering danger.	High
Modified PSO [89],[117]	Very High	Fast	Very low	Global optimization.	Computationally complex.	High
Jaya [60]	Very High	Fast	Very Low	Optimization without parameters	In large systems, slower convergence	Medium
Whale [121]	High	Medium-Fast	Low	Robust global searching	Risk of early convergence	High
Predictive [55]	Very High	Very Fast	Very Low	Precisely predicts MPP	Needs a precise FC model.	High
Modified P&O [122]	Medium-High	Medium	Medium	Straightforward, inexpensive,	Poor dynamic responsiveness	Low

				and simple to use.	and steady-state oscillations.	
Radial Basis Function Artificial Neural Network [57]	Very high	Fast	Very low	Strong convergence of nonlinearity	Excessive fitting issue	High
Feed Forward Neural Network Feed [54]	High	Low	Mdium-Fast	Strong ability for adaptability	An extensive data set is needed	High
ANFIS [62]	Very high	Fast	Very low	Integrates fuzzy inference with learning	High complexity and a need for training	Very high
Fuzzy-Predictive [123]	Very high	Very Fast	Negligible	Predicting with resilience	High complexity of design	Very High
ABC-Fuzzy [124]	Very high	Fast	Very low	Fuzzy adaptive tuning	Complex structure	High
AGA-ANFIS [118]	Very high	Very Fast	Very low	Excellent efficiency with precise tuning	Extremely high cost of calculation	Extremely High

3.3 An overview of energy management approaches

The expression "energy management strategies" (EMSs) describes a group of organized plans, techniques, or strategies used to effectively regulate and maximize the use of power sources in a specified system. In order to meet load demands and maximize energy efficiency, power management systems, or EMSs, dynamically supply and allocate energy from various sources.

Optimizing renewable energy sources necessitates an effective power management strategy. A power management strategy must prioritize three components, such as maintaining a consistent power supply to accommodate demand fluctuations, lowering expenses, and reducing fuel consumption (H2). Extending the lifespan of components is crucial for sustainability and cost-effectiveness. The effectiveness of energy management systems is limited by the complicated features of hybrid power technologies, which include multiple energy sources and complex behaviors[125].

3.3.1 Categorization of energy management approaches

Several researchers have focused on improving energy management systems as the use of DC components develops. Numerous experts in the literature have suggested these tactics [126]. Rule-based, artificial intelligence (AI), and optimization-based approaches are the three primary types of EMS. Deterministic strategies and Boolean logic strategies are the two types of rule-based strategies. Fuzzy logic, neural networks, and machine learning techniques are the three primary categories of artificial intelligence. Finally, optimization-based strategies aim to make the objective function as small or as large as possible. Emissions, expenses, energy savings, component deterioration, and overall performance are a few examples of the aim function. Optimization-based solutions come in two varieties: offline and online. Examples of offline optimization techniques that are primarily used to regulate power flow include genetic algorithms (GA), dynamic programming (DP), stochastic dynamic control strategy (SDP), and nonlinear programming (NLD). Every kind of load profile needs to be present. This results in a large amount of data. This makes implementing them extremely challenging. In online optimization, the objective function depends solely on the current states of the system. They perform better in real time and require less processing power. Although the storage devices' SoC is considered, global optimization is still not achievable. These techniques include model predictive control (MPC), the external energy maximization method (EEMS), and equivalent consumption minimization approach (ECMS) [127],[128],[129],[130],[131]. A summary of the most common energy management methods is presented in Figure 3.17.

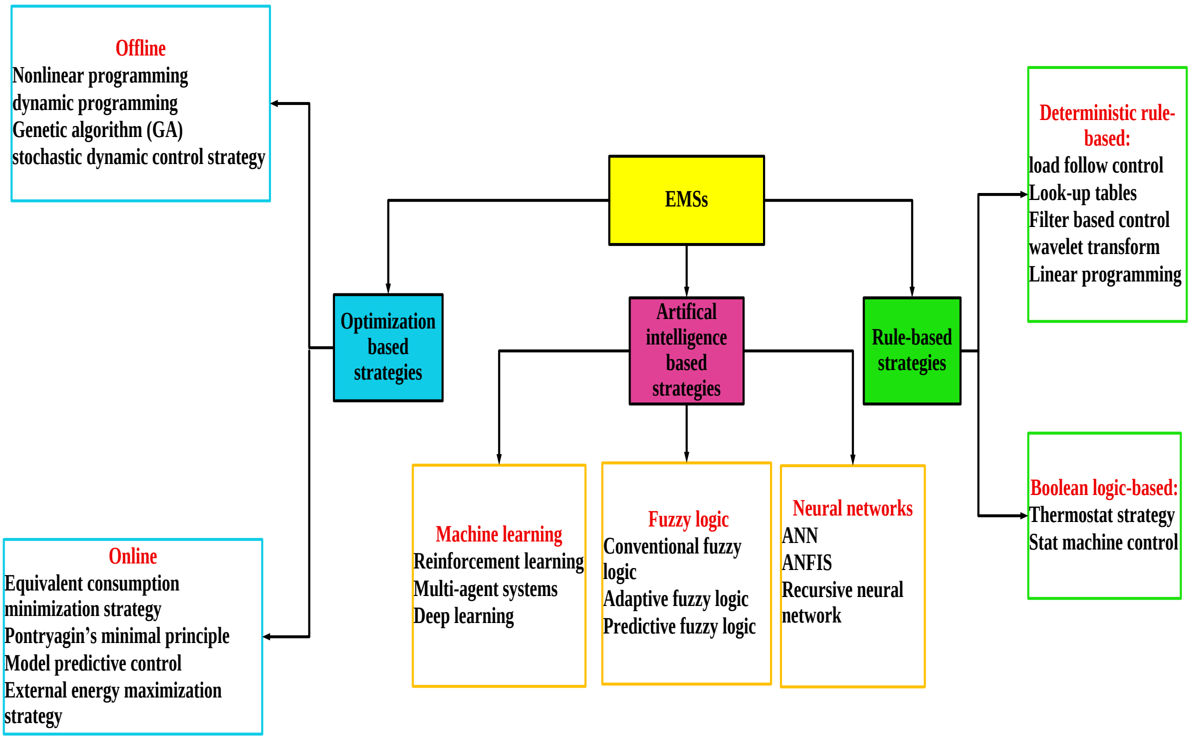

Figure 3.17: Power management strategies [128].

3.3.1.1 Rule based approaches

Traditional control systems that rely on a predetermined mode of operation are known as rules-based management methods. These technologies can be seamlessly integrated into real-time supervision to effectively control the power flow in a hybrid power complex. Usually, we develop the rules by assessing mathematical frameworks, heuristics, or human cognition. The deterministic rules-based (DRB) system and the Fuzzy Logic Rule-Based Control Method are the two main categories of rule-based procedures. A different term for DRB is static logic thresholds techniques. Furthermore, these rules are set in accordance with preset goals, such as achieving grid independence, reducing costs, and reducing emissions. One of the most commonly employed techniques within the DRB approach is the state machine method (SMM). This method represents the energy management process using a finite state machine (FSM). Every state in the FSM denotes a distinctive system mode or operational circumstance. By switching between modes in accordance with predetermined specifications, the system improves energy efficiency without sacrificing functionality. The thermostat control strategy and electric aid control are two more power management methods that fall under the DRB subclass. On the other hand, the second EMS subgroup, which falls under the rule-based algorithm category, is fuzzy rule-based control (FRBC). The latter includes three different types: predictive, adaptive, and conventional FRBC. As a result, each fuzzy logic assertion's degree of truth is defined. The simplicity, ease of use, and notable reliability of fuzzy control set it apart. It can quickly translate the conclusions of a designer into control rules. Expert knowledge can also be used in processes of decision-making and mathematically expressed as a set of rules. Fuzzy logic's ability to adjust and change, which increases control flexibility, is one of its main advantages [28], [125].

Formulating rules in rule-based management is difficult and necessitates a thorough understanding of the systems; it also lacks flexibility. However, the over-reliance on engineering knowledge and the inadequate assessment of overall operational circumstances make it challenging to achieve high performance with rule-based power management.

3.3.1.2 Optimization based approaches

Optimization-based approaches aim to maximize or minimize a function. Depending on the particular application, the cost function of a hybrid power system may include elements like power flow, hydrogen consumption, and energy expenses [128]. Although real-time energy management is not directly facilitated by these control techniques, an instantaneous cost function can be used to formulate a real-time control strategy. As a result, there are two main types of optimization-based strategies: global optimization, also known as offline optimization strategies, and real-time or online approaches. Based on a thorough comprehension of the operational characteristics and constraints of the system, the global optimization approaches optimize and improve energy consumption. These techniques are referred to as "offline," since the optimization process is carried out beforehand and makes use of forecasts or historical data rather than real-time data. The search for the best feasible solution to improve performance, lower energy costs, or accomplish specific goals within a given time frame is known as global optimization. The primary methods utilized in this context are linear programming, dynamic programming, stochastic control strategies, and genetic algorithms. When control variables are limited to a finite set, dynamic programming (DP) is a crucial technique used to solve optimal control problems. Converting the optimal control problem into a multilayer decision-making problem is a key tenet of this methodology. One of the methods most frequently used in the literature is stochastic dynamic programming, or SDP. The control law is established offline by solving an infinite horizon optimization problem offline, which yields a time-invariant state feedback controller. One heuristic technique known for its remarkable optimization effectiveness is the genetic algorithm (GA). It can swiftly identify solutions that satisfy the optimization objectives and circumvent these restrictions by utilizing its own features. Genetic algorithms are particularly useful for the iterative optimization of a power system because of the aforementioned characteristics. On the other hand, real-time data suggests that online optimization methods entail ongoing monitoring, modification, and improvement of energy usage. Unlike offline (global) optimization, which depends on preset strategies based on past data and projections, online optimization is constantly adjusted to new conditions. This approach works especially well in settings with erratic energy supply, demand, and other operational factors. The most popular techniques used here include the equivalent consumption minimization method, model predictive control, power management systems based on neural networks, and metaheuristic techniques such as beluga whale optimization (BWO)[127], salp swarm algorithm (SSA) [81], mine-blast optimization [130],[132] and coyote optimization algorithm (COA) [133] , to name a few. An effective strategy for handling dynamic process models derived from system identification is the MPC technique. The MPC's ability to maximize the current period while accounting for future timeslots is one of its core characteristics. The equivalent consumption minimization strategy (ECMS) is also covered in a number of studies. According to them, the main goal of this approach is to reduce similar fuel consumption while maintaining the battery and supercapacitor state of charge (SOC) within their optimal operating range throughout the whole load profile. For the ECMS to be effective, the equivalent fuel consumption must be accurate. A potent computational technique that learns and generalizes from training data is an artificial neural network (ANN). When compared to traditional optimization techniques, the neural network method can greatly speed up the resolution of optimization problems because of its intrinsic high concurrency [28].

3.3.1.3 AI-based approaches

Artificial Neural Networks (ANN), Machine Learning (ML), and Fuzzy Logic Control (FLC) are some of the AI techniques used to create the EMSs in AI-based strategies. By incorporating fuzzy logic (FL) into an energy management system (EMS), management techniques based on FL are created, leading to a smooth transition between rules, enhanced stability, and increased efficiency. Fuzzy logic offers considerable robustness and is easy to build. Its adaptability, which increases the EMS's flexibility, is its main benefit. Traditional FL, type 2 FL, predictive FL, and adaptive FL are examples of EMSs that use FL. While these processes are immune to model errors and have strong techniques to handle system disruptions, they require accurate designs and fast microcontrollers. Artificial neural networks (ANN), recursive neural networks (RNN), and adaptive neuro-fuzzy inference systems (ANFIS) are all examples of neural network (NN)-based management solutions. Although these tactics require a database for system training, they can result in better performance. The third category includes machine learning (ML)-based management techniques commonly used in this field, including deep learning approaches, multi-agent systems (MAS), and reinforcement learning (RL). The previously acquired database that the EMS needs to be trained with is not always available. The lack of research done in this very young market makes this process difficult. The inability to guarantee functionality with data that was not used during the training phase is another disadvantage [128],[125]. The Table 3.8 summarizes the most common and recent power management strategies used in the literature.

Table 3.8: The most common and recent power management strategies used in the literature.

Power Management Strategy	Hydrogen Consumption	Performance
Adaptive equivalent consumption minimization strategy (A-ECMS) [134]	Very low	Very High
PI-FLC [135]	Medium	High
EMMS-Based White Shark Optimizer [129]	Very low	Very High
Social Spider approach [136]	Very low	Very High
State machine control strategy [126]	High	Medium
Adaptive fuzzy management strategy [137]	Low-Medium	High

Mine Blast Algorithm (MBA) [132]	Very low	Very High
Neural network controller [138]	Low	Between high and very high
Machine learning [139]	Low	Between high and very high
Rule-Based Operation Mode Control Strategy [140]	Medium-High	Medium
Deep reinforcement learning [141]	Very low	Very high
Improved twin delayed deep deterministic policy gradient algorithm [142]	Minimum	Extremely high
Deep reinforcement learning-based predictive [143]	Minimum	Extremely high

Conclusion

This chapter provides an extensive overview and basic foundation of the predominant control mechanisms for autonomous hybrid PV-PEMFC systems. The sections addressing PV system control provide descriptions of various categories of MPPT approaches, including their limitations and current advancements in the field. The chapter presents an overview of several methods for MPPT to control PEMFC, including both traditional and intelligent approaches. The final section includes a summary of energy management techniques employed in hybrid systems.

Chapter 4 : Intelligent Control Approaches for a Standalone Hybrid PV-PEMFC System

4.1 Introduction

Due to escalating worries regarding global warming and the exhaustion of conventional sources of electricity, hybrid power plants emphasizing renewable energy are gaining significance. These mechanisms are crucial in promoting environmental initiatives. The swift expansion of clean energy incorporation into current power systems requires creative control approaches to guarantee reliability, stability, and efficiency. Advanced technology for controlling serves as an alternative approach to enhance the overall effectiveness of a power system. The maximum power point tracking method is acknowledged as an effective solution for enhancing the power output efficiency of energy generation systems and is extensively utilized in solar energy production systems, wind power production systems, and solar-wind hybrid power systems. Recent developments indicate the implementation of MPPT in fuel cell systems. This chapter delineates a variety of advanced control techniques designed to enhance and regulate the efficiency of sources of clean energy, particularly photovoltaic systems and proton exchange membrane fuel cells, with the objective of optimizing energy capture in diverse environmental conditions while maintaining system stability and delivering optimal power [12],[124],[28].

Developing effective tracking strategies for MPPT that improve the system's power-capturing performance despite variations in solar radiation and partial shading conditions is the primary objective for photovoltaic systems. Alternatively, to guarantee reliable performance, a fuel cell's functioning needs to be meticulously monitored to handle its nonlinear characteristics and dynamic changes in operating conditions, like temperature and pressure.

The next chapter provides a detailed analysis of the design concepts, implementation strategies, and efficacy of these control systems. This debate is to provide the reader with a comprehensive understanding of the real-world implications and features of current renewable energy systems.

4.2 The Development of an MPPT Controller for Photovoltaic Systems

4.2.1 The Conventional Pufferfish Optimization Approach (CPFOA)

4.2.1.1 Inspiration of Pufferfish

The pufferfish, belonging to the family Tetraodontidae and order Tetraodontiformes, inhabits coastal and estuarine regions. This fish resembles a porcupinefish and exhibits distinct spines. Although typically modest to medium in size, records indicate that pufferfish can attain lengths of up to 50 cm. Pufferfish possess a distinctive trait wherein its four teeth mimic beaks. Puffers are distinguished by the absence of pectoral fins, pelvic bones, and ribs, which are present in other species. Puffers have significantly diminished their fin and skeletal structures due to their peculiar defense mechanism of ingesting water through their mouths [144],[145].

Pufferfish exhibit sluggish movement, rendering them susceptible to predators. The pufferfish employs its distensible stomach, filled with water, to inflate into a large, spherical, spiny orb, so offering a unique protection mechanism against predators. The sharp spines of the pufferfish serve as an effective deterrent to predators, transforming a potential meal into a formidable challenge. Predators sense the danger when they receive this signal and flee the pufferfish. The inherent behaviors of pufferfish encompass notable interactions with predators and the employment of their defense mechanism, which involves inflating into a sphere of sharp spines to dissuade attacks. The proposed CPFOA approach is formulated through the modeling of natural processes that include (I) a predator's assault on pufferfish and (II) the defensive strategies employed by pufferfish against such assaults. This is elaborated about below [144].

4.2.1.2 Initialization

A population-centric approach that effectively uses iterative techniques to address optimization challenges is the proposed CPFOA methodology. CPFOA members assign values to the problem's decision variables based on where they fall in the search space. Every member of the CPFOA represents a possible solution to the problem, which can be expressed quantitatively using a vector in which each element represents a decision variable. Members of CPFOA participate in the program. Equation (4.1) provides a matrix representation of the community of these vectors, while Equation (4.2) identifies each CPFOA member's starting location at the start of the process[146],[147].

$$X = \begin{bmatrix} X_1 \\ \vdots \\ X_i \\ \vdots \\ X_N \end{bmatrix}_{N \times m} = \begin{bmatrix} x_{1,1} & \cdots & x_{1,d} & \cdots & x_{1,m} \\ \vdots & \ddots & \vdots & \cdots & \vdots \\ x_{i,1} & \cdots & x_{i,d} & \cdots & x_{i,m} \\ \vdots & \cdots & \vdots & \ddots & \vdots \\ x_{N,1} & \cdots & x_{N,d} & \cdots & x_{N,m} \end{bmatrix}_{N \times m} \tag{4.1}$$

$$x_{i,d} = lb_d + r \cdot (ub_d - lb_d) \tag{4.2}$$

X exhibits a population matrix of CPFOA. X_i is the i_{th} member of CPFOA ; $x_{i,d}$ is its d_{th} dimension in the search space. N is the population ; m is the number of decision variables ; r is a random number between 0 and 1; lb_d and ub_d are the lower and upper limits of the d_{th} decision variable.

Assessing the objective function of the problem is made easier by considering each CPFOA member as a possible solution. Equation (4.3) can be used to represent the evaluated values for the objective function as a vector.

$$F = \begin{bmatrix} F_1 \\ \vdots \\ F_i \\ \vdots \\ F_N \end{bmatrix}_{N \times 1} = \begin{bmatrix} F(X_1) \\ \vdots \\ F(X_i) \\ \vdots \\ F(X_N) \end{bmatrix}_{N \times 1} \tag{4.3}$$

Here, F_i represents the evaluated objective function associated with the i_{th} element of the CPFOA, whereas F denotes the vector of the assessed objective function.

The evaluated values of the objective function are the main factor influencing the caliber of the different recommendations made by each CPFOA member. The highest value of the objective function corresponds to the optimal member. The optimal candidate solution is another name for this. The objective function value is lowest for the least preferred member, or possible resolution. The optimal member at each operational tier can be replaced with newly computed values for the goal function. CPFOA members currently solve problems in a variety of areas[144],[146].

4.2.1.3 Mathematical Model of conventional PFOA

Inspired by pufferfish's defensive behaviors against predators, the proposed CPFOA method modifies the positioning of individuals within a population in relation to the problem-solving environment. In this usual order, the pufferfish is the first target of the predator. To ward off possible predators and make escape easier, the pufferfish's defense mechanism changes into a sphere of sharp spines. Members of the CPFOA population exhibit two distinct phases in their positions: (I) exploration, which indicates the pufferfish's proximity to a predator, and (II) exploitation, which indicates the pufferfish's defense against the predator [144],[148].

4.2.1.4 Exploration phase: Predatory attack on the pufferfish

By simulating a predator's attack on the pufferfish, the first component of the PFOA involves moving population members around. Because they move slowly, pufferfish are vulnerable to predators. The positions of PFOA members in the problem-solving environment are altered by mirroring the predator's shift in posture during the attack on the pufferfish. The algorithm's exploratory potential for global search is increased by simulating the predator's path towards the pufferfish, which causes notable changes in the PFOA members' positioning. Members with high objective function values are considered potential pufferfish attack targets. The number of pufferfish collected for each member of the population is measured by equation (4.4) [144],[146],[147].

$$CP_i = \{X_k : F_k < F_i \text{ and } k \neq i\}, \text{where i=1,2,...,N and } k \in \{1, 2, ..., N\} \tag{4.4}$$

Where X_k is the population member with a higher objective function value than the i_{th} predator, F_k is its objective function value, and CP_i is the list of potential pufferfish habitats for the i_{th} predator.

According to the CPFOA model, the designated pufferfish is chosen at random from the CP set by the predator. Equation (4.5) uses the model of predator behavior toward the pufferfish to determine a new position for each PFOA member within the problem-solving domain. If the value of the goal function rises at the new site, it supersedes the previous location, according to equation(4.6).

$$x_{i,j}^{P1} = x_{i,j} + r_{i,j} \cdot \left(SP_{i,j} - I_{i,j} \cdot x_{i,j}\right) \tag{4.5}$$

$$X_i = \begin{cases} X_i^{P1}, F_i^{P1} \le F_i; \\ X_i, \text{ else }, \end{cases} \tag{4.6}$$

Here, SP_i stands for the pufferfish's dimension, and CP_i , a group member, denotes the pufferfish selected at random from the list provided for the i_{th} predator. $x_{i,j}^{P1}$ is the j_{th} portion of the pufferfish chosen for the i_{th} predator; F_i^{P1} is the value of the objective function; $r_{i,j}$ are random numbers between 0 and 1; and $I_{i,j}$ are randomly picked values of either 1 or 2. X_i^{P1} is the new location for the i_{th} predator based on the first step of the proposed CPFOA.

4.2.1.5 Exploitation phase: Defensive Strategy of Pufferfish against Predators

The second portion of the CPFOA modifies the status of the population members by simulating a pufferfish's defense mechanism against predatory threats. When a predator attacks, the pufferfish's extremely elastic stomach expands with water, forming a spherical form with jagged spines. In these situations, when the predator receives a warning, it chooses to spare the pufferfish instead of pursuing a basic food source. The effectiveness of the local search algorithm is increased by slightly altering the PFOA member design to mimic the predator's departure from the pufferfish. Each PFOA member's new position is determined by formula (4.7) using the predator's displacement from its point of contact. If the new position increases the value of the objective function, the connected component will be substituted according to formula (4.8).

The formula (4.8) makes use of advancements in PFOA-based design techniques. To ascertain whether the newly calculated placement for the PFOA member offers a better solution to the problem at hand, the objective function values are examined. If the answer is yes, the new role is considered suitable for that particular PFOA member; if the answer is no, the individual keeps their current position because the new function is deemed unsuitable because of the limited solution. According to equation (4.8), improving the value of the objective function is a prerequisite for the updating procedure for every PFOA member [144],[146],[147].

$$x_{i,j}^{P2} = x_{i,j} + \left(1-2r_{i,j}\right)\cdot\frac{ub_j - lb_j}{t}, \tag{4.7}$$

$$X_i = \begin{cases} X_i^{P2}, F_i^{P2} \le F_i; \\ X_i, \text{ else }, \end{cases} \tag{4.8}$$

In this case, X_i^{P2} is the new position of the i_{th} predator, which was found in the second step of the suggested CPFOA. Dimension j_{th} is denotes as $x_{i,j}^{P2}$, and the value of the goal function is F_i^{P2}. The iteration counter is t, and $r_{i,j}$ stands for the random numbers that are generated from the interval $[0,\ 1]$.

4.2.1.6 Iterative Process

The placement of each PFOA member is adjusted according to the exploration and exploitation stages, so concluding the initial iteration of the algorithm. The methodology thereafter progresses to the following iteration, with Equations (4.4) through (4.8) continuously refining the positions of PFOA members until the program completes its final iteration. The position of the optimal PFOA member fluctuates based on the objective function values at each iteration. The algorithm reveals the position of the appropriate PFOA member as the resolution to the issue upon completion [144].

4.2.2 Proposed Enhanced Pufferfish Optimization Approach (EPFOA)-Based MPPT

The CPFOA has been updated to enhance its accuracy in MPPT for photovoltaic systems, as will be discussed in the subsequent section. It presently features enhanced dynamic responsiveness, accelerated convergence, and superior overall efficiency. Solar systems must effectively follow rapid movements and maintain stability; thus, their effectiveness under varying conditions dictates these enhancements. The enhanced-PFOA (EPFOA) facilitates the monitoring of GMPP and significantly diminishes the likelihood of it becoming ensnared in local optima.

4.2.2.1 Enhancements in Initialization

Typically, agents are started at random within the search area of the CPFOA. On the other hand, agents are deployed more methodically in the EPFOA for maximum power point tracking

(EPFOA-MPPT), which is especially made for solar PV applications. Intentionally, four pufferfish agents are placed at equal separations $D_1 = 0.2,\ D_2 = 0.4,\ D_3 = 0.6, \text{ and } D_4 = 0.8$. The MPPT converter is regulated by a duty cycle that varies between 0 and 1. This careful selection assists the algorithm avoid premature entrapment in local optima by ensuring thorough coverage of the entire PV power-voltage characteristic curve. In theory, more agents could improve the effectiveness of global searches, but they could also make convergence more difficult. Due to its optimal integration of processing capacity and search space exploration, the suggested design is appropriate for real-time MPPT applications.

Each pufferfish position's power, $P_i(k)$ is determined and saved as the most efficient individual power, $P_{best}(k)$ associated with the optimal personal pufferfish position, $D_{best}(k)$. When a higher power is found, the $P_{best}(k)$ value changes. With the requirement in Eq. (4.9) denoting the number of iterations, the method can efficiently search the search space for the global optimum.

$$\begin{cases} P_i(k) > P_{best}(k-1) \\ P_{best}(k-1) = P_i(k) \\ D_{best}(k) = D_i(k) \end{cases} \tag{4.9}$$

4.2.2.2 Enhancements in Exploration

The EPFOA-MPPT simulates predator hunting strategies by using predator-prey behavior modeling and modifies agent placements based on interactions. This system uses a stochastic movement mechanism driven by a randomly selected scalar $I_{i,j} \in \{1,2\}$ to find the best candidate solution for pufferfish. This randomization can increase search space diversity while causing unpredictable and unstable movements in real-time MPPT systems. Unrestrained randomness is undesirable for applications that require continuous and fast duty cycle regulation. The EPFOA-MPPT uses a more accurate Lévy flight-based mechanism (also known as a jump process) in place of the static random number $I_{i,j}$.

4.2.2.3 Levy Flights in Optimization: A General Overview

A stochastic process that has a random step whose magnitude is determined by the Lévy distribution is known as a Lévy random step. Because of its large tails, which enable rare and extreme events to occur more frequently than expected, this distribution differs from a normal distribution. In a Lévy random walk, the orientations and step sizes follow the Lévy distribution. While major steps happen occasionally in random directions, minor steps are taken frequently in a Lévy random walk. Step variation needs to be controlled; steer it in the direction of the best answers and restrict departures from the best ones. A stochastic process known as a "random walk" is defined by the sequential performance of unpredictable actions [149],[150],[151].

The Lévy distribution and Lévy random step were first proposed by French mathematician Paul Lévy in the 1920s, and they later came to be associated with his name. Modeling and stochastic events—random occurrences over time—captivated Lévy. Lévy random walks, which were first studied in physics, can accurately simulate particle motion in fluids or gases. Researchers have studied Lévy random walks, steps, and flights in great detail, showing that they are applicable to many different fields [152],[149],[153].

Apart from having heavy tails, Lévy random walks complement optimization methods and improve speed and precision. By making distinct, unpredictable jumps inside the search space, Lévy random walks make it easier to avoid obstacles and speed up access to far-off areas. This feature speeds up the search and increases the possibility of finding the global optimum [154].

The random step size of Lévy flight is represented by the Lévy distribution, as seen in the subsequent equations [154].

$$Levy\left(\gamma\right) \sim /s/^{-\gamma}; 1<\gamma<3 \tag{4.10}$$

In this context, L represents the step size of the Lévy flight, whereas γ signifies the exponential factor, often established at 1.5. The random step size of Lévy flight is determined as follows:

$$L=\frac{\mu}{/v/^{1/\beta}};\ 1<\beta<2 \tag{4.11}$$

Normal distributions are used for the values μ and v, as shown in expression(4.12).

$$\begin{cases}\mu = \mathrm{N}\left(0, \delta_{\mu}^{2}\right) \\ v = \mathrm{N}\left(0, \delta_{v}^{2}\right)\end{cases} \tag{4.12}$$

Equation (4.13) is used to show the values of δ_v and δ_μ:

$$\begin{cases}\delta_{\mu} = \left\{\dfrac{\Gamma\left(1+\lambda\right)\sin\left(\pi\lambda/2\right)}{2^{(\lambda-1)/2}\,\Gamma\left[\left(1+\lambda\right)/2\right]}\right\}^{1/\lambda} \\ \delta_{v} = 1\end{cases} \tag{4.13}$$

Where:

Γ : The typical function for Gamma.

Mantegna's methodology [155] mathematically integrates Lévy flights by employing two independent random variables derived from a Gaussian distribution, thereby reproducing Lévy-distributed step sizes. In order to promote local enhancement and allow subsequent phases to avoid confinement within limited local optima, this methodology makes sure that the majority of the stages are incremental.

In EPFOA, Lévy flights balance local enhancement and global variety by using step sizes that are derived from a heavy-tailed probability distribution. Traditional metaheuristics, on the other hand, use unconstrained Lévy flights in the search stage. To avoid premature convergence during the exploration phase, EPFOA uses sporadic long hops based on Lévy. The algorithm can simultaneously explore new regions of the P-V curve and move closer to the ideal solution when the PSCs show multiple peaks. By switching between broad searches and a more focused search, the algorithm can find the MPP faster and more accurately.

There is a conditional probability $R<P$ with $P=0.7$ added to the static location update steps in Equations (4.5) and (4.6) in Equations (4.14) and. If they pick a random number $R<P$, the position change based on Lévy flight can be shown in this way:

$$D_i^{P1}(k+1) = D_i(k) + L \cdot \left(D_{Gbest}(k) - D_i(k)\right) \tag{4.14}$$

$$D_i(k) = \begin{cases} D_i^{P1}(k+1), if \;\; F\left(D_i^{P1}\right) \le F\left(D_i(k)\right) \\ D_i(k), \text{ otherwise} \end{cases} \tag{4.15}$$

4.2.2.4 Enhancements in Exploitation

Each pufferfish's position is slightly shifted away from the optimal situation in IPFOA under the constraint $R \ge 0.7$ based on a random factor $(1-2r)$, where R and r are a random values between 0 and 1, simulating their movement to avoid predators. This model, which lacks directional bias and has flexible control, replicates the pufferfish's response to external stimuli through stochastic behavior. Under variable conditions, this approach usually results in suboptimal local adjustments and a higher risk of premature convergence in precision-sensitive domains such as MPPT. Equations (4.16) and (4.17) illustrate how the EPFOA overcomes these drawbacks by replacing the static random number with a dynamic sine decay variable (F) that is dependent on iterations. During the first iterations, F stays close to a specified constant Z, allowing for more experimental variance in the solution space. More accurate movements around the MPP are made possible by F gradually decreasing as iterations go on.

The dynamic sine decay factor's incremental step size reduction progressively reduces the search region rather than overtly limiting exploration, improving the exploitation phase's precision. With the help of this feature, the algorithm can improve local search at the ideal location, enabling faster and more accurate convergence toward GMPP. The change in F improves the accuracy of the next step in the movement. The goal of this change is to improve computing efficiency, speed up convergence, improve tracking accuracy, and reduce steady-state oscillations at the MPP. EPFOA strengthens the algorithmic base and guarantees that MPPT is quick, accurate, and has a low implementation complexity.

$$D_i^{P2}(k+1) = D_i(k) + B \cdot \left(D_{Gbest}(k) - D_i(k)\right) \tag{4.16}$$

$$D_i(k) = \begin{cases} D_i^{P2}(k+1), if \;\; F\left(D_i^{P2}\right) \le F\left(D_i(k)\right) \\ D_i(k), \text{ otherwise} \end{cases} \tag{4.17}$$

Equation (4.18) specifies the variables, with $D_i(k)$ denoting the position of the pufferfish and $D_{Gbest}(k)$ representing the global best position. In the conventional pufferfish optimization approach, the tuning parameter $(1-2r)$ is chosen at random. Conversely, to enhance convergence speed, as delineated in Eq.(4.18), the refined PFOA reinterprets F as a dynamic variable that fluctuates with iterations, ascertainable by Eq. (4.19).

$$B = Z - \sin\left(\frac{\pi}{2}\left(\frac{k}{M}\right)^2\right) \tag{4.18}$$

$$with \text{ k=1, 2, 3, 4, ..., M} \tag{4.19}$$

The constant parameter Z is set to 1.16 in this case. The max iteration is shown by M, which is 16 in this case, and the current iteration is shown by k.

The CPFOA is improved with a sophisticated exploitation phase that uses the deterministic sine decay to reduce step sizes. The update exploitation phase in EPFOA effectively monitors the GMPP under dynamic and partial shading conditions, minimizes convergence to local optima, and assists in identifying the optimal solution.

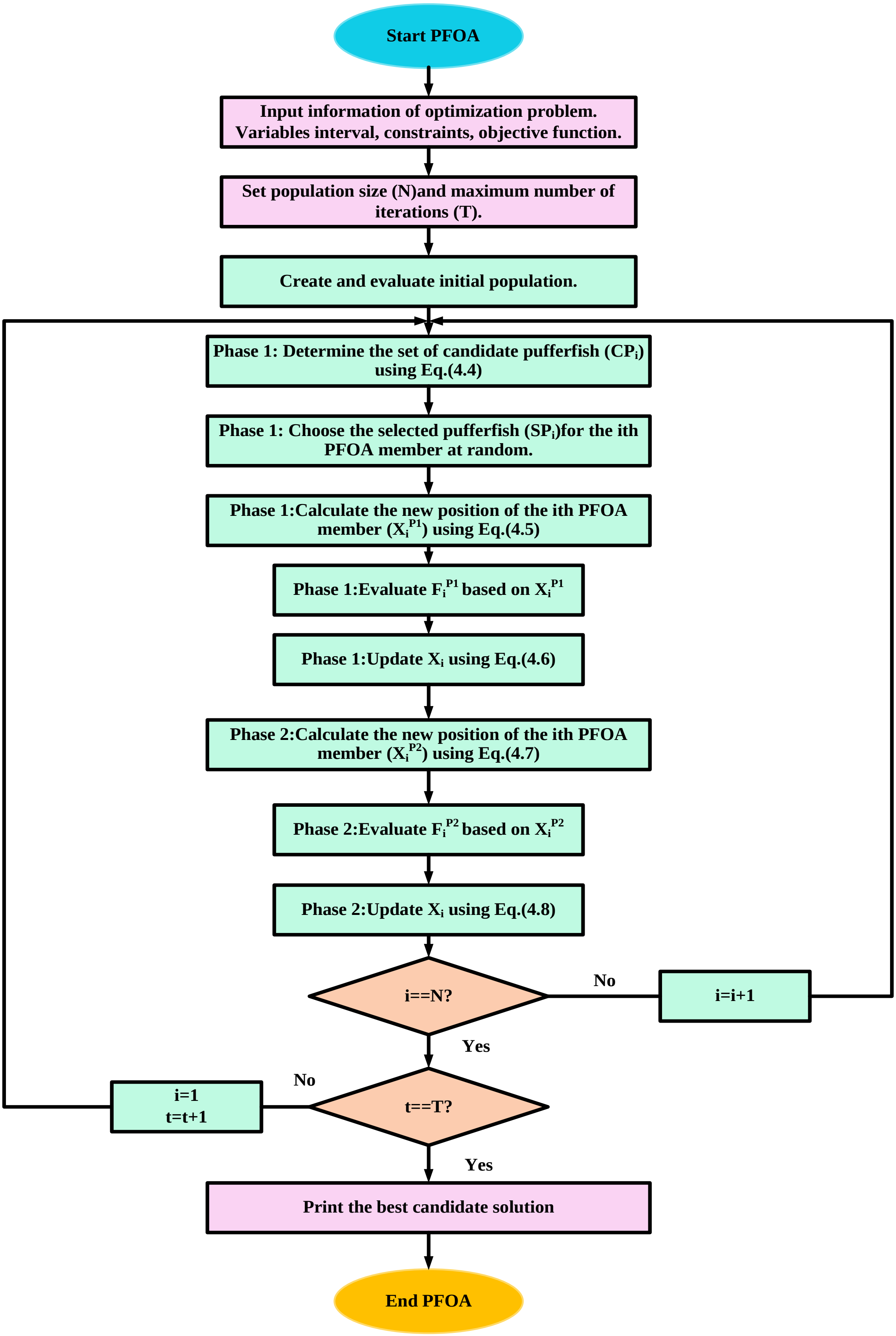

Figure 4.1: PFOA flowchart [144].

4.2.2.5 Adjustment of the condition of termination

Equation (4.20) delineates two termination criteria established to halt further research and stabilize D . Integrating the optimal powers of each pufferfish enables the determination of the global maximum power output, denoted as $(P_{Gbest}(k))$. This result in the pufferfish's position indicated as $D_{Gbest}(k)$. The search procedure concludes when the worldwide disparity in the greatest power value between the preceding $P_{Gbest}(k-1)$ and the current cycle's $P_{Gbest}(k)$ is less than 5% , and the positional difference ΔD among all pufferfish is likewise less than 5% . If (4.20) meets the termination conditions, D stabilizes at $D_{Gbest}(k)$, hence achieving the duty cycle value for the converter. The fulfillment of the ΔD requirement indicates that all four pufferfish are in greater proximity to each other, signifying the attainment of global point precision. Following the termination conditions, $P_{Gbest}(k)$, the input voltage (V_{PV}) , input current (I_{PV}) , and $D_{Gbest}(k)$ will be represented as P_{MPP} , V_{MPP} , I_{MPP} , and D_{MPP} , respectively.

$$\frac{\left|P_{Gbest}(k)-P_{Gbest}(k-1)\right|}{P_{Gbest}(k-1)} \text{ and } \Delta D < 0.05 \tag{4.20}$$

Upon meeting the stopping conditions, the technique monitors the disparity between P_{MPP} and photovoltaic power $P_{PV}(k)$ via the MPPT algorithm, provided that condition (4.21) remains fulfilled; the algorithm continues to generate D_{MPP} .

$$\frac{\left|P_{MPP}-P_{PV}(k)\right|}{P_{MPP}} < 0.05 \tag{4.21}$$

The flowchart of PFOA is presented in Figure 4.1.

4.2.3 Metaheuristic approaches used in comparative study

The next section gives an overview of the metaheuristic techniques that were selected to be compared with EPFOA. The goal of this research is to explain how each approach works, including its basic concepts, flowchart, and mathematical model.

4.2.3.1 Particle Swarm Optimization (PSO)

Using a population-based metaheuristic approach, the Particle Swarm Optimization (PSO) method uses swarm intelligence to solve optimization problems. In PSO, a swarm of particles searches the search space for the best solution. Eberhart and Kennedy proposed this technique [156]. With a position vector $x_i(k)$ and a velocity vector $v_i(k)$, each swarm particle at time k represents a possible solution. While the velocity vector determines the particle's path and speed, the location vector indicates the potential solution.

The most recent formulas for each particle's position and velocity in particle swarm optimization (PSO) are as follows [157]:

$$v_i(k+1) = w * v_i(k) + c1 * r1 * (pbesti - x_i(k)) + c2 * r2 * \left(gbest - x_i(k)\right) \tag{4.22}$$

$$x_i(k+1) = x_i(k) + v_i(k+1) \tag{4.23}$$

$x_i(k+1)$ represents the particle's updated position at time $k+1$, and $v_i(k+1)$ represents the particle's revised velocity at time $k+1$. Initial velocity influence is controlled by the inertia weight, represented by w . The acceleration factors $c1$ and $c2$, respectively, reflect the impact of the particle's global best location $(gbest)$ and personal best location $(pbesti)$. The random number generated by the function $rand(\ )$ falls between 0 and 1. The flowchart of this approach is shown in Figure 4.2.

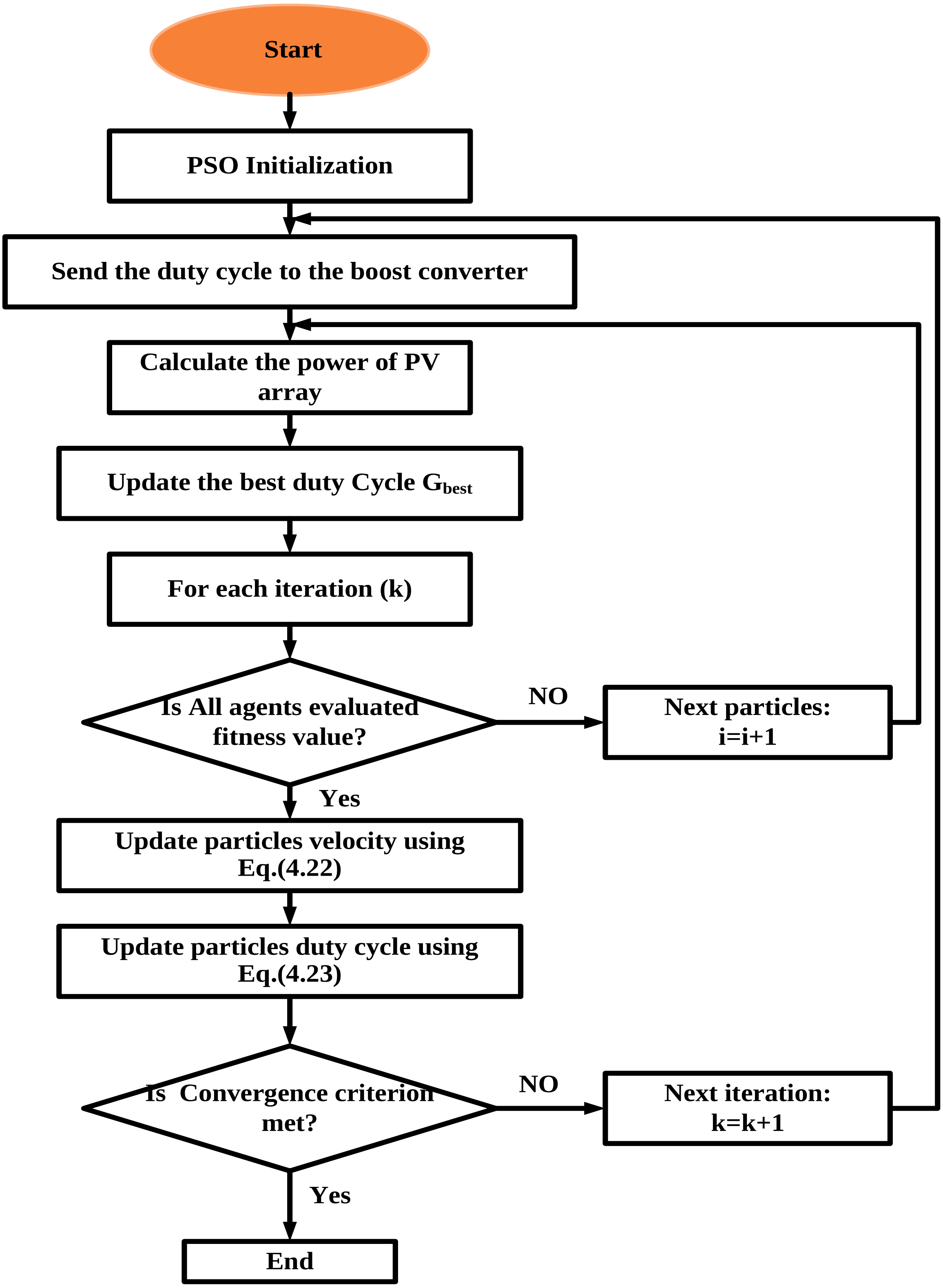

Figure 4.2: PSO approach flowchart [157].

4.2.3.2 Grey Wolf Approach (GWA)

The GW strategy is a nature-inspired optimization method that was first presented by Mirjalili et al [158]. It is similar to the social hierarchy and predatory tactics of grey wolves. To demonstrate the social hierarchy of a pack, the method uses four distinct types of grey wolves: alpha (α), beta (β), delta (δ), and omega (ω). The alpha wolf is the most advantageous option, while the beta and delta wolves rank second and third, respectively. The remaining possible answers are categorized as omega wolves. Hunting, catching, and tracking prey are the three main stages of the process. Grey wolves encircle the prey during the hunt, a phenomenon that can be accurately modeled by formulas. Formula (4.24) determines the distance between a grey wolf's current location and its prey [157].

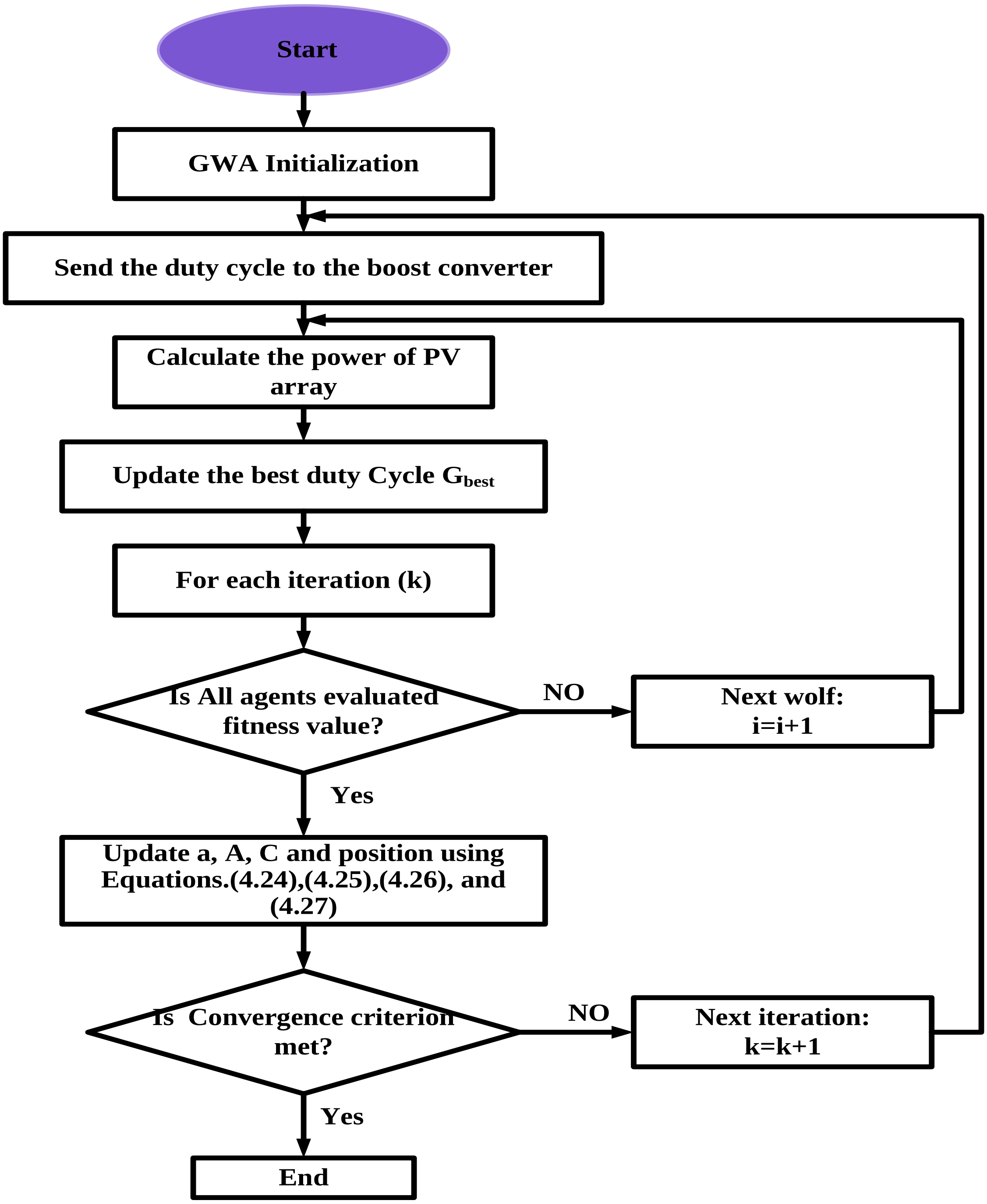

Figure 4.3: The GW strategy flowchart [157].

$$\vec{D} = \left| \vec{C} \cdot \vec{X}_P(k) - \vec{X}_P(k) \right| \tag{4.24}$$

The formula (4.25) alters the grey wolf's location based on its natural interactions.

$$\vec{X}(k+1) = \vec{X}_P(k) - \vec{A} \cdot \vec{D} \tag{4.25}$$

In the provided formulas, the current iteration is denoted by the variable k . The X denotes the grey wolf's position vectors, whereas the prey's location vectors and the vectors X_P and X are used in the calculations that follow. The symbols A and C stand for predators vectors, respectively.

$$\vec{A} = 2\vec{a} \cdot \vec{r}_1 - \vec{a} \tag{4.26}$$

$$\vec{C} = 2 \cdot \vec{r}_2 \tag{4.27}$$

As iterations proceed, the elements of vector (a) in the provided formulas exhibit a linear decrease from 2 to 0. The interval $[0, 1]$ constitutes the range of the random vectors r_1 and r_2 . The flowchart of the GW strategy is shown in Figure 4.3 .

4.2.3.3 Arithmetic optimization approach (AOA)

Abualigah introduced the revolutionary meta-heuristic optimization approach known as Arithmetic optimization approach (AOA) in 2021 [159]. The AOA was inspired by the use of mathematical operators in problem-solving. Addition (A), multiplication (M), subtraction (S), and division (D) are the basic arithmetic operators. Exploration is the first phase of an AOA, followed by exploitation [160],[161].

4.2.3.3.1 Initialization of AOA

As shown in Formula(4.28), the AOA optimization process starts with a matrix of randomly chosen solutions (X). The best outcome from each iteration is regarded as the best solution thus far [160].

$$X = \begin{pmatrix} x_{1,1} & \cdots & x_{1,n} \\ \vdots & \ddots & \vdots \\ x_{N,1} & \cdots & x_{N,n} \end{pmatrix} \tag{4.28}$$

It is crucial to choose search phases, such as intensification and diversification, before starting the AOA method. As a result, in the following search stages, the math optimizer accelerated function (MOA) is computed using Equation(4.29) .

$$MOA(C\_Iter) = Min + C\_Iter \frac{Max - Min}{M\_Iter} \tag{4.29}$$

The advanced function's minimum and maximum values are indicated by the terms Min and Max .

The value of the function at the last iteration is indicated by $MOA(C\_Iter)$. Between one and the maximum iteration limit M_Iter , C_Iter is the current iteration count.

4.2.3.3.2 Exploration stage

The exploration stage is executed using (M) or (D) arithmetic operators, which possess widely distributed values across many domains. Nonetheless, due to the extensive dispersion of operators M and D, these operators are unable to effectively close the target, unlike operators S and A. A function is built using four arithmetic steps to demonstrate the impact of the distribution values of various operators. Thus, the exploration phase facilitates the identification of a near-optimal solution, achievable after numerous iterations. Furthermore, this technique enhances the exploitation phase of the search operation by facilitating improved communication. This phase is initiated if r1 exceeds MOA, where $r1$ is a value randomly chosen from the interval $[0,1]$. The D operator applies the revised location if $r2 < 0.5$ (where $r2$ is a randomly selected value from the range $[0,1]$), while the other M operator remains inconsequential until the completion of this operator's task. The position is otherwise updated via the M operator. The mathematical formulation of this search phase is articulated in accordance with formula(4.30).

$$x_{i,j}(C\_Iter+1)=\begin{cases} best(x_j)\div(MOP+\varepsilon)\times\left((UB_j-LB_j)\times\mu+LB_j\right), & \text{r2<0.5} \\ best(x_j)\times(MOP+\varepsilon)\times\left((UB_j-LB_j)\times\mu+LB_j\right), & \text{otherwise} \end{cases} \tag{4.30}$$

The solution of the next iteration is denoted as $x_{i,j}(C\_Iter+1)$, the $best(x_j)$ denotes where the optimal solution up to this point is located, ε is a small number, and UB_j and LB_j are the upper and lower bounds of the jth location, respectively. μ, a regulating factor set to 0.499, is used to alter the search procedure. MOP stands for the math optimizer probability coefficient, which is determined by formula (4.31) based on the tests.

$$MOP(C\_Iter)=1-(C\_Iter)^{1/\alpha}/(M\_Iter)^{1/\alpha} \tag{4.31}$$

Where α, a sensitive variable that affects the exploitation's efficacy over the course of iterations is designed at 5 following multiple tries.

4.2.3.3.3 Exploitation stage

The exploitation stage is executed by (S) *or* (A) mathematical operators due of their highly concentrated outcomes. The criterion for this phase is $r1 < MOA$. Operator S is tasked with updating the position if $r3$ is less than 0.5 (where $r3$ is a random value within the range $[0,1]$), while the other operator (A) is to be disregarded until S fulfills its objective. Otherwise, the location is modified via the (A) operator. The mathematical model for this search phase is delineated in accordance with formula (4.32) to maintain the exploration during both the initial and final trials, the parameter μ is meticulously calibrated to yield a randomized outcome at each iteration.

$$x_{i,j}(C\_Iter+1)=\begin{cases} best(x_j)-(MOP+\varepsilon)\times\left((UB_j-LB_j)\times\mu+LB_j\right), & \text{r3<0.5} \\ best(x_j)+(MOP+\varepsilon)\times\left((UB_j-LB_j)\times\mu+LB_j\right), & \text{otherwise} \end{cases} \tag{4.32}$$

4.2.3.4 Snake optimization algorithm (SOA)

The snake approach explained in chapter 03 in Metaheuristic MPPT approaches section.

4.2.4 Validation of EPFOA Under different conditions

4.2.4.1 Test of Performance of the proposed EPFOA under changing irradiance conditions

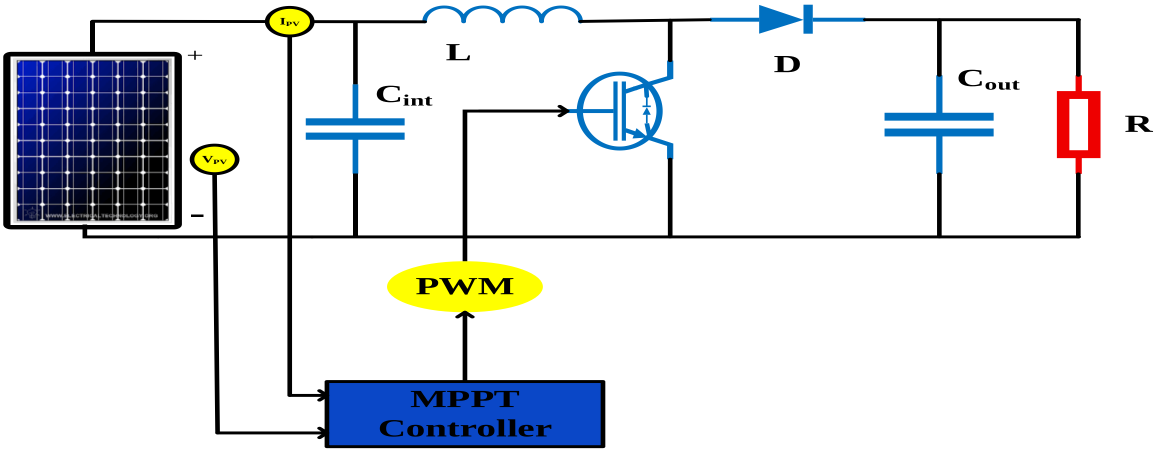

Figure 4.4: Simulation Setup.

A simulation was conducted using Simulink MATLAB, which offers a flexible framework for modeling and simulating solar systems, as illustrated in Figure 4.5. Figure 4.4 depicts this configuration, which seeks to thoroughly evaluate the efficacy of the proposed ICWOA in practical scenarios. A photovoltaic system consists of a Sun Power SPR-200-BLK PV module with specifications illustrated in **Table 2.1**, a DC-DC boost converter, and an MPPT controller with a sampling interval of 0.05, operating at a constant switching frequency of 25 kHz, all connected to a resistive load.

The efficacy of the suggested EPFOA approach was evaluated by comparing it with many recently developed and widely utilized MPPT methods, including SOA, AOA, and GWA in terms of efficiency, tracking time and convergence speed (CS). Their efficacy was examined at various irradiance levels, as depicted in the profile shown in Figure 4.6. Figures bellows illustrate the simulation results, demonstrating the efficacy of the examined approaches.

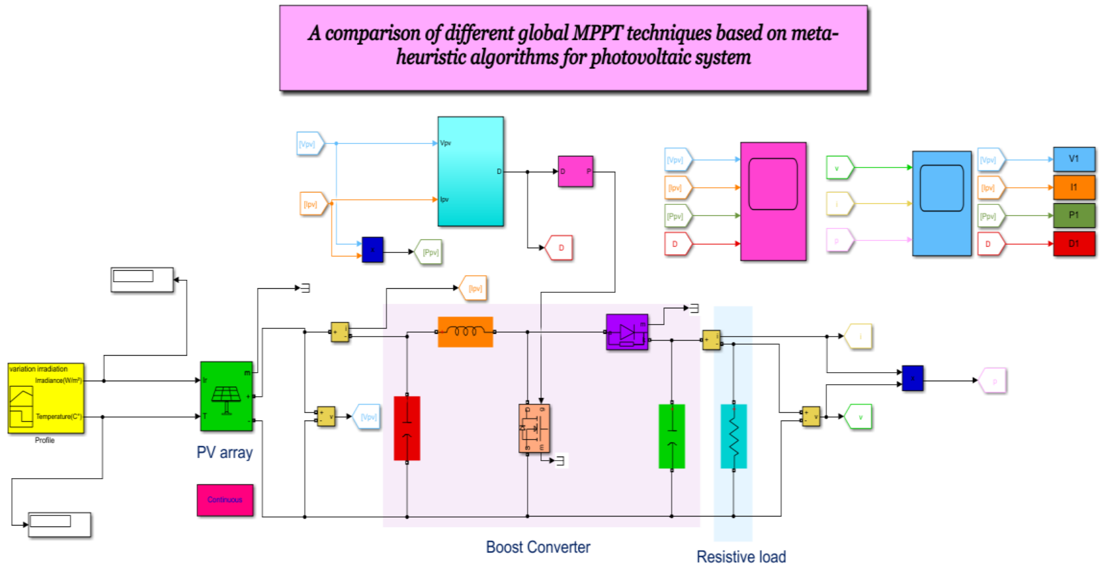

Figure 4.5: Photovoltaic system Simulink model controlled by proposed MPPT techniques.

The results underscore the efficacy of the proposed EPFOA technique, demonstrating its ability to precisely compute the GMPP, effectively overcome the extensive search space of the P-V curve, and adapt to real-time environmental fluctuations.

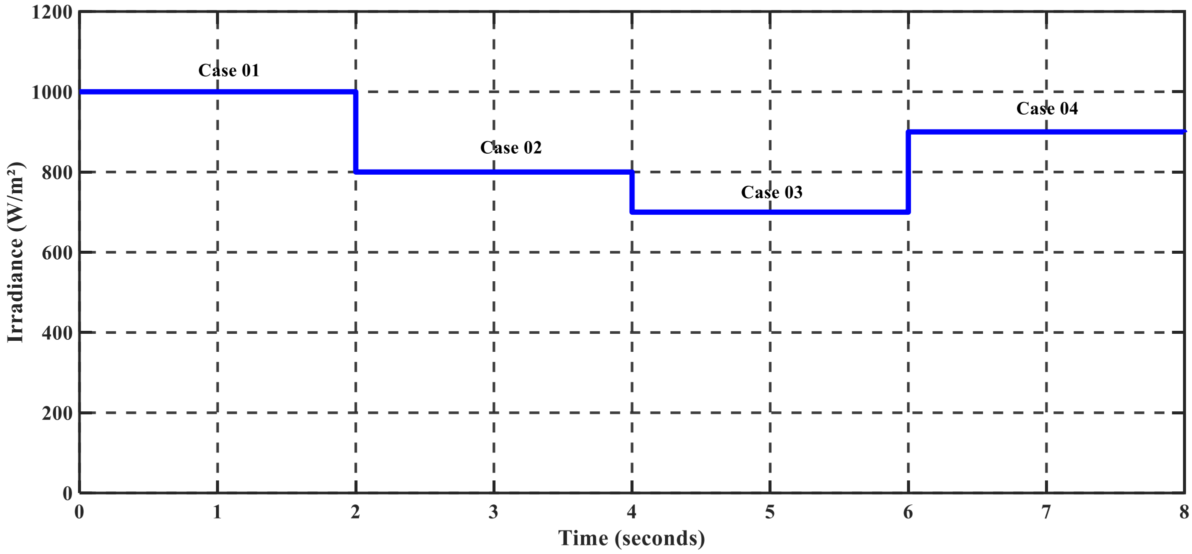

Figure 4.6: The profile of irradiance.

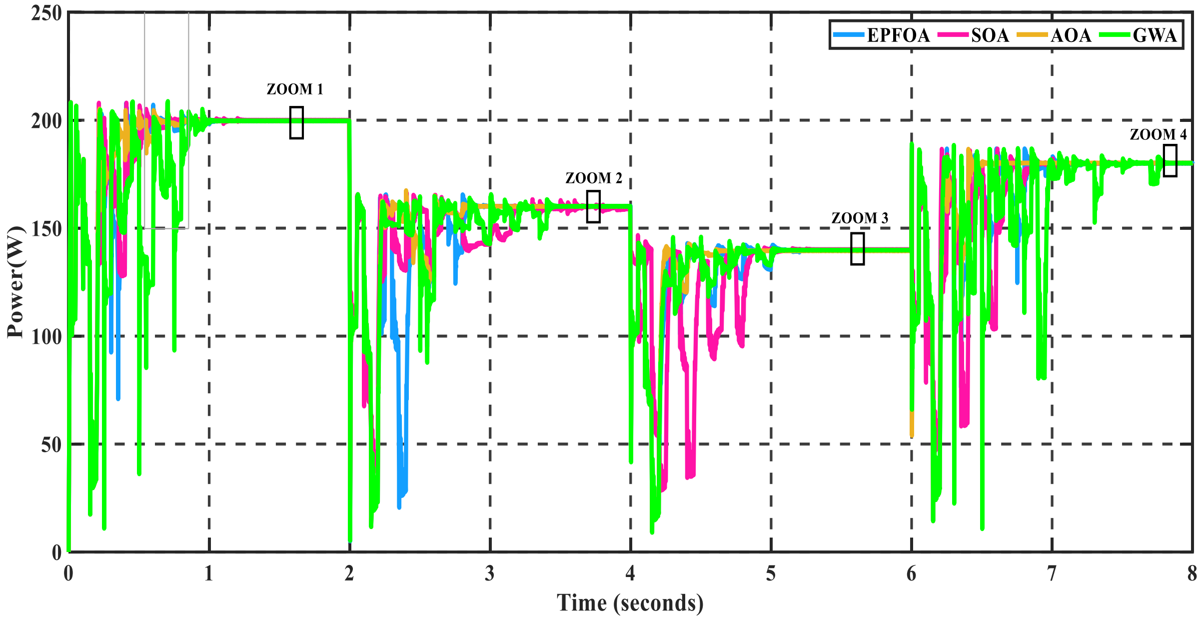

Figure 4.7: Power dynamics under changing irradiance.

Under four different irradiation scenarios, the effectiveness of the four MPPT strategies—EPFOA, SOA, AOA, and GWA—was evaluated. While Figures from Figure 4.7 until Figure 4.11 show the associated PV power, voltage, current, and duty cycle responses, Table 4.1 shows the power output (W), efficiency (%), mean efficiency (%) , tracking time (s) and mean tracking time (s) for each approach. The efficiency for each technique is determined using the Eq. (4.33) [157].

$$Efficiency = \frac{(Maximum \text{ power -stabilized power})}{Maximum \text{ power}} \times 100\% \tag{4.33}$$

EPFOA performs remarkably consistently in all circumstances. With efficiencies between 99.8% and 100%, it achieves power outputs of 199.6 W, 160.165 W, 139.84 W, and 180.036 W. Nonetheless, its tracking durations are brief and consistent, ranging from 1 to 1.25 seconds, so demonstrating rapid and seamless convergence. While the duty cycle continuously adjusts, indicating accurate control under various conditions, the related PV power and voltage plots show minimal variations around the maximum power point. In scenario 02, EPFOA achieves an efficiency of 100%, as shown in zoom 02 of Figure 4.7 , confirming that the proposed EPFOA quickly stabilizes near MPP. Furthermore, the P–V properties shown in Figure 4.12 provide a clear visual depiction of the EPFOA's precise alignment with the true MPP along the entire PV curve, efficiently tracking the shifting operating point under various irradiance situations.

With powers of 200 W, 158.8 W, 140.092 W, and 180.12 W for Cases 01–04, respectively, and efficiencies ranging from 99.15% to 100%, SOA exhibits exceptional performance. The photovoltaic power and voltage graphs show slight oscillations close to the maximum power point, and the duty cycle shows slight transient overshoots. However, its tracking times are somewhat prolonged or variable, ranging from 1 to 1.15 seconds. These results indicate that SOA converges consistently, but at a marginally slower rate than EPFOA during sudden irradiance fluctuations.

In Scenarios 02 and 03, where irradiance variations are more noticeable and typically cause significant nonlinear disruptions to the photovoltaic properties, SOA performs exceptionally well. As shown in zoom 2 and zoom 3 of Figure 4.8 , SOA maintains exceptional efficiency and dynamic stability despite these abrupt fluctuations, achieving 158.8 W and 140.092 W with efficiencies of 100% in both cases. The zoom in power response clearly shows that the method quickly converges the MPP with low oscillation.

With efficiencies between 99.58% and 99.98%, GWA offers power outputs of 199.73 W, 160.11 W, 139.83 W, and 180.1 W. This suggests that it has excellent steady-state accuracy. However, its tracking periods vary significantly (1–1.7 s), and the corresponding plots of PV power, voltage, current, and duty cycle show increased oscillations and long settling, especially in low irradiation conditions (Case 03). This suggests that GWA is more sensitive to sudden changes in irradiance, requiring longer times to evaluate the MPP. Consequently, GWA's dynamic robustness is less than that of both EPFOA and SOA, despite achieving satisfactory end efficiency.

AOA requires quick response and provides power outputs of 199.74 W, 160.07 W, 139.5 W, and 180.13 W, with efficiencies between 99.58% and 100%. It has the shortest tracking times (0.65–0.85 s) of all the methods tested, which shows that it quickly responds to changes in irradiance. Still, the duty cycle graphs that go along with them show sudden changes and the plots of PV power, voltage, and current show small differences from the exact MPP, especially after changes in irradiance. This behavior shows a distinct compromise between speed and accuracy: AOA reacts quickly, but it is not as accurate or stable as EPFOA or SOA.

With a mean efficiency of 99.89% as illustrated in Figure 4.14, the comparative analysis shows that EPFOA offers the most efficient and balanced MPPT performance under varying irradiance. The power-response zoom-ins and the steady voltage, current, and duty-cycle graphs show that it consistently achieves good performance, quick convergence, and remarkably stable operation with little oscillation with short tracking time of 1.125 s as illustrated in Figure 4.13. With an efficiency of 99.79% and a comparatively slower transient response, SOA is a reliable substitute. Despite achieving a steady-state efficiency of 99.91%, GWA exhibits notable oscillations and prolonged convergence, which reduces its effectiveness when irradiance changes quickly. With an average tracking time of 0.76 seconds, AOA has the fastest response time. However, its correction procedure causes more oscillation around the MPP and less accuracy. The results generally show that EPFOA has the best overall MPPT performance, the most stable convergence, and the most dynamic resilience, while the other methods require different trade-offs between speed, accuracy, and stability.

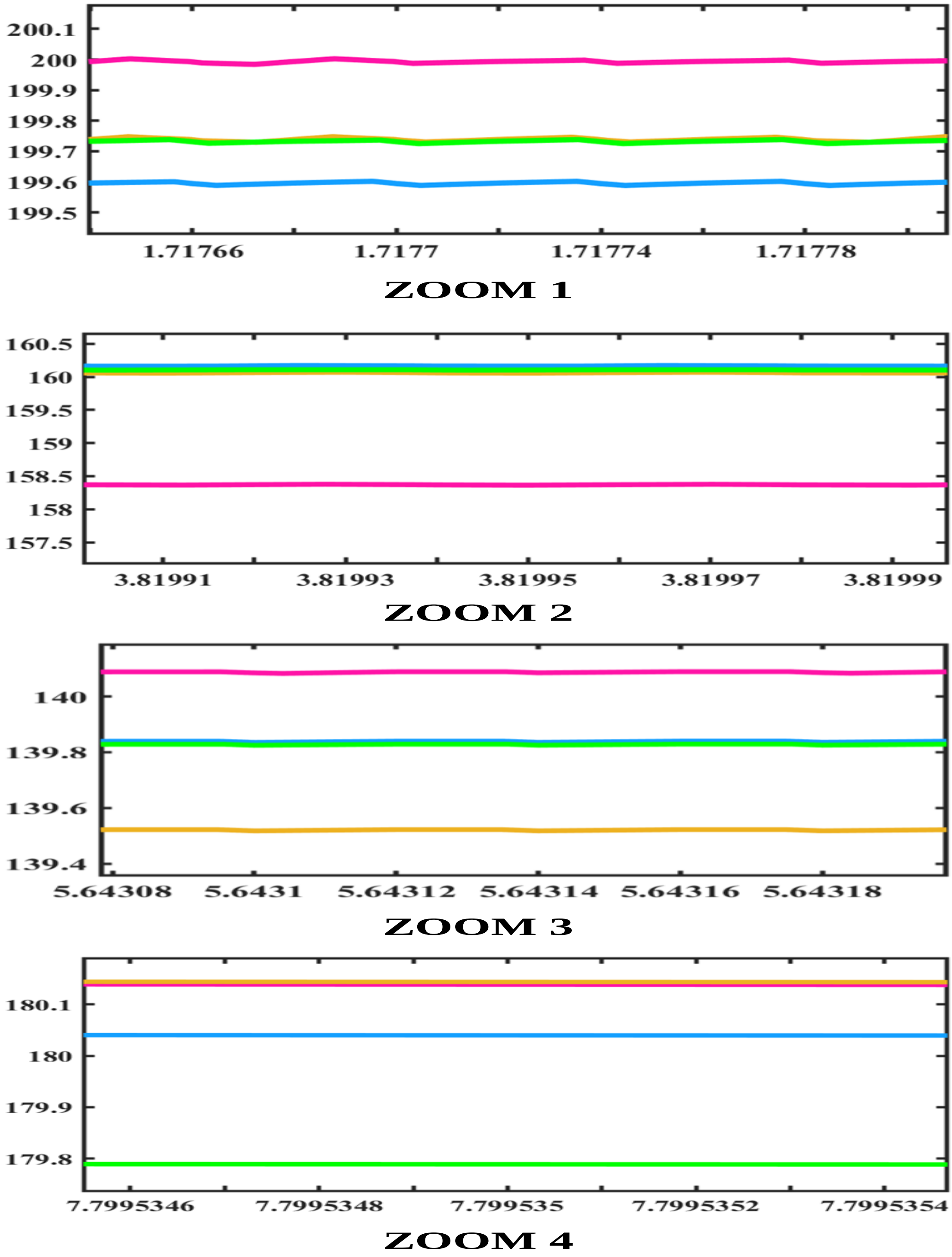

Figure 4.8: Power output zoom in.

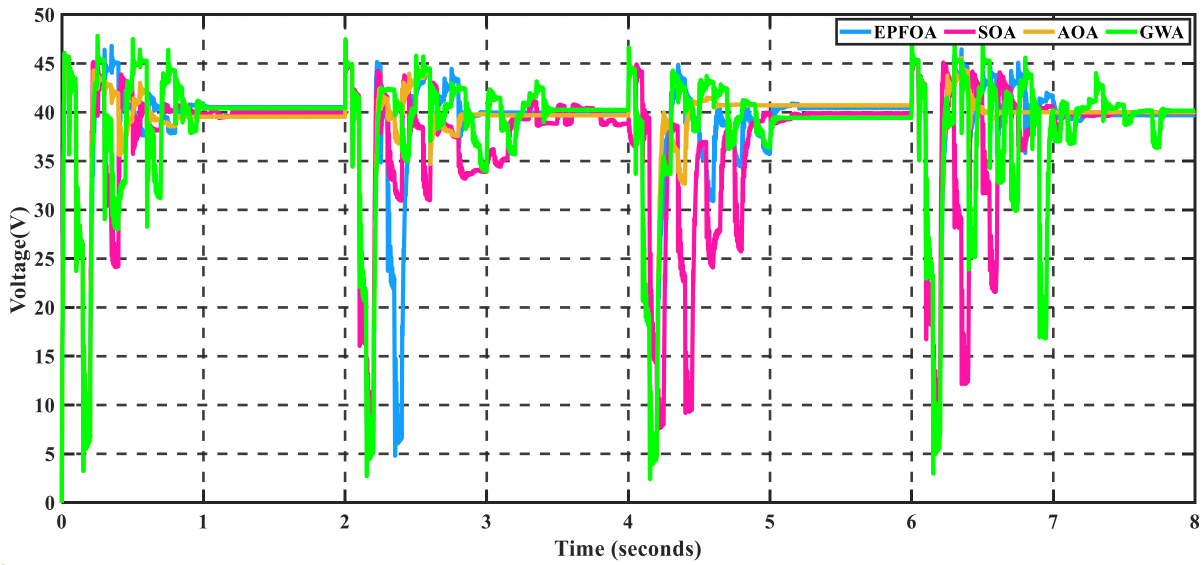

Figure 4.9: The output voltage of PV.

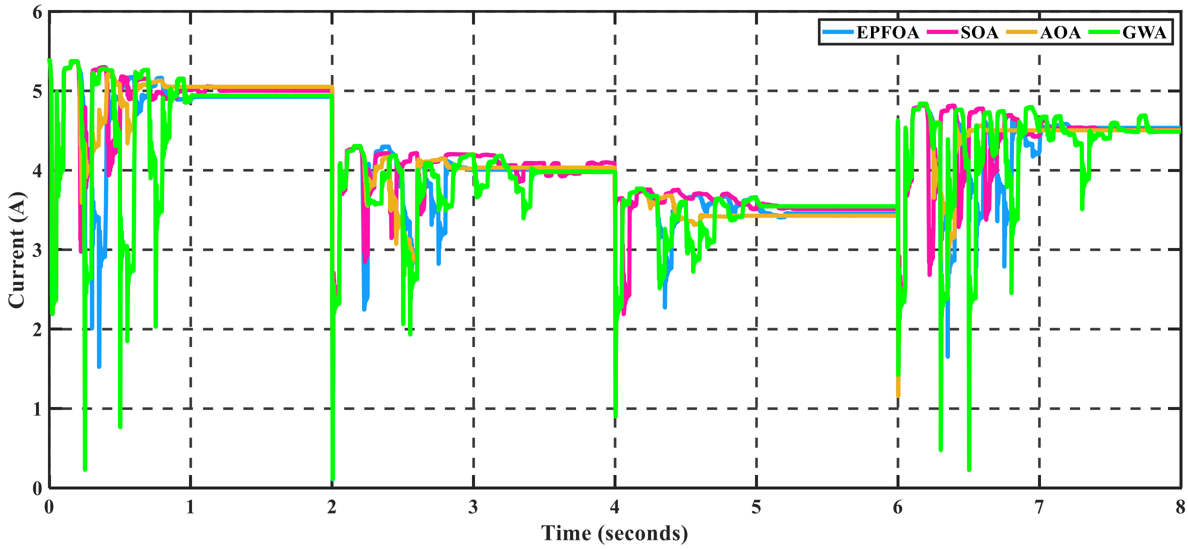

Figure 4.10: The output current of PV.

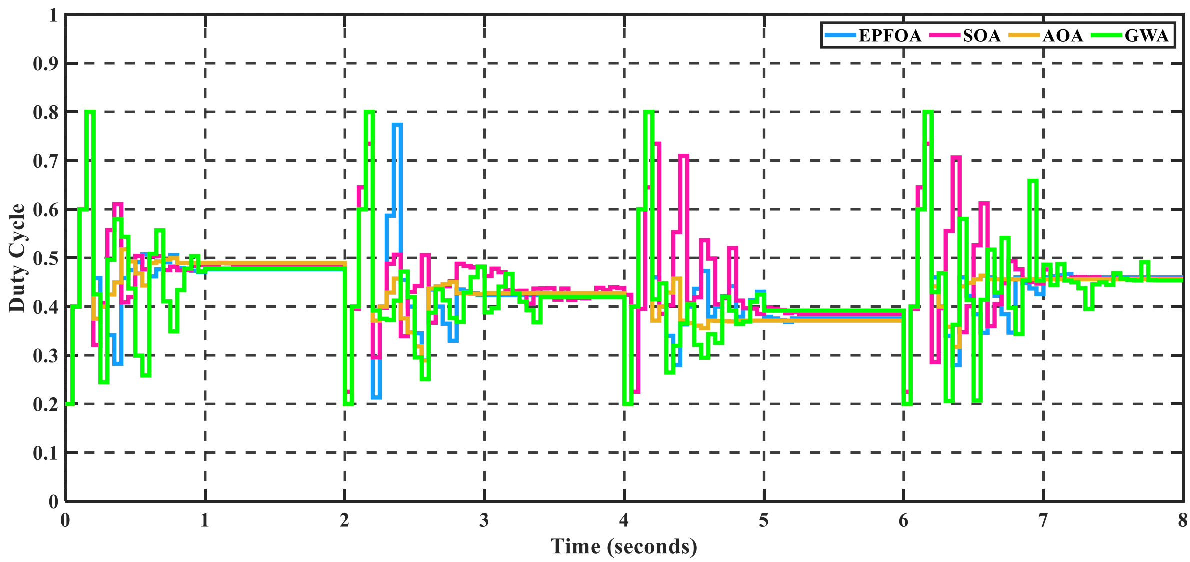

Figure 4.11: Duty cycle response of PV.

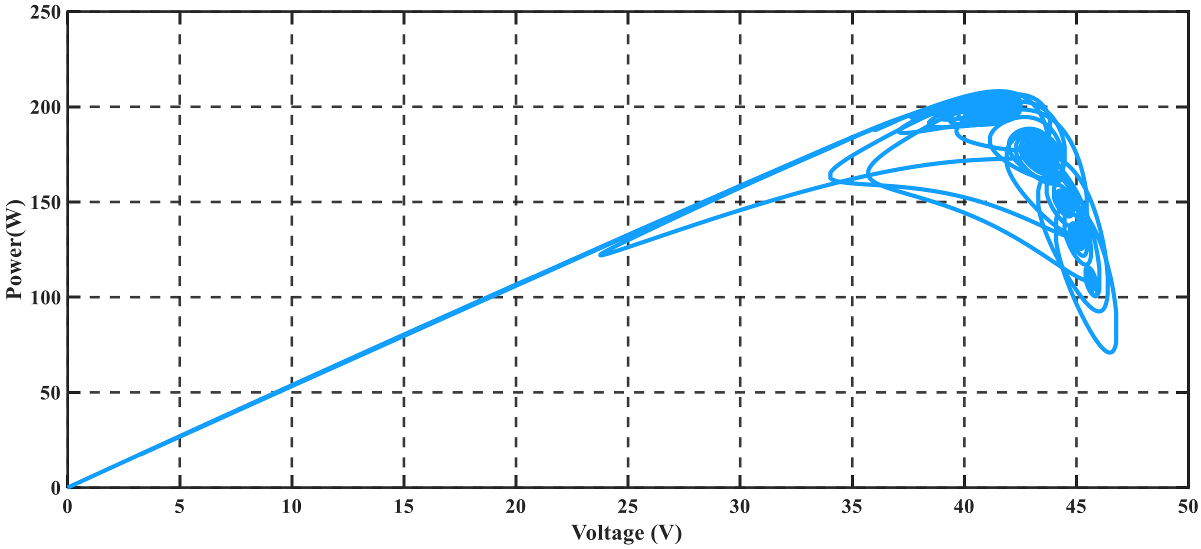

Figure 4.12: The P-V curve of the proposed EPFOA.

Table 4.1 : Summary of comparative study evaluation under change irradiance conditions.

Aspects	Metaheuristic MPPT approaches	SOA	EPFOA	GWA	AOA	Max power
Tuning parameters	-	2	1	2	3	-
Power (W)	Case 01	200	199.6	199.73	199.74	200
	Case 02	158.8	160.165	160.11	160.07	160.165
	Case 03	140.092	139.84	139.83	139.5	140.092
	Case 04	180.12	180.036	180.1	180.13	180.13
Efficiency (%)	Case 01	100	99.8	99.87	99.87	
	Case 02	99.15	100	99.97	99.94	
	Case 03	100	99.82	99.81	99.58	
	Case 04	99.99	99.95	99.98	100	
Mean efficiency (%)	The four cases	99.79	99.89	99.91	99.85	
Tracking time (s)	Case 01	1.05	1	1.65	0.85	
	Case 02	1.6	1	1.45	0.85	

	Case 03	1	1.25	1	0.7	
	Case 04	1.15	1.25	1.7	0.65	
Mean tracking time (s)	**The four cases**	1.2	1.125	1.79	0.76	

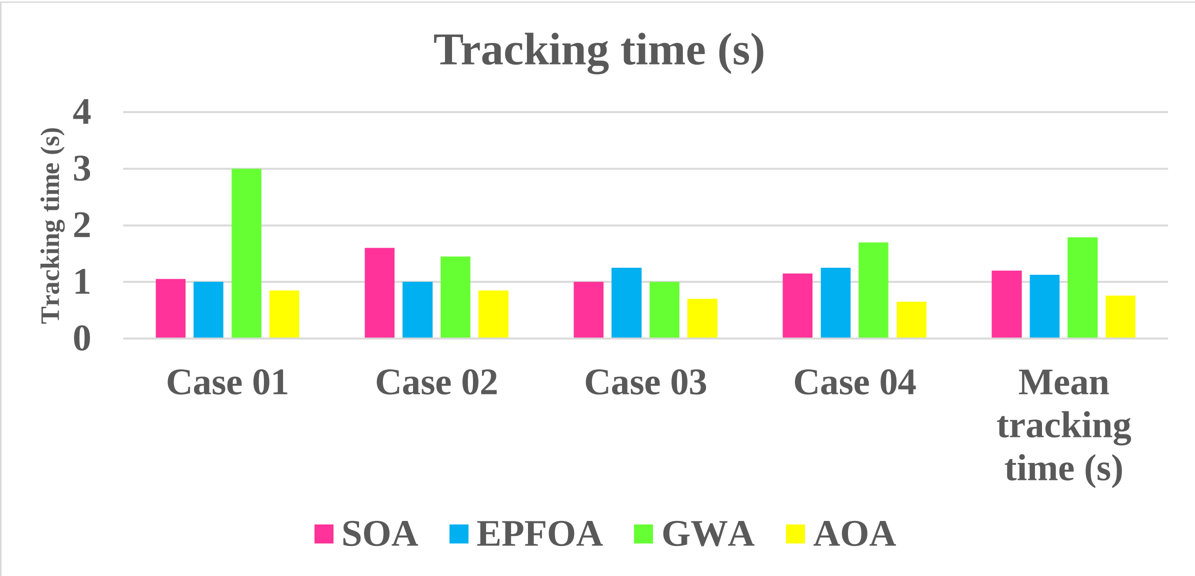

Figure 4.13: A visual representation of each approach's tracking time and mean tracking time under change irradiance conditions.

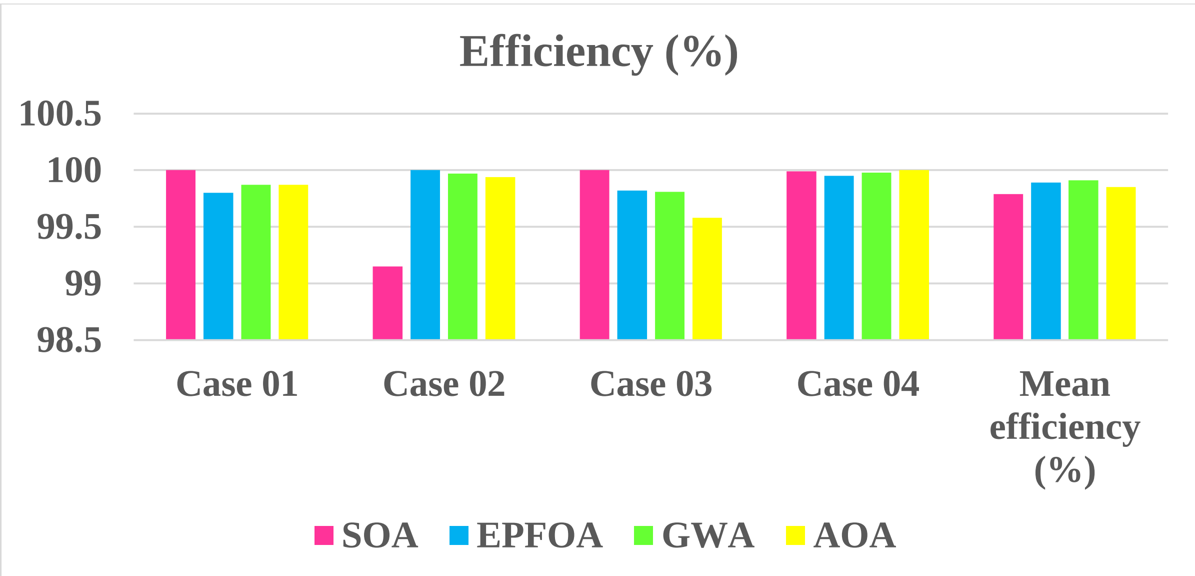

Figure 4.14: A visual representation of each approach's efficiency and average efficiency under change irradiance conditions.

4.2.4.2 Test of Performance of the proposed EPFOA under Partial shading conditions

As shown in Figure 4.16, particular MATLAB simulations were carried out to improve the validation of the method's stability under partial shading and enable a thorough assessment of its tracking precision among numerous local maxima and nonlinear P–V characteristics.

Figure 4.15 shows a block diagram used in the simulation setup that supports the recommended approach, EPFOA, over three complex PSCs with five distinct peaks (see the PV curve for each scenario in the Figure 4.17). The setup consists of five modules connected in series, which replace the Sun Power SPR-200-BLK PV panel, a boost converter, and an MPPT controller with a 0.05-second sampling period that operates at a steady switching frequency of 25 kHz and is connected to a resistive load. To ensure that the photovoltaic panel runs at its maximum power point, the recommended MPPT control system modifies the boost converter's duty cycle. However, the system's MPP and operational point are not the same. By directing the operating point to the PV modules' maximum power extraction position, an advanced MPPT algorithm can optimize system performance. This suggests that less solar panels need to be installed, increasing the efficiency of the system.

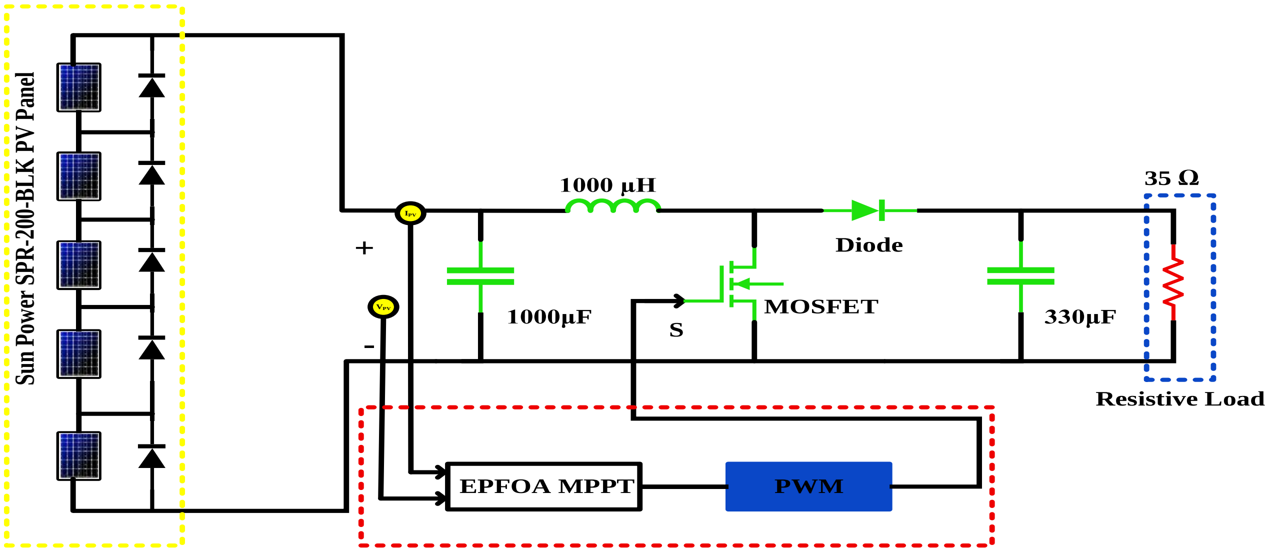

Figure 4.15 : Block diagram of the Proposed EPFOA under PSCs.

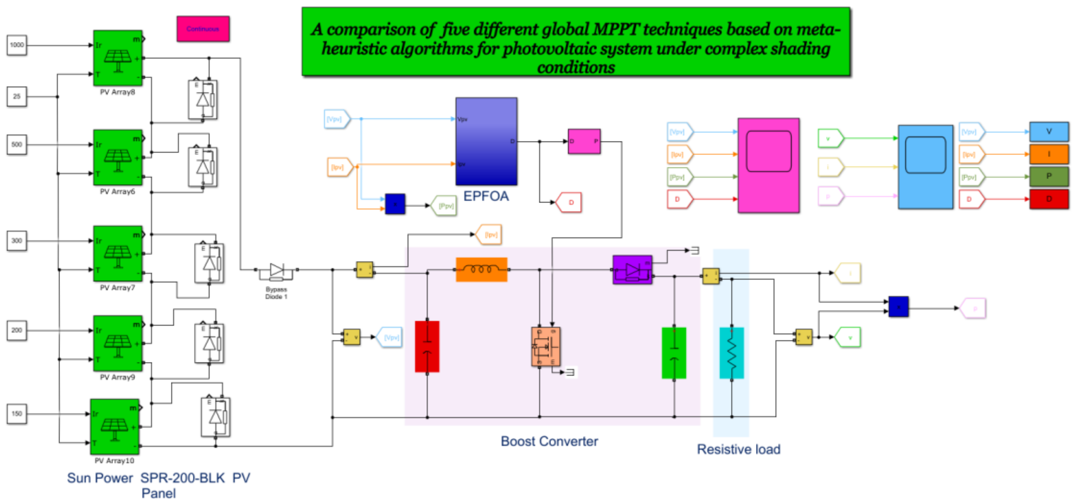

Figure 4.16: A MATLAB simulation of the suggested MPPT approaches Under Partial Shading Circumstances.

As we know, GMPP tracking performance depends significantly on the efficiency of conventional metaheuristic approaches in the presence of PSCs. The effectiveness of the proposed EPFOA method was confirmed by comparing it with four recent and existing MPPT strategies, including AOA [160], PSO [162],[163], SOA [108], and GWA [164], under three partial shade conditions (PSC-1, PSC-2, and PSC-3), each of which was characterized by five complex multiple peaks at a standard temperature of 25°C, as shown in Figure 4.18. Efficiency, tracking duration, and oscillation during GMPP tracking are used to evaluate each method's key performance indicators in relation to each other, revealing several behaviors of the approaches in different GMPPs. The combination of these factors determines the speed and accuracy with which the strategy identifies the GMPP across several PSCs. Figure 4.19 and Figure 4.20 depict a comparative analysis of the performance of MPPT algorithms under partial shading conditions using graphical representation.

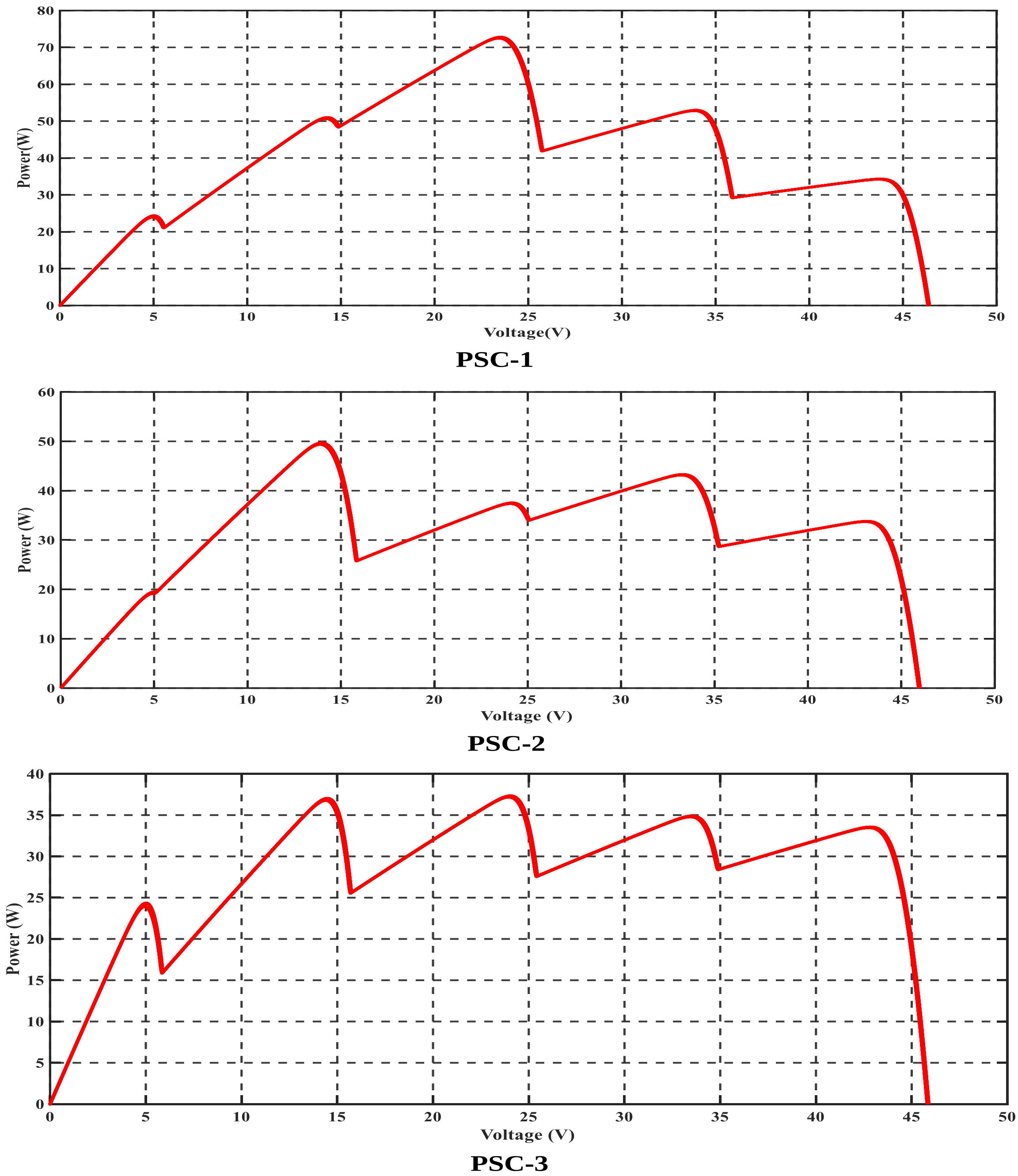

Figure 4.17: The P–V properties of PS scenarios used.

The GMPP is placed in the middle of the LMPPs in the first PSC scenario (PSC-1), and the irradiance values are determined at 1000, 700, 600, 300, and 150 W/m². With a peak of 72.31 W from a theoretical maximum of 72.75 W, the EPFOA approach demonstrates superior performance, yielding an impressive efficiency of 99.40% (see Figure 4.19) and convergence in just 1.05 seconds (see Figure 4.20). AOA compromises speed and accuracy by achieving a slightly lower power output of 70.13 W (96.40% efficiency) while achieving faster convergence with just two tuning parameters at 0.65 seconds. With a long tracking duration of 3.10 s, which indicates poor dynamic behavior, the PSO approach, which uses three tuning parameters, achieves 70.05 W (96.29%) but performs the worst in this situation with high power oscillation and a long duration to identify GMPP. With a single tuning parameter, the SOA method achieves 70.13 W with 96.40% efficiency and a moderate response time of 1.1 seconds, showing comparable performance to AOA. GWA, on the other hand, performs the least well in PSC-1, achieving 69.78 W at 95.92% effectiveness with a tracking duration of 1.45 seconds, suggesting limited robustness in global MPP identification.

Between the first and third LMPPs, the second PSC scenario (PSC-2) establishes irradiation values of 800, 700, 300, 250, and 150 W/m². The differences between approaches become more apparent as the shading becomes more intense. According to the GMPP depicted in **Figure *4.18***, EPFOA continuously outperforms all rivals, recording 49.54 W from a peak of 49.69 W, attaining an extraordinary efficiency of 99.70%, and guaranteeing a steady tracking duration of 1.05 s. The AOA method is the fastest at 0.8 seconds, but in complex shaded environments, its extracted power drops to 46.52 W (93.62%), indicating decreased accuracy. Similar to PSC-1, the PSO approach achieves 46.65 W (93.88%) but performs slowly at 3.0 seconds. The SOA strategy is the second-best performer in PSC-2, achieving satisfactory precision (49.09 W, 98.79%) with an impressive convergence duration of 1.6 seconds. By contrast, under this shade configuration, the GWA technique is unable to detect the global MPP and achieves only 39.24 W (78.97% efficiency) with an extended tracking duration of 3.0 s due to delayed convergence and high power oscillations.

The GMPP is located between the first and third LMPPs in the third PSC scenario (PSC-3), where the irradiance values are set at 1000, 500, 300, 200, and 150 W/m². With a tracking performance of 37.16 W out of 37.32 W, an efficiency of 99.57%, and a short tracking duration of 0.95 s, the EPFOA technique outperforms the GMPP. Although the AOA method is the fastest (0.75 s), it achieves lower accuracy (34.86 W, 93.41%), suggesting that its quick response is associated with the use of just two tuning parameters. The SOA approach performs well, producing 36.89 W (98.85% efficiency) with a moderate convergence time of 1.3 s, proving it to be an effective alternative. While the GWA approach shows limited capability at 34.85 W (93.38%) and records the slowest tracking time in this context at 1.8 seconds due to its performance suffering from power fluctuations, the PSO technique performs slowly because of high power oscillation at a delayed convergence time of 2.45 seconds with an efficiency of 93.38%, as presented in Figure 4.18.

As illustrated in Figure 4.18 , the most consistent and dependable MPPT technique is the EPFOA approach, which consistently achieves a mean efficiency of 99.89% and maintains average tracking times of roughly 1.125 seconds in all scenarios. While the SOA technique effectively achieves a balance between speed and precision, the AOA method consistently sacrifices accuracy while demonstrating superior convergence speed. On the other hand, PSO exhibits significant delays in every evaluation, and GWA performs the worst (see Figure 4.18) due to its inability to precisely identify the global MPP, especially in situations with severe shadowing. Table 4.3 compiles all of the performance metrics for the different MPPT methods, such as tracking duration, efficiency, and the related power, current, voltage, and duty-cycle values for each shade scenario.

PSC-1

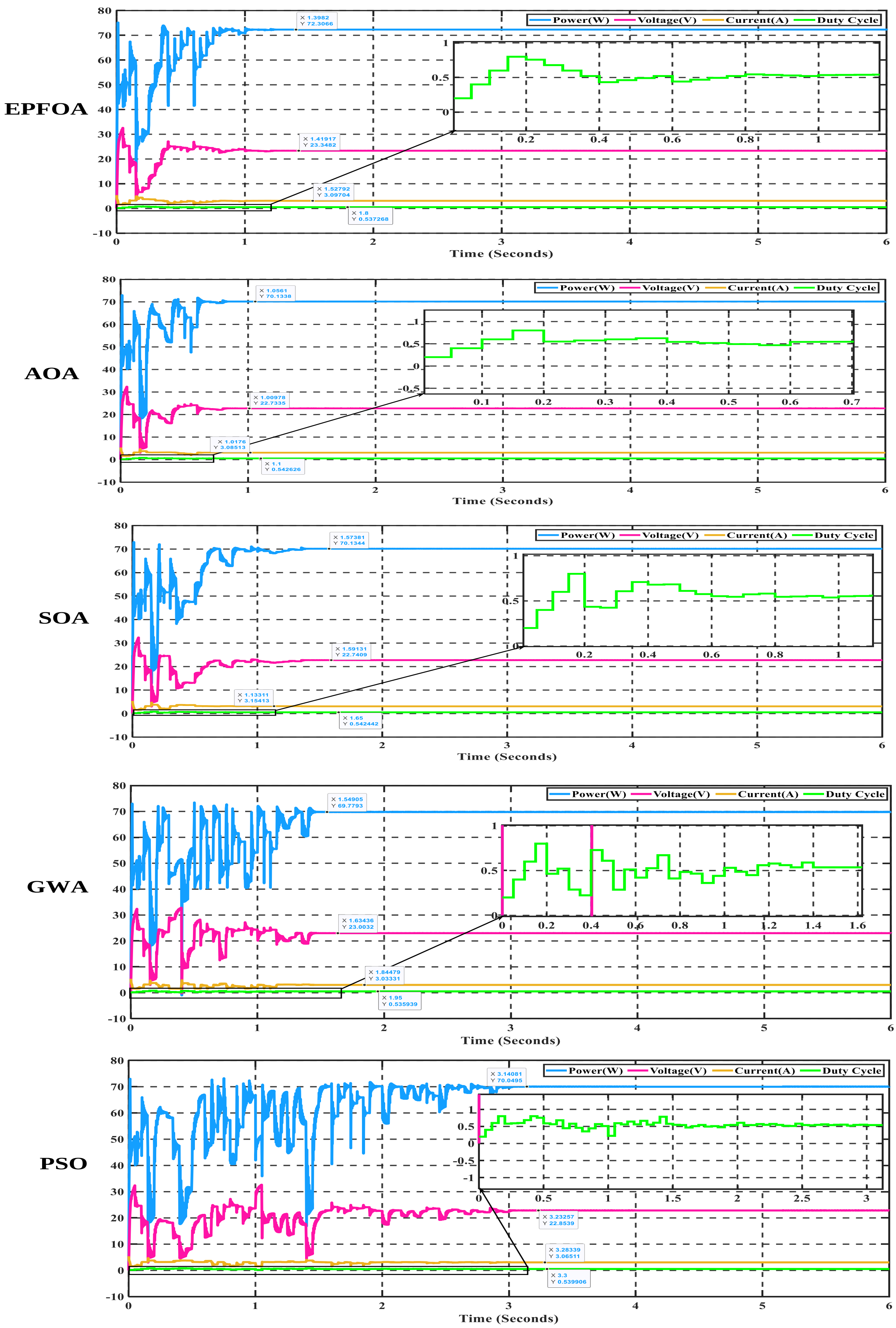

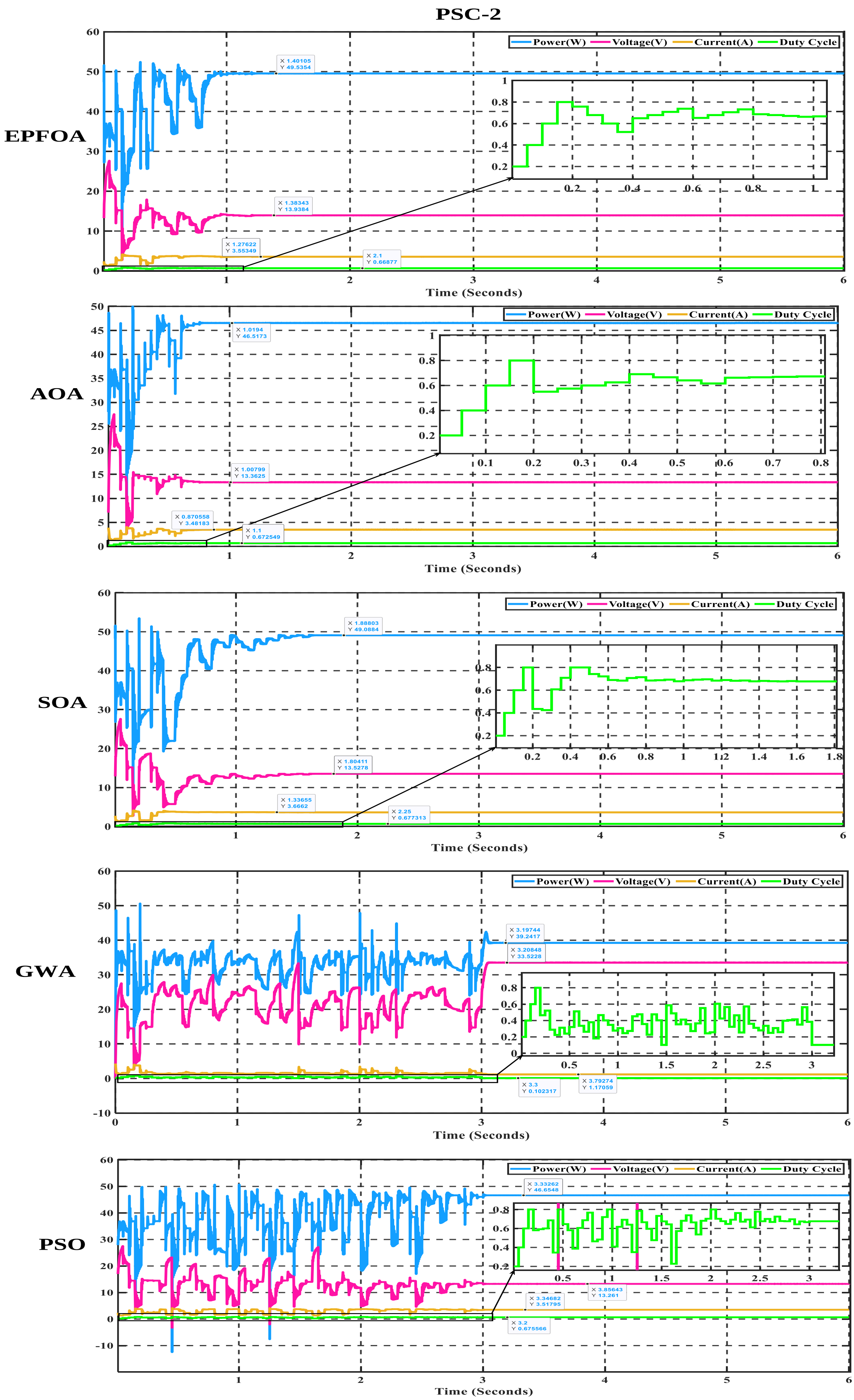
PSC-2
EPFOA
AOA
SOA
GWA
PSO
Power(W)
Voltage(V)
Current(A)
Duty Cycle
Time (Seconds)

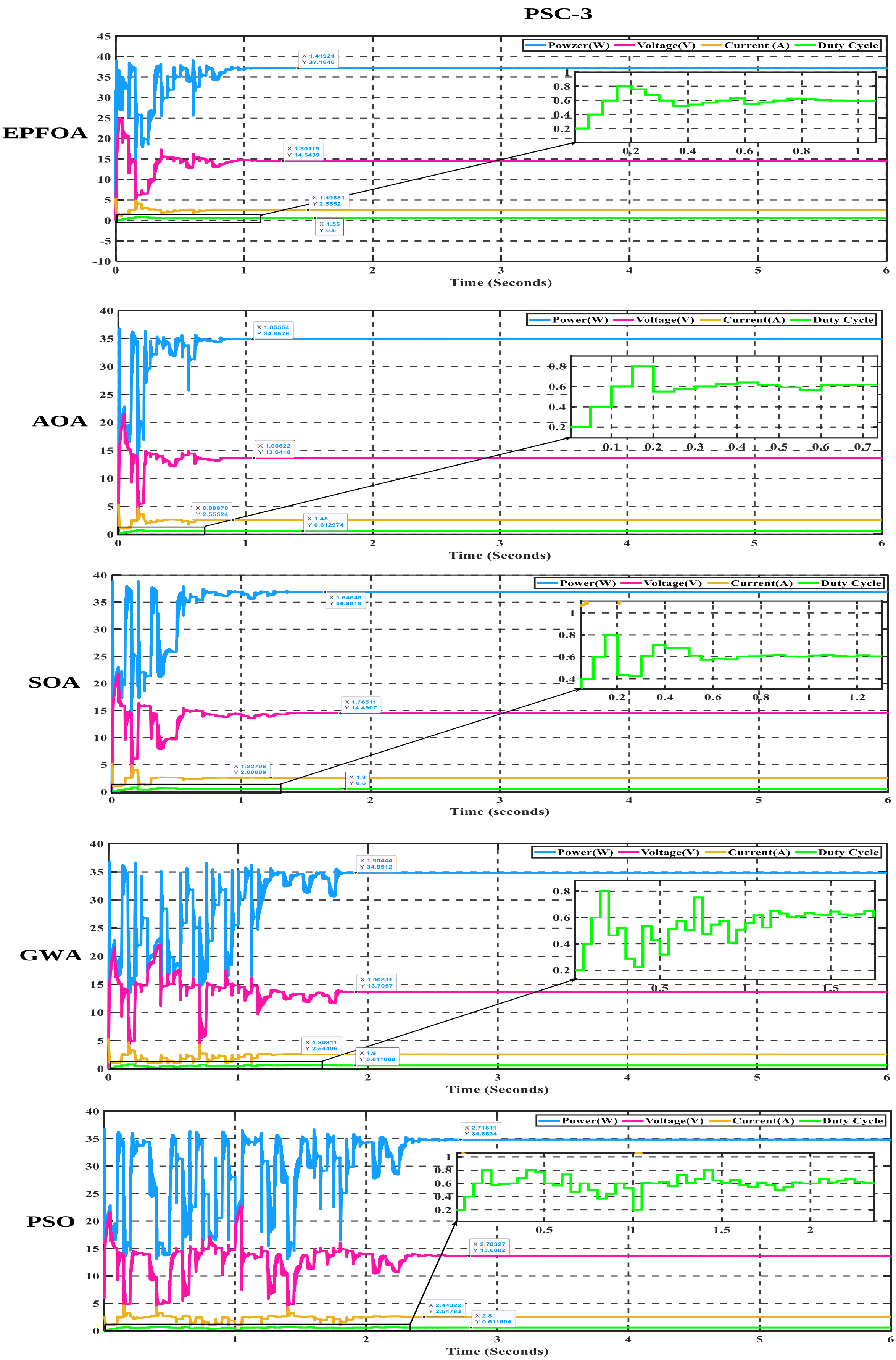

Figure 4.18: Simulation results of comparison between the proposed EPFOA with SOA, AOA, GWA, and PSO under three PSC.

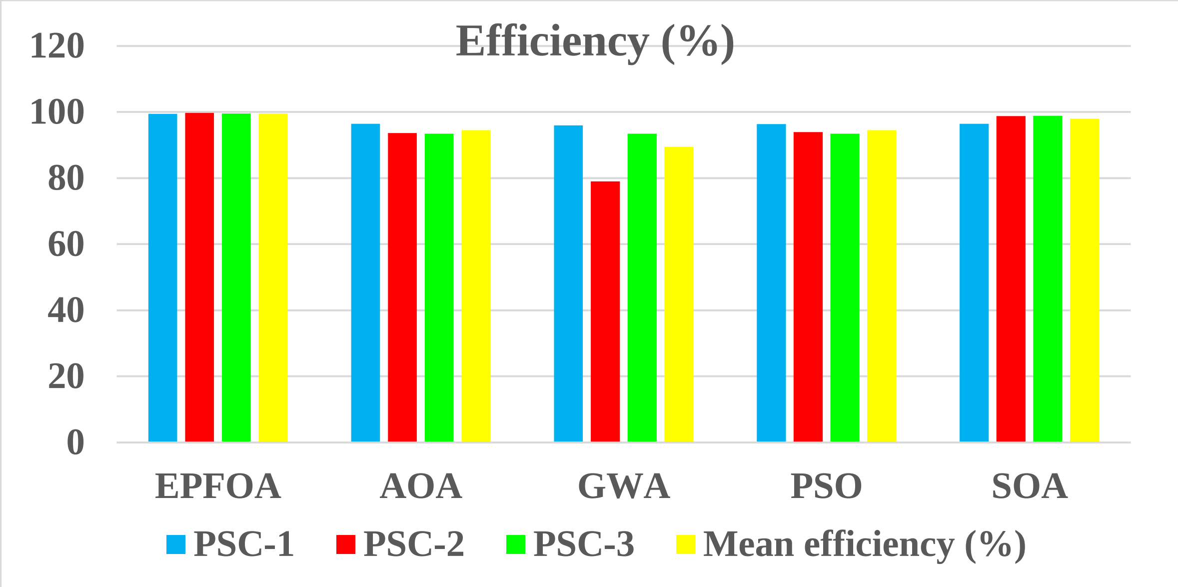

Figure 4.19: A visual representation of each approach's efficiency and average efficiency under three PS scenarios.

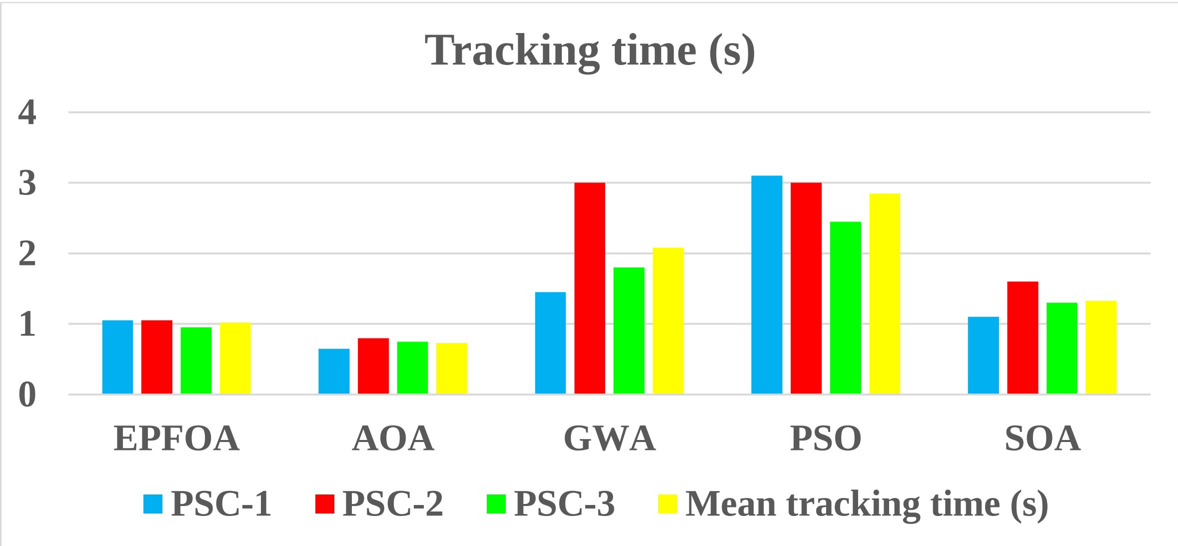

Figure 4.20: A visual representation of each approach's tracking time and mean tracking time under three PS scenarios.

Table 4.2 : Tuning parameters and random numbers for methods used.

MPPT strategy	**EPFOA**	**AOA**	**GWA**	**PSO**	**SOA**
Tuning parameters	$\lambda = 1.5$ $F = 1.16 - \sin\left(\frac{\pi}{2}\left(\frac{k}{M}\right)^2\right)$	$MOP(C\_Iter) = 1 - (C\_Iter)^{1/\alpha} / (M\_Iter)^{1/\alpha}$ μ	$a = 2$ to 0 C=2*r	$w = 0.4$ $c_1 = 1.2$ $c_2 = 2$	$c = \left(1 - \frac{t}{t_{max}}\right)$
Random numbers	1	2	2	2	1

The proposed EPFOA MPPT was evaluated in detail under complex partial-shading conditions and rapidly varying irradiance. With outstanding performance, quick convergence, and low complexity, the EPFOA is one of the most modern MPPT algorithms in all assessed scenarios. With just two tuning parameters, it continuously approaches the global maximum power point. It was able to effectively overcome local peaks due to its dynamic search strategy, which allowed for reliable tracking even in the face of abrupt environmental changes. The technique was able to achieve high output power without oscillating around the MPP. In terms of tracking speed, accuracy, and resilience, the comparative results show that it outperforms both conventional and modern MPPT techniques. The EPFOA's remarkable dependability under all circumstances attests to its suitability for realistic photovoltaic applications. In order to improve methods' practical relevance and possibly reduce computational time and algorithmic complexity, future research will focus on optimizing methods by reducing the search space and extending their application to new converter types. Table 4.4 confirms that EPFOA outperforms the common and currently used MPPT approaches for PV.

Table 4.3: Summary of comparative study analysis between five metaheuristic approaches under PSCs.

Approaches	Metrics	Power (W)	Max power (W)	Efficiency (%)	Tracking time (s)	Duty Cycle	Current (A)	Voltage (V)
AOA	PSC-1	70.13	72.75	96.40	0.65	0.542626	3.08513	22.7335
EPFOA		72.31		99.40	1.05	0.537268	3.09704	23.3482
GWA		69.78		95.92	1.45	0.535939	3.03331	23.0032
PSO		70.05		96.29	3.1	0.539906	3.06511	22.8539
SOA		70.13		96.40	1.1	0.542442	3.15413	22.7409
AOA	PSC-2	46.52	49.69	93.62	0.8	0.672549	3.48183	13.3625
EPFOA		49.54		99.70	1.05	0.66877	3.55349	13.9384
GWA		39.24		78.97	3	0.102317	1.17059	33.5228
PSO		46.65		93.88	3	0.675566	3.51795	13.261
SOA		49.09		98.79	1.6	0.677313	3.6662	13.5278

AOA		34.86		93.41	0.75	0.612974	2.55524	13.6418
EPFOA		37.16		99.57	0.95	0.6	2.5552	14.5439
GWA	PSC-3	34.85	37.32	93.38	1.8	0.611068	2.54496	13.7057
PSO		34.85		93.38	2.45	0.61104	2.54783	13.6882
SOA		36.89		98.85	1.3	0.6	2.60889	14.4907

Table 4.4 : A comprehensive comparison between the proposed EPFOA and the common and currently used MPPT approaches for PV.

MPPT strategy	**Efficiency**	**Steady state oscillation**	**Convergence Speed (CS)**	**Implementation complexity**
Proposed EPFOA	Very high	Very Low	Very Fast	Low
P&O [165]	Medium	Medium	Slow	Low
IC [166]	Medium-high	Low	Medium –Fast	Medium
PSO [167]**,**[168]	Medium-high	High	Medium –Fast	Medium
GWA [169]	Medium-high	Medium	Medium –Fast	Medium
AOA [160]	Very high	Very low	Fast	Low
SOA [108]	Very high	Very low	Very Fast	Low
COS [110]	Very high	Very low	Very Fast	Low
Artificial Bee Colony [170]	High	Low	Slow	Medium
Flower Pollination Algorithm [171]	High	Medium	Medium	Medium
Mayfly optimization algorithm [172]	High	Medium	Medium	Medium
Fuzzy Logic Adaptive Crow Search Algorithm [173]	High	Low	Fast	High
Deep reinforcement learning approach [174]	Very high	Very low	Fast	Very high

4.3 The Development of an MPPT Controller for PEMFCs

Proton Exchange Membrane Fuel Cells (PEMFCs) serve as sustainable energy systems, significantly contributing to electricity generation and interfacing with current systems using DC-DC converters.

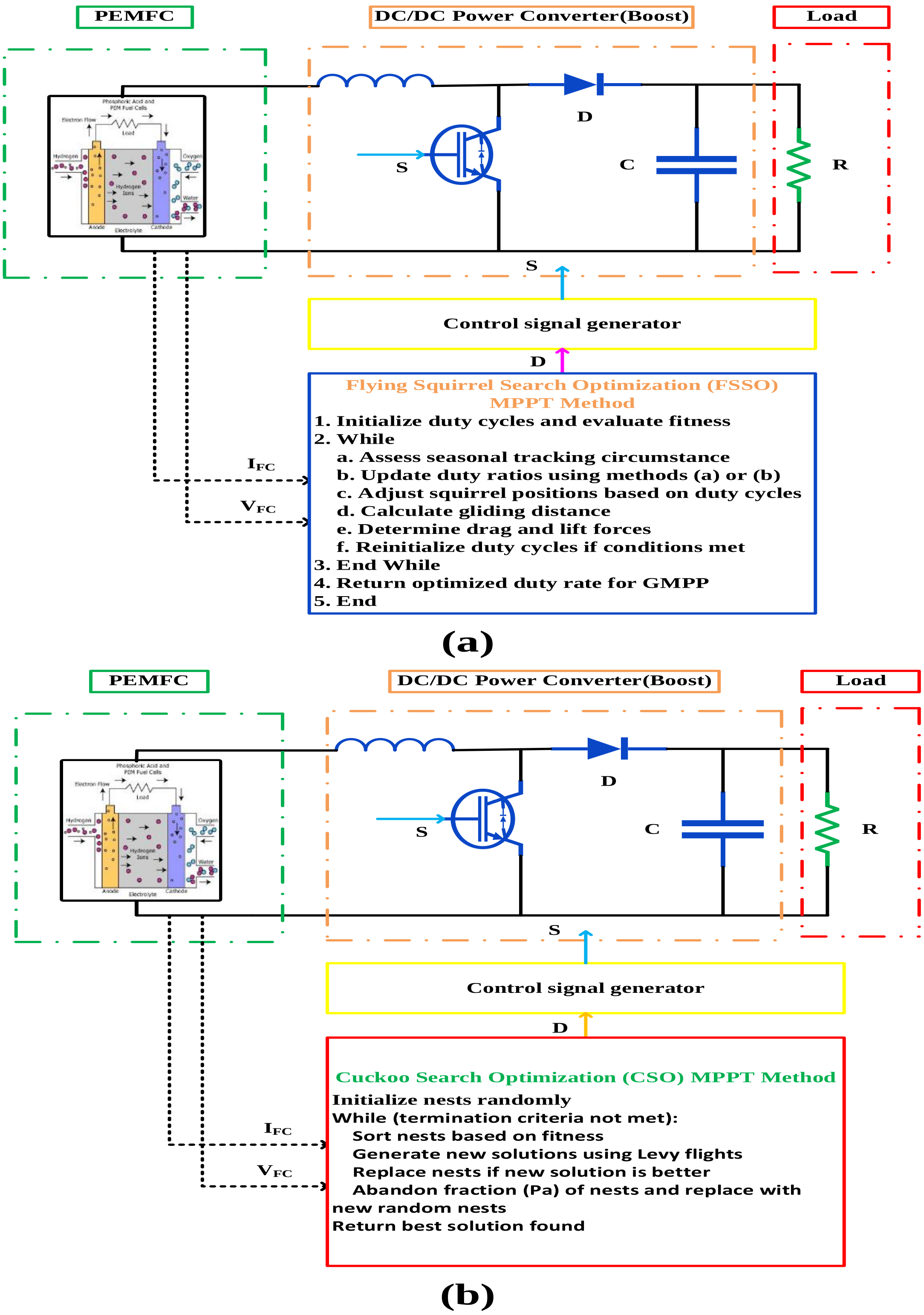

Figure 4.21 : System architecture utilizing two of the MPPT approaches: (a) FSSOS and (b) CSO.

A principal problem is the efficient extraction of power despite variations in circumstances that influence output voltage. There has been a notable increase in the utilization of intelligent control approaches and metaheuristic algorithms for diverse control applications. Despite its considerable efficiency, the power output of the fuel cell is not consistently optimal due to its fluctuating internal components. A strategy for maximum power point tracking through a DC-to-DC converter is necessary to achieve optimal power harvesting [123]. This section examines the enhancement of proton exchange membrane (PEM) fuel cell efficiency in variable settings by the application of the effective flying squirrel search optimization strategy (FSSOS) as a MPPT controller compared to the cuckoo search optimization (CSO) approach, as seen in the block diagram in Figure 4.21. A PEMFC, a DC–DC boost converter (the specifications are given in Table 4.5), and an MPPT controller that uses FSSO and CSO optimization techniques constitute the system. The MATLAB/Simulink environment is used to evaluate and analyze the entire system under different temperature and pressure circumstances. Table 4.6 illustrates that the selected parameters significantly affect the enhancement of a PEMFC system via CSO and FSSO. Meticulously defining each parameter value provides an exact compromise between exploration and exploitation dynamics, ensuring each technique's potential to attain the MPP while keeping its consistency and effectiveness.

Table 4.5: Parameter for the boost converter.

Component	**Inductance (L)**	**Capacitance (C)**	**Resistance (R)**	**Switching Frequency**
Value	98×10^{-2} H	1×10^{-6} F	26 $Ohms$	20 KHZ

4.3.1 Flying Squirrel Search Optimization Method

In 2020, Nagendra Singh, Krishna Kumar Gupta, and their team developed the Flying Squirrel Search Optimizer, which mimics the search method of flying southern squirrels (FSs), as illustrated in Figure 4.22. The location of an FS represents the possible solution vector, whereas the quality of the food source denotes the matching fitness. First, we divide the place into three zones based on fitness values: the optimum solution (OS), representing the hickory tree; the near OS, representing the acorn tree; and the random solution (RS), representing the normal tree. In the initial phase, the best solution globally determines the direction in which to move the NOS. In the second phase, some RSs are guided to the OS. The final step involves transferring the remaining RSs to NOS. One of its defining features is the degree to which OS, NOS, and RS work together. Not only does the given approach to MPPT take advantage of this aspect [175],[59].

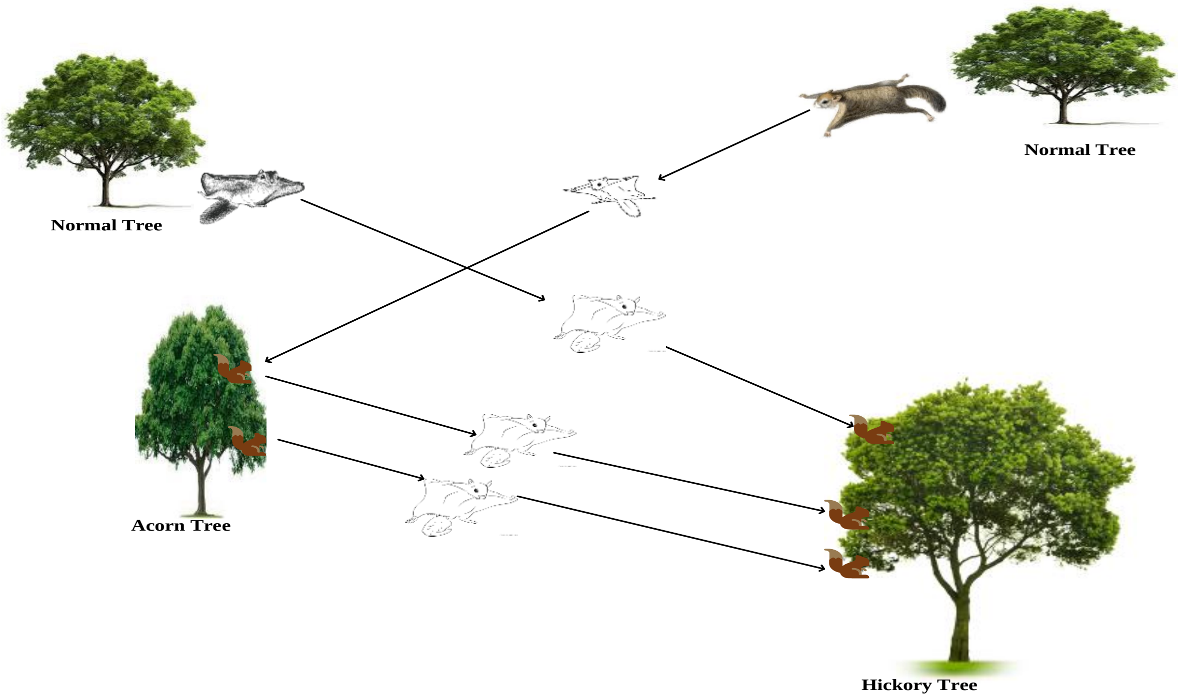

Figure 4.22: The foraging habit of the flying squirrel [175].

4.3.1.1 Application of the FSSO Method to the Tracking of GMPPs

When assessing the effectiveness of the PEMFC system, the duty ratio of the boost converter plays a crucial role. Figure 4.23 illustrates the flowchart for the FSSO MPPT technique, and the steps and formulas listed below describe this technique.

4.3.1.1.1 Getting started

Primarily set the squirrels $N_{fs} FSs$ in the resolution area to symbolize various duty rates throughout a boost converter, each defined differently [59].

$$d_i = d_{mn} + \frac{(i-1)[d_{mx} - d_{mn}]}{N_{fs}}; i = 1, 2...., N_{fs} \tag{4.34}$$

d_{mn} and d_{mx} Represent the minimum and maximum values of the converter duty cycle while enhancing, respectively.

$$0.2 < d_i < 0.8 \tag{4.35}$$

4.3.1.1.2 Fitness Evaluation

The power generated by a PEMFC system at each duty cycle is considered the quality of the nourishment resource, with the fitness function (f) defined for all duty cycles.

$$f(d) = \max P_{PV}(d) \tag{4.36}$$

4.3.1.1.3 Declaration and Arrangement

Finding the hickory tree's optimal duty cycle (G_{Best}) for a PEMFC system allows for its highest output of energy. In most cases, an oak tree ranks as the second-best placement (P_{Best}). We will assume that all remaining items FSs (NT_{FS}) are located on normal trees.

4.3.1.1.4 Location recency

After assessing the season's monitoring situation, a shift in proportion to duty occurs. If the seasonal variable $S^k{}_C$ is less than S_{min}, increase the duty rates using procedure (a); otherwise, change the duty rates using procedure (b). Afterwards, the level of fitness is evaluated.

4.3.1.1.5 Current Seasonal Monitoring Status

Monitoring conditions, helps avoid becoming trapped in the localized maximum power point. The following formula determines the seasonal value (S_C) in a single-dimensional location and its minimal value (S_{min}).

$$\begin{cases} S_C^k = \left| d_{at}^k - d_{ht} \right| \\ S_{\min} = \dfrac{10e^{-6}}{365^{k/(km/2.5)}} \end{cases} \tag{4.37}$$

d_{ht} and d_{at} denote the squirrel's location in the acorn and hickory trees Km. The symbol K represents the latest repetition, which holds the highest level of significance.

To enhance the exploration area, we use a Levy possibility to modify the range of duty rates in normal trees.

$$d_{nt}^{k+1} = d_{nt}^k + s \tag{4.38}$$

In a normal tree, the position of a squirrel is represented by d_{nt}, and the dimension of a step is shown by s using the levy dispersion, as seen below:

$$s \approx k \left(\frac{u}{|\upsilon|^{\frac{1}{\beta}}} \right) (d_{ht} - d_{nt}) \tag{4.39}$$

In which μ & v are computed employing a standard distribution model. "κ" stands for the increment factor, and "β" for the Levy value.

$$u \approx N(0, \sigma_u^2), and : u \approx N(0, \sigma_v^2) \tag{4.40}$$

When Γ one points to an integral gamma function is indicated, the following describes the variables σ_μ and σ_ν:

$$\sigma_u = \left(\frac{\Gamma(1+\beta)\sin(\pi\beta/2)}{\Gamma\left(\frac{1+\beta}{2}\right)\beta(2)^{\left(\frac{\beta-1}{2}\right)}} \right) and : \sigma_v = 1 \quad (4.41)$$

Where:

$$\Gamma\,(n) = (n-1)! \quad (4.42)$$

4.3.1.1.6 Change Routine

The squirrel on an oak tree moves towards a hickory tree, causing a shift in duty ratios. Most squirrels stay in acorn trees $(NT_{FS} - RNT_{FS})$, while a few unplanned RNT_{FS} switch to hickory trees, using specific equations.

$$d_{at}^{k+1} = d_{at}^{k} + g_d G_c (d_{ht}^{k} - d_{at}^{k}) \quad (4.43)$$

$$d_{nt}^{k+1} = d_{nt}^{k} + g_d G_C (d_{ht}^{k} - d_{nt}^{k}) \quad (4.44)$$

$$d_{nt}^{k+1} = d_{nt}^{k} + g_d G_C (d_{at}^{k} - d_{nt}^{k}) \quad (4.45)$$

The constant and the distance are used to define the gliding distance, which is defined as:

To determine the gliding space, which can be expressed using the constant glide Gc and the spacing g_d as follows:

$$\begin{cases} g_d = \dfrac{h_g}{s_f \tan\phi} \\ \tan\phi = \dfrac{F_D}{F_L} \end{cases} \quad (4.46)$$

The value of hg expresses the percentage of lower height. The two distinct forces, denoted by drag F_D and lift F_L, are calculated in the following way:

$$\begin{cases} F_D = \dfrac{1}{2}\rho V^2 S C_D \\ F_L = \dfrac{1}{2}\rho V^2 S C_L \end{cases} \quad (4.47)$$

The following variables were randomized and selected: ρ air density values, V squirrel speed, S body surface space, C_D drag factor, and C_L lift factor.

4.3.1.1.7 Evaluation of Convergence

The optimization phase must end when the change in all positions FSs reaches a specific threshold or reaches the maximum number of allowed repeats.

4.3.1.1.8 Returning to the initial state

The fitness level in the highest power point tracking process, an evolving optimization process, fluctuates based on external conditions, with duty rates varying under various scenarios.

$$\frac{P_{FC}^{k+1} - P_{FC}^{k}}{P_{FC}^{K+1}} \geq \Delta P\,(\%) \tag{4.48}$$

Table 4.6: Parameters Used in FSSO and CSO MPPT strategies.

Symbol	Value	Description
	FSSOA	
κ	1.5	The coefficient of step
Gc	0.0019	The gliding distance constant
ρ	0.01204	The density of air
β	1.5	The index of levy
V	0.0525	Squirrel velocity
C_L	0.007	The lift coefficient
C_D	0.006	The drag coefficient
S	0.00154	Space for the body
s_f	0.18	the scaling factor
hg	0.01	Height loss amount
	CSOA	
σ_v	The random walk's standard deviation	2
σ_u	The random walk's standard deviation	determined using beta
β	The scaling factor	3/2
k	Factor of step size adjustment	0.8

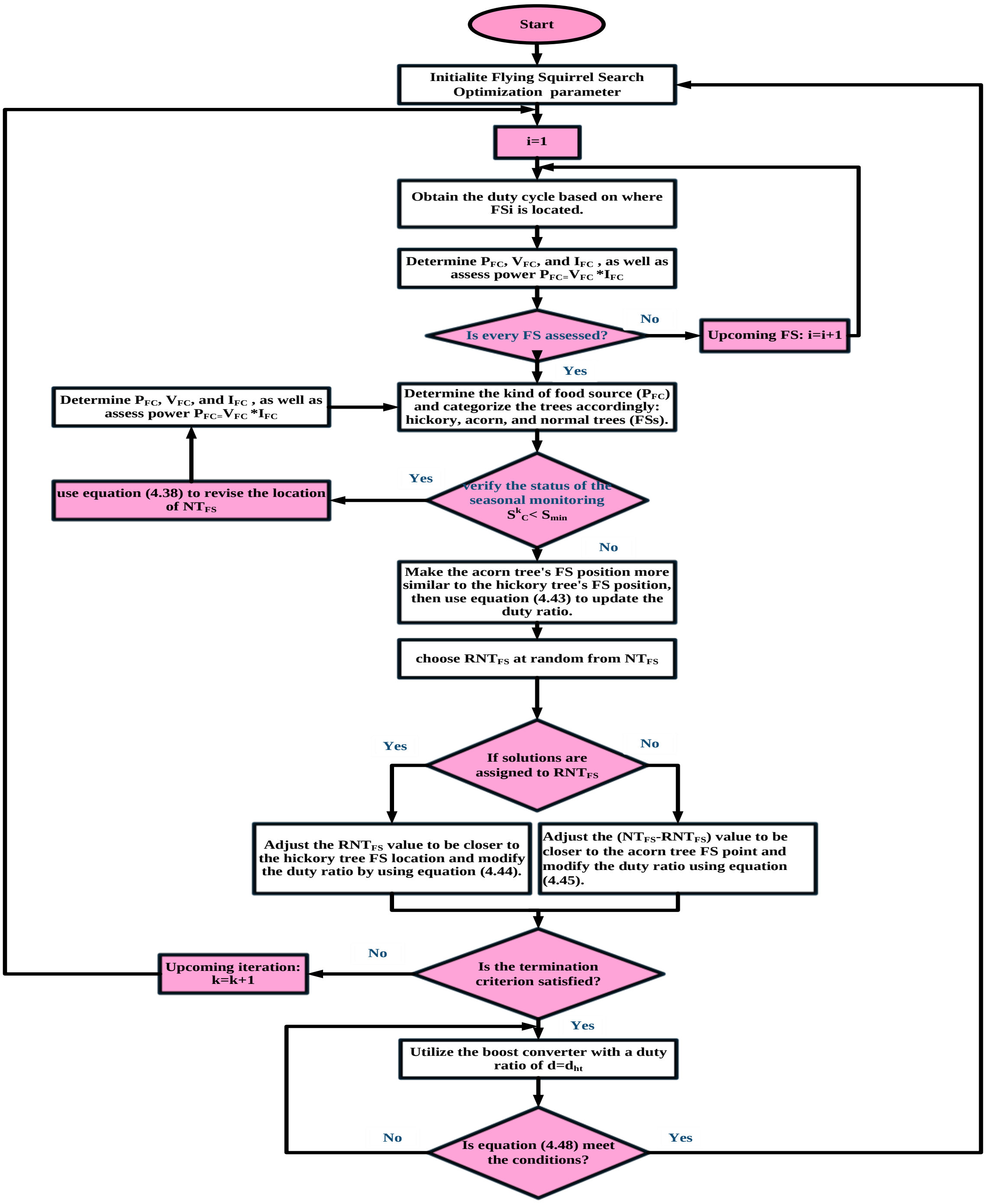

Figure 4.23: The flowchart of FSSO MPPT [59].

4.3.1.2 Cuckoo search optimization (CSO)

CSO is a nature-inspired technique based on cuckoo birds' reproductive habits. Instead of building their own nests, cuckoos are parasitic organisms that lay their eggs in the nests of other bird species. In search of suitable host candidates, cuckoos move at random between nests. They then choose the best nest to increase the chances that their eggs will hatch and produce a new generation of cuckoos. By placing their eggs in strategic locations and, in certain situations, removing the host bird's eggs from the nest, cuckoo birds increase the likelihood that their eggs will hatch. Some cuckoo species have developed the ability to lay eggs that are very similar to those of other bird species. It is possible, though, that the host bird will recognize the foreign eggs and abandon the nest. In these conditions, the cuckoo's eggs do not hatch. This innate tendency was taken into consideration when developing the CSO algorithm. This method can be applied to a single objective problem using the following three idealized characteristic rules [176]:

- ✓ A single egg will be laid by each cuckoo in a randomly chosen host nest.
- ✓ The next generation of cuckoos will inherit the superior nest, which contains high-quality organisms.
- ✓ There are a set number of host nests in the ecosystem, and the likelihood that the host bird will find alien eggs is $Pa \ [0,1]$. If the host bird recognizes the foreign eggs, it will either destroy the nest or leave it. After that, the host birds construct a new nest somewhere else.

Cuckoo eggs indicate the solution for the current iteration of the optimization problem, while cuckoo birds represent the particles assigned to find the solution. The random phase of the tracking process, as used in the CSO algorithm, is characterized by an algorithmic distribution. In their natural habitats, many organisms—especially cuckoo birds—display quasi-random movement patterns. A typical Lévy flight characteristic is demonstrated by this motion. The Lévy distribution governs the random paths and step durations of Lévy flights, which are stochastic processes. Animals and insects display Lévy flights, which are characterized by a sequence of linear trajectories punctuated by abrupt deviations. Compared to traditional random walks, Lévy flights are more effective at exploring large search areas. This is because the variances of Lévy flights increase faster than those of a conventional random walk. When compared to a typical random walk, Lévy flights can reduce the number of iterations by about four times. A key mechanism that allows the CSO algorithm to avoid local MPP while also reducing the time needed to achieve MPP is the Lévy flight [176]. The CSO method's flowchart for MPPT is shown in Figure 4.24. The local and global random walks are described by equations (4.49) and(4.50), respectively.

$$x_i^{k+1} = x_i^k + \alpha \otimes \text{ Levy}(\lambda) \tag{4.49}$$

$$Levy \sim u = k^{\lambda} \quad 1 \prec \lambda \leq 3 \tag{4.50}$$

The multiplications are carried out entry by entry, as indicated by the symbol $\otimes$. The cuckoo's subsequent walks essentially form a random walk process with a heavy tail and a power-law step-length distribution.

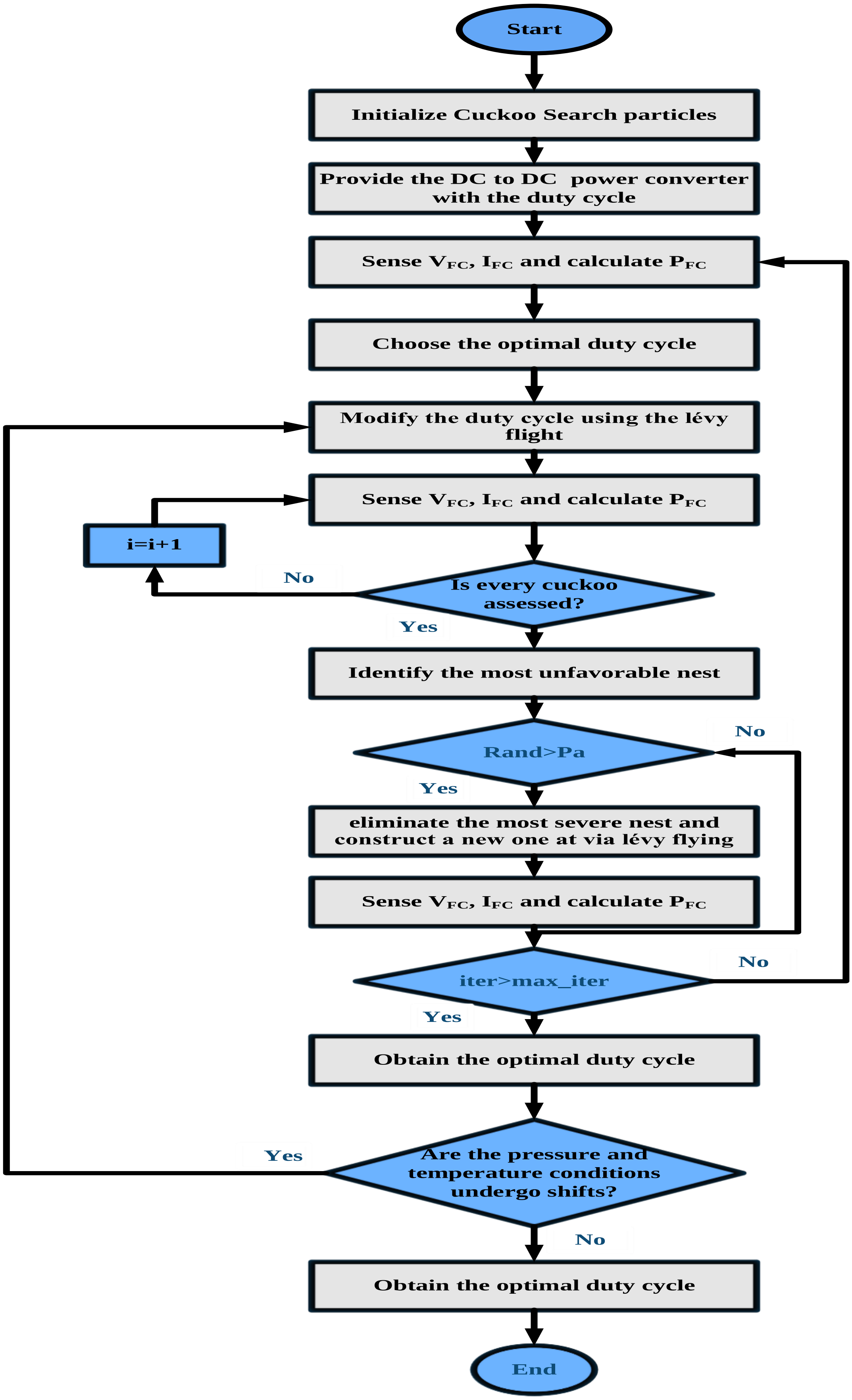

Figure 4.24: CSO flowchart [59].

4.3.2 Results and discussion

4.3.2.1 Standard Test conditions

The FSSO method evidently surpasses CSO under fixed operating conditions, which confirms its successful operation before any externally applied perturbation. For this study, a PEMFC was used to ensure that oxygen $\left(PO_2 = 1\, atm\right)$ and hydrogen $\left(PH_2 = 1.5\, atm\right)$ pressures as well as temperature were maintained constant $\left(T = 328\, K\right)$. Under these specific operating conditions, we assessed the performance of the MPPT controller using FSSO and CSO algorithms. The performance comparison of the two MPPT methods is displayed in Figure 4.25, with an emphasis on the measured results of power, current, and voltage under typical operating conditions. In observing power, current, and voltage, FSSO typically showed faster and more accurate responses (0.5 seconds for each), as compared to CSO, which showed a 0.6-second response, meaning that CSO converges more slowly to the MPP (see Figure 4.31). While both algorithms produce the same maximum power (≈1990.69 W), FSSO does so with significantly more responsiveness, tracking accurately and steadily.

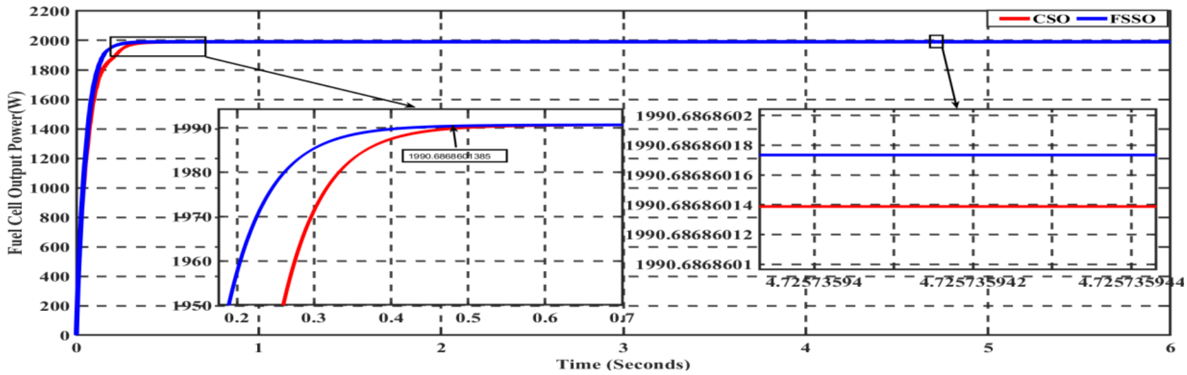

(a)

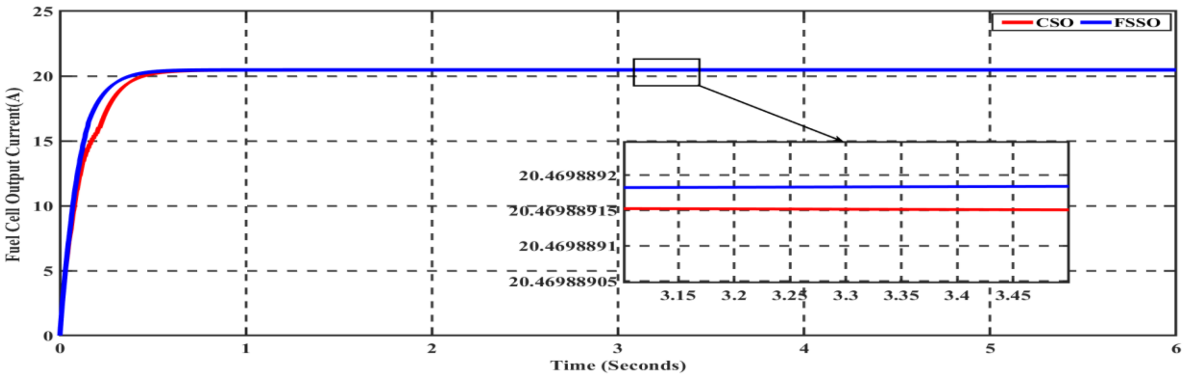

(b)

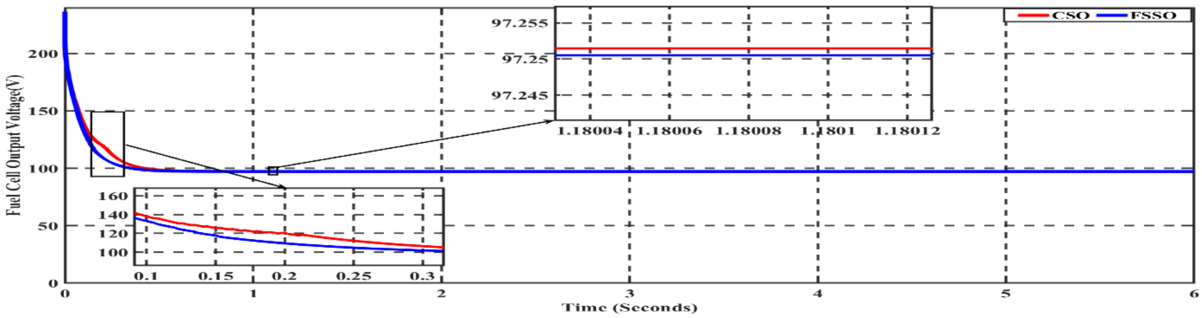

(c)

Figure 4.25: The FSSO and CSO MPPT approaches are evaluated in typical operational circumstances concerning (a) power, (b) current, and (c) voltage.

In comparison with the CSO algorithm, the FSSO algorithm generally responds more rapidly to steady-state conditions (see Figure 4.25 (a)), minimizes transitional oscillations, and reaches MPP consistently more than CSO. FSSO's adaptive search method fosters the exploration or exploitation of the search space more than CSO does. FSSO also enhances the performance of MPPT by adapting to changes, since it can continuously update the search space based on optimal conditions. Moreover, FSSO is known for enhancing the utilization of PEMFC power, but much of its outstanding performance in dynamic pressure and temperature settings stems from its original base performance in steady-state conditions.

4.3.2.2 Fast change in temperature levels

In the second scenario, sudden changes in temperature and the partial pressures of oxygen and hydrogen gas were determined under normal conditions. These changes have an impact on the performance, durability, and life of PEMFC. The ability of the strategies to work with a wide range of temperatures was tested (see profile in Figure 4.26). Variations in temperature can affect the rates of electrochemical reactions, the conductivity of membranes, and the quantity of reactants. Such variations can change the power-voltage properties of fuel cells and make it harder to track the MPP. Figure 4.27 and Table 4.7 show that the two optimizers have very different relationships with dynamics that are driven by temperature. Although FSSO has a rapid response and consistent MPPT estimation, CSO has slower convergence and nonlinear oscillation in response to disturbance temperature changes.

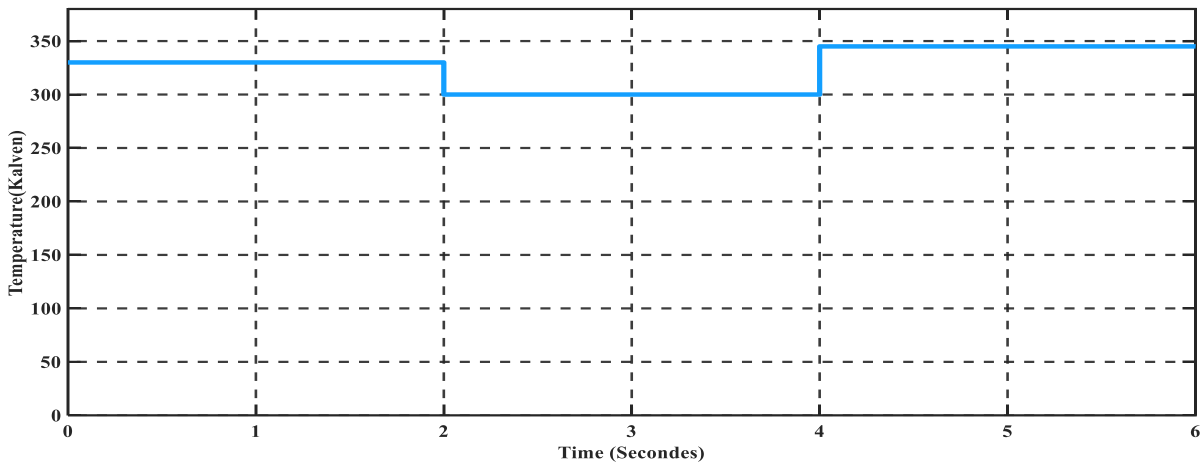

Figure 4.26: The profile of varying levels of temperature.

As shown in Figure 4.27 (a), FSSO achieves an MPP of 1995 W at 330 K for the interval of [0–2] s, while CSO achieves 1986 W, suggesting a notable advantage in power extraction at slightly higher temperatures. Both algorithms converge to almost identical maximum power points at 300 K over 2 to 4 seconds, with values of 1883.16800105 W for FSSO and 1883.168001 W for CSO. This means that both methods attain the same maximum achievable under less-than-ideal working conditions, such as lower reaction rates because of the lower temperature. FSSO, however, offers more seamless tracking performance. The PEMFC then generates more power, with FSSO at 2057.24912751 W and CSO at 2057.24912748 W, as the temperature increases to 345 K in 4 to 6 seconds. These steady-state values are similar to each other but come from distinct dynamic characteristics; FSSO settles more quickly (see figure Figure 4.31) and exhibits fewer oscillations. The results suggest that lower temperatures correspond to lower instantaneous power, while increased temperature does increase the power output. Hence, energy production decreases from lower temperatures.

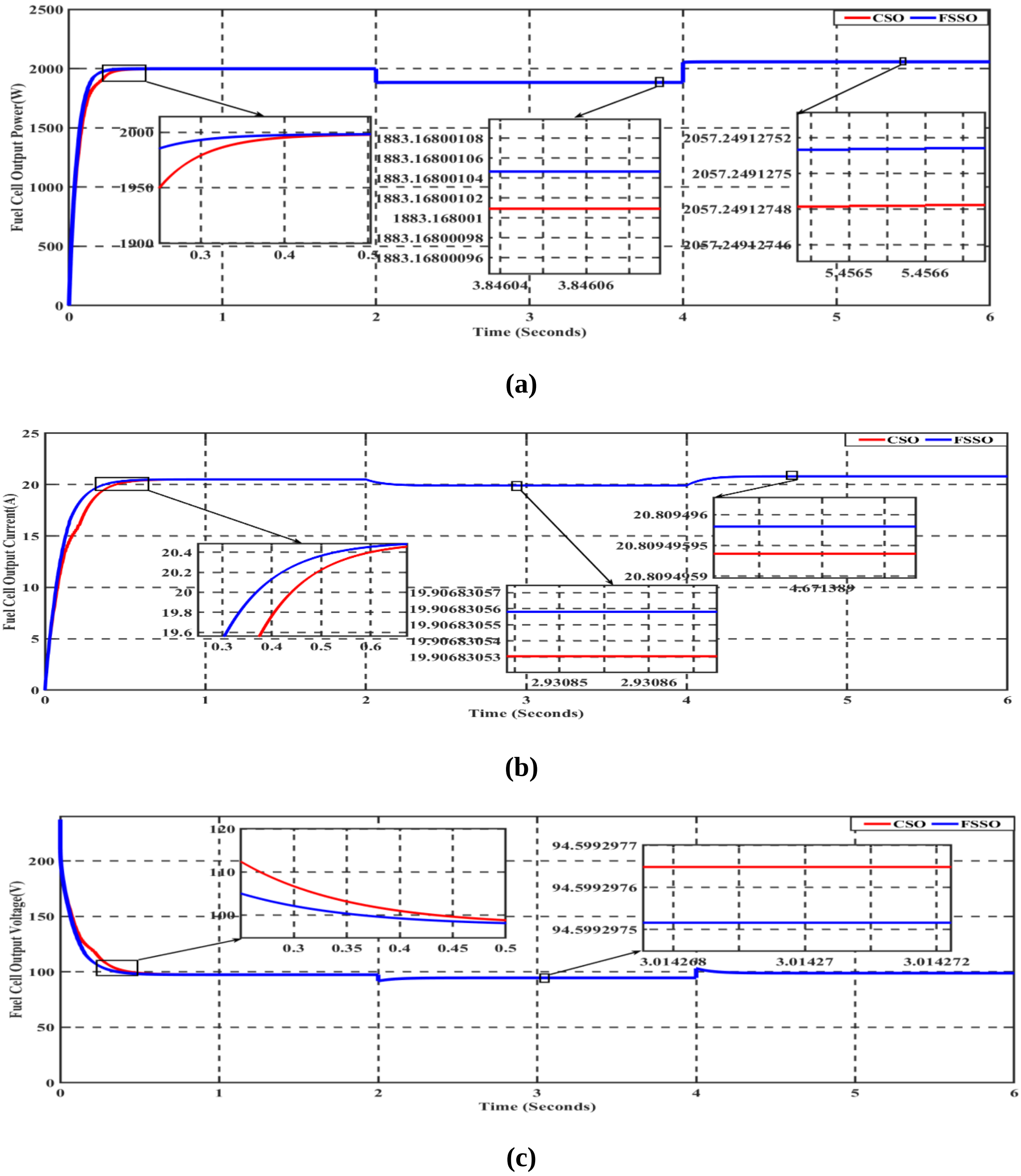

Figure 4.27 : The FSSO and CSO MPPT approaches are evaluated under change temperature conditions concerning (a) power, (b) current, and (c) voltage.

The electrochemical principles are physically consistent with these findings. Increasing the temperature typically enhances reaction kinetics and membrane ionic conductivity—shifting the operating curve and allowing more output power—until very high temperatures cause concentration losses, membrane dehydration, or failure of the membrane due to excessive temperatures. Lower temperatures, on the other hand, reduce the available power envelope because of less active reaction kinetics and decreased conductivity. Thus, a robust MPPT must (a) rapidly recognize the new MPP position for crude temperature and (b) adjust the duty cycle with minimal overshoot and oscillation at the new operation point without unnecessarily straining the fuel cell.

From an algorithmic approach, the outcomes demonstrate two synergistic advantages of FSSO over CSO in thermal stress evaluations: (1) dynamic superiority—FSSO achieves steady-state faster (shorter Tr) and with more uniform power trajectories, reducing transient oscillations that may stress the cell; and (2) robust accuracy—FSSO consistently secures equivalent or slightly elevated MPP values across a wide temperature range, demonstrating a superior balance between exploitation and exploration while converging with precision. The CSO's delayed convergence during high-temperature conditions highlights its relative vulnerability to real-time thermal disturbances. Finally, the temperature sweep experiments demonstrate that maintaining thermal robustness is critical for PEMFC MPPT. Although the two methods can achieve similar steady-state MPP values under certain conditions, FSSO provides more rapid, seamless, and thus mechanically and electrochemically safer tracking across the evaluated temperature range, making it the preferred MPPT method in thermally variable scenarios.

4.3.2.3 Fast change in Pressures levels

In the third scenario, sudden changes in the partial pressures of oxygen and hydrogen gas and temperature was determined under standard test conditions, as shown in Figure 4.28. To examine the robustness of the FSSO and the CSO algorithms, all tests performed with the PEMFC system were subjected to pressure perturbations from tiny drops to large increases in pressure. Pressure perturbations affect MPPT algorithms negatively in terms of availability of reactants, kinetics of electrochemical reaction, and performance of the stack. Pressure changes adversely affect MPPT methods by disrupting the rate of reactant supply to the fuel cell, the electrochemical reaction kinetics, and the overall efficiency of the stack. An increase in the inlet pressure allows an increased flow of hydrogen and oxygen into the PEMFC, which results in a faster electrochemical reaction and ultimately boosts power output. A reduction in the input pressure leads to a diminished electrochemical reaction rate due to the decreased availability of reactants within the fuel cell. The operating point of the boost converter was consistently adjusted to mitigate these impacts. This task was accomplished utilizing the FSSO and CSO approaches to mitigate pressure-induced changes on the P-V curve.

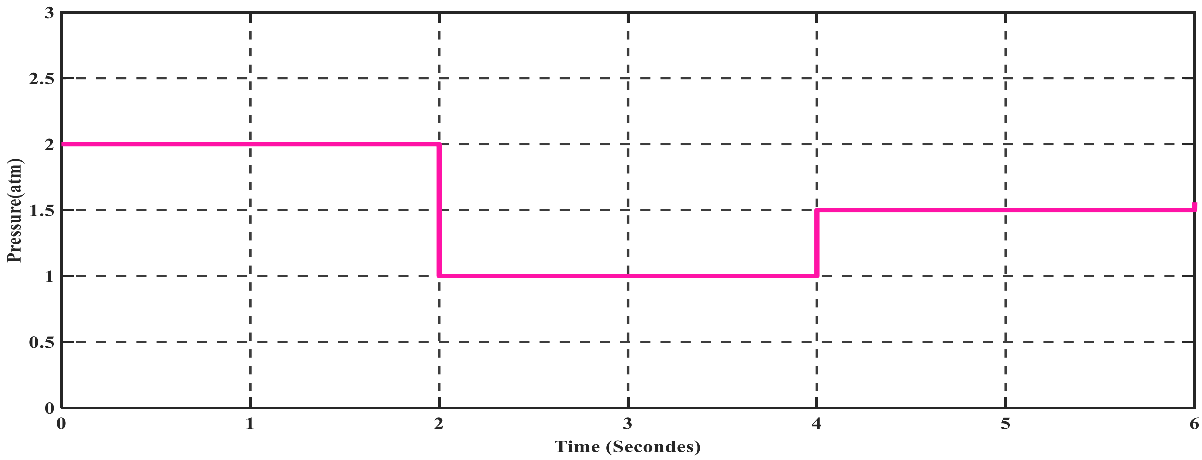

Figure 4.28 : The profile of varying levels of pressure.

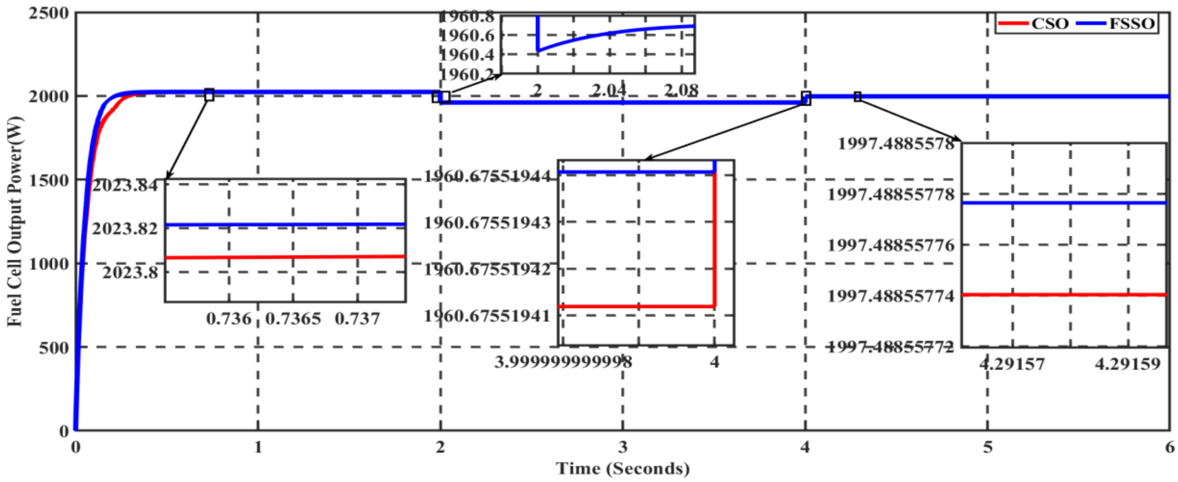

(a)

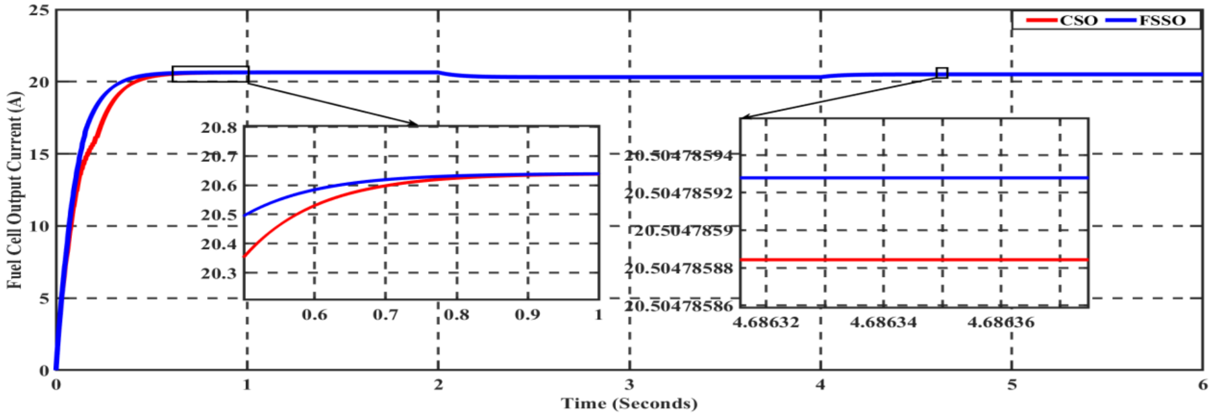

(b)

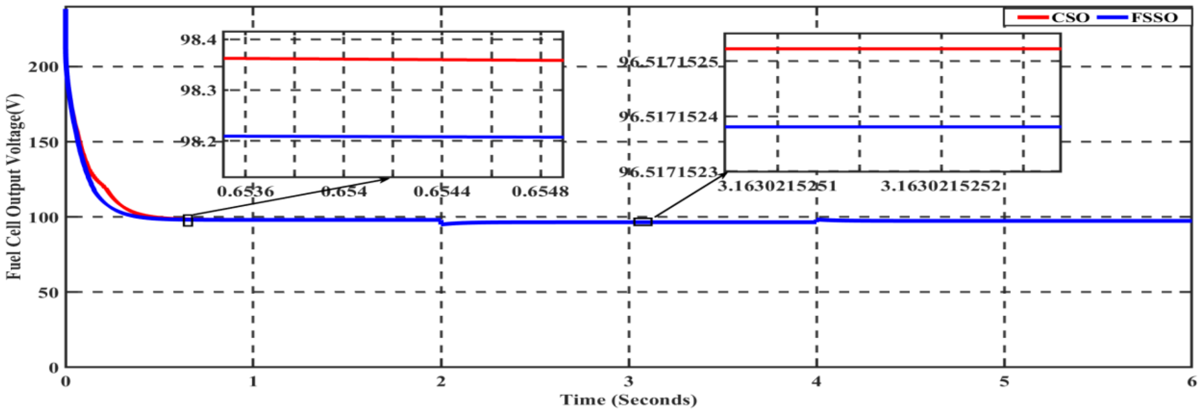

(c)

Figure 4.29: The FSSO and CSO MPPT approaches are evaluated under change pressure conditions concerning (a) power, (b) current, and (c) voltage.

The outcomes from the three simulated intervals, each characterized by varying partial pressures of hydrogen and oxygen, demonstrate significant performance disparities. Within the interval of [0–2] seconds at 2 atm, FSSO achieves an MPP of 2023.82 W, marginally surpassing

CSO's MPP of 2023.81 W. During the second interval [2–4] s, in which both gases decline to 1 atm, the attainable power diminishes as anticipated due to lowered reaction rates; nonetheless, FSSO still slightly exceeds CSO (1960.67551944 W compared to 1960.67551941 W). As pressure increases to 1.5 atm between 4 and 6 seconds, both algorithms attain elevated power outputs, with FSSO reaching 1997.48855778 W and CSO hitting 1997.48855774 W. Despite the proximity of the steady-state MPP values, the dynamic behavior illustrated in Figure 4.29 reveals a significant divergence: FSSO ensures rapid, seamless, and stable tracking amid sudden pressure fluctuations, whereas CSO demonstrates delayed convergence and marked oscillating patterns. These results affirm that although pressure fluctuations affect total energy output, FSSO continually offers enhanced flexibility and resilience, facilitating more dependable and efficient MPPT efficiency in nonlinear and swiftly varying pressure scenarios.

4.3.2.4 Sudden change in pressure and temperature levels

As referenced in our article [59], we evaluated the techniques' efficacy under changing situations by altering pressure and temperature levels, as shown in Figure 4.26 and Figure 4.28, respectively. FSSO consistently outperformed CSO, regardless of the changing circumstances.

Figure 4.30 provides a comparison of power, current, and voltage characteristics for the FSSO and CSO MPPT algorithms during simultaneous temperature and pressure deviations. The different environments depicted in this figure represent some of the most challenging modes of operation for PEMFC. As shown, the FSSO has a consistently superior ability to track the maximum power point than the CSO, owing to the improved dynamics and stability in response to perturbation under highly variable conditions. In this setup, FSSO achieves the maximum power point of 2031.88 W with a faster settling time of 330 K and $\left(\mathrm{PH}_2 = PO_2 = 2\ atm\right)$ compared with the same operating environment for CSO, which was slower to stabilize and exhibited greater transient oscillation. This observation is matched across all scenarios, indicating FSSO has a faster and more stable response to changing ambient conditions. FSSO demonstrated the generation of a more stable cluster of current and voltage trajectories with short and consistent settling times (see figure Figure 4.31) through varying operating conditions, as illustrated in Figure 4.30 (b) and Figure 4.30 (c), respectively. Contrarily, CSO demonstrated slower reaction times, unpredictable oscillations, and increased settling times, indicating vulnerable coupled heat and pressure perturbations and limited capacity to accurately track the specific MPPT.

These results demonstrate the complex interaction among temperature, pressure, and PEM fuel cell power production. Temperature affects the reaction kinetics of the electrochemical processes and the ionic conductivity of the membrane—decreasing temperature degrades reaction activity, while increasing temperature increases reaction activity and may induce thermal stress. Pressure affects reactant diffusion and overall electrochemical efficiency. Due to these coupled variations, an efficient MPPT controller must be able to quickly vary the duty cycle in order to match the varying MPP with little lag. Results show without a doubt that FSSO satisfies this requirement: the adaptive search process of FSSO enables it to deliver a very short settling time and increased stability while accurately tracking the MPP when rapid and unexpected fluctuating environmental changes occur. Therefore, FSSO is a robust and efficient MPPT technique for PEM fuel cell systems that could be considered for practical sustainable hydrogen applications under changing climate conditions.

The settling-time findings in Table 4.7 demonstrate the FSSO approach's superiority under all operational situations.

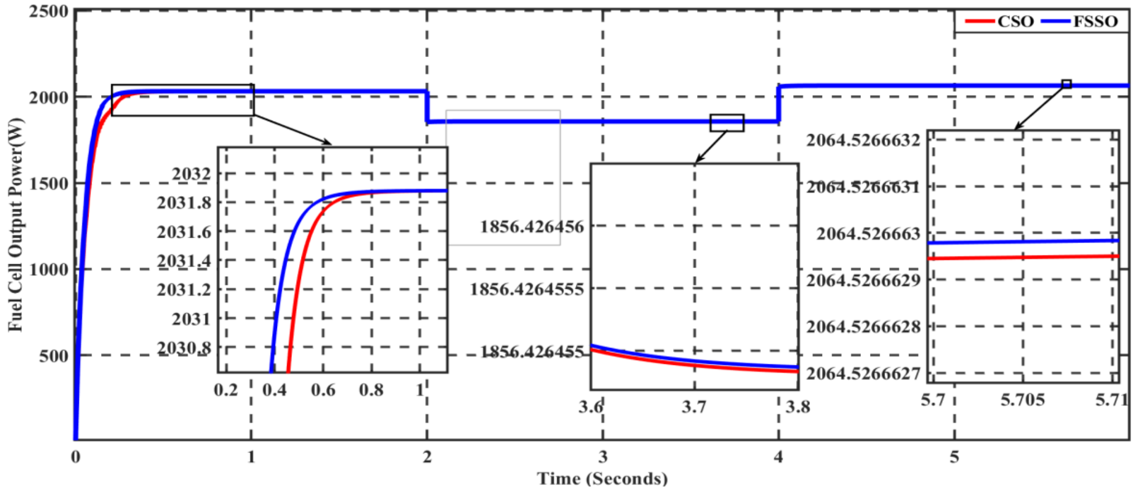

(a)

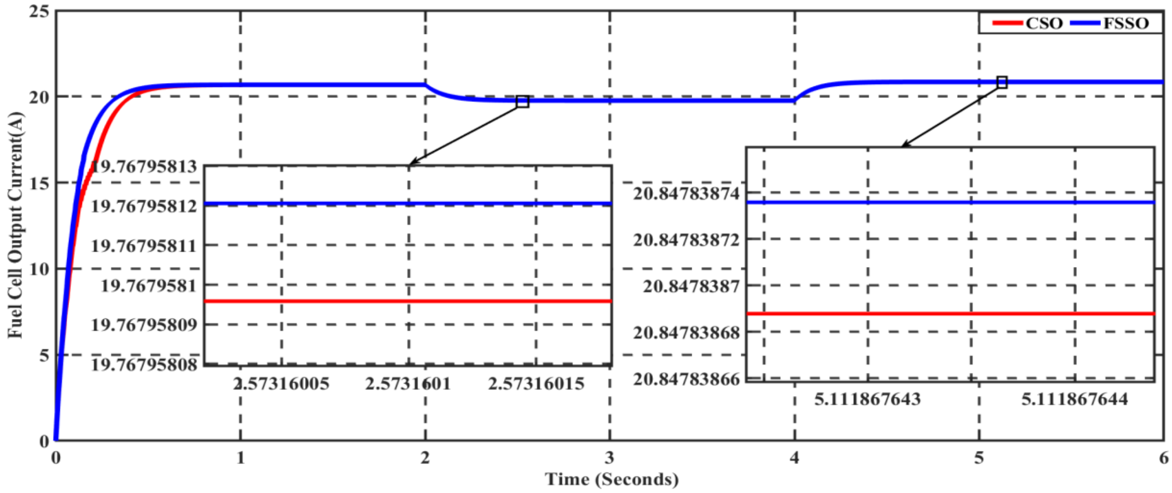

(b)

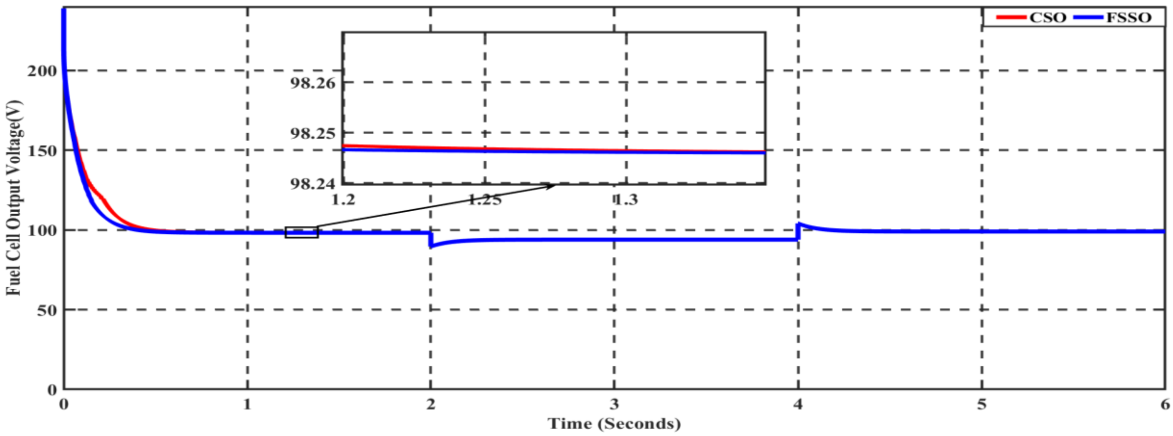

(c)

Figure 4.30: The FSSO and CSO MPPT approaches are evaluated under different pressure and temperature conditions concerning (a) power, (b) current, and (c) voltage.

Table 4.7: The results of comparative evaluation [59].

			Environmental conditions			
	approach	Elements that reacted in response time	Standard conditions	Fast change in pressure	Fast change in temperature	Fast change in temperature and pressure
Response time(seconds) [Tr(s)]	Flying squirrel search Optimization (FSSO)	Power	0.5	0.3	0.32	0.8
		Current	0.5	0.6	0.6	0.6
		Voltage	0.5	0.4	0.5	0.64
		Max Power P_{max}(W)	1990.68686017	2023.822	2057.2412752	2064.526663
	Cuckoo Search Optimization (CSO),	Power	0.6	0.4	0.35	0.84
		Current	0.6	0.9	0.7	0.68
		Voltage	0.6	0.5	0.6	0.76
		Max Power P_{max}(W)	1990.68686014	2023.807	2057.24912748	2064.5266605

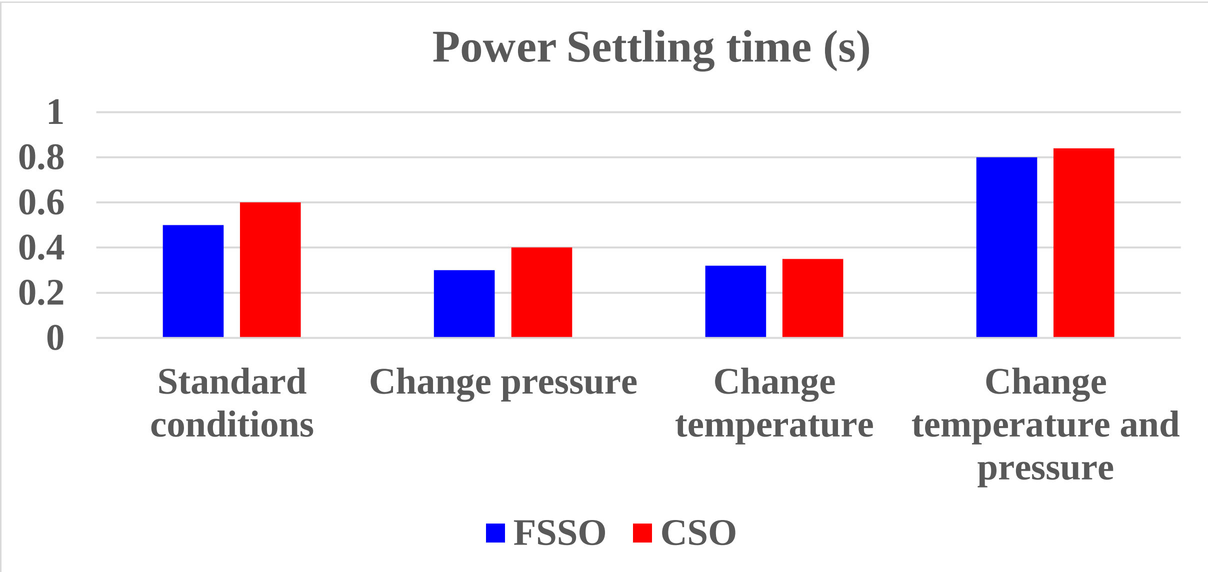

Figure 4.31: power settling time graphical representation.

The FSSO and CSO strategies may improve the MPPT and efficiency of PEM hydrogen fuel cell systems, as indicated by the findings. Our findings suggest these new optimization strategies may provide initial benefits. They represent a real step to optimize PEMFC dynamism and efficiency in various locations of operation. This study demonstrates the principles of adaptability for the optimization components and distinguishes the benefits of FSSO and CSO, which expands our understanding of MPPT optimization strategies associated with green energy technologies. The study also calls for continued research and innovation around MPPT optimization. The study calls for research and innovation to address new challenges and to accelerate the uptake of PEM fuel cell technology into practice. The involvement of MPPT researchers to investigate future improvements to PEM fuel cell technology should include testing their ideas in practical fuel cell systems, improving the resilience of those systems to failures and disturbances, developing optimal control techniques to manage energy storage systems in parallel with the MPPT strategy, exploring other energy applications outside of automotive transportation, investigating machine learning techniques for adaptive control, and moving the problem forward in an appropriate way.

Table 4.8 illustrates a comprehensive comparison between the proposed FSSO and the common and currently used MPPT approaches for PEMFC, such as cuckoo search optimization (CSO), particle swarm optimization (PSO),whale optimization approach (WOA), grey wolf approach (GWA), differential evolution optimization (DEO), and salp swarm approach (SSA) in terms of power oscillation, convergence speed, complexity, scalability, and robustness. The MPPT methods' responsiveness to changing environments is determined by their rate of convergence. Because of their quick convergence rates, FSSO, CSO, SSA, WOA, and PSO show quick adaptation to changes in temperature and pressure. Even though DEO converges satisfactorily, MPPT algorithms need to be highly precise in order to maximize the extraction of renewable energy. The maximum power point is closely monitored by several systems, including FSSO, CSO, SSA, WOA, and GWO. Stability is indicated by power oscillation. With the exception of PSO, every technique produces a steady energy output with little variation in production. Algorithms are delicate in their complexity. Due to their complex algorithms and processing requirements, FSSO, CSO, SSA, WOA, GWO, and DE are categorized as moderate to high complexity. The FSSO, CSO, SSA, and WOA are strong and capable of facing unusual operational situations [59].

Table 4.8: A comprehensive comparison between the proposed FSSO and the common and currently used MPPT approaches for PEMFC [59].

Approach	**Power oscillation**	**CS**	**Complexity**	**Scalability**	**Robustness**
Proposed FSSO [59]	Very low	Very fast	Low	Very high	High
CSO [59]	Very low	High- fast	Medium-High	Very High	High
PSO [177]	High	Medium-Fast	Medium	Medium-High	Medium
WOA [121]	Low	Fast	High	Medium-High	High
GWA [178]	Medium	Medium-Fast	High	Medium-High	Medium-High
DEO [179]	Low	Fast	Medium	Medium	Medium

SSA [180]	Low	High -Fast	High	High	High

4.4 Conclusion

This chapter introduces enhanced control systems for photovoltaic and proton exchange membrane fuel cell renewable energy sources, which are the focus of this thesis. Initially, we have focused on the extraction of the MPP in photovoltaic systems by proposing an improved PFO MPPT algorithm, in comparison to four contemporary metaheuristic MPPT strategies: PSO, GWA, AOA, and SOA) under varying irradiance and five intricate peak shading patterns. The FSSO has been proposed, developed, and evaluated against the CSO for the PEMFC control system across several scenarios. The results endorse the preeminence of the proposed methodologies for various applications. The suggested EPFOA MPPT for photovoltaic systems was thoroughly assessed in intricate partial-shading situations and fluctuating irradiance levels. The EPFOA demonstrates exceptional performance, rapid convergence, and little complexity, making it one of the most advanced MPPT algorithms across all evaluated scenarios. Conversely, the findings unequivocally indicate that FSSO is a resilient and effective MPPT methodology for PEM fuel cell systems, rendering it a feasible choice for sustainable hydrogen applications amid fluctuating climate conditions.

Chapter 5 : Design of Energy Management and Power Flow Strategies

5.1 Introduction

This study examines a hybrid system that relies on photovoltaic (PV) energy as its main renewable energy source, supplemented by fuel cells (FC) and battery storage. In order to accomplish this hybridization and the main objective, an approach to energy management (EM) is needed to ensure an effective distribution of load demand among available energy sources and to handle the difficulties presented by the dynamic features of energy flows, particularly the unpredictable nature of renewable production and the fluctuating demand profiles.

The EMS increases energy efficiency and substantially decreases the use of hydrogen. A range of traditional EMSs has been suggested in the literature to effectively control load demand across the components of the hybrid system. Many of the analyzed approaches require a high initial state of charge (SOC) for the battery and supercapacitor with too much data, particularly for methods that use ANFIS; they also require substantial implementation efforts and have flaws in the complex architecture of the energy management strategy (EMS). Additionally, local optima may have an impact on a number of heuristic optimization techniques used in EMS [133].

The primary contribution of this research is the provision of an optimized energy management system designed to reduce hydrogen consumption and mitigate fuel cell performance loss. Novel optimizers are still useful in the field of managing energy research, according to the No Free Lunch principle, which states that no single optimizer can successfully handle all optimization problems.

The accurate heuristic methodology of the elk herd optimization algorithm (EHOA), which maintains a balance between exploration and exploitation in the optimization process, controls storage cycles, and ensures the stability of the DC-Link voltage, is used in this chapter to discuss a number of issues and present a carefully designed EMS. This feature prevents the approach from being stuck in local optima and includes comparison simulations and mathematical formulations of various energy management techniques intended to verify the effectiveness of the suggested EMS in raising the system's overall efficiency. Each EMS's efficacy is evaluated in comparable situations, with a focus on crucial comparison metrics such as SOC of battery storage system, hydrogen consumption, and overall system performance.

5.2 A brief overview of the different power management approaches used

To verify the effectiveness of the suggested EMS in improving the system's overall efficiency, this section describes some previous strategies used for managing the energy of the hybrid-generated system.

5.2.1 Proportional-integral (PI) control approach

As shown in Figure 5.4 (a), this technique uses a proportional-integral (PI) regulator to control the battery's SOC. The fuel cell's target power is calculated by subtracting the controller's output, which represents the battery's power contribution, from the total load requirement (ΔP). The fuel cell operates at reduced power while the battery supplies its full capacity when the battery's state of charge surpasses the predetermined minimum threshold.

The fuel cell must meet nearly all of the load demand if the SOC falls below this threshold. Compared to other strategies, this approach is relatively straightforward and simple to implement. To achieve the best system performance, the PI controller's variables are modified repeatedly[81],[181],[28].

$$\Delta P = P_{Load} - P_{PV} \tag{5.1}$$

5.2.2 The Equivalent Consumption Minimization Approach (ECMA)

The equivalent consumption minimization approach (ECMA) (see Figure 5.4 (b)) is a well-known optimization method that uses instantaneous cost functions. The goal is to use less fuel by lowering the amount of fuel the fuel cell needs and the amount of fuel needed to keep the battery's state of charge stable. This method uses a dynamic equivalency factor that changes based on the battery's SOC. In addition, adding this part directly to the optimization objective function makes the method less likely to be affected by changes in the SOC balancing coefficient (μ) . Therefore, we can say the objective function for the optimization problem like this [181],[81]:

$$F = \left(P_{FC} + \alpha_p P_{Battery}\right) \times \Delta T \tag{5.2}$$

With regard to the equality constraints

$$\Delta P = P_{FC} + P_{Battery} \tag{5.3}$$

$$\alpha_p = 1 - 2\mu \frac{\left(SOC - 0.5\left(SOC_{Max} + SOC_{Min}\right)\right)}{\left(SOC_{Max} + SOC_{Min}\right)} \tag{5.4}$$

Within the constraints of the boundaries

$$\begin{cases} P_{FC}^{Min} \le P_{FC} \le P_{FC}^{Max} \\ P_{Battery}^{Min} \le P_{Battery} \le P_{Battery}^{Max} \\ 0 \le \alpha_p \le 2 \end{cases} \tag{5.5}$$

In relation to the DC bus, P_{FC} and $P_{Battery}$ represent the power from the fuel cell, and battery, respectively, taking converter losses into account. The punishment coefficient is denoted by α_p . The sample interval is denoted by ΔT .The fuel cell's minimum and maximum power output are indicated by P_{FC}^{Min} and P_{FC}^{Max} .

The minimum and maximum battery power are denoted by $P_{Battery}^{Min}$ and $P_{Battery}^{Max}$, respectively. The battery's lowest and highest states of charge are denoted by SOC_{Min} and SOC_{Max} . The state of charge balance coefficient is represented by μ .

5.2.3 The External Energy Maximization Approach (EEMA)

A common ECMS functions by balancing the use of hydrogen fuel cells with the battery's energy consumption. This equivalence is established using a penalty factor that ensures the battery remains within its state of charge limits during the driving cycle. This approach's drawback is that it is dependent on the load profile, which can be extremely unexpected in practical scenarios. Consequently, the external energy maximization strategy (EEMS) represents a key change in technique (see Figure 5.4 (c)). Rather than computing an equivalence factor for fuel savings, it optimizes battery energy consumption at all times. This ensures that the system meets SOC and voltage limits without requiring predictive modeling of future energy requirements. The primary goal of this function is to increase the energy output offered by both the battery and the DC bus. This is represented mathematically in the following way [28],[181]:

$$J = -\left(\Delta T \cdot P_{Battery} + 0.5 \cdot C_{Dc} \cdot (\Delta \nu)^2\right) \tag{5.6}$$

Where the DC-bus voltage perturbation is denoted by $\Delta \nu$.

The negative sign in formula (5.6) is employed to move between minimization and maximization problems in optimization theory.

This equation is governed by the following inequality constraint:

$$\begin{cases} P_{Battery} \cdot \Delta T \leq \left(SOC - SOC_{Min}\right) V_{Battery} \cdot Q_{Battery} \\ V_{Dc}^{Min} - V_{Dc} \leq \Delta \nu \leq V_{Dc}^{Max} - V_{Dc} \\ P_{Battery}^{Min} \leq P_{Battery} \leq P_{Battery}^{Max} \end{cases} \tag{5.7}$$

5.2.4 PARTICLE SWARM OPTIMIZER

The behavior of known animal social structures, like fish schools and flocks of birds, is mimicked by particle swarm optimization (PSO). It consists of the two steps required to find the best solution. After moving in their individual directions, each particle first shares its information with other particles. After every iteration, they can learn to calibrate the parameters and modify their trajectory. PSO has been used in the literature as a successful technique to handle a variety of optimization problems, such as the global maximum power point tracking of photovoltaic systems under partial shading conditions and the optimal distribution of distributed renewable resources and electric vehicle charging stations in power distribution networks [133]. In this work, PSO is designed as EMS, as illustrated in Figure 5.4 (d).

5.2.5 The proposed Elk Herd Optimization Approach

Al-Betari et al. presented the EHO method in 2024 [182]. One way to think of elk herds' reproductive process is as an optimizing mechanism. To create a herd that is more resilient and able to deal with environmental issues, the elks are selectively bred over several generations. The breeding process and optimization concepts are related in this section. The first conversation concerns the source of inspiration for EHO. The general optimization process of EHO and the mathematical structure are then described.

5.2.5.1 Inspiration of EHOA

The largest deer type after the moose is the elk, also known as the wapiti. Elks prefer warmer climates over colder ones and live in the forests and woodlands of Central East Asia and North America. As herbivores, elks eat grasses, plants, leaves, and bark. Elks are therefore thought to be at the bottom of the food chain hierarchy. However, elks are strong animals that can jump, swim, and run short distances at up to 50 km/h, particularly when they sense danger. Elks also have keen senses of smell and hearing. Therefore, elk herds are vulnerable relative to higher hierarchical levels; thus, they reside in extensive familial groups including 200 or more individuals for protection [182].

Males, females, and juveniles make up the elk herd, with females (cows) making up the majority. Because of their aggressive behavior in the competition for protection and dominance, the number of males (bulls) is reduced. Calves are young elk that typically follow their mothers or herds led by adult bulls. The herd communicates in a variety of ways. During the breeding season, bulls use a unique sound called bugling to show off their fitness and attract potential mates. The bull's location within the herd is also indicated by this sound. Calves make high-pitched squeals when they are in danger, but cows grunt to warn others of danger and to find their calves.

Rutting and calving are the two distinct stages of the mating season, which mostly occurs from September to October. Bulls become more aggressive toward one another and other animals during the rutting season. They fight for dominance through vocalizations and physical altercations, often using their antlers. Larger harems, often exceeding 20 cows, are acquired by more dominant bulls, while smaller harems of up to five cows are assembled by less dominant bulls. These encounters typically result in damage to the antlers. A dominant bull is in charge of each harem and is responsible for providing protection.

Cows mate with bulls at the start of the calving season in order to become pregnant, and then they separate from the herd to give birth to their calves in safe places away from predators. After a gestation period, cows give birth to calves, which can be either male or female. These calves grow antlers in the upcoming months, initiating a reproductive cycle that resumes the breeding season and forces the group of bulls and their harems to select the strongest bull for upcoming competitions and mating opportunities [182].

5.2.5.2 The EHOA's mathematical model

5.2.5.2.1 Initialization of EHOA population

The population of elk solutions, comprising harem groups and bulls, is represented by the elk herd (EH), as illustrated in Figure 5.1. The equation (5.8) shows how the EHOA is arranged as a matrix of dimensions $n \times EHS$ [183].

$$\begin{bmatrix} x_1^1 & x_2^1 & \cdots & x_d^1 \\ x_1^2 & x_2^2 & \cdots & x_d^2 \\ \vdots & \vdots & \cdots & \vdots \\ x_1^N & x_2^N & \cdots & x_d^N \end{bmatrix} \tag{5.8}$$

The population size is denoted by N . Equation (5.9) is used to estimate the position of each elk.

$$x_j^i = lb_j + \left(ub_j - lb_j\right) \times rand \tag{5.9}$$

In this case, rand denotes a uniformly distributed random number within the interval $[0,\ 1]$, ub_j denotes the upper bound of the $j-th$ dimension, lb_j displays the lower bound of the $j-th$ dimension, and x_j^i indicates the location of the $i-th$ elk in the $j-th$ dimension. Equation (5.8) is used to determine the fitness value of each elk's solution. Elks in EH are ranked according to how fit they are.

5.2.5.2.2 Rutting Season

During the rutting season, the elk herd divides into family groups based on the bull ratio B_r . $B = |B_r \times N|$ determines the total number of families. According to the equation(5.10), the top B individuals with the highest fitness values in the EH are selected as bulls by the herd based on their fitness values[183].

$$B = \arg_{j=(1,2,\ldots,B)} f\left(x^j\right) \tag{5.10}$$

Each bull in the herd is given a harem using the roulette wheel selection method; harems are distributed among family groups based on the fitness values of the bulls, as outlined in equation (5.11) .

$$p_j = \frac{\left|f\left(x^i\right)\right|}{\left|\Sigma_{k=1}^{B} f\left(x^k\right)\right|} \tag{5.11}$$

Where p_j denotes the selection probability for each bull x^i in B , $f\left(x^k\right)$ indicates the absolute fitness value of bull x^i , all bulls, and B is the parameter utilized to compute the number of familial groups. $\left|\Sigma_{k=1}^{B} f\left(x^k\right)\right|$ denotes the overall absolute fitness.

5.2.5.2.3 Calving Season

During the calving season, the calves, $x_i^j(t+1)$, within each familial group are predominantly produced based on the characteristics of the sire bull, $x^{h_j}(t)$, and the maternal harem, $x_i^j(t)$. If calf $x_i(t+1)$ maintains an identical index i as its bull progenitor, the calf is produced as specified in equation(5.12)[183].

$$x_i^j(t+1) = x_i^j(t) + \alpha \cdot \left(x_j^k(t) - x_i^j(t)\right) \tag{5.12}$$

In this context, $x_i^j(t+1)$ signifies the $i-th$ elk in the $j-th$ dimension during the $t+1$ iteration, while $x_j^k(t)$ indicates a randomly chosen elk from the herd, where $k \in (1,2,\ldots,EHS)$. Additionally, α is a stochastic value within the interval $[0,\ 1]$ that dictates the proportion of random factors involved in new calf reproduction. When the calf shares the same index as its mother, it receives traits from both its sire and harem dam, as delineated in equation(5.13).

$$x_i^j(t+1) = x_i^j(t) + \beta \cdot \left(x^{h_j}(t) - x_i^j(t)\right) + \gamma\left(x^r(t) - x_i^j(t)\right) \tag{5.13}$$

Where j, r is the index of a randomly chosen bull from the current bull set such that $r \in B$, $x^{h_j}(t)$ represents the bull of harem, and γ *and* β are two random values within the interval $[0,\ 2]$, with inherited traits from previously created calves being randomly assigned.

5.2.5.2.4 Selection Season

Bulls, harems, and calves are all grouped into a single solution space during the selection process. The temporary matrix, EH_temp , is created by combining the population matrix, EH, which includes the current generation of bulls and harems, with the new solution matrix, EH′, which contains the calves. The top EHS individuals are selected as the next-generation population to replace the original population matrix EH after the individuals in EH_temp are sorted in ascending order according to their fitness values [183].

Figure 5.2 depicts the EHOA flowchart, while Figure 5.3 depicts the proposed methodology that includes EHOA.

The suggested EMS employed the elk herd algorithm to optimize the fitness function in formula (5.6) alongside the associated restrictions outlined in Eq. (5.7). Figure 5.9 (e) illustrates the suggested optimization configuration.

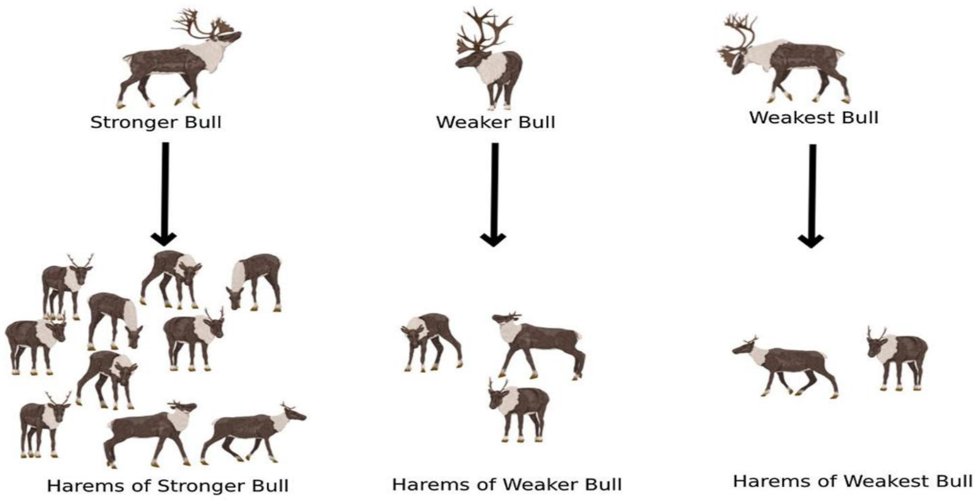

Figure 5.1: Families of elk herds [182].

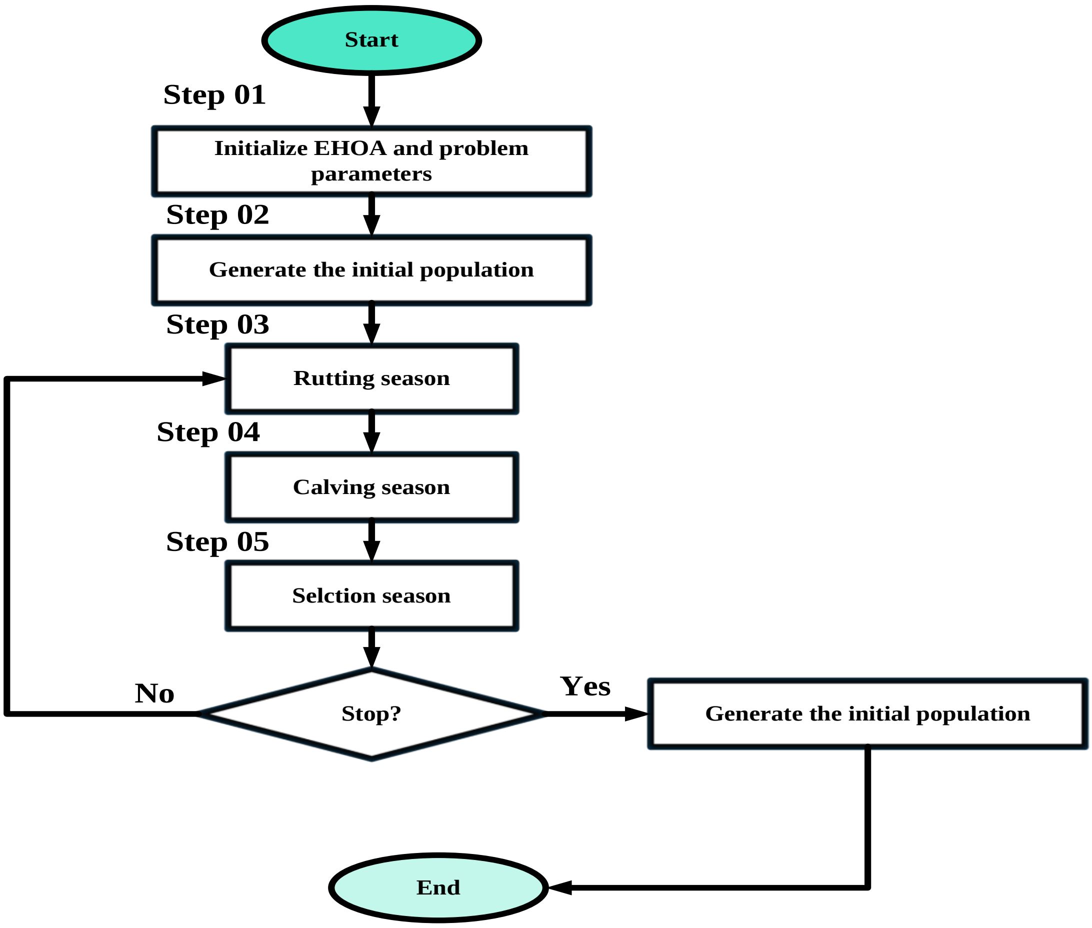

Figure 5.2 : A flowchart delineating the basic EHOA [184].

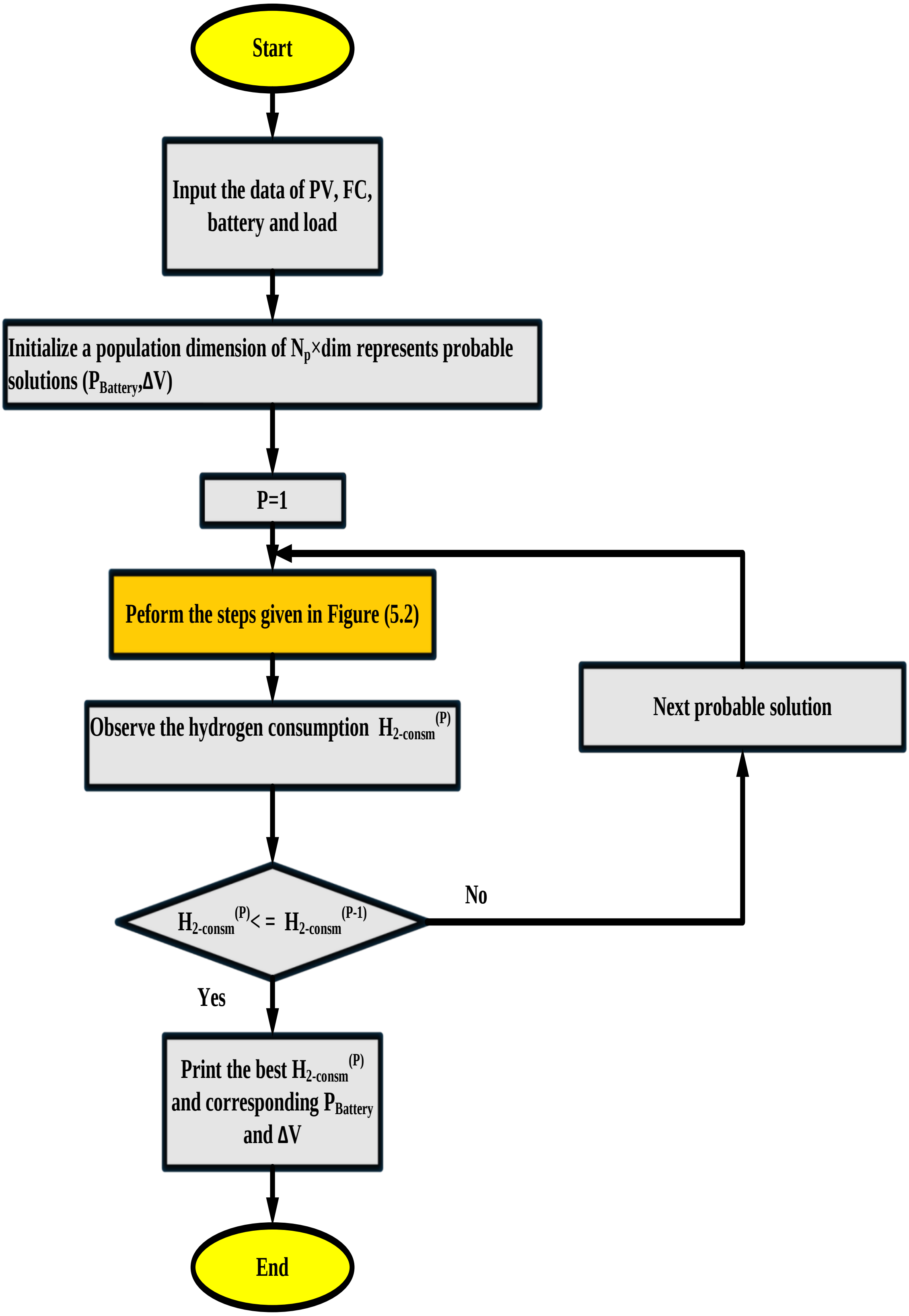

Figure 5.3: the proposed methodology that includes EHOA.

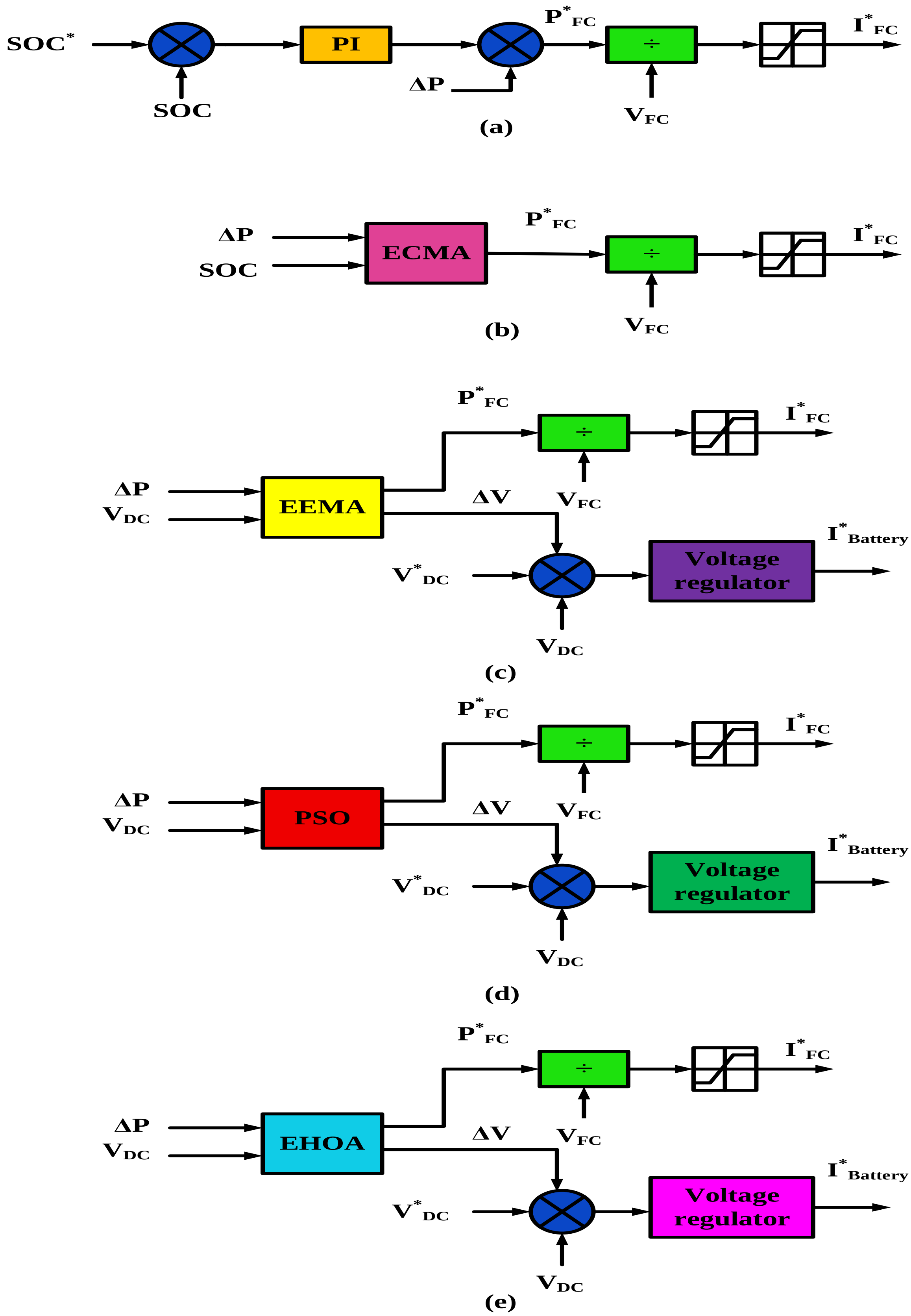
SOC*
SOC
PI
ΔP
P*FC
÷
VFC
I*FC
(a)
ΔP
SOC
ECMA
P*FC
÷
VFC
I*FC
(b)
ΔP
VDC
EEMA
P*FC
÷
VFC
I*FC
ΔV
V*DC
VDC
Voltage regulator
I*Battery
(c)
ΔP
VDC
PSO
P*FC
÷
VFC
I*FC
ΔV
V*DC
VDC
Voltage regulator
I*Battery
(d)
ΔP
VDC
EHOA
P*FC
÷
VFC
I*FC
ΔV
V*DC
VDC
Voltage regulator
I*Battery
(e)

Figure 5.4: Configurations for power management approaches: (a) PI approach [81], (b) Equivalent consumption minimization approach [81], (c) External energy maximization approach [81], (d) PSO, and (e) EHOA.

5.3 Simulation setup and discussion

A comparative MATLAB/Simulink simulation study is used to examine the operational effectiveness of the suggested power management approaches. Before the hybrid PV-FC-battery system (see Figure 5.5) is experimentally validated in an RT-Lab real-time simulation environment, this analysis confirms the EMS's performance. The main factors for performance evaluation include hydrogen consumption, battery state of charge, longer lifespan, DC bus voltage adjustment, and the overall effectiveness of the system.

The proposed model includes the following components: a primary source consisting of a 10 kW solar photovoltaic generator operating in maximum power point tracking mode; a proton exchange membrane fuel cell (PEMFC) rated at 10 kW with a terminal voltage range of 30-60 V; and a lithium-ion battery with a voltage of 48 V and a capacity of 40 Ah. A protective resistor is employed to prevent overvoltage or undervoltage conditions that may arise during system initiation or abrupt load reductions. Figure 5.6 depicts the utilized solar irradiation profiles, whereas Figure 5.7 presents the variable load profile. Table 5.1 shows the electrical details of the PEMFC and battery used in the present research.

Each EMS's simulated performance is assessed over a 200-second period (3 minutes and 20 seconds). All simulations use the same initial circumstances—a battery state of charge of 65% and a DC bus voltage of 270 V—to ensure accurate comparisons. Fuel cell output power (P_{FC}), battery output power $(P_{Battery})$, and battery state of charge are among the optimization variables. The following delineates their various limits: $P_{FC}^{Min} = 850$, $P_{FC}^{Max} = 8800$, $P_{Battery}^{Min} = 1500$, $P_{Battery}^{Max} = 3400$, $SOC_{Min} = 60$, $SOC_{Max} = 90$, to enable a fair comparison with alternative approaches, the PI controller's SOC reference is set at SOC_{Min} .

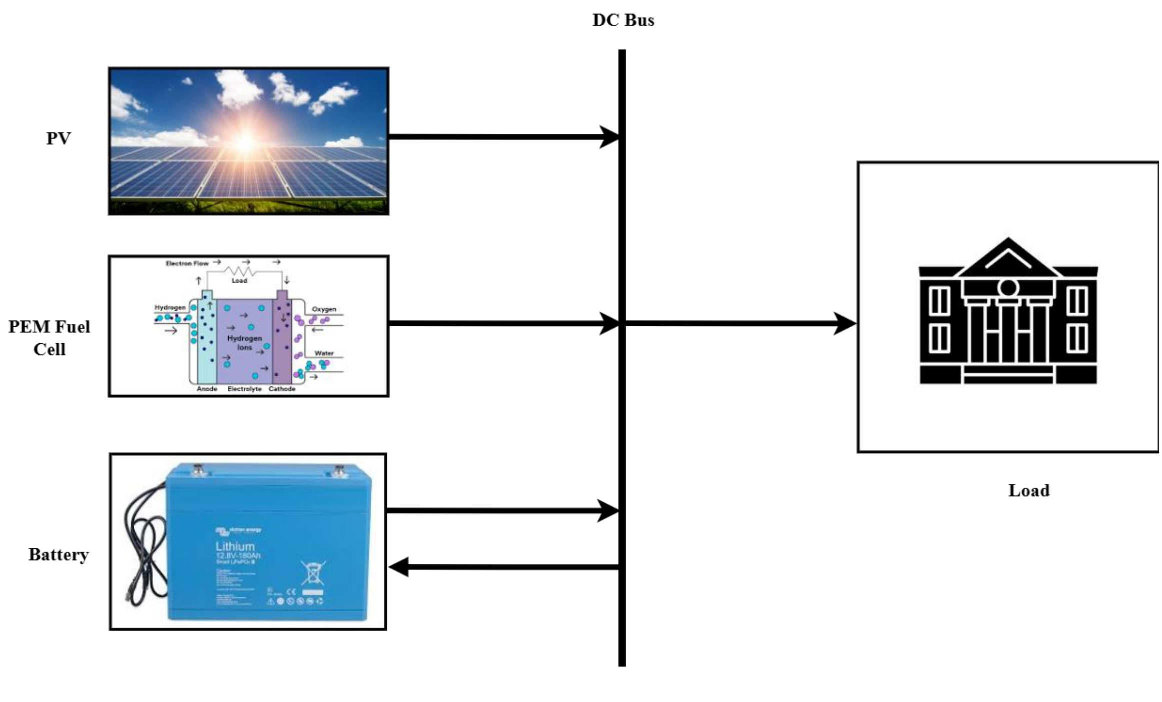

Proposed Hybrid system

Figure 5.5: Power flow for the suggested hybrid renewable energy system.

Table 5.1: The hybrid power system part's electrical details.

Component specifications	**Values**
	PEMFC
Cells Number	65
Efficiency	50 %
The nominal voltage of operation	41.15 V
The nominal current of operation	250 A
Flow rate of air	732 Ipm
Operating temperature	45°C
Air pressure	1 bar
Fuel pressure	1.16 bar
	Battery
Max capacity	40 Ah
Nominal capacity	40 Ah
Nominal voltage	48 V
Nominal current discharge	17.4 A
Full charged voltage	55.88 V
Internal resistance	0.012 Ohm

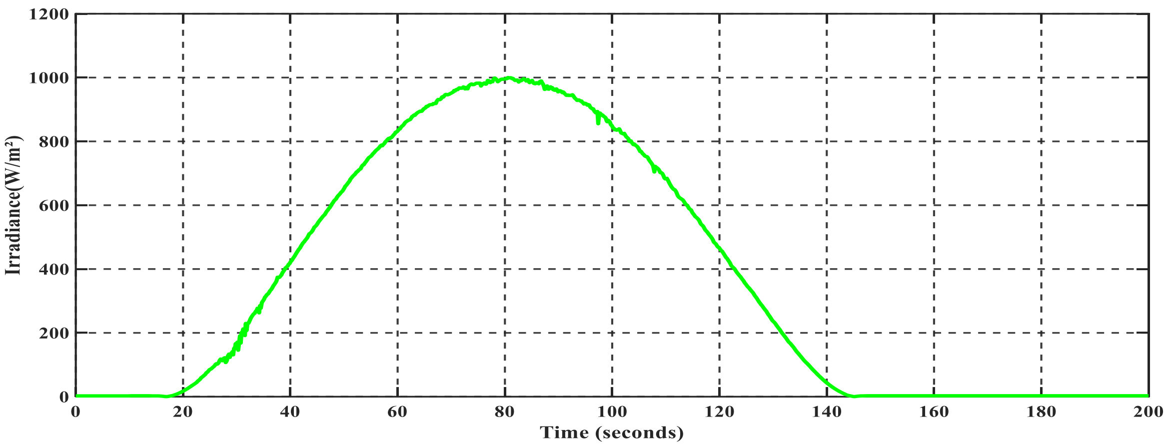

Figure 5.6 : Irradiance profile.

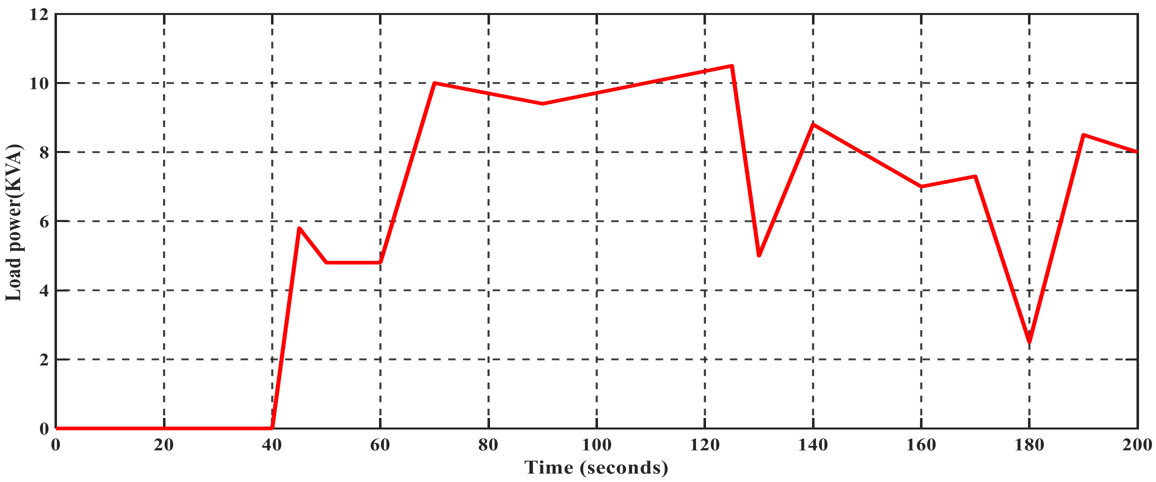

Figure 5.7: Load profile.

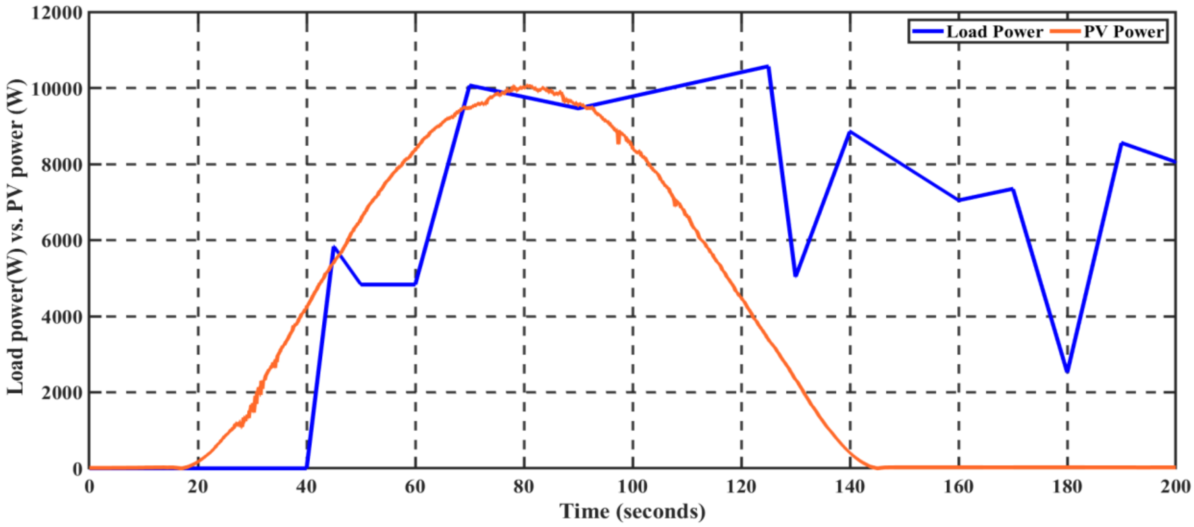

Figure 5.8: Power production versus the amount of power needed.

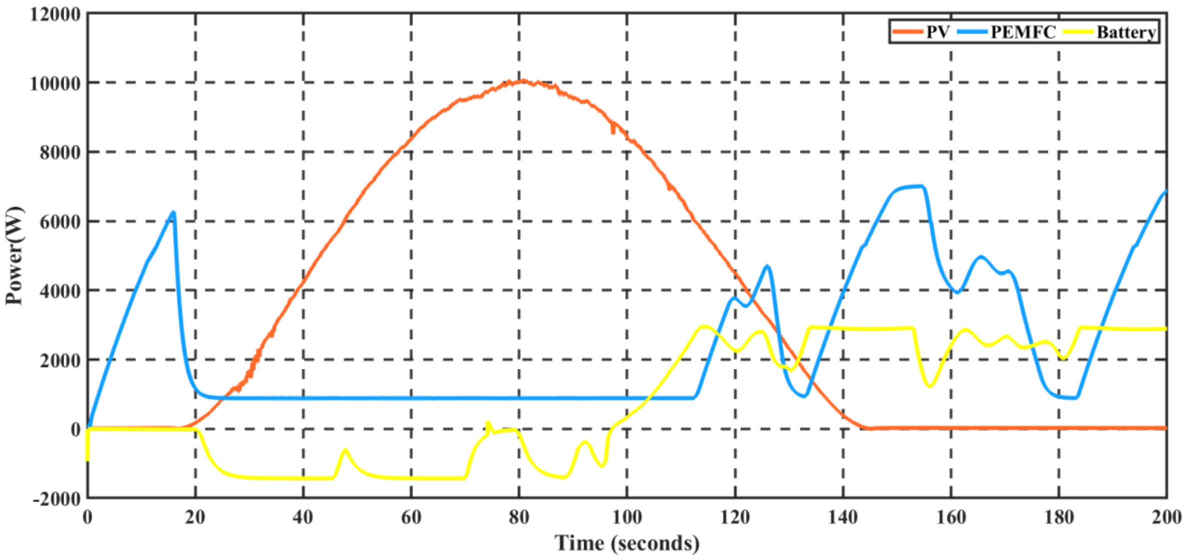

(a)

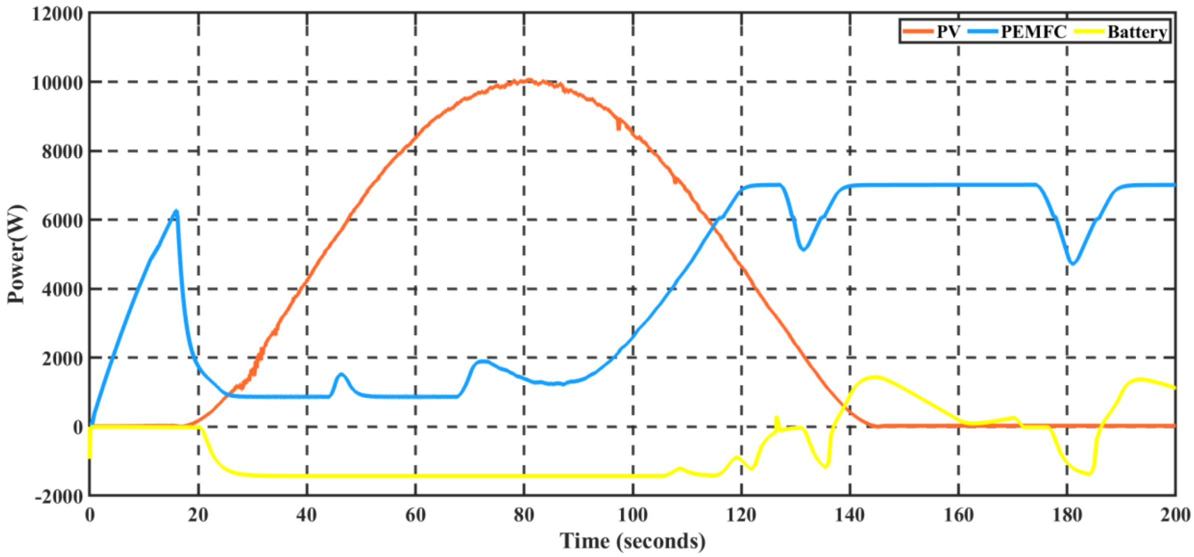

(b)

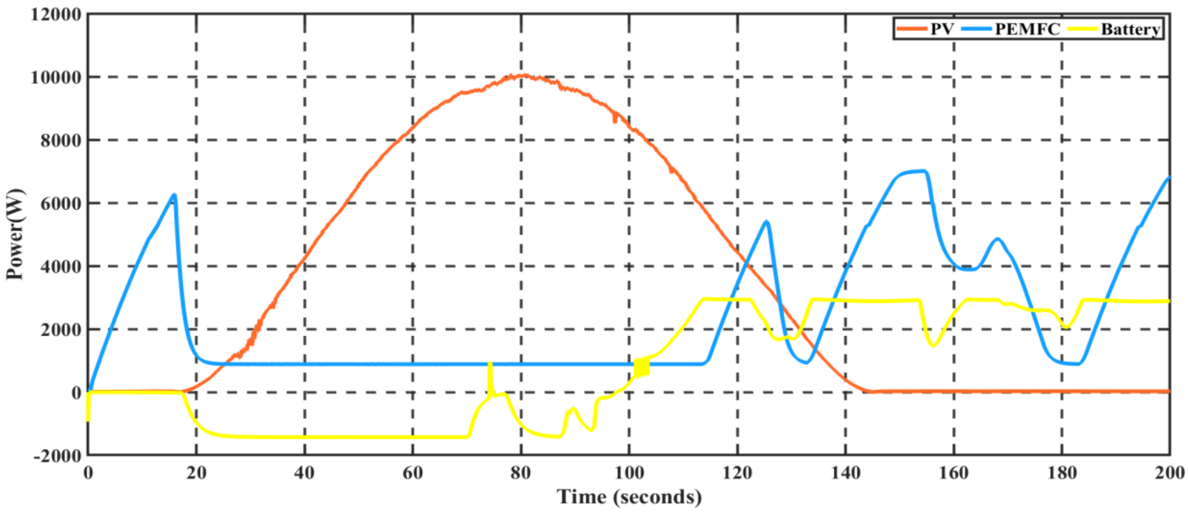
PV
PEMFC
Battery
Power(W)
Time (seconds)

(c)

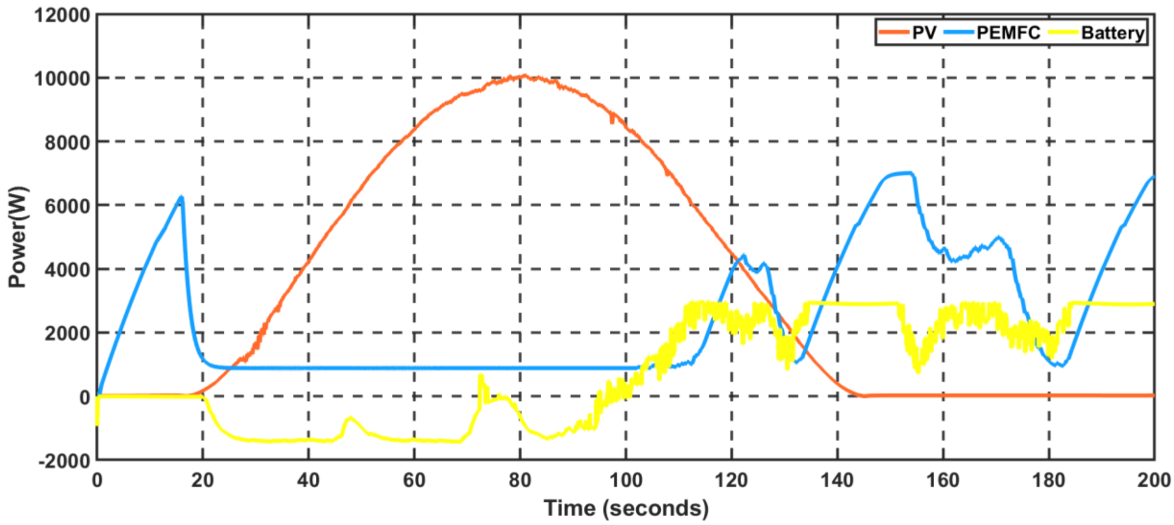
PV
PEMFC
Battery
Power(W)
Time (seconds)

(d)

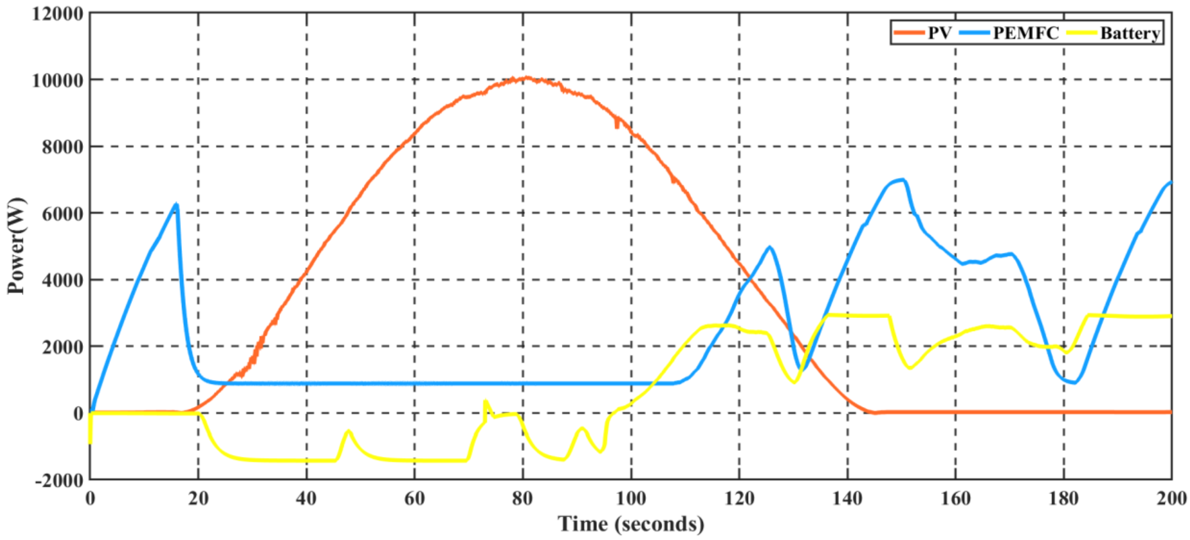
PV
PEMFC
Battery
Power(W)
Time (seconds)

(e)

Figure 5.9: PV, PEMFC, and battery power response using (a) PI, (b) ECMS, (c) EEMS, (d) PSO, and (e) EHOA.

The power output of the primary photovoltaic source and the secondary sources—the PEMFC and battery—across different methods for energy management are shown in Figure Figure 5.9. The power response using the Classical PI is shown in Figure 5.9 (a). Photovoltaic power starts out high and gradually drops, simulating a real drop in solar radiation, which could happen because of clouds or sunset. The PEMFC gradually increases its output from a minimal power level as photovoltaic generation decreases, making up for the solar energy shortfall and meeting load demand; however, it exhibits abrupt fluctuations, indicating sudden variations in power output rather than a consistent response. Concurrently, the battery power operates in a complementary and dynamic capacity, starting at about –1500 W, indicating that the excess photovoltaic power is charging the battery. The battery power shift turns positive during the transition as photovoltaic power drops, signifying that the battery discharges to help the fuel cell meet the required load. This pattern highlights the battery's susceptibility to notable fluctuations, indicating frequent cycles of charging and discharging.

The power response under the equivalent consumption minimization approach (ECMA) is shown in Figure 5.9 (b). As a result, when compared to other approaches, ECMS shows a more balanced and efficient power distribution between the PEMFC and battery. The method optimizes hydrogen utilization while meeting load requirements by dynamically allocating power between the fuel cell and the battery. In this arrangement, the PV is the main source that determines how management will react when its output declines. The PEMFC operates as a slow, effective base load generator; maintaining the fuel cell's longevity and improving its efficiency require a gradual ramp-up. In order to stabilize the load on the fuel cell and enhance the system's autonomy and overall energy efficiency, the battery simultaneously serves as a quick, dynamic power reservoir, quickly charging from excess photovoltaic energy and discharging to address brief shortfalls. The power response under the EEMS is shown in Figure 5.9 (c). EEMS provides the most consistent and efficient power response by emphasizing external energy sources to reduce internal fuel usage. Unlike ECMS, which optimizes energy distribution for efficiency, EEMS actively enhances contribution.

This entails employing external resources while methodically overseeing the operation of the fuel cell and batteries. The battery depletes more rapidly to reach its minimal state of charge (60%).When PV available, power initially peaks and thereafter declines. The PEMFC progressively enhances its output from a minimal power level as photovoltaic generation diminishes, compensating for the solar energy deficit and fulfilling load demand. The steady and smooth ramp-up, as opposed to an abrupt transition, safeguards the fuel cell's longevity and enhances its efficiency.

On the other hand, the power responses under optimization algorithms such as PSO- and EHOA-based EMS are shown in Figure 5.9 (d) and Figure 5.9 (e), respectively. According to the response, PV is the main source, but when PV reaches its maximum output, PEMFC and the battery are used as supplemental providers to meet further demand.

The results show that, in the absence of PV, the suggested EHOA with smooth FC ramping is superior and efficient, with power responses that are similar to those of EEMS. However, PSO may cause significant changes in the battery power response. Due to the method's search process, this behavior differs from that of EEMS.

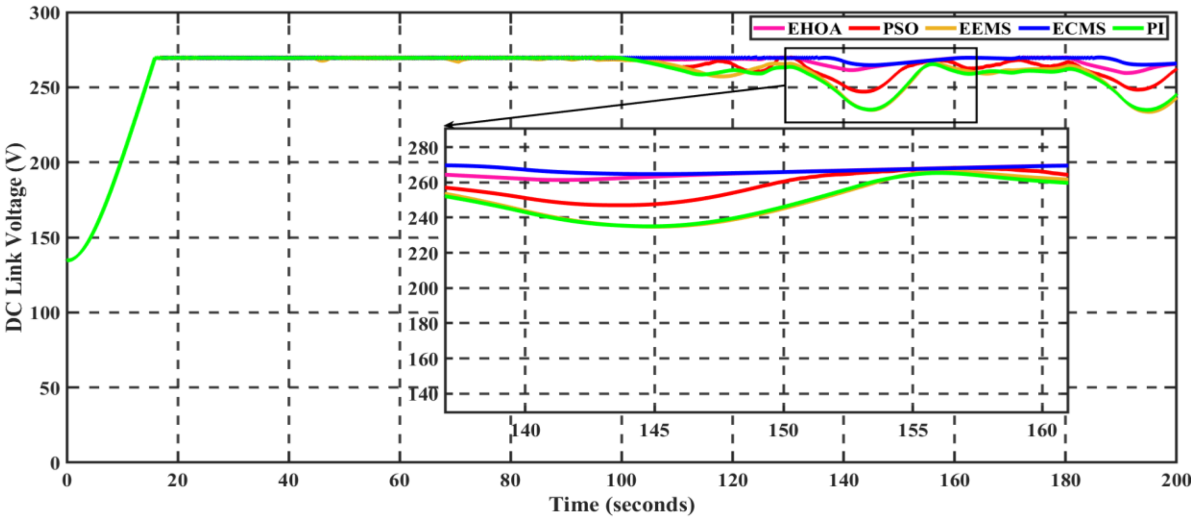

Figure 5.10: DC Link Voltage.

The DC link voltage's temporal response for the evaluated power management solutions is shown in Figure 5.10. During the first 100 seconds of the period, all strategies show an initial voltage increase that stabilizes at about 270 V. However, during the last 100 seconds, variations in load demand lead to varying degrees of overshoot and oscillations among the different strategies, resulting in the DC bus voltage falling below the reference voltage. The DC bus voltage falls below the reference voltage but stays significantly above the minimum DC bus voltage as PSO and EHOA show slight fluctuations but quickly stabilize. On the other hand, PI and EEMS show the most variability, suggesting a longer reaction time to changes in load. However, ECMS provides the smoothest DC link voltage stabilization.

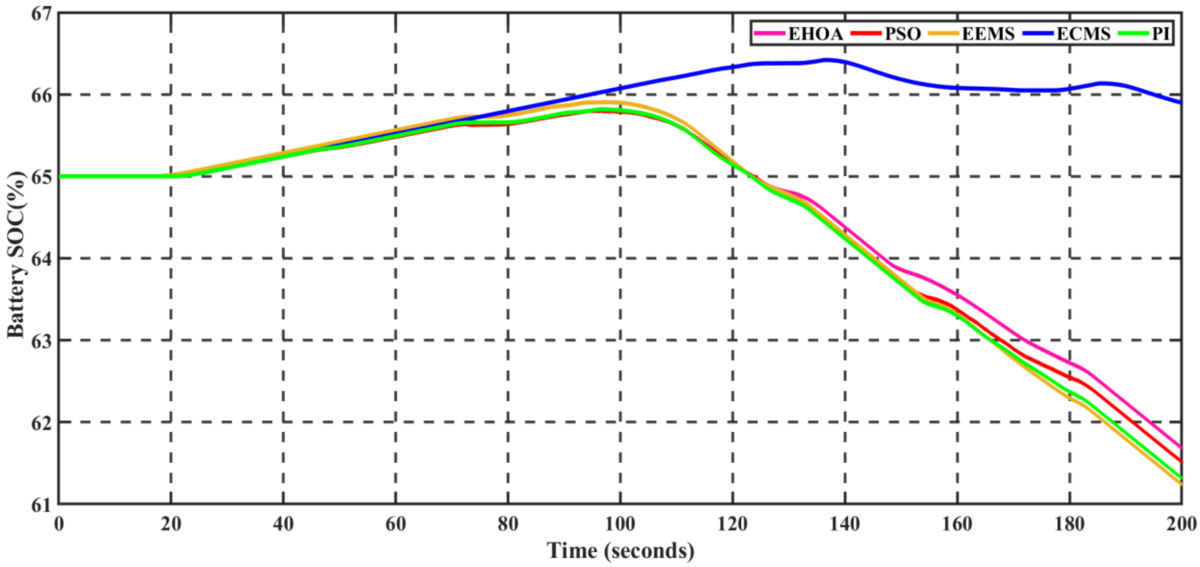

Figure 5.11: The SOC response of the battery for the proposed power management approaches.

The following formula is used to calculate the hydrogen consumption and overall efficiency obtained from each method:

The expression for overall efficiency is:

$$Efficiency = \frac{\int P_{Load}\,dt}{\int \left(P_{PV} + P_{FC} + P_{Battery}\right)dt} \tag{5.14}$$

The expression for hydrogen consumption (gm) is indicated by:

$$Consumption\ \text{H2}=\frac{N}{F}\int_{0}^{1800} I_{FC}\,dt \tag{5.15}$$

Where:

The Faraday constant $(A\ s/mol)$ is represented by F .

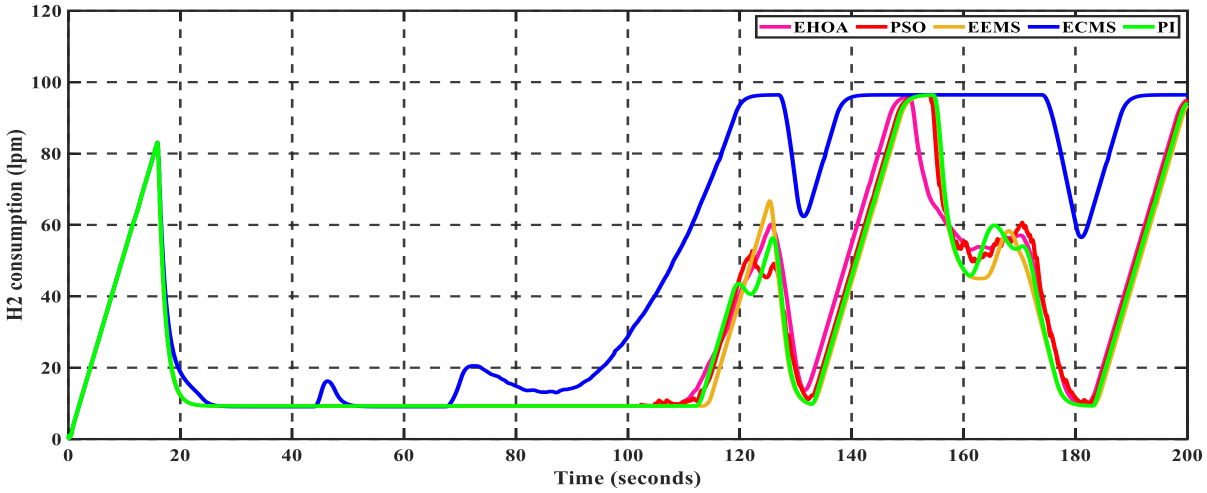

Figure 5.12: Hydrogen consumption in (Ipm) for the proposed power management approaches.

Figure 5.12 and Figure 5.13 provide a basis for evaluating how much hydrogen is consumed by the various power management approaches studied. EEMS has the least total hydrogen consumption of 8.34925 grams. This shows that EEMS uses less hydrogen when compared to other controllers.

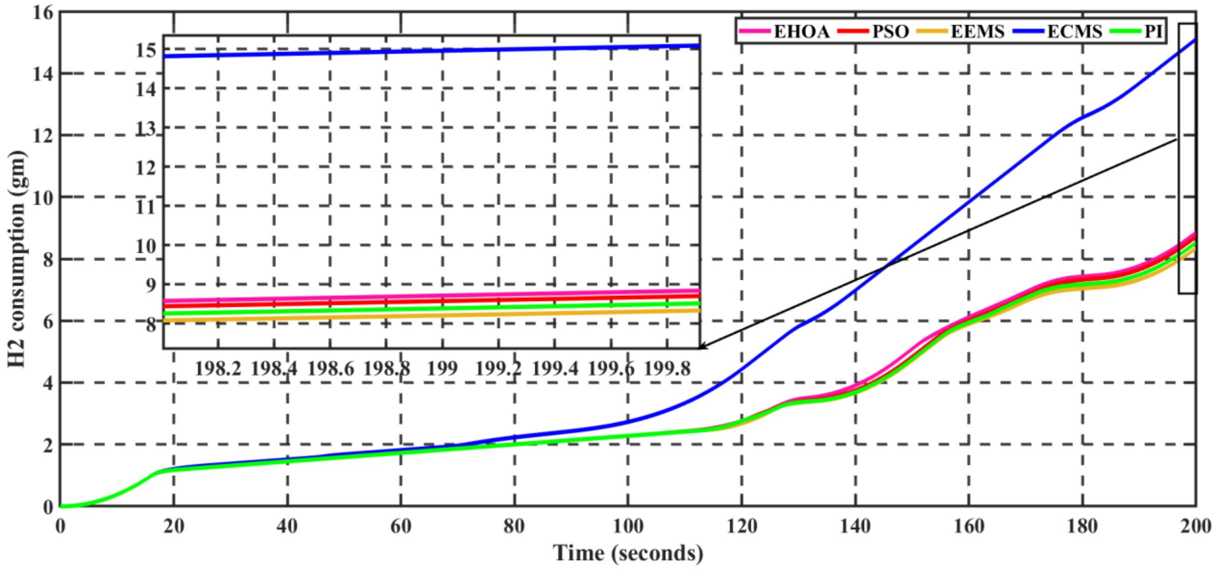

Figure 5.13: Hydrogen consumption in (gm) for the proposed power management approaches.

On the other hand, ECMS has the highest hydrogen consumption with 15.1042 grams; this implies that more importance is attached to the stability of the fuel cells than to other components of the system by ECMS. For example, PI-based EMS has a total hydrogen consumption of 8.52983 grams, making it between EHOA and PSO in fuel efficiency, whereas EHOA used 8.8564 grams and PSO used 8.71795 grams, which is slightly more hydrogen than EEMS.

As related to final battery SOC (see Figure 5.11), EEMS had the lowest with 61.24% vs ECMS with 65.90%, EHOA had 61.768%, PSO had 61.53%, and PI had 61.33%. While ECMS uses more fuel for its higher final SOC than any of these other scenarios, it also emphasizes the conservation of the battery by limiting its maximum depth of discharge. Although EHOA, PSO, and PI use more fuel for their SOCs, they remain below the reference SOC of 65%.

As illustrated in Figure 5.14, EEMS achieves the highest overall system efficiency of 90.99%, closely followed by PSO at 90.00% and the traditional PI method at 90.21%. With an efficiency of 89.91%, the EHOA approach performs competitively, while ECMS has the lowest efficiency at 87.89%, which is related to its higher hydrogen consumption and increased reliance on fuel-cell power. The comparison shows that EMSs have well-defined and comparable dynamic performance characteristics. Furthermore, there is a clear trade-off among fuel consumption, SOC preservation, and system performance, as summarized in Table 5.2.

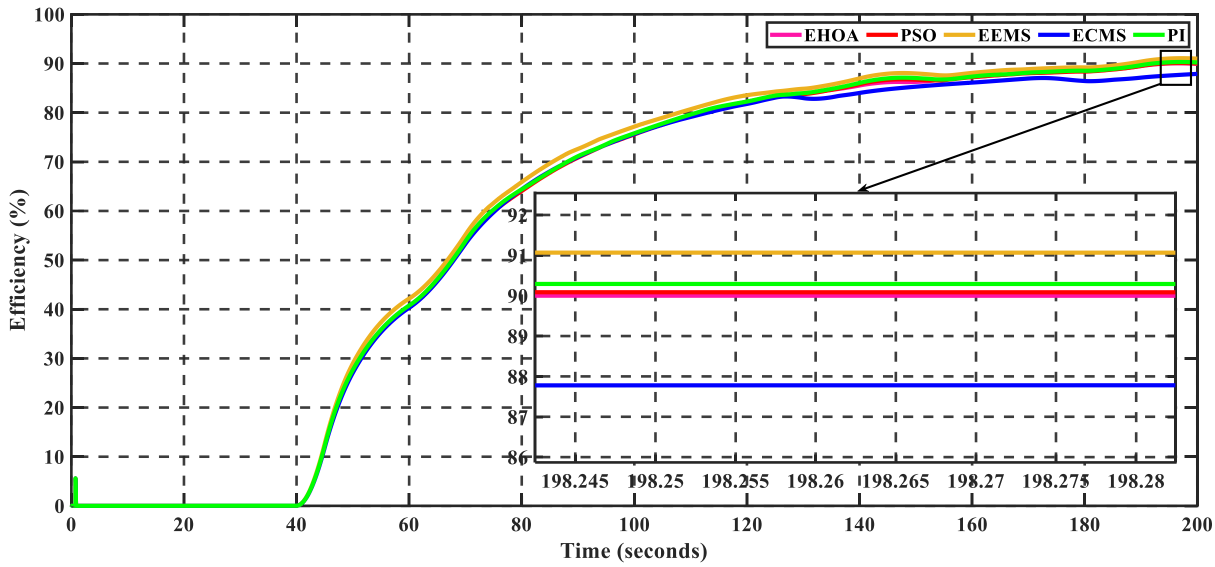

Figure 5.14: Efficiency of the proposed power management approaches.

Table 5.2 : Comparison between different performance metrics for the proposed power management approaches.

Performance metrics	EHOA	PSO	EEMS	ECMS	PI
Final SOC (%)	61.768	61.53	61.24	65.90	61.33

H2 Consumption (gm)	8.8564	8.71795	8.34925	15.1042	8.52983
Efficiency (%)	89.91	90	90.99	87.89	90.21

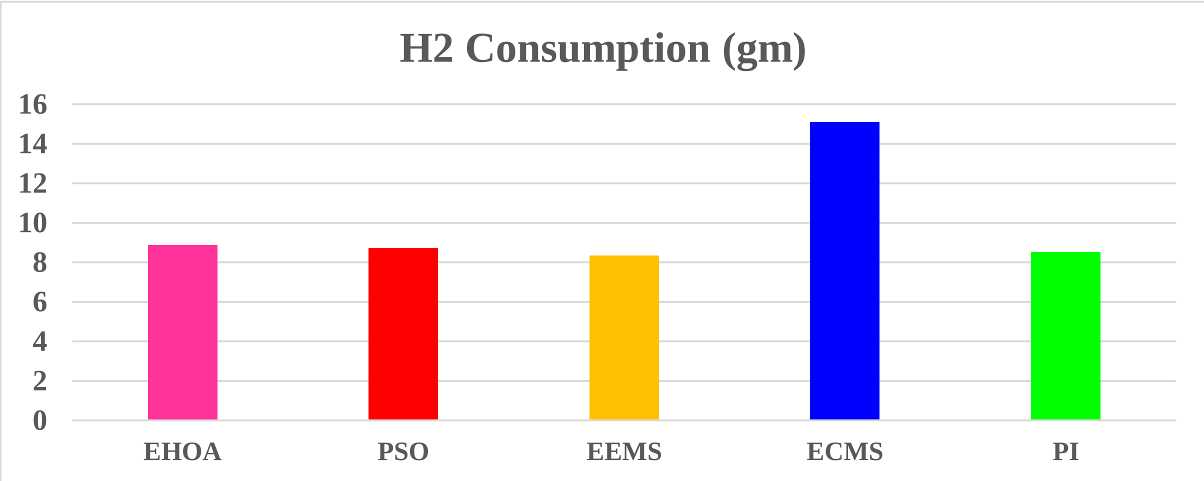

(a)

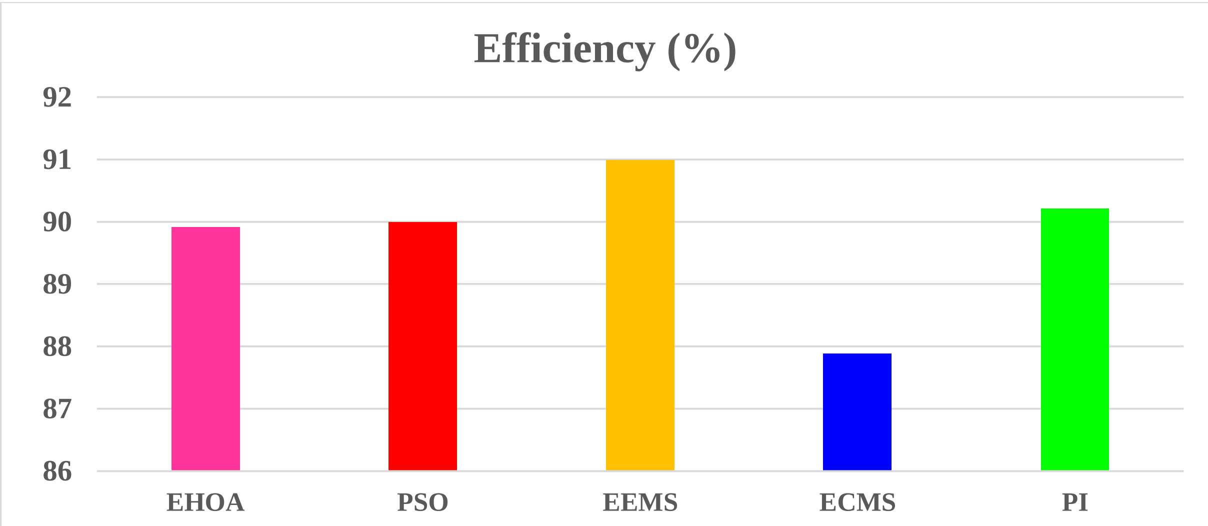

(b)

Figure 5.15: Graphical representation of the proposed power management approaches: (a) Hydrogen consumption, and (b) Efficiency.

Table 5.3 : A comprehensive comparison between the proposed EHOA and the common and currently used EMSs.

Power management strategy	**H2 Consumption**	**Efficiency**

Proposed EHOA	Very Low	Very High
PI [81]	Low	Medium
Genetic algorithm (GA) [81]	Low	Medium-High
EEMS [81]	Low	High
ECMS [81]	Medium	Medium
Frequency decoupling and state machine strategy (FDSMS) [81]	Low	High
SSA [81]	High -Low	Medium-High
Harris hawks optimizer (HHO) -EEMS [128]	Very low	High
Coyote Optimization Approach [133]	High-Low	High

5.4 Conclusion

For testing, modeling, and comparison, the most popular and modern energy management techniques are selected. For a fair comparison, the energy management strategies had been developed to satisfy the same requirements. The strategies included the equivalent consumption minimization approach (ECMA) and the proportional-integral (PI) control approach. The strategies included the newly introduced elk herd optimization approach (EHOA), the external energy maximization strategy (EEMS), and particle swarm optimization (PSO). Compared to existing techniques for lowering H2 consumption, the suggested approach is less complicated, simple, and more adaptable to variations in the load profile. Hydrogen consumption, battery state of charge, DC bus voltage stabilization, and overall efficiency were among the performance evaluation criteria (see Table 5.3).

Compared to other techniques, the PI controller was more efficient and used less hydrogen; however, it needed more battery power and showed different degrees of DC bus voltage overshoot. These results demonstrated that the PI controller's performance was inadequate in all assessments. Because the ECMS approach prioritizes battery state of charge retention, it uses more hydrogen and is less efficient overall. By maintaining a nearly constant DC bus voltage while guaranteeing a smooth response and minimal battery usage, the suggested technique, EHOA, outperformed the ECMS in efficiency and fuel consumption, thereby increasing lifespan. Although it uses more batteries, EEMS is the best option for cutting hydrogen consumption while maintaining competitive efficiency.

Chapter 6 : Conclusions

6.1 General conclusion

It can be challenging to develop an efficient control strategy and choose the right hybrid system, especially when multiple energy sources are involved. The primary aim of this thesis is to improve the control and management of the hybrid standalone PV-FC system. The proposed methods have addressed key challenges associated with fluctuating weather conditions, nonlinear output characteristics, dynamic operating environments, and dynamic load demands, which can compromise system efficiency, stability, and reliability.

Firstly, we have concentrated on extracting the MPP in photovoltaic systems by developing an enhanced pufferfish optimization (PFO) MPPT strategy, compared to four existing and recent metaheuristic MPPT strategies, including particle swarm optimization, the grey wolf approach, the arithmetic optimization approach, and the snake optimization approach, under fast-changing irradiance conditions and five complex peak shading patterns. The proposed EPFOA MPPT for solar systems underwent comprehensive evaluation under complex partial-shading scenarios and varying irradiance levels. With just two tuning parameters, EPFOA continuously approaches the global maximum power point. It was able to effectively overcome local peaks due to its dynamic search strategy, which allowed for reliable tracking even in the face of abrupt environmental changes. The technique was able to achieve high output power without oscillating around the MPP. In terms of tracking speed, accuracy, and resilience, the comparative results indicate that it outperforms both conventional and modern MPPT techniques. The EPFOA's remarkable dependability when deployed in complex real-world solar panel issues affected by uneven and changing shading and fast-varying conditions attests to its suitability for realistic photovoltaic applications. To improve methods' practical relevance and possibly reduce computational time and algorithmic complexity, future research will focus on optimizing methods by reducing the search space and extending their application to new converter types.

Through extensive simulations, the proposed methods have been shown to be effective, all the while showing substantial improvements in robustness, efficiency, and dynamic response as compared to current methods. The results confirm the practical viability of the proposed control strategies by showing the ability of the hybrid system to adapt to rapid changes in environmental variables. However, unlike other methods, real-time experiments using hardware-in-the-loop (HIL) demonstrated the EPFOA's stable and sustained system performance in real-world operating conditions.

On the other hand, in PMEFC, the FSSO has been suggested, developed, and assessed in comparison to the CSO for the PEMFC control system specifically under varying pressure and temperature conditions. The results demonstrate the adaptive search process enables the FSSO to deliver a minimal settling time and increased stability while accurately tracking the MPP during rapid and unexpected fluctuations in environmental conditions. FSSO is a robust and efficient MPPT approach for PEM fuel cell systems, making it a viable option for sustainable hydrogen applications under varying climate conditions.

An effective EHOA energy management strategy has been developed to manage the operation of many energy sources and assure that power is always available. This method optimally distributes energy, focuses on renewable sources, and protects the system from exceeding the operating limits of any part, ensuring a steady flow of power to the demand. The results show that the hybrid system can quickly adjust to changes in the environment and the load's needs. This result indicates that the proposed EHOA control, along with other common and modern management methods, can be used successfully in the real world. This research has developed a scalable and systematic framework for the integration of hybrid renewable energy systems, accommodating diverse configurations, sizes, and operational requirements, extending beyond mere technical efficiency.

The solutions provided in this thesis have advanced intelligent control for hybrid green systems, providing a comprehensive approach to increase efficiency and achieve stability. The outcomes from this research advance sustainable, longer lasting, and intelligent energy systems in the future by opening up avenues for further research into more adaptive, data-driven, and predictive control methods, while also providing a robust foundation for the practical and real-time implementation of hybrid energy systems.

6.2 Perspectives & Future Directions

This thesis lays the foundation for future research opportunities aimed at improving the efficiency, versatility, flexibility, and scalability of hybrid green power systems.

- ✓ Investigate deep and reinforcement learning for predictive power management and adaptive control.
- ✓ Develop energy management to encompass smart grid integration and demand response initiatives.
- ✓ Enhance hybrid systems to incorporate supplementary renewable sources (hydropower, biomass, tidal) with combined control mechanisms.
- ✓ Design, develop, and implement of AI and machine learning-based real-time predictive EMS for electric vehicles.
- ✓ Develop and Implement hybrid strategies combining machine learning and conventional MPPT approaches.
- ✓ Integrate soft-switching converters with advanced MPPT approaches for expedited and precise tracking in partial shade and changing irradiance scenarios.
- ✓ Explore new power converters topologies to enhance low conversion.
- ✓ Develop AI methods for hydrogen demand forecasting.
- ✓ Hydrogen-powered gas turbines for grid backup.

References

[1] J. O. Petinrin and M. Shaaban, "Renewable energy for continuous energy sustainability in Malaysia," *Renew. Sustain. Energy Rev.*, vol. 50, pp. 967–981, 2015, doi: 10.1016/j.rser.2015.04.146.

[2] "CO_2 and Greenhouse Gas Emissions - Our World in Data." Accessed: Aug. 14, 2025. [Online]. Available: https://ourworldindata.org/co2-and-greenhouse-gas-emissions

[3] J. Delbeke, A. Runge-Metzger, Y. Slingenberg, and J. Werksman, "The paris agreement," *Towar. a Clim. Eur. Curbing Trend*, pp. 24–45, 2019, doi: 10.4324/9789276082569-2.

[4] N. Fulghum, "Total electricity generation as share of primary energy," *Our World Data*, no. April, 2024, [Online]. Available: https://archive.ourworldindata.org/20250624-125417/grapher/electricity-as-a-share-of-primary-energy.html

[5] X. Li *et al.*, "Carbon footprint and environmental impact of China's PV production and reduction potential of PV power generation," *Environ. Impact Assess. Rev.*, vol. 115, no. September 2024, p. 107977, 2025, doi: 10.1016/j.eiar.2025.107977.

[6] B. Yang *et al.*, "Salp swarm optimization algorithm based MPPT design for PV-TEG hybrid system under partial shading conditions," *Energy Convers. Manag.*, vol. 292, no. April, p. 117410, 2023, doi: 10.1016/j.enconman.2023.117410.

[7] C. Ceylan and Y. Devrim, "Design and simulation of the PV/PEM fuel cell based hybrid energy system using MATLAB/Simulink for greenhouse application," *Int. J. Hydrogen Energy*, vol. 46, no. 42, pp. 22092–22106, 2021, doi: 10.1016/j.ijhydene.2021.04.034.

[8] M. Z. Yousaf *et al.*, "Improved MPPT of solar PV Systems under different Environmental conditions utilizes a Novel Hybrid PSO," *Renew. Energy*, vol. 244, no. November 2024, p. 122709, 2025, doi: 10.1016/j.renene.2025.122709.

[9] B. Shboul *et al.*, "New hybrid photovoltaic-fuel cell system for green hydrogen and power production: Performance optimization assisted with Gaussian process regression method," *Int. J. Hydrogen Energy*, vol. 59, no. February, pp. 1214–1229, 2024, doi: 10.1016/j.ijhydene.2024.02.087.

[10] M. Tawalbeh, A. Al-Othman, F. Kafiah, E. Abdelsalam, F. Almomani, and M. Alkasrawi, "Environmental impacts of solar photovoltaic systems: A critical review of recent progress and future outlook," *Sci. Total Environ.*, vol. 759, 2021, doi: 10.1016/j.scitotenv.2020.143528.

[11] M. S. Okundamiya, "Integration of photovoltaic and hydrogen fuel cell system for sustainable energy harvesting of a university ICT infrastructure with an irregular electric grid," *Energy Convers. Manag.*, vol. 250, no. November, p. 114928, 2021, doi: 10.1016/j.enconman.2021.114928.

[12] S. M. Abu *et al.*, "An effective optimization algorithm for hydrogen fuel cell-based hybrid energy system: A sustainable microgrid approach," *Int. J. Hydrogen Energy*, vol. 98, no. October 2024, pp. 1341–1355, 2025, doi: 10.1016/j.ijhydene.2024.12.176.

[13] M. K. Deshmukh and S. S. Deshmukh, "Modeling of hybrid renewable energy systems," *Renew. Sustain. Energy Rev.*, vol. 12, no. 1, pp. 235–249, 2008, doi: 10.1016/j.rser.2006.07.011.

[14] N. G. Chatzigeorgiou, S. Theocharides, G. Makrides, and G. E. Georghiou, "Assessment of the economic feasibility of hybrid Photovoltaic – Battery Energy Storage Systems in public buildings with flexible load demand : Examination study in Southern Europe," *Renew. Energy*, vol. 256, no. PD, p. 124089, 2026, doi: 10.1016/j.renene.2025.124089.

[15] A. Maturo, C. Vallianos, A. Buonomano, A. Athienitis, and B. Delcroix, "Clustering-driven design and predictive control of hybrid PV-battery storage systems for demand response in energy communities," *Renew. Energy*, vol. 253, no. April, p. 123390, 2025, doi: 10.1016/j.renene.2025.123390.

[16] R. Zhu, K. Das, P. E. Sørensen, and A. D. Hansen, "International Journal of Electrical Power and Energy Systems Enhancing profits of hybrid wind-battery plants in spot and balancing markets using data-driven two-level optimization," *Int. J. Electr. Power Energy Syst.*, vol. 159, no. May 2023, p. 110029, 2024, doi: 10.1016/j.ijepes.2024.110029.

[17] K. Zhao, K. Zheng, C. Shen, and J. Ge, "Configuration optimization and performance analysis of hybrid PV / wind systems in building groups," *J. Build. Eng.*, vol. 97, no. August, p. 110696, 2024, doi: 10.1016/j.jobe.2024.110696.

[18] S. Lee, L. Al-ghussain, M. Alrbai, and S. Al-dahidi, "International Journal of Hydrogen Energy Integrating hybrid PV / wind-based electric vehicles charging stations with green hydrogen production in Kentucky through techno-economic assessment," *Int. J. Hydrogen Energy*, vol. 71, no. April, pp. 345–356, 2024, doi: 10.1016/j.ijhydene.2024.05.053.

[19] M. A. Alotaibi, U. K. Seng, H. Malik, and A. Afthanorhan, "Fuzzy logic-based intelligent energy management framework for hybrid PV-wind-battery system : A case study of commercial building in Malaysia," vol. 102, no. March, 2024, doi: 10.1016/j.est.2024.114109.

[20] N. A. S. Elminshawy, S. Diab, Y. El, S. Yassen, and O. Elbaksawi, "An energy-economic analysis of a hybrid PV / wind / battery energy-driven hydrogen generation system in rural regions of Egypt," *J. Energy Storage*, vol. 80, no. December 2023, p. 110256, 2024, doi: 10.1016/j.est.2023.110256.

[21] A. A. Hassan and S. H. E. A. Aleem, "OPEN A modified energy management strategy for PV / diesel hybrid system to reduce diesel consumption based on artificial protozoa optimizer Artificial Protozoa optimizer," pp. 1–24, 2025.

[22] A. Olalekan, S. Kumar, A. Kumar, and A. Mane, "e-Prime - Advances in Electrical Engineering , Electronics and Energy Design ,

modeling , and simulation of a PV / diesel / battery hybrid energy system for an off-grid hospital in Ethiopia," *e-Prime - Adv. Electr. Eng. Electron. Energy*, vol. 8, no. March, p. 100607, 2024, doi: 10.1016/j.prime.2024.100607.

[23] R. Sebastián-fernández, J. L. Monroy-morales, R. Peña-alzola, D. Campos-gaona, J. Q. Castellano, and J. L. Guardado, "Frequency control in an isolated wind-diesel hybrid system with energy storage and an irrigation water supply system," no. April 2023, pp. 1040–1054, 2024, doi: 10.1049/rpg2.12950.

[24] S. Sarmast, S. Séjourné, A. Wigston, R. A. Fraser, and M. B. Dusseault, "Adaptive hybrid energy system for remote Canadian communities : Optimizing wind-diesel systems integrated with adiabatic compressed air energy storage," *Energy Convers. Manag.*, vol. 315, no. December 2023, p. 118778, 2024, doi: 10.1016/j.enconman.2024.118778.

[25] A. S. Rahi and S. F. Alwash, "Accurate Power Control for Hybrid PV-Battery / Supercapacitor System," vol. 57, no. 4, pp. 1127–1133, 2024.

[26] K. Raut, A. Shendge, J. Chaudhari, R. Lamba, and N. F. Alshammari, "Modeling and simulation of photovoltaic powered battery-supercapacitor hybrid energy storage system for electric vehicles," *J. Energy Storage*, vol. 82, no. February 2023, p. 110324, 2024, doi: 10.1016/j.est.2023.110324.

[27] H. Rezk and A. Fathy, "Hydrogen reduction-based energy management strategy of hybrid fuel cell / PV / battery / supercapacitor renewable energy system," *J. Energy Storage*, vol. 86, no. PB, p. 111316, 2024, doi: 10.1016/j.est.2024.111316.

[28] D. Nassir, "Développement d ' une stratégie intelligente de contrôle et de gestion d ' un système hybride connecté au réseau," 2025.

[29] P. Joshi, A. B. Rao, and R. Banerjee, "Review of solar PV deployment trends, policy instruments, and growth projections in China, the United States, and India," *Renew. Sustain. Energy Rev.*, vol. 213, no. February, pp. 1–17, 2025, doi: 10.1016/j.rser.2025.115436.

[30] F. J. Vivas, A. De las Heras, F. Segura, and J. M. Andújar, "A review of energy management strategies for renewable hybrid energy systems with hydrogen backup," *Renew. Sustain. Energy Rev.*, vol. 82, no. August 2017, pp. 126–155, 2018, doi: 10.1016/j.rser.2017.09.014.

[31] B. F. Silinto, C. van der Laag Yamu, C. Zuidema, and A. P. C. Faaij, "Hybrid renewable energy systems for rural electrification in developing countries: A review on energy system models and spatial explicit modelling tools," *Renew. Sustain. Energy Rev.*, vol. 207, no. September 2024, 2025, doi: 10.1016/j.rser.2024.114916.

[32] Y. Yuan, J. Wang, X. Yan, B. Shen, and T. Long, "A review of multi-energy hybrid power system for ships," *Renew. Sustain. Energy Rev.*, vol. 132, no. June, p. 110081, 2020, doi: 10.1016/j.rser.2020.110081.

[33] A. F. Bendary and M. M. Ismail, "Battery charge management for hybrid PV/wind/fuel cell with storage battery," *Energy Procedia*, vol. 162, pp. 107–116, 2019, doi: 10.1016/j.egypro.2019.04.012.

[34] T. Jeyaraj, A. Ponnusamy, and D. Selvaraj, "Hybrid renewable energy systems stability analysis through future advancement technique: A review," *Appl. Energy*, vol. 383, no. November 2024, p. 125355, 2025, doi: 10.1016/j.apenergy.2025.125355.

[35] J. S. Kumari and C. S. Babu, "Mathematical Modeling and Simulation of Photovoltaic Cell using Matlab-Simulink Environment," vol. 2, no. 1, pp. 26–34, 2012.

[36] M. G. Villalva, J. R. Gazoli, and E. R. Filho, "Comprehensive Approach to Modeling and Simulation of Photovoltaic Arrays," vol. 24, no. 5, pp. 1198–1208, 2009.

[37] S. R. Wenham and M. A. Green, "Silicon Solar," vol. 4, no. December 1995, pp. 3–33, 1996.

[38] "The World's First GW-Level Perovskite PV Module Production Line Commences Operation - Shanghai Metal Market." Accessed: Aug. 31, 2025. [Online]. Available: https://www.metal.com/en/newscontent/103165746

[39] M. R. Ranga, V. Raobathina, and S. Kotni, "A review of solar cell parameters extraction using metaheuristic optimization methods based on various diode models," *2024 Int. Conf. Comput. Intell. Green Sustain. Technol.*, pp. 1–6, 2024, doi: 10.1109/ICCIGST60741.2024.10717470.

[40] Y. Mahmoud, W. Xiao, and H. H. Zeineldin, "A Simple Approach to Modeling and Simulation of Photovoltaic Modules," *IEEE Trans. Sustain. Energy*, vol. 3, no. 1, pp. 185–186, 2012, doi: 10.1109/TSTE.2011.2170776.

[41] A. Chouder, S. Silvestre, N. Sadaoui, and L. Rahmani, "Simulation Modelling Practice and Theory Modeling and simulation of a grid connected PV system based on the evaluation of main PV module parameters," *Simul. Model. Pract. Theory*, vol. 20, no. 1, pp. 46–58, 2012, doi: 10.1016/j.simpat.2011.08.011.

[42] Vinod, R. Kumar, and S. K. Singh, "Solar photovoltaic modeling and simulation: As a renewable energy solution," *Energy Reports*, vol. 4, pp. 701–712, 2018, doi: 10.1016/j.egyr.2018.09.008.

[43] C. Mai, L. Zhang, X. Chao, X. Hu, X. Wei, and J. Li, "A novel MPPT technology based on dung beetle optimization algorithm for PV systems under complex partial shade conditions," *Sci. Rep.*, vol. 14, no. 1, pp. 1–23, 2024, doi: 10.1038/s41598-024-57268-8.

[44] D. J. K. Kishore, M. R. Mohamed, K. Sudhakar, and K. Peddakapu, "A new meta-heuristic optimization-based MPPT control technique for green energy harvesting from photovoltaic systems under different atmospheric conditions," *Environ. Sci. Pollut. Res.*, vol. 30, no. 35, pp. 84167–84182, 2023, doi: 10.1007/s11356-023-28248-8.

[45] M. T. Hussain, M. Tariq, A. Sarwar, S. Urooj, A. BaQais, and M. A. Hossain, "Atomic Orbital Search Algorithm for Efficient Maximum Power Point Tracking in Partially Shaded Solar PV Systems," *Processes*, vol. 11, no. 9, 2023, doi: 10.3390/pr11092776.

[46] S. K. Vankadara, S. Chatterjee, P. K. Balachandran, and L. Mihet-Popa, "Marine Predator Algorithm (MPA)-Based MPPT Technique for Solar PV Systems under Partial Shading Conditions," *Energies*, vol. 15, no. 17, 2022, doi: 10.3390/en15176172.

[47] S. M. Kabeb and N. H. A. Bakar, "Polymer blend nanocomposites for polymer electrolyte membrane fuel cell (PEMFC) applications," *Polym. Blend Nanocomposites Energy Storage Appl.*, no. January, pp. 479–493, 2023, doi: 10.1016/B978-0-323-99549-8.00002-9.

[48] I. Sebbani, M. K. Ettouhami, and M. Boulakhbar, "Fuel cells: A technical, environmental, and economic outlook," *Clean. Energy Syst.*, vol. 10, no. January, p. 100168, 2025, doi: 10.1016/j.cles.2024.100168.

[49] S. Mekhilef, R. Saidur, and A. Safari, "Comparative study of different fuel cell technologies," *Renew. Sustain. Energy Rev.*, vol. 16, no. 1, pp. 981–989, 2012, doi: 10.1016/j.rser.2011.09.020.

[50] A. K. M. Mohiuddin, N. Basran, and A. A. Khan, "Modelling and validation of Proton exchange membrane fuel cell (PEMFC)," *IOP Conf. Ser. Mater. Sci. Eng.*, vol. 290, no. 1, pp. 0–12, 2018, doi: 10.1088/1757-899X/290/1/012026.

[51] I. Chaouki and K. V. Fedorovich, "Future pem fuel cell system renewable energy systems based on hydrogen equipment for microgrid networks," *IOP Conf. Ser. Earth Environ. Sci.*, vol. 1045, no. 1, 2022, doi: 10.1088/1755-1315/1045/1/012005.

[52] N. H. Jawad *et al.*, "Fuel Cell Types, Properties of Membrane, and Operating Conditions: A Review," *Sustain.*, vol. 14, no. 21, 2022, doi: 10.3390/su142114653.

[53] D. Manzo, R. Thai, H. T. Le, and G. K. Venayagamoorthy, "Fuel cell technology review: Types, economy, applications, and vehicle-to-grid scheme," *Sustain. Energy Technol. Assessments*, vol. 75, no. January, p. 104229, 2025, doi: 10.1016/j.seta.2025.104229.

[54] B. Karthikeyan, V. Kalyanasundaram, S. Vidyasagar, K. Sundararaju, and R. Palanisamy, "Ffnn Based Mppt Controller for Pemfc Powered Non-Isolated High Gain Dc-Dc Converter With Spwm Inverter Fed Bldc Motor," *IOP Conf. Ser. Mater. Sci. Eng.*, vol. 1055, no. 1, p. 012147, 2021, doi: 10.1088/1757-899x/1055/1/012147.

[55] J. Y. Fam, S. Y. Wong, H. B. M. Basri, M. O. Abdullah, K. B. Lias, and S. Mekhilef, "Predictive maximum power point tracking for proton exchange membrane fuel cell system," *IEEE Access*, vol. 9, pp. 157384–157397, 2021.

[56] R. Subbulakshmy, R. Palanisamy, S. Alshahrani, and C. A. Saleel, "Implementation of Non-Isolated High Gain Interleaved DC-DC Converter for Fuel Cell Electric Vehicle Using ANN-Based MPPT Controller," *Sustain.*, vol. 16, no. 3, 2024, doi: 10.3390/su16031335.

[57] Y. Foughali *et al.*, "A RBF artificial neural network to predict a fuel cell maximum power point," *Prz. Elektrotechniczny*, vol. 98, no. 7, pp. 100–104, 2022, doi: 10.15199/48.2022.07.17.

[58] A. Daya and A. S. Nesaraj, "Review of materials, functional components, fabrication technologies and assembling characteristics for polymer electrolyte membrane fuel cells (PEMFCs) - An update," *J. Met. Mater. Miner.*, vol. 33, no. 4, 2023, doi: 10.55713/JMMM.V33I4.1775.

[59] A. Bouguerra, A. E. Badoud, S. Mekhilef, B. Kanouni, M. Bajaj, and I. Zaitsev, "Enhancing PEM fuel cell efficiency with flying squirrel search optimization and Cuckoo Search MPPT techniques in dynamically operating environments," *Sci. Rep.*, vol. 14, no. 1, pp. 1–28, 2024, doi: 10.1038/s41598-024-64915-7.

[60] R. Gugulothu, B. Nagu, and D. Pullaguram, "A computationally efficient jaya optimization for fuel cell maximum power tracking," *Energy Sources, Part A Recover. Util. Environ. Eff.*, vol. 44, no. 1, pp. 1541–1565, 2022, doi: 10.1080/15567036.2022.2055229.

[61] A. Zaidy, P. Pokharkar, R. Krishnan, and D. Sonawane, "Dynamic modeling and simulation of a PEM fuel cell: MATLAB and LabVIEW modeling approach," *Proc. 2014 1st Int. Conf. Non Conv. Energy Search Clean Safe Energy, ICONCE 2014*, no. Iconce, pp. 272–276, 2014, doi: 10.1109/ICONCE.2014.6808744.

[62] A. Zouggaret *et al.*, "An Efficient Fuel Cell Maximum Power Point Tracker based on an Adaptive Neural Fuzzy Inference System," *Prz. Elektrotechniczny*, vol. 99, no. 2, pp. 135–139, 2023, doi: 10.15199/48.2023.02.23.

[63] C. System, "Fuzzy logic MPPT control algorithm for a Proton-Exchange Membrane Fuel Cells System," no. August, 2021, doi: 10.46657/ajresd.2021.3.1.2.

[64] M. G. Santarelli and M. F. Torchio, "Experimental analysis of the effects of the operating variables on the performance of a single PEMFC," *Energy Convers. Manag.*, vol. 48, no. 1, pp. 40–51, 2007, doi: 10.1016/j.enconman.2006.05.013.

[65] M. A. Salam *et al.*, "Effect of Temperature on the Performance Factors and Durability of Proton Exchange Membrane of Hydrogen Fuel Cell: A Narrative Review," *Mater. Sci. Res. India*, vol. 17, no. 2, pp. 179–191, 2020, doi: 10.13005/msri/170210.

[66] A. Bouguerra, A. E. Badoud, and S. Mekheilef, "Proton Exchange Membrane Fuel Cells: An Effective Neural Fuzzy System for Optimal Power Tracking," *J. Renew. Energies*, vol. 2024, no. Special Issue, pp. 151–164, 2024, doi: 10.54966/jreen.v1i3.1299.

[67] M. Aly and H. Rezk, "An improved fuzzy logic control-based MPPT method to enhance the performance of PEM fuel cell system," *Neural Comput. Appl.*, vol. 34, no. 6, pp. 4555–4566, 2022, doi: 10.1007/s00521-021-06611-5.

[68] A. N. Suthar, J. Venkataramanaiah, and Y. Suresh, "Conventional, wide-bandgap, and hybrid power converters: A comprehensive review," *Renew. Sustain. Energy Rev.*, vol. 213, no. November 2023, p. 115419, 2025, doi: 10.1016/j.rser.2025.115419.

[69] S. S. Mohammed and D. Devaraj, "Simulation and analysis of stand-alone photovoltaic system with boost converter using MATLAB/Simulink," *2014 Int. Conf. Circuits, Power Comput. Technol. ICCPCT 2014*, pp. 814–821, 2014, doi: 10.1109/ICCPCT.2014.7054991.

[70] H. A. Mohamed, H. A. Khattab, A. Mobarka, and G. A. Morsy, "Design, control and performance analysis of DC-DC boost converter for stand-alone PV system," *2016 18th Int. Middle-East Power Syst. Conf. MEPCON 2016 - Proc.*, pp. 101–106, 2017, doi: 10.1109/MEPCON.2016.7836878.

[71] J. L. Seguel, S. I. Seleme, and L. M. F. Morais, "Comparative Study of Buck-Boost, SEPIC, Cuk and Zeta DC-DC Converters Using Different MPPT Methods for Photovoltaic Applications," *Energies*, vol. 15, no. 21, 2022, doi: 10.3390/en15217936.

[72] S. Alatai *et al.*, "A review on state-of-the-art power converters: Bidirectional, resonant, multilevel converters and their derivatives," *Appl. Sci.*, vol. 11, no. 21, 2021, doi: 10.3390/app112110172.

[73] R. Hvljq, I. R. U. Ssolfdwlrqv, D. G. D. O. Eul, and D. Rxvhi, "'& '& %Rrvw &Rqyhuwhu &Rqwuroohu 'Hvljq Iru 39 $Ssolfdwlrqv," pp. 5–10, 2017.

[74] R. Reshma Gopi and S. Sreejith, "Converter topologies in photovoltaic applications – A review," *Renew. Sustain. Energy Rev.*, vol. 94, no. December 2017, pp. 1–14, 2018, doi: 10.1016/j.rser.2018.05.047.

[75] W. Erickson, "Dc – Dc Power Converters Choppers Switching Power Supplies," *Power*, no. 2, pp. 1–18, 2007, [Online]. Available: https://onlinelibrary.wiley.com/doi/abs/10.1002/047134608X.W5808.pub2.[Accessed 06%0AJuly 2018].

[76] A. Pradhan and B. Panda, "A simplified design and modeling of boost converter for photovoltaic sytem," *Int. J. Electr. Comput. Eng.*, vol. 8, no. 1, pp. 141–149, 2018, doi: 10.11591/ijece.v8i1.pp141-149.

[77] A. M. Atallah and A. Y. Abdelaziz, "I MPLEMENTATION O F P ERTURB A ND O BSERVE MPPT O F PV S YSTEM W ITH D IRECT C ONTROL M ETHOD U SING B UCK A ND B UCK -," no. February 2014, 2015.

[78] B. M. Hasaneen and A. A. E. Mohammed, "Design and simulation of DC/DC boost converter," *2008 12th Int. Middle East Power Syst. Conf. MEPCON 2008*, pp. 335–340, 2008, doi: 10.1109/MEPCON.2008.4562340.

[79] F. Akter, T. K. Roy, M. S. Islam, A. F. Alkhateeb, and M. A. Mollah, "Design of a Nonlinear Integral Terminal Sliding Mode Controller for a PEM Fuel Cell Based on a DC-DC Boost Converter," *IEEE Access*, vol. 10, no. August, pp. 97419–97428, 2022, doi: 10.1109/ACCESS.2022.3205733.

[80] K. Badreddine, "KANOUNI Badreddine TH È ME C ontribution to the control and energy management of multi- source system connected to the network Presented to the Department of Electrical Engineering Ph . D Contribution to the control and energy management of multi-source system connected to the network," 2024.

[81] A. Fathy, H. Rezk, and A. M. Nassef, "Robust hydrogen-consumption-minimization strategy based salp swarm algorithm for energy management of fuel cell/supercapacitor/batteries in highly fluctuated load condition," *Renew. Energy*, vol. 139, pp. 147–160, 2019, doi: 10.1016/j.renene.2019.02.076.

[82] S. Nyamathulla and C. Dhanamjayulu, "A review of battery energy storage systems and advanced battery management system for different applications: Challenges and recommendations," *J. Energy Storage*, vol. 86, no. PA, p. 111179, 2024, doi: 10.1016/j.est.2024.111179.

[83] B. Kanouni, "Contribution to the control and energy management of multi-source system connected to the network," 2024.

[84] R. Kumar, R. A. Gupta, and A. Kumar, "Economic analysis and power management of a stand-alone wind / photovoltaic hybrid energy system using biogeography based optimization algorithm," *Swarm Evol. Comput.*, vol. 8, pp. 33–43, 2013, doi: 10.1016/j.swevo.2012.08.002.

[85] A. Refaat *et al.*, "Extraction of maximum power from PV system based on horse herd optimization MPPT technique under various weather conditions," *Renew. Energy*, vol. 220, no. May 2023, p. 119718, 2024, doi: 10.1016/j.renene.2023.119718.

[86] S. Motahhir, A. El Hammoumi, and A. El Ghzizal, "The most used MPPT algorithms: Review and the suitable low-cost embedded board for each algorithm," *J. Clean. Prod.*, vol. 246, p. 118983, 2020, doi: 10.1016/j.jclepro.2019.118983.

[87] N. Karami, N. Moubayed, and R. Outbib, "General review and classification of different MPPT Techniques," *Renew. Sustain. Energy Rev.*, vol. 68, no. July 2016, pp. 1–18, 2017, doi: 10.1016/j.rser.2016.09.132.

[88] M. İnci and U. Aydemir, "Maximum power harvesting from fuel cell systems: A comprehensive review on critical role of MPPT methods, parameters and control algorithms," *Int. J. Hydrogen Energy*, vol. 138, no. May, pp. 823–842, 2025, doi: 10.1016/j.ijhydene.2025.05.169.

[89] C. Zhou, Z. Y. Liu, Y. N. Sun, and L. Mao, "A novel maximum power point tracking technique with improved particle swarm optimization for proton exchange membrane fuel cell," *J. Phys. Conf. Ser.*, vol. 2347, no. 1, 2022, doi: 10.1088/1742-6596/2347/1/012017.

[90] I. M. M. Eltigani and U. Nangia, "Intelligent PSO- PID Controller Based Maximum Power Point Tracking (MPPT) for Photovoltaic System," *2022 Int. Virtual Conf. Power Eng. Comput. Control Dev. Electr. Veh. Energy Sect. Sustain. Futur. PECCON 2022*, no.

August, 2022, doi: 10.1109/PECCON55017.2022.9851173.

[91] M. L. Katche, A. B. Makokha, S. O. Zachary, and M. S. Adaramola, “A Comprehensive Review of Maximum Power Point Tracking (MPPT) Techniques Used in Solar PV Systems,” *Energies*, vol. 16, no. 5, 2023, doi: 10.3390/en16052206.

[92] R. B. Bollipo, S. Mikkili, and P. K. Bonthagorla, “Hybrid, optimal, intelligent and classical PV MPPT techniques: A review,” *CSEE J. Power Energy Syst.*, vol. 7, no. 1, pp. 9–33, 2021, doi: 10.17775/CSEEJPES.2019.02720.

[93] S. A. Kanth and N. Gupta, “A Comprehensive Review on MPPT Methods for Enhanced Photovoltaic System Efficiency,” *2025 IEEE 1st Int. Conf. Smart Sustain. Dev. Electr. Eng. SSDEE 2025*, pp. 1–6, 2025, doi: 10.1109/SSDEE64538.2025.10968420.

[94] S. I. Saadi and I. K. Mohammed, “Power Control Approach for PV Panel System Based on PSO and INC Optimization Algorithms,” *J. Eur. des Syst. Autom.*, vol. 55, no. 6, pp. 825–834, 2022, doi: 10.18280/jesa.550615.

[95] M. S. Bouakkaz, A. Boukadoum, O. Boudebbouz, N. Boutasseta, I. Attoui, and A. Bouraiou, *Classification of conventional and modern maximum power point tracking techniques for photovoltaic energy generation systems*. 2022. doi: 10.1002/9781119786511.ch9.

[96] A. A. Petcut-Lasc, V. E. Balas, and F. M. Petcut, “A Survey of MPPT Techniques Under Partial Shading Conditions: Evaluating the Firefly Algorithm’s Performance,” *2025 18th Int. Conf. Eng. Mod. Electr. Syst. EMES 2025*, pp. 1–6, 2025, doi: 10.1109/EMES65692.2025.11045613.

[97] Ö. F. Tozlu and H. Çalık, “A Review and Classification of Most Used MPPT Algorithms for Photovoltaic Systems,” *Hittite J. Sci. Eng.*, vol. 8, no. 3, pp. 207–220, 2021, doi: 10.17350/hjse19030000231.

[98] S. Y. Wong and J. Li, “Enhancing efficiency in photovoltaic hydrogen production: A comparative analysis of MPPT and electrolysis control strategies,” *MethodsX*, vol. 14, no. August 2024, p. 103220, 2025, doi: 10.1016/j.mex.2025.103220.

[99] M. S. Endiz, G. Gökkuş, A. E. Coşgun, and H. Demir, “A Review of Traditional and Advanced MPPT Approaches for PV Systems Under Uniformly Insolation and Partially Shaded Conditions,” *Appl. Sci.*, vol. 15, no. 3, 2025, doi: 10.3390/app15031031.

[100] H. E. N. Hiber and H. Miloua, *Numerical Study of an Aircraft Cargo Compartment Fire: The Impact of Fire Retardant Sheets*, vol. 1238 LNNS. 2025. doi: 10.1007/978-3-031-80301-7_28.

[101] M. Sarvi and A. Azadian, *A comprehensive review and classified comparison of MPPT algorithms in PV systems*, vol. 13, no. 2. Springer Berlin Heidelberg, 2022. doi: 10.1007/s12667-021-00427-x.

[102] M. H. Ibrahim, S. P. Ang, M. N. Dani, M. I. Rahman, R. Petra, and S. M. Sulthan, “Optimizing Step-Size of Perturb & Observe and Incremental Conductance MPPT Techniques Using PSO for Grid-Tied PV System,” *IEEE Access*, vol. 11, no. February, pp. 13079–13090, 2023, doi: 10.1109/ACCESS.2023.3242979.

[103] A. Chellakhi and S. El, *Optimizing Solar Photovoltaic Systems*. doi: 10.1007/978-3-031-93283-0.

[104] S. J. Yaqoob, “Advanced Maximum Power Point Tracking in Photovoltaic Systems : A Comprehensive Review of Classical , AI-Based , and Metaheuristic Optimization Techniques”, doi: 10.1002/eng2.70404.

[105] N. Koshkarbay *et al.*, “Improved MPPT technology for PV systems using Social Spider optimization (SSO): Efficient handling of partial shading and load variations,” *Electr. Power Syst. Res.*, vol. 247, no. May, p. 111822, 2025, doi: 10.1016/j.epsr.2025.111822.

[106] F. Abdelmalek *et al.*, “Experimental validation of effective zebra optimization algorithm-based MPPT under partial shading conditions in photovoltaic systems,” *Sci. Rep.*, vol. 14, no. 1, pp. 1–21, 2024, doi: 10.1038/s41598-024-77488-2.

[107] F. A. Hashim and A. G. Hussien, “Snake Optimizer: A novel meta-heuristic optimization algorithm,” *Knowledge-Based Syst.*, vol. 242, p. 108320, 2022, doi: 10.1016/j.knosys.2022.108320.

[108] K. K. Mohammed and S. Mekhilef, “Improved Snake Optimizer Algorithm-Based GMPPT With a Fast Response to the Load Variations Under Different Weather Conditions for PV Systems,” *IEEE Trans. Ind. Electron.*, vol. 71, no. 7, pp. 7147–7157, 2024, doi: 10.1109/TIE.2023.3301526.

[109] I. Naruei and F. Keynia, “A new optimization method based on COOT bird natural life model,” *Expert Syst. Appl.*, vol. 183, no. June, p. 115352, 2021, doi: 10.1016/j.eswa.2021.115352.

[110] A. Talib Naser, K. Khairullah Mohammed, N. Fadilah Ab Aziz, A. Elsanabary, K. Binti Kamil, and S. Mekhilef, “A fast-tracking MPPT-based modified coot optimization algorithm for PV systems under partial shading conditions,” *Ain Shams Eng. J.*, vol. 15, no. July 2023, 2024, doi: 10.1016/j.asej.2024.102967.

[111] K. K. Mohammed, S. Mekhilef, and S. Buyamin, “Improved Rat Swarm Optimizer Algorithm-Based MPPT Under Partially Shaded Conditions and Load Variation for PV Systems,” *IEEE Trans. Sustain. Energy*, vol. 14, no. 3, pp. 1385–1396, 2023, doi: 10.1109/TSTE.2022.3233112.

[112] E. H. de Vasconcelos Segundo, V. C. Mariani, and L. dos S. Coelho, “Design of heat exchangers using Falcon Optimization Algorithm,” *Appl. Therm. Eng.*, vol. 156, no. April, pp. 119–144, 2019, doi: 10.1016/j.applthermaleng.2019.04.038.

[113] M. J. Alshareef, “An Effective Falcon Optimization Algorithm Based MPPT Under Partial Shaded Photovoltaic Systems,” *IEEE Access*, vol. 10, no. December, pp. 131345–131360, 2022, doi: 10.1109/ACCESS.2022.3226654.

[114] F. Abdelmalek, H. Afghoul, F. Krim, M. Bajaj, and V. Blazek, “Experimental validation of novel hybrid Grey Wolf Equilibrium Optimization for MPPT to improve the efficiency of solar photovoltaic system,” *Results Eng.*, vol. 25, no. December 2024, p. 103831, 2025, doi: 10.1016/j.rineng.2024.103831.

[115] H. Alhusseini, M. Niroomand, and B. M. Dehkordi, “A Fuzzy-Based Adaptive P&O MPPT Algorithm for PV Systems With Fast Tracking and Low Oscillations Under Rapidly Irradiance Change Conditions,” *IEEE Access*, vol. 12, no. June, pp. 84374–84386, 2024, doi: 10.1109/ACCESS.2024.3412848.

[116] C. Restrepo, N. Yanẽz-Monsalvez, C. González-Castaño, S. Kouro, and J. Rodriguez, “A fast converging hybrid mppt algorithm based on abc and p&o techniques for a partially shaded pv system,” *Mathematics*, vol. 9, no. 18, pp. 1–25, 2021, doi: 10.3390/math9182228.

[117] B. Laxman, R. Gugulothu, and S. R. Salkuti, “A modified particle swarm optimization-based adaptive maximum power point tracking approach for proton exchange membrane fuel cells,” *Franklin Open*, vol. 8, no. June, p. 100161, 2024, doi: 10.1016/j.fraope.2024.100161.

[118] E. Touti, M. Aoudia, C. H. Hussaian Basha, and I. M. Alrougy, “A Novel Design and Analysis Adaptive Hybrid ANFIS MPPT Controller for PEMFC-Fed EV Systems,” *Int. Trans. Electr. Energy Syst.*, vol. 2024, 2024, doi: 10.1155/2024/5541124.

[119] M. Aly, E. A. Mohamed, H. Rezk, A. M. Nassef, M. A. Elhosseini, and A. Shawky, “An Improved Optimally Designed Fuzzy Logic-Based MPPT Method for Maximizing Energy Extraction of PEMFC in Green Buildings,” *Energies*, vol. 16, no. 3, 2023, doi: 10.3390/en16031197.

[120] J. Hahm, H. Kang, J. Baek, H. Lee, and M. Park, “Design of incremental conductance sliding mode MPPT control applied by integrated photovoltaic and proton exchange membrane fuel cell system under various operating conditions for BLDC motor,” *Int. J. Photoenergy*, vol. 2015, 2015, doi: 10.1155/2015/828129.

[121] H. Bektas and A. Caliskan, “ScienceDirect Whale optimization algorithm based MPPT control of a fuel cell system,” *Int. J. Hydrogen Energy*, vol. 48, no. 60, pp. 23230–23241, 2023, doi: 10.1016/j.ijhydene.2023.03.180.

[122] R. Celikel, O. Aydogmus, and M. Yilmaz, “OPEN A modified perturb and observe MPPT algorithm for PEMFC with rapid convergence and low power oscillation,” pp. 1–20, 2025.

[123] B. Kanouni, A. E. Badoud, S. Mekhilef, A. Elsanabary, M. Bajaj, and I. Zaitsev, “A fuzzy-predictive current control with real-time hardware for PEM fuel cell systems,” *Sci. Rep.*, vol. 14, no. 1, pp. 1–18, 2024, doi: 10.1038/s41598-024-78030-0.

[124] L. Fan and X. Ma, “Maximum power point tracking of PEMFC based on hybrid artificial bee colony algorithm with fuzzy control,” *Sci. Rep.*, vol. 12, no. 1, pp. 1–13, 2022, doi: 10.1038/s41598-022-08327-5.

[125] J. J. Jui, M. A. Ahmad, M. M. I. Molla, and M. I. M. Rashid, “Optimal energy management strategies for hybrid electric vehicles: A recent survey of machine learning approaches,” *J. Eng. Res.*, vol. 12, no. 3, pp. 454–467, 2024, doi: 10.1016/j.jer.2024.01.016.

[126] B. Kanouni, A. E. Badoud, S. Mekhilef, M. Bajaj, and I. Zaitsev, “Advanced efficient energy management strategy based on state machine control for multi-sources PV-PEMFC-batteries system,” *Sci. Rep.*, vol. 14, no. 1, pp. 1–20, 2024, doi: 10.1038/s41598-024-58785-2.

[127] A. G. Alharbi, A. G. Olabi, H. Rezk, A. Fathy, and M. A. Abdelkareem, “Optimized energy management and control strategy of photovoltaic/PEM fuel cell/batteries/supercapacitors DC microgrid system,” *Energy*, vol. 290, no. February 2023, p. 130121, 2024, doi: 10.1016/j.energy.2023.130121.

[128] H. Rezk and A. Fathy, “Hydrogen reduction-based energy management strategy of hybrid fuel cell/PV/battery/supercapacitor renewable energy system,” *J. Energy Storage*, vol. 86, no. PB, p. 111316, 2024, doi: 10.1016/j.est.2024.111316.

[129] H. Alhumade, H. Rezk, M. Louzazni, I. A. Moujdin, and S. Al-Shahrani, “Advanced Energy Management Strategy of Photovoltaic/PEMFC/Lithium-Ion Batteries/Supercapacitors Hybrid Renewable Power System Using White Shark Optimizer,” *Sensors*, vol. 23, no. 3, 2023, doi: 10.3390/s23031534.

[130] H. Rezk, A. M. Nassef, M. A. Abdelkareem, A. H. Alami, and A. Fathy, “Comparison among various energy management strategies for reducing hydrogen consumption in a hybrid fuel cell/supercapacitor/battery system,” *Int. J. Hydrogen Energy*, vol. 46, no. 8, pp. 6110–6126, 2021, doi: 10.1016/j.ijhydene.2019.11.195.

[131] H. Rezk, A. Fathy, M. Aly, and M. N. Ibrahim, “Energy Management Control Strategy for Renewable Energy System Based on Spotted Hyena Optimizer,” *Comput. Mater. Contin.*, vol. 67, no. 2, pp. 2271–2281, 2021, doi: 10.32604/cmc.2021.014590.

[132] A. M. Nassef, A. Fathy, and H. Rezk, “An effective energy management strategy based on mine-blast optimization technique applied to hybrid PEMFC/supercapacitor/batteries system,” *Energies*, vol. 12, no. 19, pp. 1–16, 2019, doi: 10.3390/en12193796.

[133] A. Fathy, M. Al-Dhaifallah, and H. Rezk, “Recent Coyote Algorithm-Based Energy Management Strategy for Enhancing Fuel Economy of Hybrid FC/Battery/SC System,” *IEEE Access*, vol. 7, pp. 179409–179419, 2019, doi: 10.1109/ACCESS.2019.2959547.

[134] D. Algorithm *et al.*, “A Novel A-ECMS Energy Management Strategy Based on,” pp. 1–23, 2023.

[135] H. Rezk and A. Fathy, “Combining proportional integral and fuzzy logic control strategies to improve performance of energy management of fuel cell electric vehicles,” *Int. J. Thermofluids*, vol. 26, no. January, p. 101076, 2025, doi: 10.1016/j.ijft.2025.101076.

[136] A. Fathy, K. Kaaniche, and T. M. Alanazi, "Recent Approach Based Social Spider Optimizer for Optimal Sizing of Hybrid PV/Wind/Battery/Diesel Integrated Microgrid in Aljouf Region," *IEEE Access*, vol. 8, pp. 57630–57645, 2020, doi: 10.1109/ACCESS.2020.2982805.

[137] A. Fathy, S. Ferahtia, H. Rezk, D. Yousri, M. A. Abdelkareem, and A. G. Olabi, "Optimal adaptive fuzzy management strategy for fuel cell-based DC microgrid," *Energy*, vol. 247, p. 123447, 2022, doi: 10.1016/j.energy.2022.123447.

[138] A. N. Ribeiro and D. M. Muñoz, "Neural network controller for hybrid energy management system applied to electric vehicles," vol. 104, no. July, 2024.

[139] A. R. Singh, R. S. Kumar, M. Bajaj, C. B. Khadse, and I. Zaitsev, "Machine learning - based energy management and power forecasting in grid - connected microgrids with multiple distributed energy sources," *Sci. Rep.*, pp. 1–23, 2024, doi: 10.1038/s41598-024-70336-3.

[140] J. Uralde, O. Barambones, A. Rio, and I. Calvo, "Rule-Based Operation Mode Control Strategy for the Energy Management of a Fuel Cell Electric Vehicle," 2024.

[141] C. Jia, W. Liu, H. He, and K. T. Chau, "Deep reinforcement learning-based energy management strategy for fuel cell buses integrating future road information and cabin comfort control," *Energy Convers. Manag.*, vol. 321, no. July, p. 119032, 2024, doi: 10.1016/j.enconman.2024.119032.

[142] R. Huang and H. He, "ScienceDirect A novel data-driven energy management strategy for fuel cell hybrid electric bus based on improved twin delayed deep deterministic policy gradient algorithm," *Int. J. Hydrogen Energy*, vol. 52, pp. 782–798, 2023, doi: 10.1016/j.ijhydene.2023.04.335.

[143] C. Jia, H. He, J. Zhou, J. Li, Z. Wei, and K. Li, "International Journal of Hydrogen Energy A novel deep reinforcement learning-based predictive energy management for fuel cell buses integrating speed and passenger prediction," *Int. J. Hydrogen Energy*, vol. 100, no. December 2024, pp. 456–465, 2025, doi: 10.1016/j.ijhydene.2024.12.338.

[144] O. Al-Baik *et al.*, "Pufferfish Optimization Algorithm: A New Bio-Inspired Metaheuristic Algorithm for Solving Optimization Problems," *Biomimetics*, vol. 9, no. 2, 2024, doi: 10.3390/biomimetics9020065.

[145] B. K. Veedhi, K. Das, D. Mishra, S. Mishra, and M. P. Behera, "Balancing data imbalance in biomedical datasets using a stacked augmentation approach with STDA, DAGAN, and pufferfish optimization to reveal AI's transformative impact," *Int. J. Inf. Technol.*, vol. 17, no. 1, pp. 455–480, 2024, doi: 10.1007/s41870-024-02234-w.

[146] R. Mahaveerakannan, B. Rajakumar, R. R. Sharma, and S. Pushpa, "Pufferfish Optimizer based Enhanced UNETR for Accurate Lung Cancer Segmentation and Classification," *2024 Asian Conf. Intell. Technol. ACOIT 2024*, pp. 1–7, 2024, doi: 10.1109/ACOIT62457.2024.10939909.

[147] W. Peng and W. Zheng, "An AI-based badminton smash detection using residual-shuffle network optimized based on upgraded pufferfish optimizer," *Ain Shams Eng. J.*, vol. 16, no. 7, p. 103414, 2025, doi: 10.1016/j.asej.2025.103414.

[148] R. Pattanayak and B. Mohanty, "Energy Management Strategy for a DC Micro-Grid system using FOPID Controller and POA Optimization Technique," *2024 Int. Conf. Intell. Comput. Sustain. Innov. Technol. IC-SIT 2024*, pp. 1–6, 2024, doi: 10.1109/IC-SIT63503.2024.10862804.

[149] S. Barua and A. Merabet, "Lévy Arithmetic Algorithm: An enhanced metaheuristic algorithm and its application to engineering optimization," *Expert Syst. Appl.*, vol. 241, no. October 2023, p. 122335, 2024, doi: 10.1016/j.eswa.2023.122335.

[150] S. Wang, W. Cai, and L. Zeng, "Research on MPPT Based on Gray Wolf Algorithm improved by Levy Flight," *J. Phys. Conf. Ser.*, vol. 1865, no. 4, 2021, doi: 10.1088/1742-6596/1865/4/042089.

[151] J. Kołodziejczyk and Y. Tarasenko, "Particle Swarm Optimization and Lévy Flight integration," *Procedia Comput. Sci.*, vol. 192, no. 2019, pp. 4658–4671, 2021, doi: 10.1016/j.procs.2021.09.244.

[152] W. Wang and J. Tian, "An Improved Nonlinear Tuna Swarm Optimization Algorithm Based on Circle Chaos Map and Levy Flight Operator," *Electron.*, vol. 11, no. 22, 2022, doi: 10.3390/electronics11223678.

[153] C. Charin, D. Ishak, M. A. A. Mohd Zainuri, B. Ismail, and M. K. Mohd Jamil, "A hybrid of bio-inspired algorithm based on Levy flight and particle swarm optimizations for photovoltaic system under partial shading conditions," *Sol. Energy*, vol. 217, no. February, pp. 1–14, 2021, doi: 10.1016/j.solener.2021.01.049.

[154] L. gang Kong, B. Wang, D. jin Fan, S. Shi, X. Ouyang, and M. Xu, "Optimize photovoltaic MPPT with improved snake algorithm," *Energy Reports*, vol. 11, no. May 2023, pp. 5033–5045, 2024, doi: 10.1016/j.egyr.2024.04.064.

[155] L. S. Processes, "',,and a= —," vol. 49, no. 5, 1994.

[156] A. Bouguerra, A. E. Badoud, S. Mekheilef, and A. Chouder, "Comparative Study of Perturb and Observe Incremental Conductance and Particle Swarm Optimisation for Maximum Power Point Tracking Under Changing Irradiance," *Proc. - 2023 2nd Int. Conf. Electron. Energy Meas. IC2EM 2023*, vol. 1, no. Ic2em, pp. 1–7, 2023, doi: 10.1109/IC2EM59347.2023.10419737.

[157] A. T. Naser, K. Khairullah Mohammed, N. F. Ab Aziz, K. Binti Kamil, and S. Mekhilef, "A Comparative Study of Three Meta-Heuristic MPPT Techniques for PV Systems Under Complex Partial Shading Conditions," *2023 33rd Australas. Univ. Power Eng. Conf. AUPEC 2023*, pp. 1–6, 2023, doi: 10.1109/AUPEC59354.2023.10502884.

[158] S. Mirjalili, S. Mohammad, and A. Lewis, “Advances in Engineering Software Grey Wolf Optimizer,” *Adv. Eng. Softw.*, vol. 69, pp. 46–61, 2014, doi: 10.1016/j.advengsoft.2013.12.007.

[159] C. Methods, A. Mech, L. Abualigah, A. Diabat, S. Mirjalili, and M. Abd, “ScienceDirect The Arithmetic Optimization Algorithm,” *Comput. Methods Appl. Mech. Eng.*, vol. 376, p. 113609, 2021, doi: 10.1016/j.cma.2020.113609.

[160] M. Ahmed, E. Mohamed, and S. N. Ahmed, “Arithmetic optimization algorithm based maximum power point tracking for grid - connected photovoltaic system Maximum PowerPoint tracking,” *Sci. Rep.*, no. 0123456789, pp. 1–19, 2023, doi: 10.1038/s41598-023-32793-0.

[161] S. Chtita, A. Derouich, S. Motahhir, and A. EL Ghzizal, “A new MPPT design using arithmetic optimization algorithm for PV energy storage systems operating under partial shading conditions,” *Energy Convers. Manag.*, vol. 289, no. May, p. 117197, 2023, doi: 10.1016/j.enconman.2023.117197.

[162] K. Ishaque, Z. Salam, M. Amjad, and S. Mekhilef, “An improved particle swarm optimization (PSO)-based MPPT for PV with reduced steady-state oscillation,” *IEEE Trans. Power Electron.*, vol. 27, no. 8, pp. 3627–3638, 2012, doi: 10.1109/TPEL.2012.2185713.

[163] Y. H. Liu, S. C. Huang, J. W. Huang, and W. C. Liang, “A particle swarm optimization-based maximum power point tracking algorithm for PV systems operating under partially shaded conditions,” *IEEE Trans. Energy Convers.*, vol. 27, no. 4, pp. 1027–1035, 2012, doi: 10.1109/TEC.2012.2219533.

[164] S. Mohanty, B. Subudhi, and P. K. Ray, “A new MPPT design using grey Wolf optimization technique for photovoltaic system under partial shading conditions,” *IEEE Trans. Sustain. Energy*, vol. 7, no. 1, pp. 181–188, 2016, doi: 10.1109/TSTE.2015.2482120.

[165] V. H. Bui, V. Du Ha, V. A. Truong, and T. L. Duong, “A Hybrid P&O and PV Characteristics Simulation Method for GMPPT in PV Systems Under Partial Shading Conditions,” *Sensors*, vol. 25, no. 6, pp. 1–23, 2025, doi: 10.3390/s25061908.

[166] A. Chellakhi, S. El Beid, Y. Abouelmahjoub, and H. Doubabi, “An Enhanced Incremental Conductance MPPT Approach for PV Power Optimization: A Simulation and Experimental Study,” *Arab. J. Sci. Eng.*, vol. 49, no. 12, pp. 16045–16064, 2024, doi: 10.1007/s13369-024-08804-1.

[167] W. Hayder, E. Ogliari, A. Dolara, A. Abid, M. Ben Hamed, and L. Sbita, “Improved PSO: A comparative study in MPPT algorithm for PV system control under partial shading conditions,” *Energies*, vol. 13, no. 8, 2020, doi: 10.3390/en13082035.

[168] H. Li, D. Yang, W. Su, J. Lu, and X. Yu, “An Overall Distribution Particle Swarm Optimization MPPT Algorithm for Photovoltaic System under Partial Shading,” *IEEE Trans. Ind. Electron.*, vol. 66, no. 1, pp. 265–275, 2019, doi: 10.1109/TIE.2018.2829668.

[169] H. Gundogdu, A. Demirci, S. M. Tercan, and U. Cali, “A Novel Improved Grey Wolf Algorithm Based Global Maximum Power Point Tracker Method Considering Partial Shading,” *IEEE Access*, vol. 12, no. December 2023, pp. 6148–6159, 2024, doi: 10.1109/ACCESS.2024.3350269.

[170] C. Gonzalez-Castano, C. Restrepo, S. Kouro, and J. Rodriguez, “MPPT Algorithm Based on Artificial Bee Colony for PV System,” *IEEE Access*, vol. 9, pp. 43121–43133, 2021, doi: 10.1109/ACCESS.2021.3066281.

[171] Jahid, M. Ehtesham, S. Kirmani, and Manaullah, “Application of Flower Pollination Algorithm and its Comparative Analysis for MPPT of Solar Panels Under Partial Shading Conditions,” *J. Inst. Eng. Ser. B*, 2025, doi: 10.1007/s40031-025-01197-1.

[172] S. Mo, Q. Ye, K. Jiang, X. Mo, and G. Shen, “An improved MPPT method for photovoltaic systems based on mayfly optimization algorithm,” *Energy Reports*, vol. 8, pp. 141–150, 2022, doi: 10.1016/j.egyr.2022.02.160.

[173] M. A. Zeddini, S. Krim, M. Mansouri, M. F. Mimouni, and A. Sakly, “Fuzzy Logic Adaptive Crow Search Algorithm for MPPT of a Partially Shaded Photovoltaic System,” *IEEE Access*, vol. 12, no. September, pp. 119246–119271, 2024, doi: 10.1109/ACCESS.2024.3434523.

[174] L. Avila, M. De Paula, M. Trimboli, and I. Carlucho, “Deep reinforcement learning approach for MPPT control of partially shaded PV systems in Smart Grids,” *Appl. Soft Comput. J.*, vol. 97, p. 106711, 2020, doi: 10.1016/j.asoc.2020.106711.

[175] N. Singh, K. K. Gupta, and S. K. Jain, “A Flying Squirrel Search Optimization for MPPT under Partial Shaded Photovoltaic System,” no. January 2021, 2020, doi: 10.1109/JESTPE.2020.3024719.

[176] A. A. Al-Shammaa, A. M. Abdurraqeeb, A. M. Noman, A. Alkuhayli, and H. M. H. Farh, “Hardware-In-the-Loop Validation of Direct MPPT Based Cuckoo Search Optimization for Partially Shaded Photovoltaic System,” *Electron.*, vol. 11, no. 10, 2022, doi: 10.3390/electronics11101655.

[177] A. Bouguerra, A. E. Badoud, S. Mekheilef, and B. Kanouni, “Energy Sustainability: Using Particle Swarm Optimization to Evaluate Hydrogen Exchange Membrane Fuel Cells in altering instances,” *2024 2nd Int. Conf. Electr. Eng. Autom. Control. ICEEAC 2024*, pp. 1–6, 2024, doi: 10.1109/ICEEAC61226.2024.10576566.

[178] K. P. S. Rana, V. Kumar, N. Sehgal, and S. George, “A Novel dPdI feedback based control scheme using GWO tuned PID controller for efficient MPPT of PEM fuel cell.,” *ISA Trans.*, vol. 93, pp. 312–324, Oct. 2019, doi: 10.1016/j.isatra.2019.02.038.

[179] M. Aly, “A Differential Evolution-Based Optimized Fuzzy Logic MPPT Method for Enhancing the Maximum Power Extraction of Proton Exchange Membrane Fuel Cells,” pp. 172219–172232, 2020, doi: 10.1109/ACCESS.2020.3025222.

[180] A. Fathy, M. Ali, and A. G. Olabi, “ScienceDirect A novel strategy based on salp swarm algorithm for extracting the maximum

power of proton exchange membrane fuel cell," *Int. J. Hydrogen Energy*, vol. 46, no. 8, pp. 6087–6099, 2020, doi: 10.1016/j.ijhydene.2020.02.165.

[181] "Souleman Njoya Motapon 2013," 2013.

[182] M. Azmi, A. Betar, M. A. Awadallah, and M. S. Braik, *Elk herd optimizer : a novel nature - inspired metaheuristic algorithm*, vol. 57, no. 3. Springer Netherlands, 2024. doi: 10.1007/s10462-023-10680-4.

[183] G. Zheng, W. Wei, H. Jia, Y. Liu, and J. Lin, "An Improved Elk Herd Optimization Algorithm for Maximum Power Point Tracking in Photovoltaic Systems Under Partial Shading Conditions," pp. 1–26, 2025.

[184] M. Azmi, A. M. Sh, B. Qusai, and Y. Shambour, "Ameliorated elk herd optimizer for global optimization and engineering problems," 2025.